

EXPERIMENTAL INVESTIGATIONS OF
WATER BREAKDOWN

by

DAVID LOJEWSKI, B.S., B.S.E.E., M.S.E.E.

A DISSERTATION

IN

ELECTRICAL ENGINEERING

Submitted to the Graduate Faculty
of Texas Tech University in
Partial Fulfillment of
the Requirements for
the Degree of

DOCTOR OF PHILOSOPHY

 Approved

May, 1996

11
801
T3
1996
110.8
Cop. 2

AK9 - 50212
1m 4/25

ACKNOWLEDGMENTS

First and foremost, I want to thank my wife, Cheryl Lojewski, for putting up with me going to school for most of our married life. Without her love and understanding, I would not be completing this. I also want to thank my children, Jenifer and Randy, for their support and understanding.

I am grateful to the United States Air Force, without their programs for higher education, I would never have been able to do this work. A special note of thanks goes to Dr. M. Kristiansen who was my mentor and committee chairman. Without his guidance and assistance, I would not be where I am today. I also want to thank the other members of my committee -- Drs. Lynn Hatfield, Hermann Krompholtz, Greg Engel, and Michael Giesselmann -- for all of their help and guidance. I want to thank Dr. Raghu Narayan and Aashish Ahuja, from the Chemical Engineering Department, for their help with the polymer coatings.

A project like this cannot be done without help from a lot of different people. Many problems were solved by discussions with my fellow graduate students, and it would take considerable space to acknowledge each and every person that helped me, so I will have to thank them as a group. I also received considerable help and support from the technicians in both the Physics and the Electrical Engineering Departments. I have to thank Kim Zinsmeyer for solving many of the problems I was having with various pieces

of equipment. John Bridges calibrated my oscilloscopes which was a big help and also built the analog integrator.

I received considerable help from Danny Garcia and Dino Castro. They helped me find parts for the experiment and helped with the manual labor portion of the project. Lonnie Stephenson built the D-Dot probe and was very patient with my faulty drafting skills, he did an excellent job in spite of my mistakes. I want to also thank the following people for their help: Dick Miller and Bill Rix, Maxwell Laboratories; Peter Sincerny and Ken Childers, Physics International; Van Kenyon, Naval Surface Warfare Center; and Tom Martin, Sandia National Laboratory.

I am grateful for the help I received from Travis Simpson, he was always there when I needed someone to talk to. I want to thank Marie Byrd for being a friend and also helping me through the administrative parts of my education. Donna Srader was also very helpful in this same area. Last but not least, I have to acknowledge the help I received from the undergraduate assistants that worked on the project. Without Nora Chang, Bill Conover, Mark Barkley, and Kharuum Salim, I would not have been able to complete this effort.

Finally, I need to thank the Defense Nuclear Agency for their small contribution to help pay for the materials used during the course of this project and the salaries of my undergraduate assistants.

Nam et ipsa scientia potestas est (Knowledge is power), Francis Bacon,
Meditationes Sacrae [1597].

TABLE OF CONTENTS

ACKNOWLEDGMENTS.....	ii
ABSTRACT.....	vi
LIST OF TABLES	viii
LIST OF FIGURES	ix
LIST OF ABBREVIATIONS	xiv
CHAPTER	
I. INTRODUCTION	1
II. LITERATURE REVIEW.....	4
III. EXPERIMENTAL SETUP AND MODELS	31
IV. EXPERIMENTAL DESIGN AND DATA.....	63
V. DATA ANALYSIS	129
VI. CONCLUSIONS	142
REFERENCES	150
APPENDICES	
A. WATER BREAKDOWN FORMULAS	154
B. D-DOT PROBE.....	169
C. MATLAB PROGRAMS	183
D. ASSEMBLY LANGUAGE PROGRAMS	234
E. READING LIST	263

ABSTRACT

The Water Breakdown System was designed to investigate various techniques for increasing the high voltage breakdown strength of water and increase the time before breakdown. The interest in water for high voltage applications is because of water's unusually high dielectric constant (ϵ_r) which is typically 80. This is about 30 to 40 times higher than most other insulator materials. If the insulating ability of water could be improved, then high energy capacitors could be made 30 to 40 times smaller than they presently are. The initial breakdown mechanism is believed to be an electrode surface effect in which case the use of a coating to grade the field effects at the electrode surface would have the greatest chance for improvement in the voltage holdoff capability of water.

Several techniques were tried during this investigation which included magnetic fields, SF_6 gas, and HCl. The electrodes were also coated with two different polymers, poly(ethersulfone) (PES) and polycarbonate (PC) to see if there would be an improvement in voltage holdoff. The use of anodized aluminum electrodes and coating the electrodes with black wax have been tried by other researchers. These experiments were conducted to see if the results could be repeated.

For the magnetic field experiments, neodymium iron boron magnets were placed inside hollowed out copper tungsten electrodes. The magnetic

fields showed a small, though, statistically significant effect on the maximum voltage and the effective time-width of the pulse. The amount of the effect depended on the orientation of the magnetic field and whether the magnets were used in both electrodes or only one electrode, possibly because of the change in magnetic flux density or the divergence of the field.

Initial use of SF₆ gas with the water appeared promising but the results could not be reproduced. The lack of a reproducible effect may have been due to an insufficient amount of the gas mixing with the water.

The HCl experiments were similar to work done by Russian scientists except that the voltage level was measured rather than the prebreakdown current measured by the Russians. Adding HCl caused the voltage holdoff capability of the water to decrease with increasing amounts of HCl.

Copper tungsten and stainless steel electrodes were coated with either a thin layer of poly(ethersulfone) or polycarbonate. No noticeable beneficial effects were seen with either of these coatings. The anodized aluminum electrodes did not show the same increase in holdoff strength as previous research in which ethylene glycol was mixed with the water and then cooled. The electrodes coated with black wax also did not show an increase in holdoff strength as in previous research. It was shown that over larger surface areas, the use of black wax to coat the electrode surfaces did not increase the voltage breakdown level.

LIST OF TABLES

1. Matrix of variables versus effects in water breakdown research	6
2. Electrical breakdown strength properties of mixtures of ethylene glycol and water	10
3. Summary of the data with a history of the highest applied voltages without breakdown	13
4. Results of the t -tests for τ_{eff} for the second HCl experiment	135
5. Results of the t -tests for V_{max} for the second HCl experiment	136
6. Results of the t -tests for fall-rate for the second HCl experiment.....	137

LIST OF FIGURES

1.	Relationship between pressure and electric breakdown strength of water	7
2.	Isothermal static permittivity versus molar fraction x for mixtures (methanol) _{x} / (water) _{$1-x$}	12
3.	The j - v dependence for different cathode materials for the same spacing between the cathode and the anode.....	14
4.	Schematic representation of the j - v curves obtained with different electrodes in pure water.....	16
5.	The j - v dependence for Au and Ni electrodes for the same spacing between the cathode and the anode	17
6.	The j - v dependence for a platinum electrode covered with (a) 0.1 mm and (b) 0.5 mm thick film of black wax.....	18
7.	The value of $\langle M \rangle_{20}$ as a function of the shot sequence number.....	20
8.	Action density as a function of applied voltage for various electrode materials. The threshold breakdown voltages (V_{th}) are included	21
9.	Action density as a function of applied voltage for #304 stainless steel. The threshold breakdown voltages (V_{th}) are included	23
10.	Differences between measurements of ϵ_s as a function of temperature; $\Delta\epsilon = \epsilon_s - \epsilon_{smm}$	26
11.	Proton mobility mechanism in water (1) Displacement of a proton and (2) displacement of an electron.....	28
12.	High voltage breakdown in water system diagram, side view.....	32
13.	Air line diagram for trigger switch.....	38
14.	Trigger switch electrical connections	39
15.	Electrical wiring diagram for the trigger switch	49

16.	System model for simulation	52
17.	Output of system model at the probe point.....	54
18.	Comparison of an actual signal with a 5 MHz sine wave	56
19.	Diagram of the D-Dot probe.....	58
20.	Circuit model used for the D-Dot probe	60
21.	Normalized input and output voltages for the D-Dot probe simulation.	61
22.	Comparison of D-Dot probe with calculated versus measured C_2	62
23.	Average waveforms for the magnet in the anode	72
24.	Effective time (τ_{eff}) with a magnet in the anode.....	73
25.	Maximum voltage (V_{max}) with a magnet in the anode	74
26.	Fall-time with a magnet in the anode	75
27.	Fall-rate with a magnet in the anode.....	76
28.	Average waveforms for the magnet in the cathode	77
29.	Effective time (τ_{eff}) with a magnet in the cathode.....	78
30.	Maximum voltage (V_{max}) with a magnet in the cathode	79
31.	Fall-time with a magnet in the cathode	80
32.	Fall-rate with a magnet in the cathode.....	81
33.	Average waveforms with magnets in the anode and cathode	82
34.	Effective time (τ_{eff}) with magnets in the anode and cathode	83
35.	Maximum voltage (V_{max}) with magnets in the anode and cathode	84
36.	Fall-time with magnets in the anode and cathode	85
37.	Fall-rate with magnets in the anode and cathode	86

38.	Average waveforms with SF ₆ added to the water (first series).....	87
39.	Effective time (τ_{eff}) with SF ₆ added (first series).....	88
40.	Maximum voltage (V_{max}) with SF ₆ added (first series).....	89
41.	Fall-time with SF ₆ added (first series).....	90
42.	Fall-rate with SF ₆ added (first series).....	91
43.	Average waveforms with SF ₆ added to the water (second series).....	93
44.	Effective time (τ_{eff}) with SF ₆ added (second series).....	94
45.	Maximum voltage (V_{max}) with SF ₆ added (second series).....	95
46.	Fall-time with SF ₆ added (second series).....	96
47.	Fall-rate with SF ₆ added (second series).....	97
48.	The ten baseline waveforms for the SF ₆ second series of shots.....	98
49.	The ten waveforms with SF ₆ added to the water (second series).....	99
50.	Average waveforms with SF ₆ added to the water (third series).....	100
51.	Effective time (τ_{eff}) with SF ₆ added (third series).....	101
52.	Maximum voltage (V_{max}) with SF ₆ added (third series).....	102
53.	Fall-time with SF ₆ added (third series).....	103
54.	Fall-rate with SF ₆ added (third series).....	104
55.	Waveforms for various amounts of HCl added to the water.....	105
56.	Average waveforms for various amounts of HCl added to the water (second series).....	107
57.	Effective time (τ_{eff}) with HCl added (second series).....	108
58.	Maximum voltage (V_{max}) with HCl added (second series).....	109

59.	Fall-time with HCl added (second series)	110
60.	Fall-rate with HCl added (second series).....	111
61.	Average waveforms with polymer coatings on the electrodes.....	112
62.	Effective time (τ_{eff}) with polymer coatings on the electrodes.....	113
63.	Maximum voltage (V_{max}) with polymer coatings on the electrodes	114
64.	Fall-time with polymer coatings on the electrodes	115
65.	Fall-rate with polymer coatings on the electrodes.....	116
66.	Average waveforms with black wax coatings on the electrodes.....	118
67.	Effective time (τ_{eff}) with black wax coatings on the electrodes.....	119
68.	Maximum voltage (V_{max}) with black wax coatings on the electrodes....	120
69.	Fall-time with black wax coatings on the electrodes.....	121
70.	Fall-rate with black wax coatings on the electrodes.....	122
71.	Average waveforms with anodized aluminum electrodes	123
72.	Effective time (τ_{eff}) with anodized aluminum electrodes	124
73.	Maximum voltage (V_{max}) with anodized aluminum electrodes	126
74.	Fall-time with anodized aluminum electrodes	127
75.	Fall-rate with anodized aluminum electrodes	128
76.	Typical Gaussian curve.....	156
77.	Comparison of the breakdown field equations (F) versus surface area (A)	159
78.	Normalized energy (E_c) versus relative dielectric constant (ϵ_r) for $AF^2d = 2/\epsilon_0$	163

79. Normalized energy (E_c) versus normalized electric field (F) for $Ad = 2/\epsilon_0$	164
80. Normalized energy (E_c) versus area (A) for the JCM and EL equations.....	168
81. Typical Bode plot with one zero and two poles	175
82. Coax geometry for Eqs. (87) and (88)	180
83. Output of the D-Dot probe. The top trace is the input signal with a 75 MHz bandwidth probe. The bottom trace is the output of the D-Dot probe.....	182

LIST OF ABBREVIATIONS

A - area.

α - statistical probability of error.

AD - action density, energy density times τ_{eff} (Gehman [9]).

Al - aluminum.

ANOVAR - Analysis of Variance - statistical test.

atm - atmosphere.

Au - gold.

BW - bandwidth.

C - capacitance.

C - degree Celsius.

CLC - capacitor - inductor - capacitor model for estimating risetime.

cm - centimeter.

C_s - stray capacitance.

Cu - Copper.

CuSO_4 -Cupric Sulfate.

CuW - Copper Tungsten (Elconite).

δ - skin depth.

d - distance between capacitor plates.

D-Dot - derivative of the electric flux density (D).

dB - decibel.

df - degrees of freedom (statistics).

E - electric field strength (volts/meter).

ϵ_0 - dielectric permittivity of free space (8.85×10^{-12} Farad/meter).

E_{BD} - electric field breakdown value (volts/meter).

E_c - energy stored in a capacitor (joules).

EHD - electro-hydrodynamic.

E_{JCM+} , E_{JCM-} , E_{EL+} , and E_{EL-} for JCM positive, JCM negative, Elbert-Lupton positive, and Elbert-Lupton negative, respectively, electric field breakdown values (volts/meter).

EL - Elbert Lupton.

E_{max} - maximum electric field (volts/meter).

ϵ_r - relative dielectric constant.

ϵ_s - static dielectric constant, similar to ϵ_r .

F - electric field, used by J. C. Martin, same as E (volts/meter).

F - statistical distribution used for the ANOVAR.

$FeCl_3$ - Iron Chloride.

HCl - Hydrochloric acid.

HV - high voltage.

$j-v$ - current density versus voltage (Szklarczyk, Kainthla, and Bockris [7]).

JCM - J. C. Martin.

kG - kiloGauss.

kJ - kilojoules.

kPa - kiloPa (Pascal), a measure of air pressure (1 atm = 101 kPa).

kV - kilovolts.

l - length (meters).

l/min - liters/minute.

m - meter.

M - constant used by Fenneman [8] in J. C. Martin's equations.

M - molar.

$\langle M \rangle_{20}$ - average of 20 values of M (Fenneman [8]).

μ, μ_0 - permeability and permeability of free space ($4\pi \times 10^{-7}$ Henry/meter).

μF - microfarads.

MHz - megahertz.

ml/s - milliliters/second.

μm - micrometers.

mm - millimeters.

MPa - megaPa (Pascal), a measure of air pressure (1 atm = 0.101 MPa).

μs - microseconds.

ms - milliseconds.

MV/cm - megavolts/centimeter.

MV/m - megavolts/meter.

NdFeB - neodymium iron boron (magnet material).

Ni - nickel.

ns - nanoseconds.

Pa - Pascal, a measure of air pressure (1 atm = 1.01×10^5 Pa).

PC - polycarbonate.

PES - poly(ethersulfone).

π - pi = 3.141593....

ρ - resistivity (Ωm).

r - radius.

R - resistance (Ω).

σ - conductivity ($1/\Omega\text{m}$).

SF₆ - Sulfur Hexafluoride.

SS - stainless steel.

STP - standard temperature and pressure (1 atm, 25 C).

T - temperature or Tesla (magnetic field).

t-test - statistical test.

t_{dc} - discharge time of the Marx bank capacitor.

τ - time to breakdown.

τ_{eff} - effective time width of a signal which is the time that the voltage is

above 63% of V_{max} .

V - voltage.

V_{\max} - maximum voltage.

V_{th} - threshold breakdown voltage.

ω - 2π x frequency.

Ω - ohms.

x - molar fraction.

CHAPTER I

INTRODUCTION

The Water Breakdown System was designed to investigate various techniques for increasing the high voltage breakdown strength of water and increase the time before breakdown. The interest in water for high voltage applications has been around since the 1950s. The reason for this interest is water's unusually high dielectric constant (ϵ_r) which is typically 80. This is about 30 to 40 times higher than most other insulator materials. If we could improve the insulating ability of water, then high energy capacitors could be made 30 to 40 times smaller than they presently are. Much of the initial work in characterizing water insulation was done by J. C. Martin; however, most of his work was done for systems with limited surface area. Many of the pulsed power systems today are much larger than they were in Martin's time, and his equations are limited to smaller surface areas than we are seeing today, but Martin's work is still used for comparison with the work being done today. Martin's equations are discussed in Appendix A.

The Russians have also done considerable work with water insulation. Recently claims of quadrupling the field strength above the J. C. Martin levels over large areas [1] has brought considerable interest into this area. This type of improvement is what we have been looking for these many years to make water a more practical insulator. It will be interesting to see what

the future holds for research in this area. Some of the Russian work will be discussed in Chapter II.

As can be seen, the interest in water has been around for a long time. One reason for this is that water exhibits the quality of being self-healing; if there is a breakdown in the water, it quickly returns to its original and undamaged state. Other liquid insulators are prone to carbonization after breakdown and tend to lose some of their voltage holdoff strength.

The drawback to using water is the short length of time it can hold off the voltage, typically in the microsecond (μs) range. Considerable research has been done to make water a more viable dielectric material. For now, water capacitors are used for intermediate energy storage in pulsed power systems. This is usually in the form of peaking capacitors placed between the Marx bank and the load. The use of peaking capacitors sharpens the rise time of the pulse before it goes to the load. What we would like to see is the use of water in the primary energy storage portion of the pulsed power system.

Water is relatively inexpensive and is environmentally safe. These characteristics along with the high dielectric constant make water an excellent choice for building large capacitors. If a way can be found to increase the voltage holdoff time and the field strength, then there will be more applications for water capacitors.

A review of the literature is given in Chapter II. This consists of a discussion of a subset of over 225 articles that were reviewed for this work and a review of some of the Russian literature. Chapter III presents a description of the experimental setup and an analysis of the electrical circuit model developed for this experiment. Experimental design and data are given in Chapter IV and a discussion of the data is in Chapter V. Conclusions are given in Chapter VI along with some suggestions for future work.

As mentioned above, Appendix A goes through some of the information on J. C. Martin's equation and some of the more recent work done in that area. Appendix B presents the mathematical derivation of the D-Dot probe and the development of the design criteria for construction of the probe. Appendices C and D consist of the MATLAB and assembly language programs that were written for the data collection and analysis for this dissertation. Appendix E contains the list of articles found in the literature search.

CHAPTER II

LITERATURE REVIEW

The literature search for this project consisted of a review of over 225 journal articles and books that pertained to high voltage breakdown in liquids with the emphasis on water. The literature review is presented in two sections; the first will be a discussion of thirteen representative articles that deal with techniques to increase the ability of the water insulator to hold-off high electric fields and, the second, presents a discussion of the prebreakdown phenomena described by Russian scientists at the Siberian Scientific-Research Institute of Power Generation, Novosibirsk, Russia. A reading list of all of the articles reviewed is included at the end of the dissertation in Appendix E.

High voltage water breakdown review

In the course of this review, there were so many variables involved that attempting to analyze the work that had been done was like comparing “apples and oranges.” Thirteen articles were selected that provided a good representation of the research previously done.

An analysis of the data showed three overriding effects. Any change made to the water affected (1) its voltage breakdown strength which was usually measured as its electric field breakdown (E_{BD}) strength, (2) its

dielectric constant (ϵ_r), and/or (3) its effective time (τ_{eff}) of holdoff. Typically, there were tradeoffs between these three effects, e.g., something that improves E_{BD} causes a decrease in ϵ_r .

A matrix of Variables versus Effects was developed from the 13 journal articles to show these relationships (see Table 1). The numbers in the matrix relate to the references listed at the end of this dissertation. The variables that have been researched are pressure, additives (ethylene glycol and alcohol), electrode material, polarity, temperature, resistivity, distillation, diffusion electrodes, and electrode coatings. The respective effects of each of these variables will be summarized. More in-depth information can be found by reviewing the articles referenced in Table 1.

Abramyan and Kornilov [2] did considerable work looking at the effects of pressure on the voltage breakdown and the time to breakdown. They showed that an increase in the pressure from 1.7 MPa to 13.4 MPa increased E_{BD} from 360 kV/cm to 640 kV/cm, effectively doubling E_{BD} . Figure 1 shows the nearly linear relationship between the breakdown field and pressure. Over the range of pressures that were measured, the relationship between the E_{BD} and pressure was approximately 24 kV/(cm MPa). They also reported an increase in the time until breakdown ($\sim\tau_{\text{eff}}$) from 50 ns to 10 μs with an increase in pressure from 0.3 MPa to 10.1 MPa. According to Abramyan and Kornilov, this suggested a gaseous process occurring in the water during the breakdown.

Table 1. Matrix of Variables versus Effects in water breakdown research (numbers in table refer to reference numbers at the end of this thesis).

Variables / Effects	E_{BD}	ϵ_r	τ_{eff}
Pressure	2,3		2,3
Ethylene Glycol/Water	4	4	4
Alcohol/Water		5	
Same Electrode Material (anode and cathode)	6,7	8,9,10	
Different Electrode Material (anode and cathode)	6	10	
Polarity		10	11
Temperature	3	5,12,14	3,12
Resistivity (Conductivity)		12	12
Diffusion Electrodes	13		13
Electrode Coatings	7		

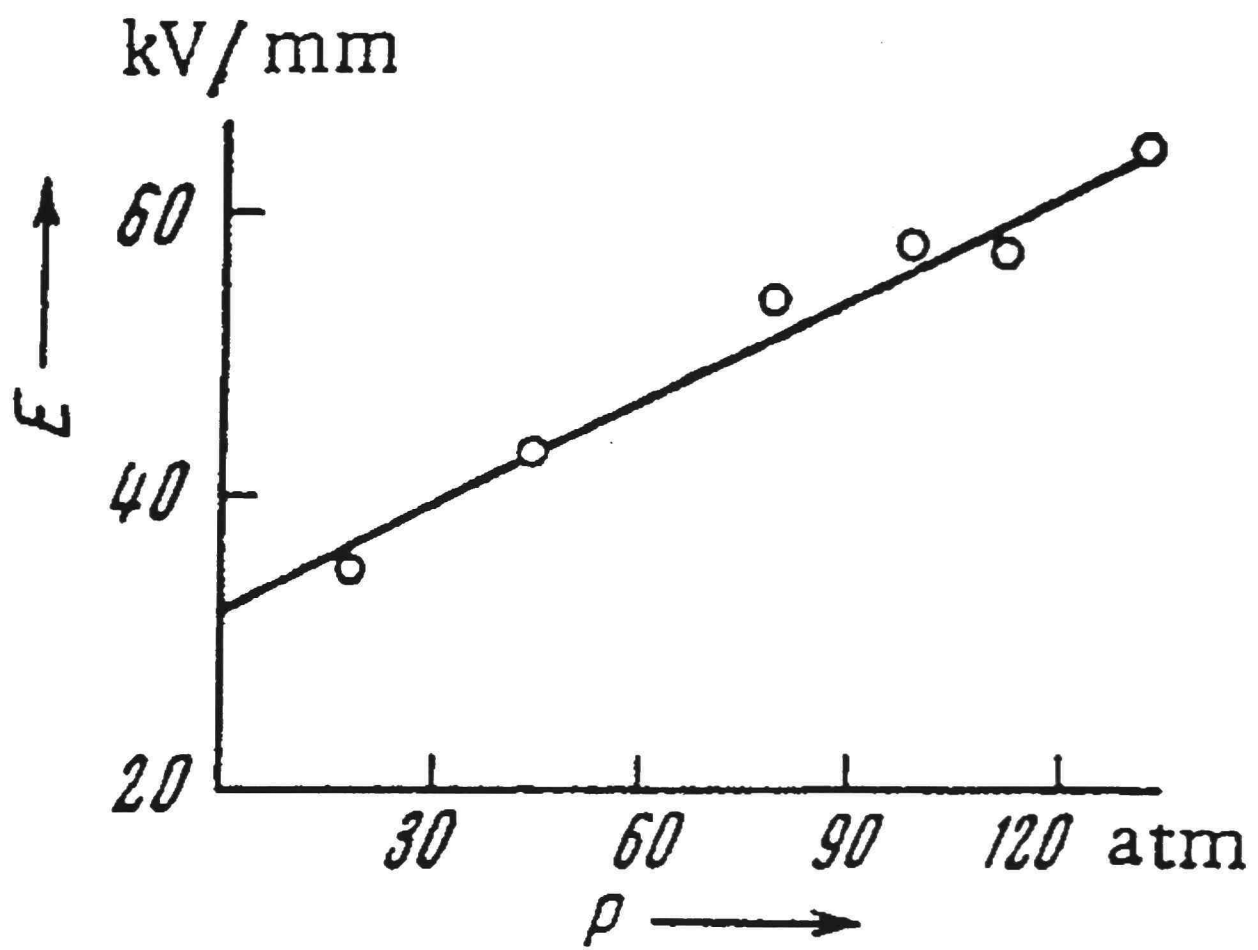


Figure 1. Relationship between pressure and electric breakdown strength of water [2].

Sincerny [3] looked at flow rate, temperature, resistivity, pressure, and percentage of deaeration on E_{BD} and τ_{eff} . He varied the water pressure from 101 kPa to 308 kPa with an increase of E_{BD} from 218 kV/cm to 236 kV/cm, and an increase in τ_{eff} from 2.9 μ s to 3.5 μ s. Even though he claims no effect due to temperature, a small effect was seen when three measurements were made at different temperatures: 8°C, 20°C, and 33°C. The electric breakdown field (E_{BD}) went from 220 kV/cm to 224 kV/cm, and τ_{eff} went from 2.9 μ s to 3.1 μ s as the temperature decreased.

Varying the deaeration level from 0% to 90% did not have any significant effect on the electrical breakdown level but did have an effect on the recovery time of the test cell. The level of deaeration affected the amount of time required to wait between shots to allow the bubbles that formed in the water to dissipate. Without deaeration, this typically took about an hour.

The flow rate of the water was varied between 126 ml/s and 630 ml/s with no significant effect seen on E_{BD} or τ_{eff} . He did observe a difference in the breakdown site on the electrode with a difference in flow rate. The breakdown region tended to be more localized when there was no flow as opposed to a more generalized breakdown region with the higher flow rate. This was attributed to the arc following the motion of the particles involved in the discharge as they are being swept across the surface of the electrode. The resistivity of the water was varied from 14 M Ω -cm to 37 M Ω -cm. There

was no significant effect on breakdown strength with the change of resistivity of the water.

Fenneman [4] looked at the effects of mixing ethylene glycol with the water on E_{BD} , ϵ_r , and τ_{eff} . With pure water at room temperature and no ethylene glycol, he measured E_{BD} at 130 kV/cm. With a 95% mixture of ethylene glycol at +28°C, E_{BD} went up to 270 kV/cm, effectively doubling the breakdown voltage. By varying the water/ethylene glycol mixture and the temperature, he was able to get an ϵ_r of 80 with a 60% mixture cooled to -30°C, and was able to get τ_{eff} up to 1 ms with an 80% mixture cooled to -10°C. Table 2 summarizes the data on the water and ethylene glycol investigation. By varying the amount of ethylene glycol added to the water and the temperature of the mixture, Fenneman was able to vary E_{BD} , ϵ_r , and τ_{eff} .

Noyel, Jorat, Derriche, and Huck [5] looked at the change in the dielectric constant with different mixtures of alcohol and supercooled water. The alcohols used were methanol, ethanol, propanediol 1-2, and propanetriol 1-2-3. They determined the relationship between temperature (T), molar fraction (x) of the alcohol, and static dielectric constant (ϵ_s) to be

$$\epsilon_{s,x} = A_x + \frac{B_x}{T} + \frac{C_x}{T^2}, \quad (1)$$

where A, B, and C are constants that were determined experimentally and varied with the molar fraction of the alcohol used. They showed that an

Table 2. Electrical breakdown strength properties of mixtures of ethylene glycol and water [4].

Mix (%)	T (C)	ϵ_r	τ_{eff} (ms)	E_{BD} (kV/cm)
0	0	88	0.25	130
40	25	67	0.10	160
40	-11	79	0.40	160
60	30	58	0.18	160
60	-23	77	0.97	140
80	25	49	0.45	210
80	-10	60	1.00	170
95	28	40	0.20	270

increase in alcohol decreased ϵ_s while a decrease in temperature increased ϵ_s (Figure 2). The highest value of ϵ_s was found to be 120 by using a 40% methanol molar fraction cooled to -100°C . They did not look at E_{BD} or τ_{eff} .

Zahn, Ohki, Rhoads, LaGasse, and Matsuzawa [6] looked at the E_{BD} of different types of electrodes. They found that stainless steel (SS) electrodes performed better than aluminum (Al) and were able to increase E_{BD} from 110 kV/cm (Al) to 125 kV/cm (SS). Overall, brass electrodes had the best holdoff with an E_{BD} of 145 kV/cm. Copper electrodes had the most consistent holdoff (least variation) with an average E_{BD} of 135 kV/cm. They also looked at using different materials for the anode and cathode. The most significant finding was that brass for the cathode and aluminum for the anode gave the worst holdoff with an E_{BD} of 90 kV/cm. Table 3 summarizes the data from this investigation.

These data were taken using parallel plane electrodes, 1 m x 3.2 cm, placed 1 cm apart. This may explain why the E_{BD} 's are lower than what is seen in other research. The larger is the surface area, the lower the E_{BD} . They did not look at ϵ_r or τ_{eff} .

Szklarczyk, Kainthla, and Bockris [7] compared platinum, copper, iron, nickel, gold, and cobalt electrodes. Figure 3 shows the current density-voltage (j - v) relationship for various types of electrodes with a 5 mm gap. The horizontal axis is the voltage (v) in volts and the vertical axis is the current density (j) in amps/cm². Shown in Figure 3, of the four materials

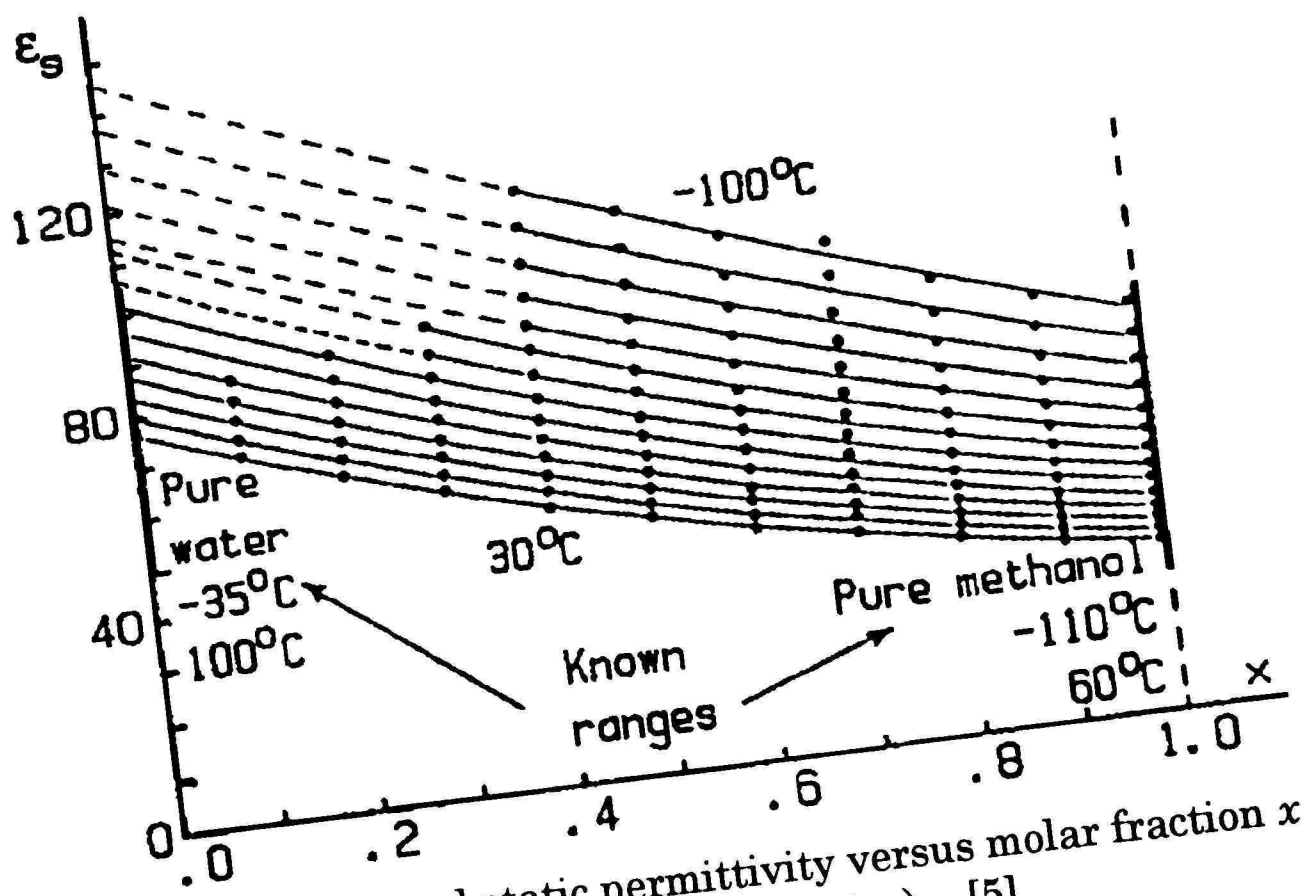


Figure 2. Isothermal static permittivity versus molar fraction x for mixtures $(\text{methanol})_x / (\text{water})_{1-x}$ [5].

Table 3. Summary of the data with a history of the highest applied voltages without breakdown [6].

Stainless Steel + / Stainless Steel - 110 kV/cm (12 times) 115 kV/cm (12 times) 120 kV/cm (4 times) 125 kV/cm (16 times)	Aluminum + / Aluminum - 110 kV/cm (29 times) 115 kV/cm (9 times) 120 kV/cm (2 times)
Brass + / Brass - 115 kV/cm (9 times) 125 kV/cm (10 times) 130 kV/cm (1 time) 145 kV/cm (2 times)	Copper + / Copper - 135 kV/cm (24 times)
Stainless Steel + / Aluminum - 125 kV/cm (4 times) 130 kV/cm (14 times) 140 kV/cm (2 times)	Aluminum + / Stainless Steel - 105 kV/cm (20 times) 110 kV/cm (1 time)
Brass + / Copper - 110 kV/cm (19 times) 115 kV/cm (8 times)	Copper + / Brass - 110 kV/cm (10 times) 115 kV/cm (8 times) 120 kV/cm (1 time)
Stainless Steel + / Brass - 115 kV/cm (20 times) 120 kV/cm (6 times)	Brass + / Stainless Steel - 125 kV/cm (19 times)
Stainless Steel + / Copper - 115 kV/cm (19 times) 125 kV/cm (2 times) 130 kV/cm (1 time)	Copper + / Stainless Steel - 110 kV/cm (19 times) 115 kV/cm (3 times)
Aluminum + / Brass - 90 kV/cm (19 times) 95 kV/cm (17 times)	Brass + / Aluminum - 125 kV/cm (22 times) 130 kV/cm (13 times) 135 kV/cm (2 times)
Aluminum + / Copper - 110 kV/cm (20 times)	Copper + / Aluminum - 100 kV/cm (19 times) 125 kV/cm (2 times)

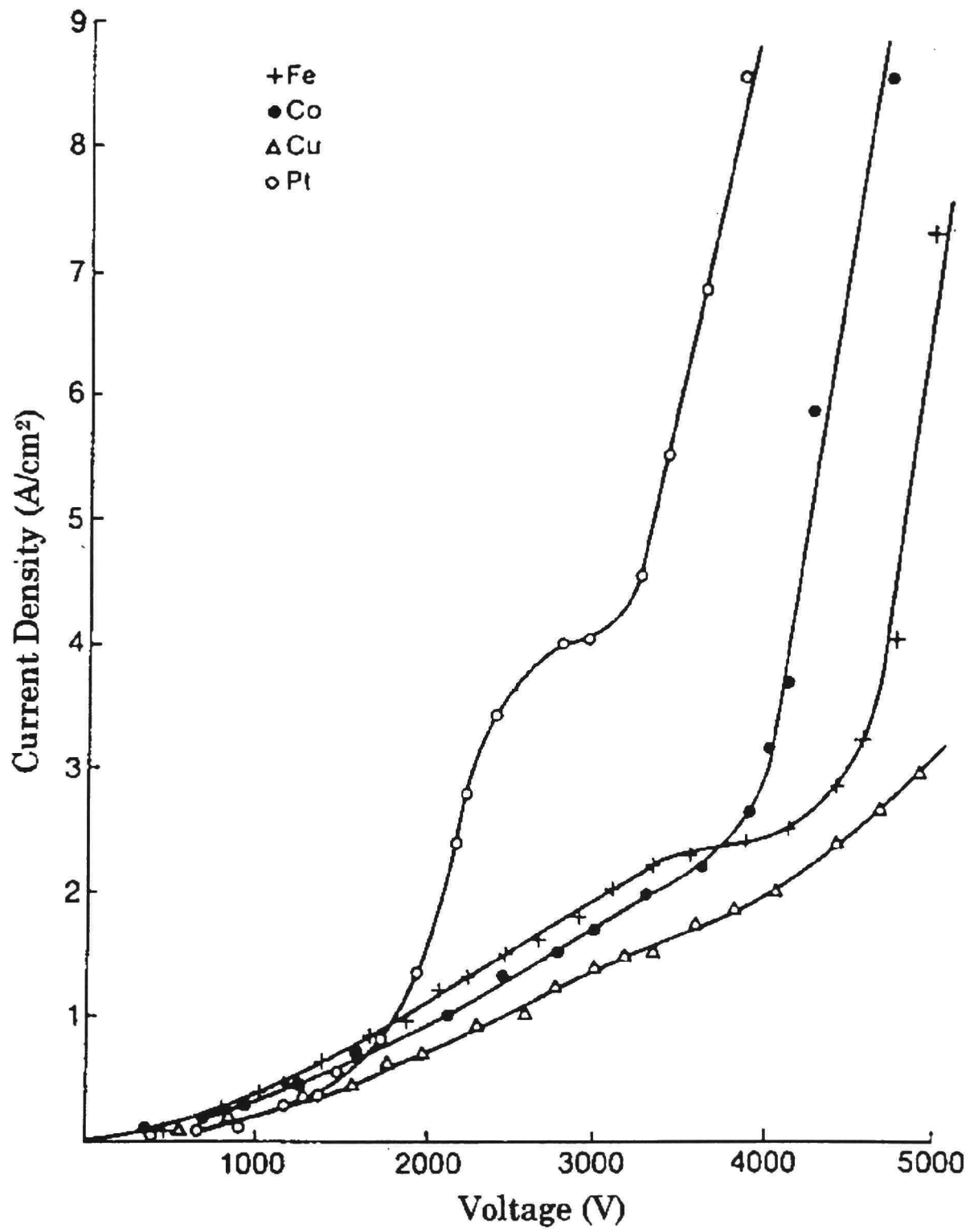


Figure 3. The j - v dependence for different cathode materials for the same spacing between the cathode and the anode [7].

used, copper (Cu) had the best response. Figure 4 describes the various portions of the j - v curve and what the mechanism was at various parts of the curve. The section of the curve at A is due to the electrode kinetics for H_2 and O_2 evolution in a low conductance solution. In this region, the current is limited by the solution resistance. The next portion of the curve (B) represents the dissociation of the water molecules. The electric field is high enough to cause the ionization and dissociation of the water. The next stage is the plateau region (C) where so much H_2 has built up on the electrode surface that the water will no longer be in contact with the electrode, surface thus preventing the increase of the current density. At the end of the plateau region (D), an intermittent glow discharge is seen. Region E represents the breakdown of the gap. Szklarczyk et al. suggest that at the breakdown point (D) the Fermi level of the electrons in the cathode is equal to the conduction band of the water. They also looked at gold (Au) and nickel (Ni) electrodes with the results shown in Figure 5. Comparing Figures 3 and 5 shows that Au performs much better than Cu, and Ni was the worst.

Szklarczyk et al. also looked at coatings of paraffin and black wax on the anode. Figure 6 shows the results of the black wax coating on the electrode. The black wax showed the best overall performance with an E_{BD} of about 60 kV/cm with a 0.5 mm thick film of black wax on a platinum electrode compared with only about 8 kV/cm without. No explanation was

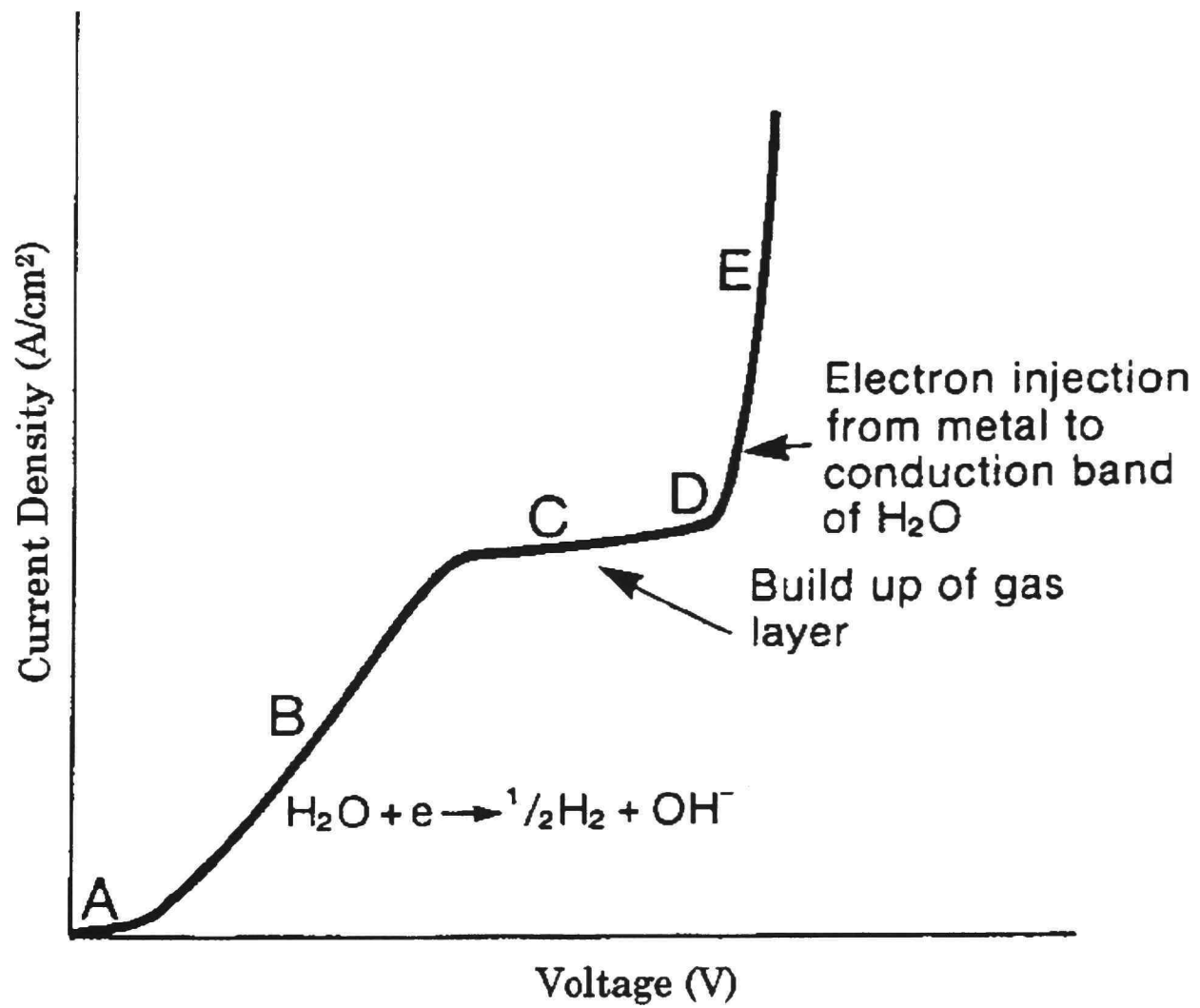


Figure 4. Schematic representation of the j - v curves obtained with different electrodes in pure water [7].

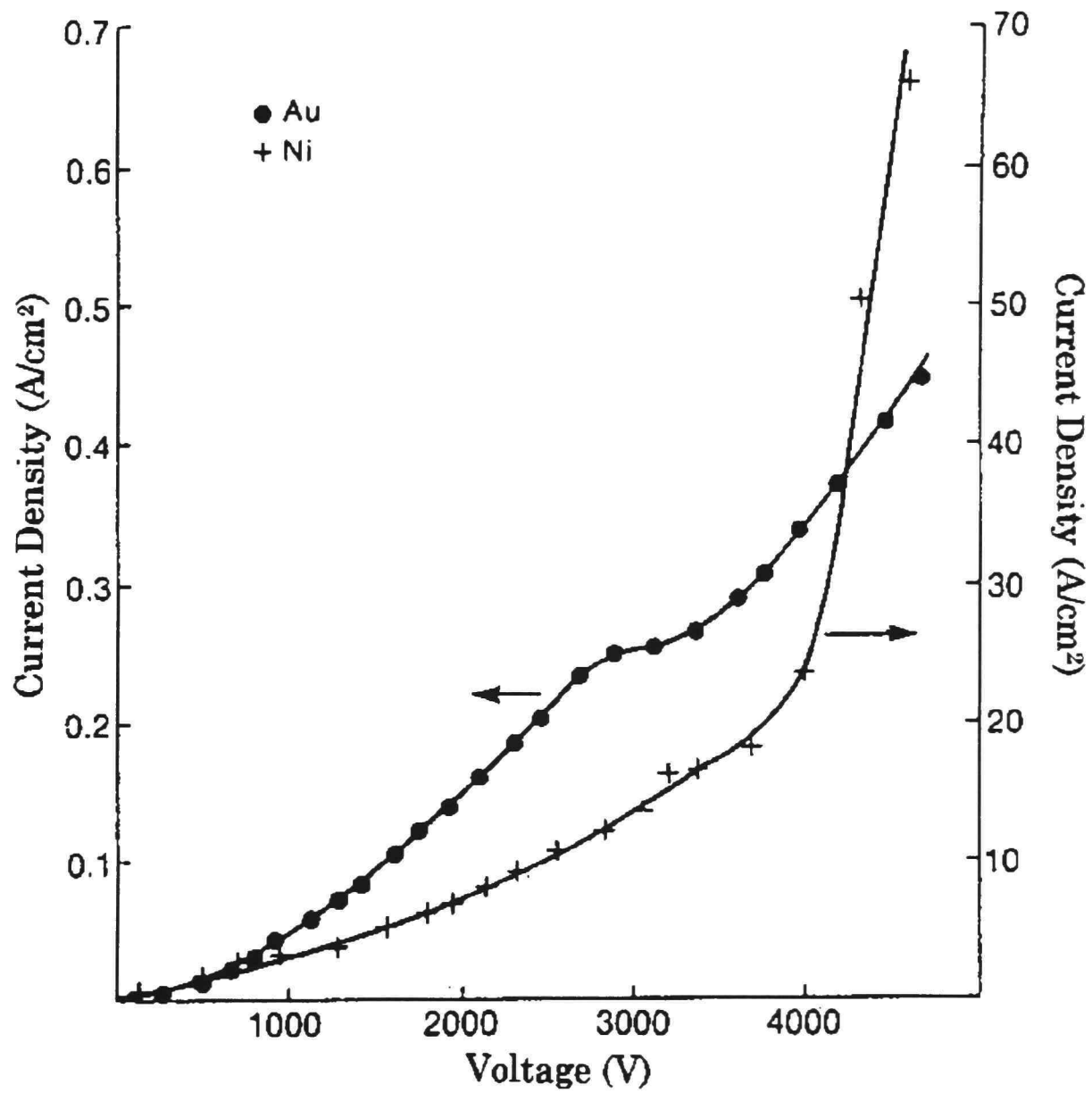


Figure 5. The j - v dependence for Au and Ni electrodes for the same spacing between the cathode and the anode [7].

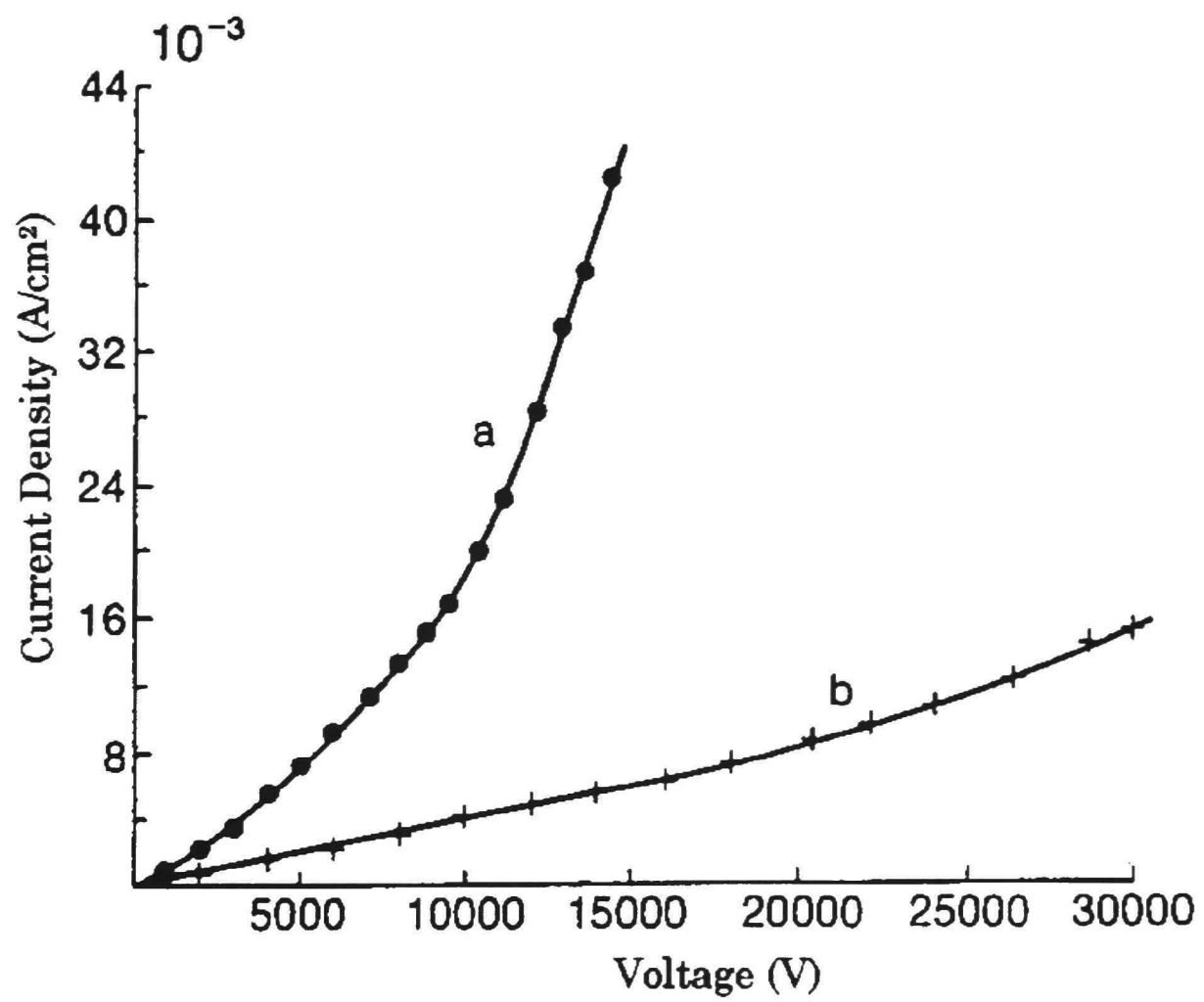


Figure 6. The j - v dependence for a platinum electrode covered with (a) 0.1 mm and (b) 0.5 mm thick film of black wax [7].

offered as to why the E_{BD} 's were low compared to other field strengths seen in similar research. The electrodes consisted of a 100 μm diameter planar tip platinum anode and a 0.6 cm diameter platinum cathode. The wax was placed on the anode. The small size of the electrodes and gap may explain the low breakdown values.

Fenneman [8] looked at the performance of copper (Cu), steel (SS), brass, and aluminum (Al) electrodes. Using J. C. Martin's relationship, Fenneman measured the value of M from Martin's equation (see Appendix A)

$$E_{\max} \tau_{\text{eff}}^{1/3} = \frac{M}{A^{1/10}}, \quad (2)$$

as a measure of the performance of the different electrodes where E_{\max} was the maximum electric field in MV/cm, τ_{eff} was the effective time in μs , A was the electrode area in cm^2 , and M was a value usually between 0.3 and 0.6. Figure 7 shows the values of M over a sequence of 200 shots for each of the different electrode materials. Fenneman averaged each set of 20 shots ($\langle M \rangle_{20}$) for the plot in Figure 7. The most significant result was the poor performance of Al to withstand repeated breakdowns.

Gehman [9] examined various electrode materials and measured their action density (AD) which is a figure of merit defined as the energy density multiplied by the effective time (τ_{eff}). Figure 8 shows the AD for Al, anodized Al, brass, and Cu. Of these four electrode types, the anodized Al had the best performance. Also shown in Figure 8 for the various electrode types are the

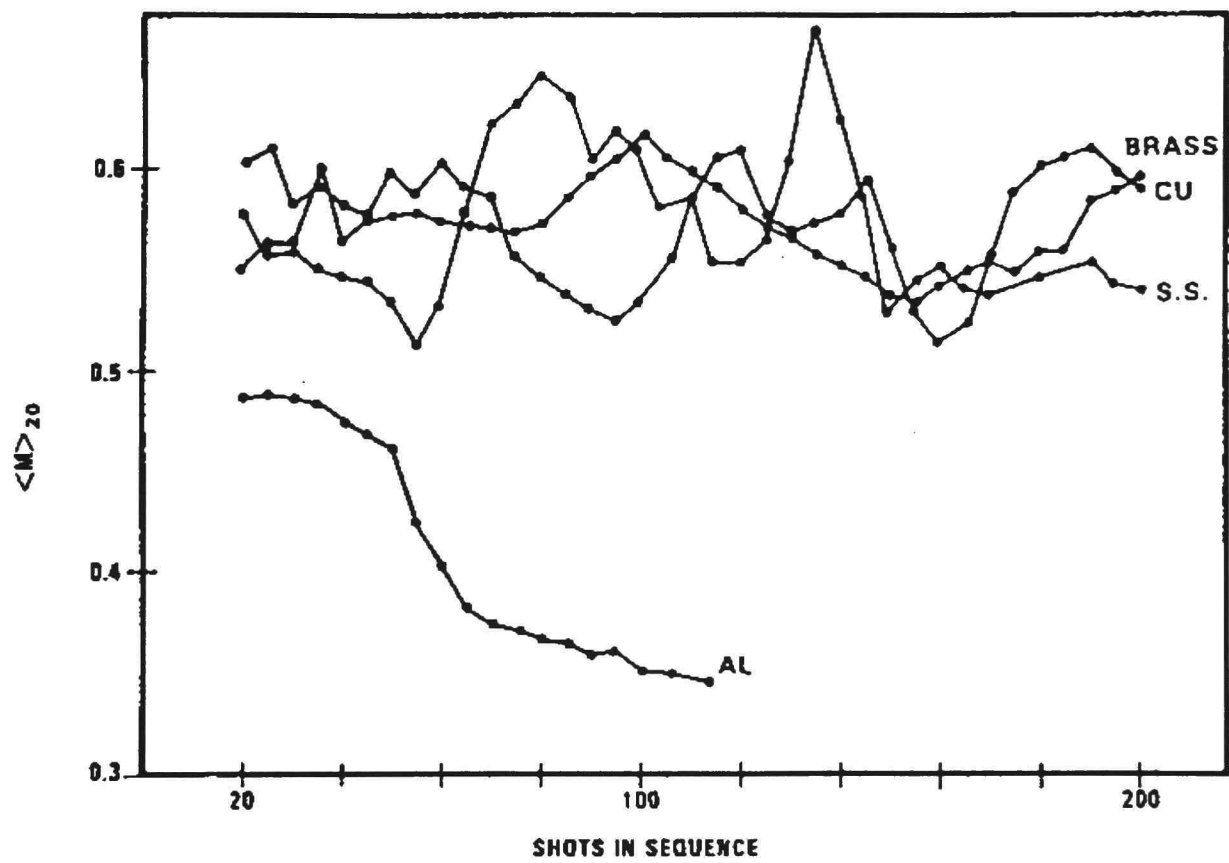


Figure 7. The value of $\langle M \rangle_{20}$ as a function of the shot sequence number [8].

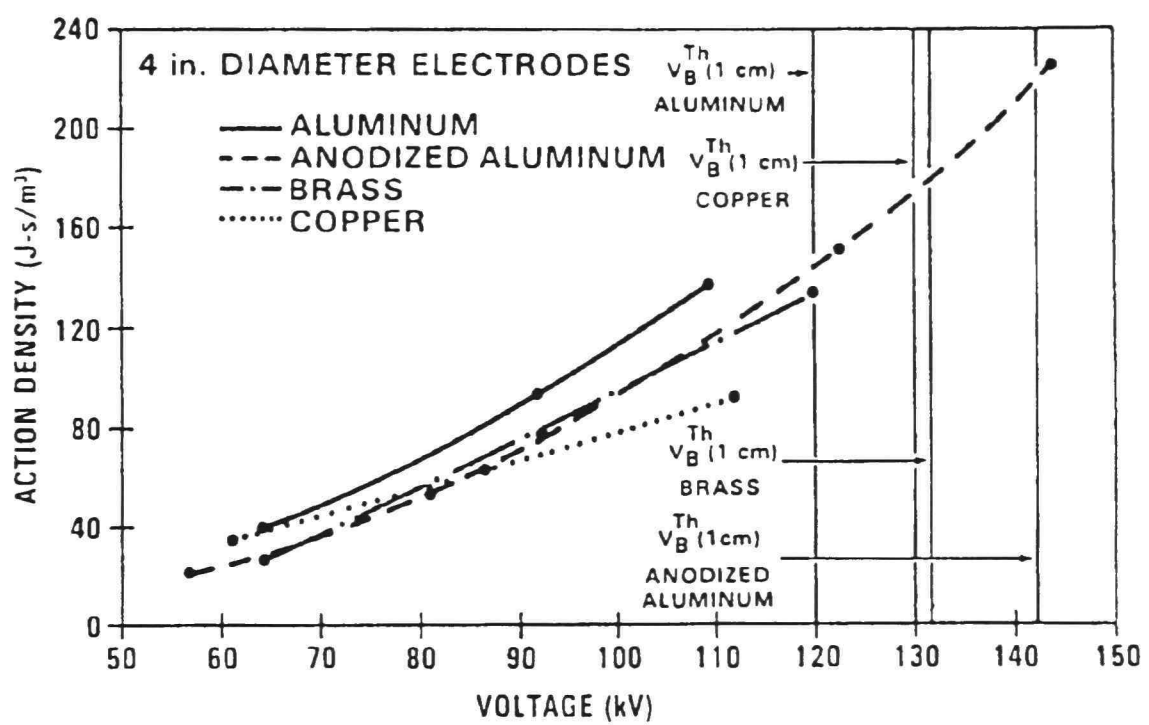


Figure 8. Action density as a function of applied voltage for various electrode materials. The threshold breakdown voltages (V_{th}) are included [9].

threshold breakdown strengths (V_B^{TH}) which were calculated by dividing the maximum voltage before the onset of breakdown by the electrode spacing. Figure 9 shows the AD for SS for various configurations of bead blasted and electropolished passivated electrodes. Passivation forms a contiguous layer of chromic oxide across the surface of the steel to prevent metal ions from contaminating the water. To do this, the electrodes were dipped into a solution of nitric acid and potassium dichromate which was heated to 43.3°C. If both electrodes had the same surface preparation, the data points are labeled either with “BB” or “EP” for bead blasted or electropolished passivated, respectively. For the trials run with a mix of surface treatment, the data points are labeled “EP(+), BB(-)” for an electropolished passivated anode and a bead blasted cathode, and “BB(+), EP(-)” for a bead blasted anode and an electropolished passivated cathode. The electropolished SS had the best performance. Comparing Figure 9 with Figure 8, the SS had overall better performance than the other materials.

McLeod and Gehman [10] looked at several different types of SS and Al electrodes, and compared their voltage holdoff capability. There were four SS electrodes: #304, #310, #316, #430, and four Al electrodes: #7075, #5083, #2024, #6061. The best performance was achieved with #430 SS and #6061 Al which both showed an average breakdown strength of 170 kV/cm. By using mixed electrodes of #304 SS and #2024 Al, he showed that with +SS

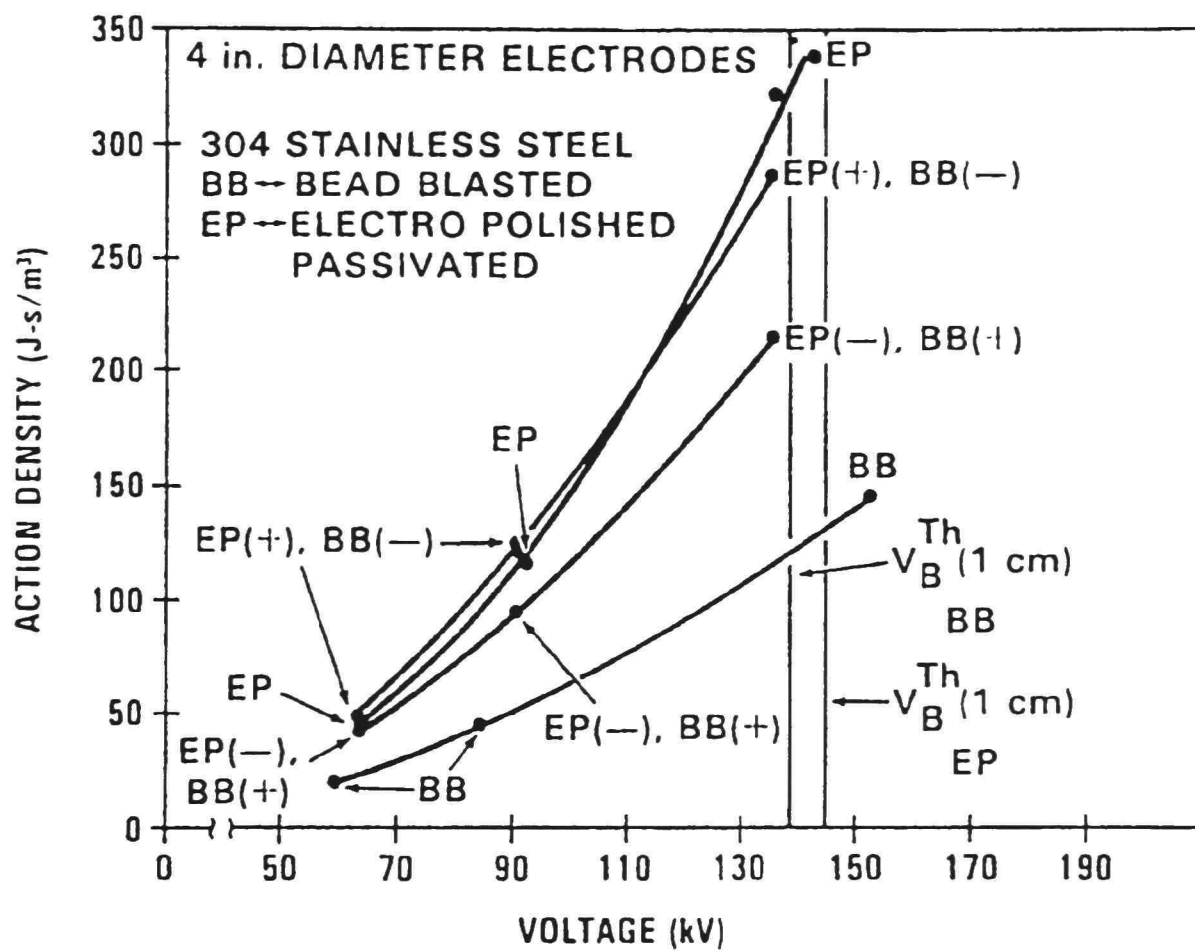


Figure 9. Action density as a function of applied voltage for #304 stainless steel. The threshold breakdown voltages (V_{th}) are included [9].

and $-Al$, E_{BD} was 145 kV/cm; with $-SS$ and $+Al$, E_{BD} was 100 kV/cm; but after the electrodes stayed in the water for 23 days, E_{BD} was about the same for both polarities. The authors state the reason for this is “related to the theoretical modeling of the breakdown initiation process” (p. 59).

Kuzhekin [11] looked at the effects that the polarity and the type of electrode had on voltage breakdown and the time to breakdown (τ). He used a rod electrode 0.8 cm in diameter and a plane electrode which was SS, 25 cm in diameter. Kuzhekin demonstrated a polarity effect at 95 kV/cm using a $+rod$ and $-plane$, τ was 0.5 μs ; with $-rod$ and $+plane$, τ was 20 μs ; which increased τ by a factor of 40. This shows the importance of the polarity of the machine if the electrodes are non-symmetrical.

Buttram and O'Malley [12] showed that the water temperature affected both the resistivity and the dielectric constant of the water. By purifying the water to its intrinsic resistivity level, $\rho = 18 M\Omega\text{-cm}$ (room temperature), and then chilling the water to near freezing, $T \approx 0^\circ C$, they could get the water up to its theoretical maximum resistivity of 80 $M\Omega\text{-cm}$. Using water at its maximum resistivity, they were able to get an ϵ_r of 90 and τ_{eff} of 640 μs .

Vorov'ev, Kapitonov, and Kruglyakov [13] used “diffusion” electrodes made up of cupric sulfate ($CuSO_4$) adjacent to the upper electrode, which was the anode, and iron chloride ($FeCl_3$) adjacent to the lower electrode. The different solutions were used to keep the diffusion layer close to the surface

of the electrode by the difference in densities between the water and the two solutions. The electrodes were SS with 2 μm to 5 μm pores for introducing the solutions into the experimental chamber. They were able to show an increase in E_{BD} from 0.3 MV/cm to 1.3 MV/cm by using the diffusion electrodes. This was for pulse lengths of less than 3 μs ; above 3 μs , the diffusion electrodes did not perform as well.

Hasted [14] looked at much of the research done on the static dielectric constant (ϵ_s) of water and showed that there was a very complicated relationship between water temperature and ϵ_s . Figure 10 shows a comparison of findings by eight different sets of research. These were plots of the differences between Malmberg and Maryott's [15] equation for ϵ_s which was given by

$$\log(\epsilon_{\text{SMM}}) = 1.94404 - \frac{1.991 \cdot 10^{-3}}{T}, \quad (3)$$

and the actual data. Figure 10 shows that there was a lot of variation between the different sets of data.

Prebreakdown phenomena

Many theories have been proposed in an attempt to describe what is occurring in the water during the breakdown. It is important to understand the phenomena that lead to the breakdown so that ways can be devised to delay or prevent the breakdown. Probably the most extensive investigation

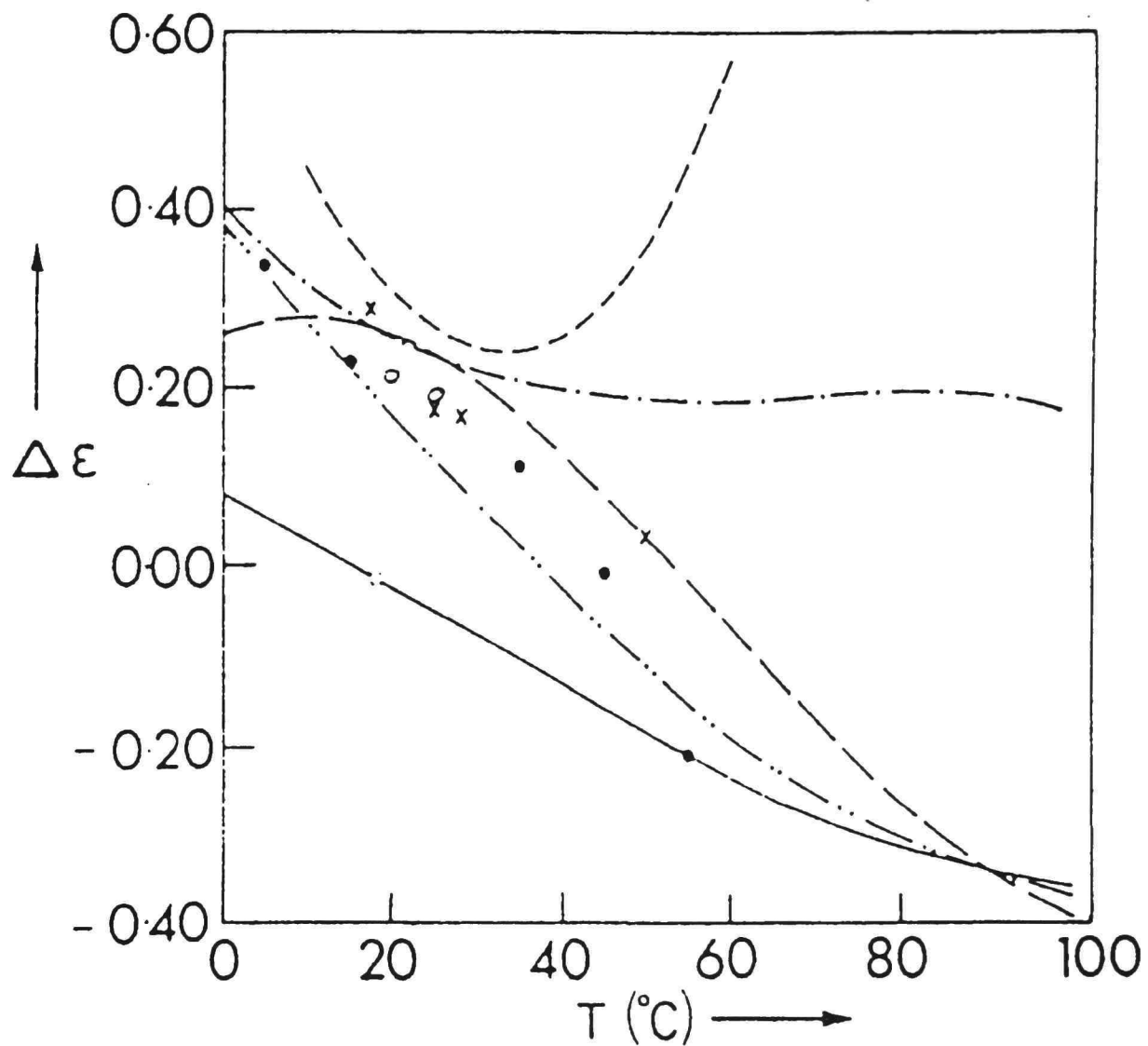


Figure 10. Differences between measurements of ϵ_s as a function of temperature; $\Delta\epsilon = \epsilon_s - \epsilon_{SMM}$ (Malmberg and Maryott) [14]. \square mean of 17 values selected from literature by Lattey et al.; \times Albright; \dashrightarrow Wyman and Ingalls; --- Lattey et al.; \circ Jones and Davies; \bullet Albright and Gosting; --- Drake et al.; -- -- Wyman; --- Akerlof and Oshry.

of the prebreakdown phenomena has been conducted by the Academy of Sciences of the USSR, Scientific-Research Institute of Energetics, Novosibirsk, USSR. Their development and use of the electrooptical bridge made it possible to study the effects of a high voltage pulse on the water between the electrodes [15].

Yanshin, Ovchinnikov, and Vershinin [16] describe the primary mechanism of charge transport through the water gap as proton motion, similar to "hole" motion in semiconductors. Figure 11 shows how this motion occurs. The water molecule (H_2O) is pictured on the right as it would be oriented in an electric field in the direction shown on the top of the figure. On the left side of the figure, an H^+ ion is shown combining with an H_2O molecule to form a hydronium ion (H_3O^+). According to the authors,

when a voltage is applied across the discharge gap, electron vacancies appear on the anode with a surface charge density $\sigma = \epsilon_0 \epsilon_r E$. The appearance of vacancies is accompanied by an adiabatic or nonadiabatic transition of electrons from nearby water molecules to these vacancies; hydronium ions form. The subsequent motion of charge carriers occurs by the mechanism described above, which converts electric-field energy into thermal energy. (pp. 1305-1306)

This thermal energy causes the water to "boil" causing bubble formation.

In a later article, Yanshin, Yanshin, and Korobeynikov [17] concluded that the bubble formation in the water was due to gas released from micropores on the electrode surface by a mechanism similar to cavitation. They used the Kerr effect in nitrobenzene to study the

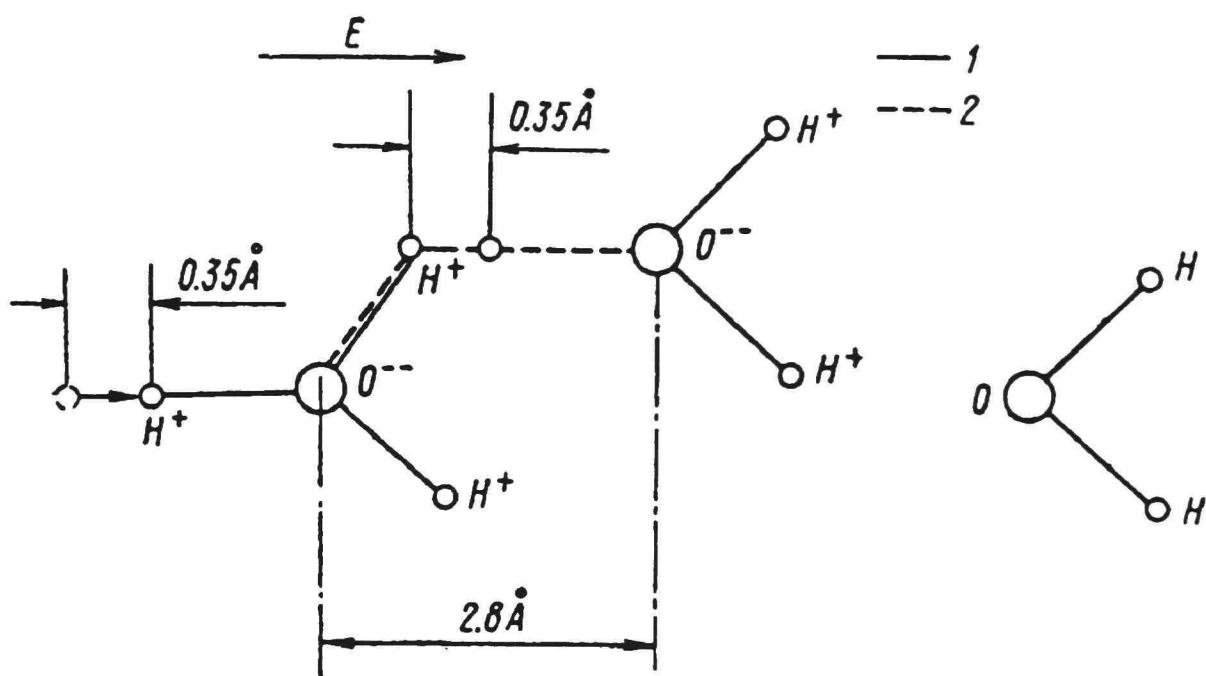


Figure 11. Proton mobility mechanism in water.
 (1) Displacement of a proton and (2) displacement of an electron [16].

prebreakdown fields because of its high Kerr constants. A 50 kV to 150 kV pulse was applied to the test gap that contained a 0.1 mm to 0.3 mm stainless steel electrode and a plane electrode. Field strengths in the gap were between 500 kV/cm and 1 MV/cm. They looked at the formation of space charges and bubbles in the electrode gap. Their conclusion based on the results of the experiment was that the bubbles appeared as a result of gases being released from micropores on the electrode surface due to Coulomb forces and electro-hydrodynamic (EHD) flow.

Ovchinnikov, Yanshin, and Yanshin [18] were able to show through the use of the Kerr effect and a streak camera that there was not a space charge buildup around the cathode even with fields up to 10 MV/cm. They interpret this to mean that the electron mobility in the water is very low and that the electrons are bound to the water molecules even under high electric fields. The electron velocity in water was estimated to be less than 1.5×10^5 cm/sec with a field of 10 MV/cm. This gives an electron mobility of less than 1.5×10^{-2} cm²/Vsec. This supports the contention by Yanshin et al. [16] that it is proton motion that carries the charges across the water gap.

The development of a new technology that creates conductive layers in the liquid near the electrode was recently claimed by E. V. Yanshin at the Pulsed Power Conference [19]. This technology supposedly builds on the findings generated by the diffusion electrode experiments and provides a practical means of quadrupling the breakdown field strength. No

explanation was given as to what this new technology is and how it works.

Whatever the conductive layer is made of, it does not diffuse into the water and can be used in any configuration since it is not dependent on gravity to hold it in place as was needed with the diffusion electrodes.

CHAPTER III

EXPERIMENTAL SETUP AND MODELS

System description

Overview

Figure 12 shows a simple diagram of the components that make up the pulsed power system. It consists of a Marx bank, a coaxial line, and the test chamber. The system also includes a control panel, power supply, screen room, and diagnostics. Each of these components will be described in detail in the following sections.

Marx bank

The Marx bank consisted of six Maxwell Model 31334 capacitors which were rated at 0.1 μF , 100 kV, and 20 nH; these were later replaced with Model 31885 capacitors which were rated at the same capacitance but only 75 kV and 40 nH. The total capacitance of the erected Marx bank was the series capacitance of the capacitors which would simply be

$$C = \frac{0.1 \mu\text{F}}{6} = 16.6 \text{ nF}. \quad (4)$$

The inductance of the bank was the series inductance of the capacitors and the inductance of the connections between the bank and the center coaxial line. The inductance of the Marx bank connections was estimated by

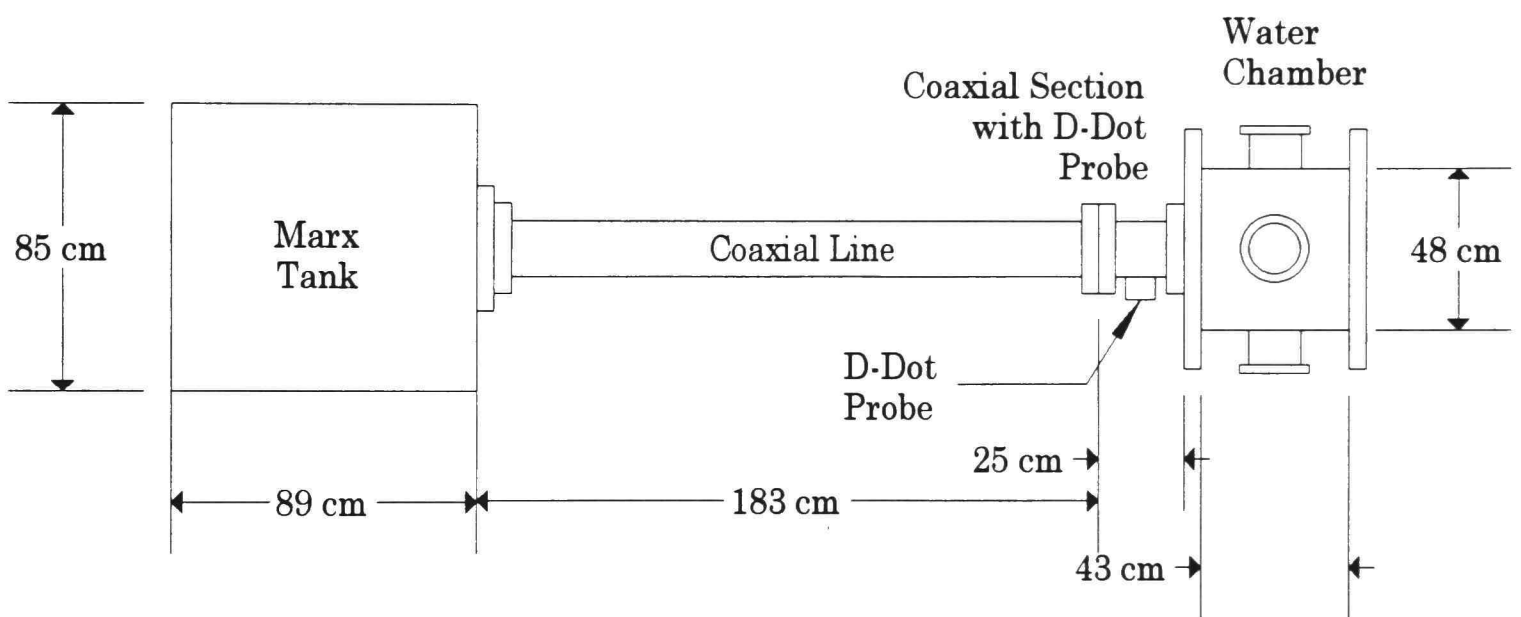


Figure 12. High voltage breakdown in water system diagram, side view.

modeling them as a rectangle of rectangular wire. Terman [20] gives the following equation for a rectangle that has sides that are S_1 by S_2 and is made up of a rectangular bar that is b by c ,

$$L = 0.02339 \left[(S_1 + S_2) \log \left(\frac{2S_1 S_2}{b + c} \right) - S_1 \log(S_1 + g) - S_2 \log(S_2 + g) \right] + 0.01016 \left[2g - \frac{S_1 + S_2}{2} + 0.447(b + c) \right] \mu\text{H}, \quad (5)$$

where g is the diagonal distance in the rectangle formed by S_1 and S_2 . All distances are in inches. For S_1 equal to 12 inches (30.48 cm); S_2 , 22 inches (55.88 cm); b , 1/16 inch (0.16 cm); and c , 1 inch (2.54 cm), the inductance of the Marx bank connectors is 1.185 μH . The capacitors used were rated at 20 nH each, so the total inductance would be 1.305 μH . The impedance of the Marx bank would be

$$Z = \sqrt{\frac{L}{C}} = 8.9 \Omega. \quad (6)$$

This produced a very low impedance Marx bank.

The capacitors are charged to 66 kV to give an erected voltage of about 400 kV. The capacitors are linked together with Physics International Model 670 air pressure spark gaps which are rated at 100 kV at 415 kPa air pressure. The pressure in the spark gaps is set at about 345 kPa with the pressure in the last sparkgap set to 415 kPa. This helps reduce the prebreakdown current in the coaxial line.

The charging resistors are water resistors made from 1.9 cm diameter polyvinyl tubing with 1.9 cm copper end caps. Electrical connectors are soldered to the flat portion of the end caps. The tubing that makes up the body of the resistors is about 9 cm long and the end caps are forced into the end of the tubing. The resistors are filled with 0.008 grams/liter of CuSO_4 . The CuSO_4 is mixed with purified water in order to increase the resistivity of the mixture.

The switches and resistors are attached to the capacitors by copper plates, the same as those described by Coulter [21]. These had to be modified when the new capacitors were used because the capacitor cases were wider and the mounting hardware would not allow the switches to fit properly. The bank is assembled on a fiberglass frame and is made up of a row of three capacitors on the bottom of the frame and another row above them. Because of the size of the Marx tank, the Marx bank could not be assembled with six capacitors in one row. This configuration caused some erection problems and some changes had to be made to the Marx bank.

If there is not enough stray capacitance around the Marx bank, then the bank will not erect properly. To estimate the stray capacitance, it is possible to treat the sides of the capacitor and the side of the Marx tank as a parallel plate capacitor. The following equation can be used to calculate the value of the capacitance around one of the Marx bank capacitors

$$C_s = \epsilon_r \epsilon_o \left(\frac{A_1}{d_1} + \frac{A_2}{d_2} + \frac{A_3}{d_3} + \frac{A_4}{d_4} \right), \quad (7)$$

where A is the area of the side of the capacitor and d is the distance from the capacitor and the side of the Marx tank. To adjust for electric field fringes, one-fourth of the distance from the capacitor and the Marx tank is added to each dimension of the area term. For example, for A_1 , the area would be

$$A_1 = \left(w + \frac{d_1}{4} \right) \left(l + \frac{d_1}{4} \right), \quad (8)$$

where w is the width of the capacitor and l is the length of the capacitor. For the capacitors used, w was 15.24 cm, l was 71.12 cm, and t (thickness) was 6.35 cm. The distances from the capacitor to the surrounding structures were 24.13 cm, 7.62 cm, 1.91 cm, and 15.24 cm for d_1 , d_2 , d_3 , and d_4 , respectively. Using these values gives a stray capacitance of about 150 pF.

To increase the stray capacitance, ground planes were added above and below each row of capacitors. These consisted of 15 cm x 37 cm copper plates that are connected together by grounding straps and are insulated from the capacitors by 0.6 cm plastic sheets on the bottom row of capacitors and 1.2 cm plastic sheets on the top row of capacitors. The grounding plates on the top row were later removed because of arcing between the capacitors and the ground plates. The ground plates were added to increase the amount of stray capacitance the bank sees. For proper erection, the time it takes for the capacitor to discharge through the charging resistors must be longer than

the time it takes for the arc to form in the sparkgap [22]. This time is given by

$$t_{dc} = \frac{1}{2}RC_s , \quad (9)$$

where t_{dc} is the discharge time, R is the resistance of the charging resistors, and C_s is the stray capacitance. The discharge time is one-half the RC time constant because there are two resistors in parallel with the capacitor when the Marx bank is erected. Normally, the sides of a Marx tank are close enough to the Marx bank to ensure sufficient stray capacitance but the way the bank was positioned in the tank, the capacitors were a considerable distance from the sides of the tank. Adding the grounding planes improved the performance of the Marx bank. Also, to ensure sufficient capacitance on the second stage, a booster capacitor was added to the ground side of the sparkgap switch. This consists of four 2700 pF, 40 kV, capacitors connected in series with 2 cm corona balls. This gives a calculated capacitance of 675 pF added to the second stage between the electrode and ground. This greatly improved the performance of the bank and when it was removed, because one of the 2700 pF capacitors broke, the Marx bank started having erection problems again. Putting the booster capacitor back on solved the problem. The bank was fired over 500 times in this configuration before it was removed for maintenance.

Another addition to the Marx bank was a sparkgap trigger. This is used to trigger the first switch of the bank. Several attempts at a trigger generator were made before a successful design was found. Because of grounding problems, which burned up the first two triggers, an air pressure controlled switch was opted for. This consists of a BIMBA Model 041-D air pressure cylinder connected to a Ross Engineering HV Relay Model E-DTA-30-2, 7.6 cm, high-voltage switch. Figure 13 shows the connections for the air lines. The electric solenoid was removed from the HV switch and the BIMBA air pressure cylinder was attached to the end of the fiberglass rod.

The switch was placed into a Lexan cylinder 46 cm long with 1.3 cm Lexan end plates. The connections to the air valve and the HV switch are made through the top end plate. The whole assembly is pressured with 140 kPa of air to prevent breakdown between the ends of the switch during charging; the air pressure is controlled by a C. A. Norgren Co., R07-200-RNKA pressure regulator. Figure 14 shows the electrical connections to the HV switch. In the open position, the trigger capacitors, which are two Maxwell Model 31247, 0.02 μ F, 50 kV capacitors connected in series, are charged by the main power supply. When the switch is closed, the connection between the capacitors and the trigger pin in the first sparkgap switch is closed. This provides 66 kV between the end of the trigger point and the ground electrode in the first switch. The trigger point is approximately 0.6 cm from the edge of the electrode which gives it a 110 kV/cm field

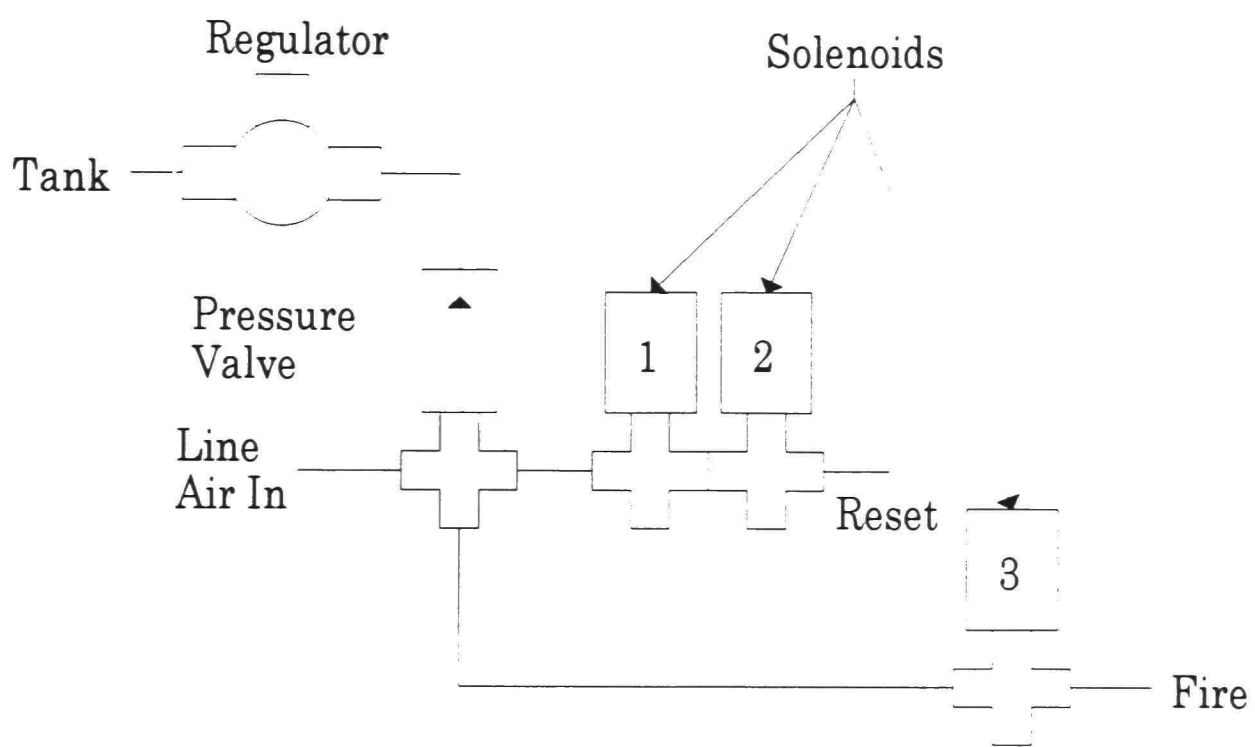


Figure 13. Air line diagram for trigger switch.

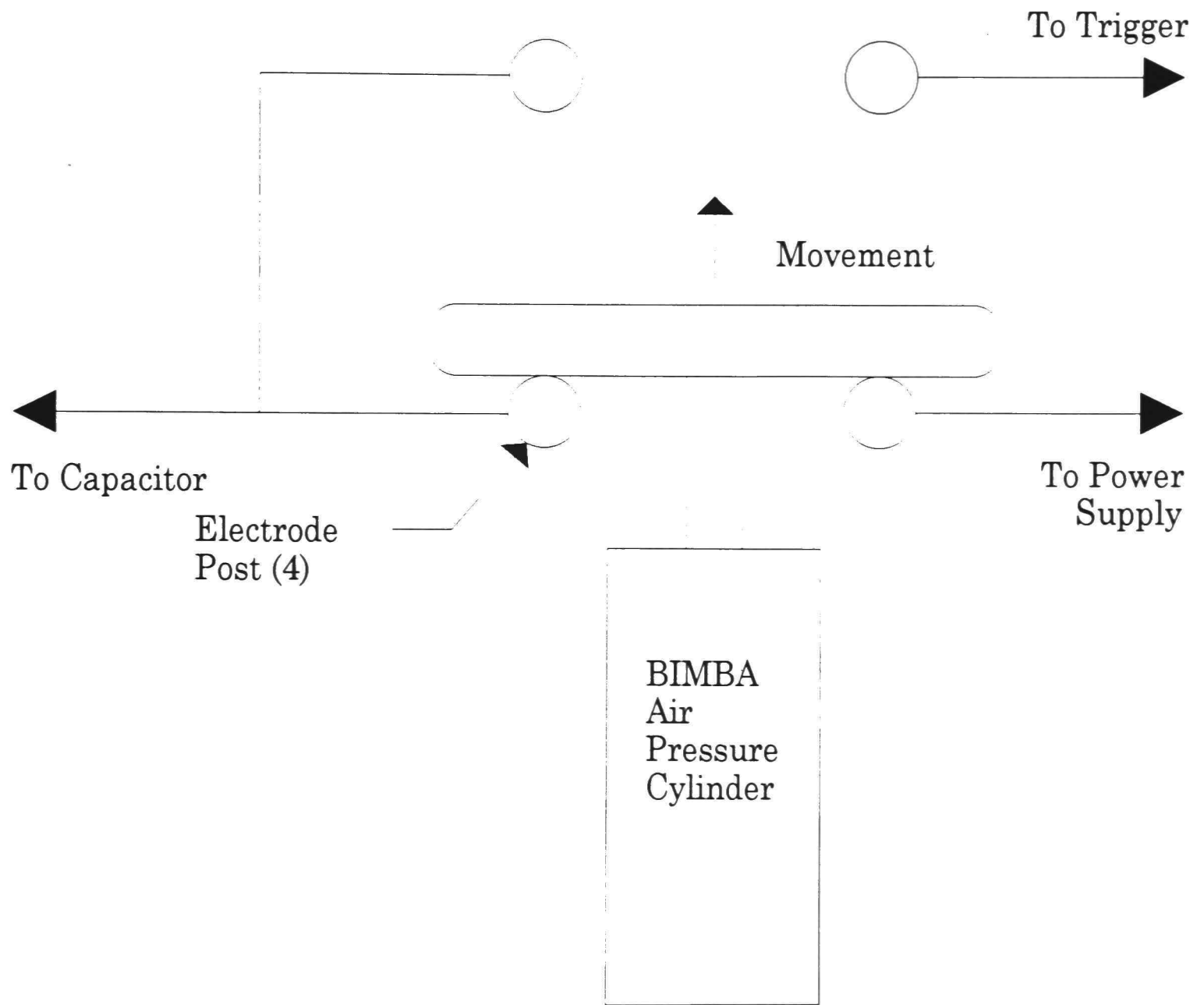


Figure 14. Trigger switch electrical connections.

between the two points which is more than enough field strength to initiate a breakdown in the sparkgap switch.

The air pressure for the air cylinder comes from the same line as that used in the spark gaps. This is typically at 550 kPa and is routed to and from the trigger switch through ASCO 104R General Purpose Valves. There was a 50 ms time delay measured between the signal from the firing switch to the actual closing of the trigger switch, so that signal could not be used to initiate the trace on the oscilloscope.

Coaxial line

The coaxial line consists of an aluminum outer electrode which has an inside diameter of 16.4 cm and a stainless steel center electrode which is 2.3 cm in diameter. The distance from the Marx tank to the test chamber is 208 cm. The coaxial line is filled with transformer oil which is circulated continuously through the coaxial line and the Marx tank. A water-lock filter is used to remove any moisture that was present in the oil and also removed any contaminants, including carbonization caused by occasional arcs in the Marx tank usually seen around the booster capacitor and the bottom of the tank.

The capacitance and inductance of the line is needed in order to calculate the impedance of the coaxial line. The capacitance of the coaxial line is given by the equation

$$C = \frac{2\pi\epsilon_r\epsilon_0 l}{\ln\left(\frac{b}{a}\right)} = 130 \text{ pF}, \quad (10)$$

where ϵ_r is equal to 2.2 for transformer oil, ϵ_0 is the permittivity of free space, a is the radius of the inner conductor, b is the inner radius of the outer conductor, and l is the length of the coaxial line. The inductance is given by the equation

$$L = \frac{\mu_0 l}{2\pi} \cdot \ln\left(\frac{b}{a}\right) = 817 \text{ nH}, \quad (11)$$

where μ_0 is the permeability of free space. Then the impedance of the coaxial line is

$$Z = \sqrt{\frac{L}{C}} = 79 \text{ } \Omega. \quad (12)$$

We also needed to know the one-way transit time in the coaxial line. This can be calculated by

$$t = \frac{l\sqrt{\epsilon_r}}{c} = 10.3 \text{ ns}, \quad (13)$$

where c is the speed of light in free space. This gives us an estimate of the delay between the erection of the Marx bank and the voltage at the D-Dot probe located at the end of the coaxial line.

Previous work by Coulter looked at ways to increase the operating voltage of the system but these were not successful. The limiting factor on

the maximum voltage of the system was the coaxial line. The maximum voltage of a coaxial line is given by the equation [23]

$$V_{\max} = aE_{\max} \ln\left(\frac{b}{a}\right), \quad (14)$$

where a is the radius of the inner conductor, and b is the radius of the outer conductor. For the values listed above with E_{\max} of 200 kV/cm (nominal value for transformer oil), then $V_{\max} = 450$ kV. In order to prevent a breakdown in the coaxial line, the Marx bank was charged to 66 kV in order to have an erected voltage of about 400 kV.

Experimental Chamber

The test chamber is a cylinder with a 48 cm inside diameter and 43 cm in length. The end plates were made from 5 cm thick Lexan. There are six ports evenly spaced around the chamber. The tank is filled with deionized water which is continuously circulated through two deionizing bottles at about 3.8 l/min. This provides water with a resistivity of over 10 M Ω -cm measured with a Myron L Series 570 Resistivity Meter. The circulation clears away any contaminants from the test chamber. The water was initially filtered through two U. S. Filter, poly string wound, 5 μ m cartridge filters and put into a storage tank before pumping it through the deionizer bottles and into the test chamber. This method removes only particulate matter from the water, not organic contaminants such as solvents. Air

bubbles are removed from the water by the difference in pressure between the experimental chamber and the storage tank due to the weight of the water; this is not the same as deaeration.

As with the coaxial line, the impedance of the experimental chamber is calculated by treating the chamber as a coaxial line. The capacitance is given by the equation

$$C = \frac{2\pi\epsilon_r\epsilon_0 l}{\ln\left(\frac{b}{a}\right)} = 630 \text{ pF}, \quad (15)$$

where ϵ_r is equal to 80 for the water, ϵ_0 is the permittivity of free space, a is the radius of the inner conductor, b is the radius of the outer conductor, and l is the length of the water chamber. The inductance is given by the equation

$$L = \frac{\mu_0 l}{2\pi} \cdot \ln\left(\frac{b}{a}\right) = 261 \text{ nH}, \quad (16)$$

where μ_0 is the permeability of free space. Then the impedance of the coaxial line is

$$Z = \sqrt{\frac{L}{C}} = 20 \text{ } \Omega. \quad (17)$$

The one-way transit time to the center of the water gap ($l/2$) is calculated to be

$$t = \frac{l\sqrt{\epsilon_r}}{c} = 6.4 \text{ ns}, \quad (18)$$

where c is the speed of light in free space. This is also the transit time from the gap to the load resistor since the gap is centered in the chamber.

The electrodes in the experimental chamber consist of two copper-tungsten rods 2.3 cm in diameter with a 7.6 cm radius of curvature on the electrode surface. The edge of the electrode surface is rounded to reduce field enhancements. For most of the data collected, the gap was set at 1.27 cm. The average breakdown strength of water is typically given to be 200 kV/cm, so, with a 1.27 cm spacing, the gap should break down at approximately 250 kV. With the Marx bank delivering a 400 kV pulse, there should be sufficient over-voltage to ensure gap breakdown regardless of the treatment given to the water.

Load resistor

The load resistor was built by Coulter [21] and provided both matching and damping of the voltage at the end of the experimental chamber. It consists of two water resistors, 14 cm in diameter and 36 cm in length, connected together at the inner conductor extending from the end of the experimental chamber and connected to two of the return paths around the experimental chamber.

D-Dot probe

The design of the D-Dot probe is given in Appendix B and will not be covered here. The use of a D-Dot probe for the Water Breakdown System was recommended by both Mr. Van Kenyon [24] from the Naval Surface Warfare Center and Mr. Richard Miller [25] from Maxwell Laboratories. The design resulted from a paper provided by Mr. Miller which is referenced in the probe model section later in the chapter.

There were several attempts made to calibrate the probe without any success. The initial attempt used a Mercury Relay Pulse Generator Model L4 line pulser with a 1.6 kV, 200 ns, pulse. This was not sufficient voltage to measure an integrated signal at the oscilloscope because of the voltage drop across the probe and across the integrator. By using a high voltage power supply and a mechanical switch, it was determined that in order to calibrate the probe, a 10 kV pulse was needed. The equipment needed to generate a test signal with a fast rise time and with a short pulse duration, and the equipment needed to make a direct measurement was not available. To get around this, the experiments were designed to look at changes in the voltage pulse rather than being concerned about the actual value of the voltage seen across the gap.

Cable

The probe is connected to the screen room with LDF 2-50 semi-rigid coaxial cable, commonly referred to as "foam" cable. Initial measurements made with the Tektronix 7104 oscilloscope were plagued by noise. This resulted in a lot of back-writing on the oscilloscope trace which was due to changes in the oscilloscope's ground level. Considerable time was spent trying to eliminate ground loops between the experiment and the screen room. At one point, the main power to the screen room was disconnected and a 12 V battery and a power inverter was used to run the oscilloscope.

To completely eliminate the noise problem, the coaxial cable had to be covered with three layers of Olympic tinned copper flat braid, 2.54 cm wide (Allied #876-4169), along with 7.3 meters of 3.8 cm outside diameter solid conduit added from the probe towards the screen room. The solid conduit accounted for about 80% of the total cable length between the experiment and the screen room. In order to ensure there was no noise on the coaxial line when the machine was fired, the line was terminated at the probe end with a 50 Ω terminator and the outer shield was connected to the outer shell of the probe with aluminum tape. The machine was fired with the oscilloscope at its lowest input amplifier level (5 mV/div). The copper braid and the solid conduit was added to the coaxial cable until the machine could be fired without triggering the oscilloscope. The line was then connected to the probe, and the tinned copper braid and the solid conduit were connected

to the outer shell of the probe with several layers of aluminum tape. This was also done to the connection at the screen room wall. Through trial and error, it was determined that the cable from the oscilloscope to the connection on the inside of the screen room needed to be as short as possible. This completely eliminated the noise seen on the oscilloscope trace.

Power supply

The power supply for the Marx bank consists of a Beta Electric Corp. Model MP-120-50R, 120 kV, DC Power Supply connected to a Universal Voltronics Corporation High Voltage D. C. Power Supply transformer rated at 160 kV, 5.5 mA. This is set so that the Marx bank is charged with a 2.5 mA constant current up to 66 kV. The transformer is attached to the Marx bank with an RG-19 coaxial cable with the outer braid cut back about 30 cm from both ends and allowed to "float" electrically. The ground between the power supply and the Marx bank is through a single point (MECCA) ground connection.

Control panel

The control panel for the system was assembled by Coulter [21]. It provides control for the air pressure in the sparkgap switches, dump switch, warning buzzer and light, and circulation pumps for both the oil and water. Control for the air pressure switch for triggering the Marx bank was added

later. Figure 15 shows the electrical connections for the trigger switch. The electrical control of the trigger switch consists of a main power switch, a keyed HV switch to prevent firing the machine if the key is removed, and a double-throw switch for firing and resetting the trigger switch.

Diagnostics

Initially, diagnostics for the Water Breakdown System consisted of two Tektronix 7104 oscilloscopes using either a 7A29 plug-in (50 Ω input, 1 GHz BW) or a 7A16A plug-in (1 M Ω , 200 MHz BW) vertical amplifier, and a 7B15 or 7B10 horizontal time base. The 7A16A was used with the analog integrator. Initially, a Polaroid C-53 camera was used to capture the waveforms on Polaroid 667 film. This was later replaced with a Tektronix C1002R digital camera which was connected to a Tektronix DX01 video board installed in a COMPAQ 386/20 computer. Images from the digital camera were converted into waveforms with the Tektronix DCS01GPH version 3.05 software and stored on the COMPAQ computer.

All of the signals were saved in the raw video format. These were then loaded into the DCS01GPH program and saved as a binary waveform file, and then printed out. For data analysis, the waveform file had to be converted to ASCII file format. To do this, the file was loaded into DCS01GPH and saved as an ASCII file through the Save File function. Several files could be saved this way at one time, usually a complete set of

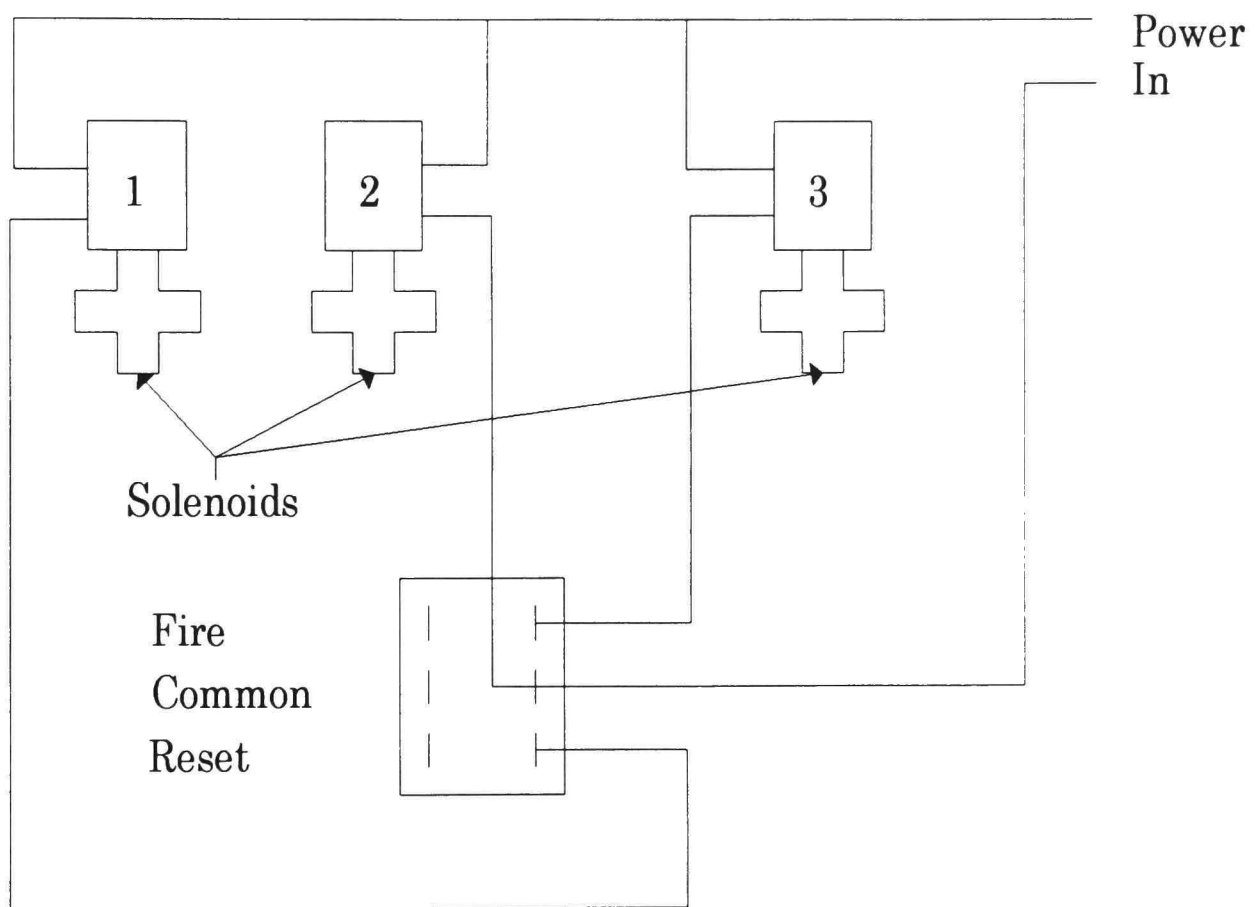


Figure 15. Electrical wiring diagram for the trigger switch.

signals were saved as a group with a unique filename prefix -- first four characters of the filename. The software then saved the group of files adding the corresponding letter of the alphabet of the waveform to the fifth character of the filename and the video port number as the last three characters. This gave us an eight character filename.

We would then exit the software to DOS. Using the rename command (ren), the video port number could be stripped off of the filename. For example, entering the following at the DOS prompt

```
“ren file?258.asc file?.asc”
```

would get rid of the video port number. In order to import the file into MATLAB for analysis, the text header had to be stripped from each of the files. This was accomplished by using a program called STRIPASC.COM which is described in Appendix D. This would take out all the text that DCS01GPH put at the beginning of the file and then check to see if there were 512 data points in the file. For some reason, some of the ASCII files would have an extra character added at the end of the file which would look like an extra data point to the MATLAB program. To do more than one file, the following DOS command

```
“for %a in (*.asc) do stripasc %a”
```

would run the STRIPASC.COM program for each file.

One problem encountered with the Tektronix DX01 video board and the DCS01GPH software was the inability of the program to follow fast

changing signals. The waveform that was generated tended to have the signal peaks rounded off. This caused us to lose the high frequency components of the waveforms. This was particularly prevalent when the D-Dot signal was measured without an integrator. Adjusting the intensity of the trace and the threshold level did not improve the waveform generated by the software. It seemed to be an inherent problem with the program.

The Tektronix 7104s have been replaced by Tektronix SCD-5000 digitizers. These are on loan from the Defense Nuclear Agency (DNA). These provide 4.5 GHz bandwidth input with 1024 points over the signal's time-width. The high bandwidth made it possible to measure the D-Dot signal directly and integrate it digitally. The high frequency components of the signal is preserved. The digitizers were controlled through the computer with the Data Acquisition, Archival, Analysis, and Instrument Control (DA³C) System software provided by DNA which was prepared by Voss Scientific, Inc.

Models

System model

Figure 16 shows the PSPICE model used for the Water Breakdown system. The Marx bank was modeled as a single 16.6 nF capacitor (C_1) with an initial charge of 400 kV and a 1.305 μ H (L_1) inductor between the Marx

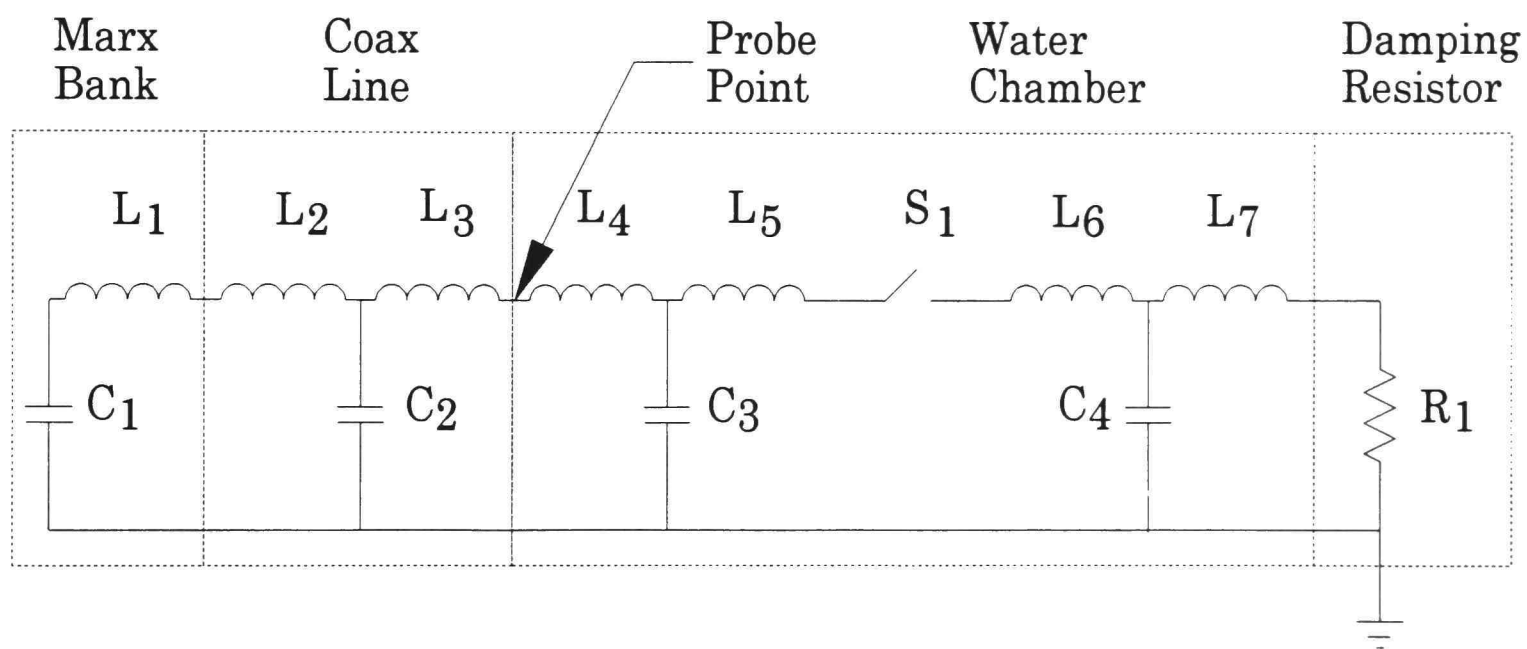


Figure 16. System model for simulation.

bank and the rest of the circuit. This inductance was the rated inductance of the capacitors specified by the manufacturer (120 nH) plus the estimated inductance of the Marx bank connections (1.185 μ H). The coaxial line was modeled as a lumped parameter transmission line with a total inductance of 817 nH and a capacitance of 130 pF ($L_2 = L_3 = 408.5$ nH, $C_2 = 130$ pF). These values were the calculated values using Eqs. (10) and (11). The water chamber was modeled as two transmission lines, one before the gap and one after the gap ($L_4 = L_5 = L_6 = L_7 = 65.25$ nH, $C_3 = C_4 = 315$ pF). The water gap was modeled as a voltage controlled switch (S_1) with the controlling voltage the voltage seen across the switch. The damping resistor (R_1) was modeled as a simple 80 Ω resistor.

Figure 17 shows the output measured at the point where the D-Dot probe would be located. The waveform was similar to the actual waveform seen with the D-Dot probe.

To get an idea of what the rise time of the system would be, the ringing frequency was needed. This was done by modeling the system as a CLC circuit. The first capacitor was the total capacitance of the erected Marx bank which was calculated to be 16.7 nF. The second capacitor was the calculated capacitance of the coaxial line which was calculated to be 130 pF. The inductor is the sum of the bank inductance and the coaxial inductance. The bank inductance was 1.305 μ H and the coaxial inductance was

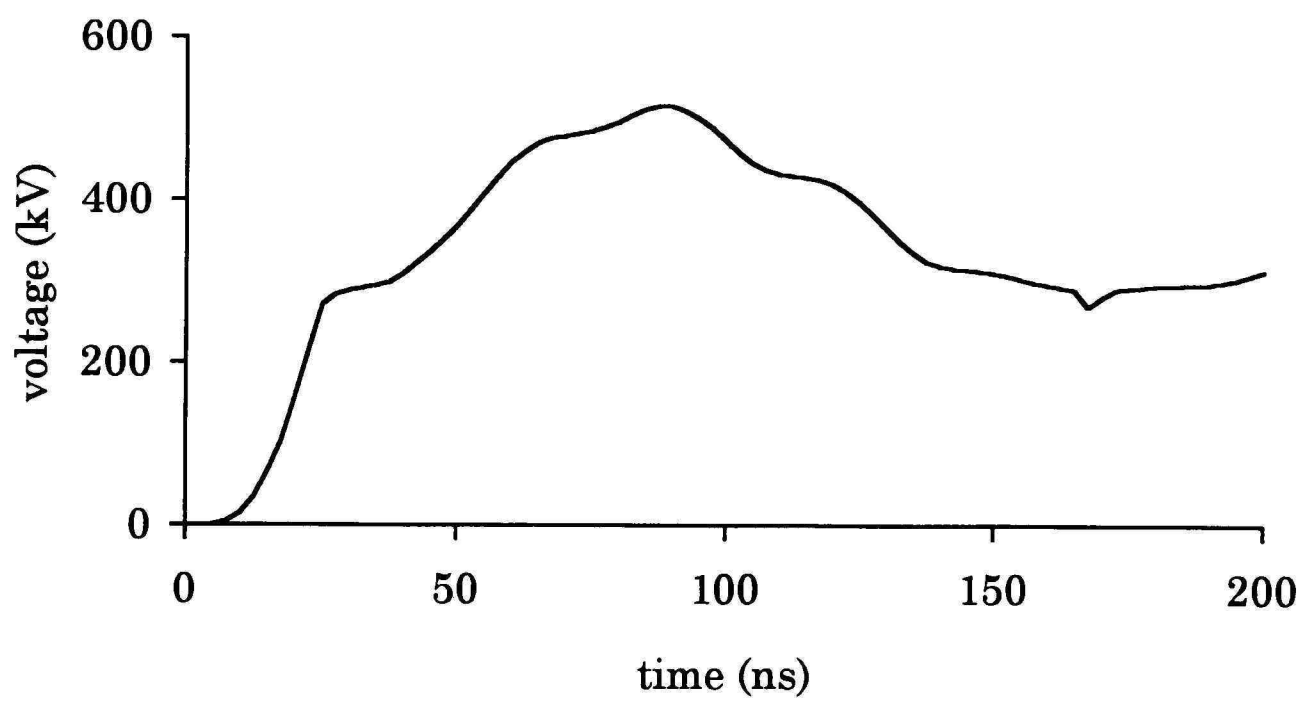


Figure 17. Output of system model at the probe point.

calculated to be 817 nH for a total of 2.122 μH . Solving the CLC circuit for the voltage across the second capacitor gives the equation

$$V_{c2} = \frac{V_o}{\omega L} (1 - \cos \omega t), \quad (19)$$

with

$$\omega = \sqrt{\frac{1}{L} \left(\frac{1}{C_1} + \frac{1}{C_2} \right)}. \quad (20)$$

Dividing Eq. (20) on both sides by 2π gives us the ringing frequency equation

$$f = \frac{1}{2\pi} \sqrt{\frac{1}{L} \left(\frac{1}{C_1} + \frac{1}{C_2} \right)}. \quad (21)$$

For the values listed above, the ringing frequency is 9.6 MHz. If a sinusoidal shaped pulse is assumed, the risetime (t_r) for a sinusoid can be calculated by

$$t_r = \frac{1}{2\pi f} \left[\sin^{-1}(.9) - \sin^{-1}(.1) \right], \quad (22)$$

which simplifies to

$$t_r = \frac{0.16227}{f}. \quad (23)$$

For a frequency of 9.6 MHz, t_r would be 16.9 ns. This gave us an idea of the signal that the system would be capable of producing. To compare this to an actual system, a sine wave was produced and then overlaid on an actual signal from the Water Breakdown System. Figure 18 shows how the initial portion of the actual signal (solid line) and a 5 MHz sine wave have the same rise time. After the initial rise in voltage, the capacitances and inductances

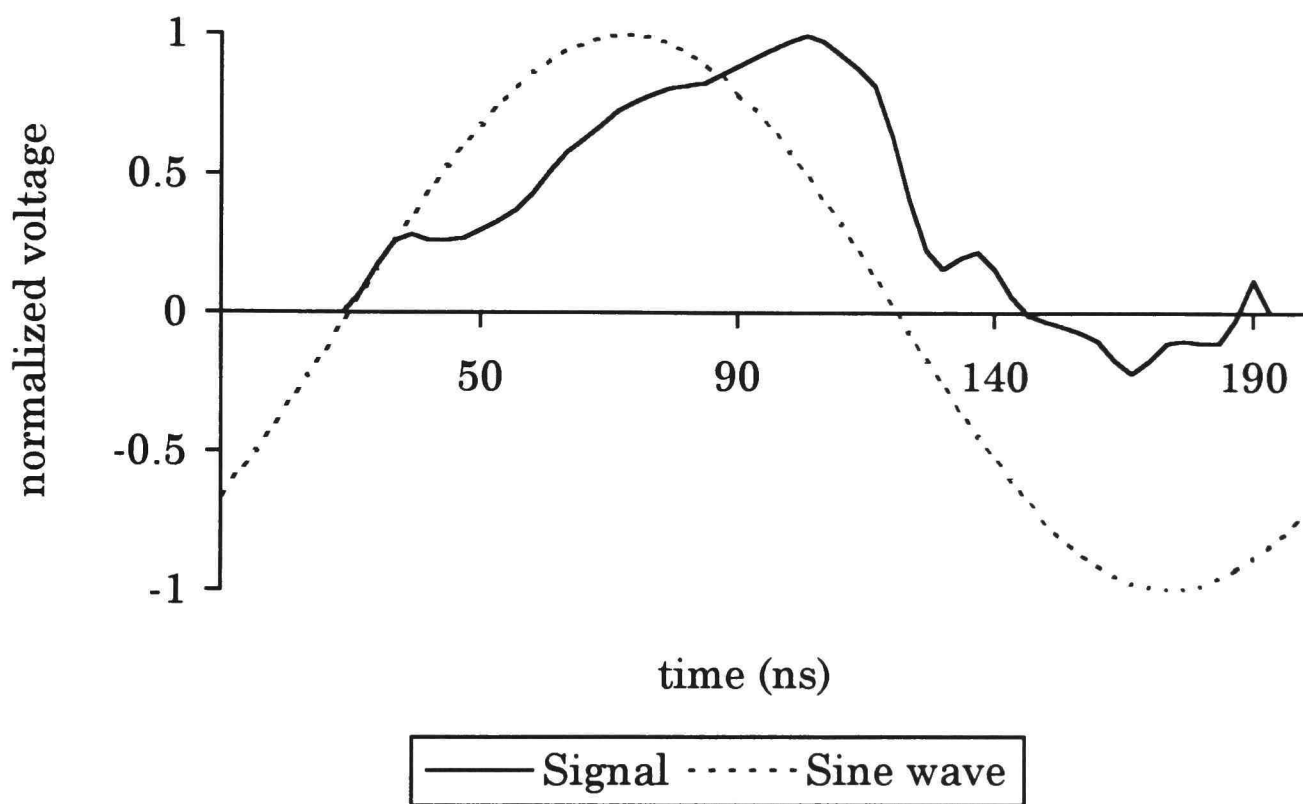


Figure 18. Comparison of an actual signal with a 5 MHz sine wave.

in the rest of the system begin to affect the waveform. A 5 MHz sine wave has a risetime of about 33 ns. This is a factor of about two greater than what the CLC model gives for the risetime. This would require a factor of about four increase in the combination of the inductance and capacitance of the Marx bank and the coaxial line. The total inductance of the Marx bank would be expected to be more than the rated inductance of just the individual capacitors and the loop inductance approximation calculated earlier due to the inductance of the Marx bank connections and the inductances of the individual spark gap switches.

Probe model

The model used for the D-Dot probe was described by Wilkinson [26]. Figure 19 shows a graphic representation of the probe as it would look connected to the system. The probe was modeled as a capacitive divider with the two capacitances, C_1 and C_2 , connected to an RC integrator as shown in Figure 19. The first capacitor was the capacitance between the face of the center section of the probe and the inner conductor of the coaxial line. This value was estimated by assuming a flat plate capacitor with the surface area equal to the cross sectional area of the probe's center section. The second capacitor of the capacitive divider was the capacitance between the side of the probe's center section and the outer shell of the probe body. This value

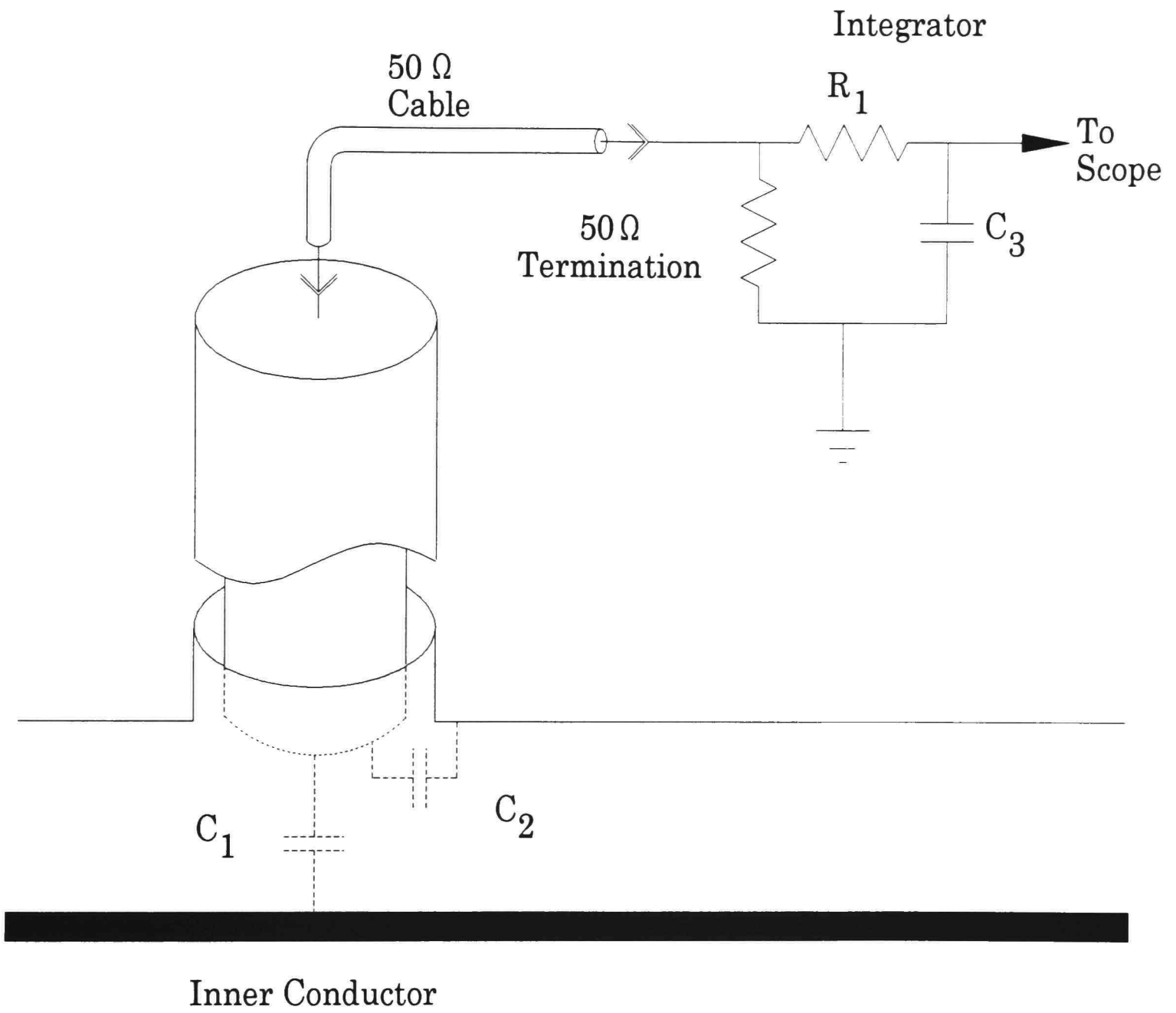


Figure 19. Diagram of the D-Dot probe.

was estimated by assuming a coaxial capacitor.

The probe was connected to a $50\ \Omega$ cable and terminated into a $50\ \Omega$ resistor either at the oscilloscope or the integrator. The integrator was modeled as a simple RC circuit. In practice, simple resistors and capacitors could not be used because of the high frequency components of the signal from the probe. The signal had to be integrated digitally or through the use of a special high-bandwidth integrator.

Figure 20 shows the circuit model used for the derivation and simulation of the probe. Appendix B contains the mathematical derivation and will not be repeated here. For simulation, the following values were used: $C_1 = 0.65\ \text{pF}$, $C_2 = 32.5\ \text{pF}$, $C_3 = 1.66\ \text{nF}$, $R = 50\ \Omega$, and $R_1 = 1.21\ \text{k}\Omega$. Figure 21 shows the output of the probe model using PSPICE. Actual measurement of C_2 was done with the Tektronix Type 130 LC meter and was found to be $67\ \text{pF}$. This was over twice what was expected and was due to not including the capacitance at the connector end of the probe. The PSPICE simulation was run again to see what effect the increase in C_2 would have on the output of the probe. Figure 22 shows the output of the probe with C_2 equal to $32.5\ \text{pF}$ (calculated value), solid line, and then equal to $67\ \text{pF}$ (measured), dotted line, to the same $400\ \text{kV}$ square input (solid line) in Figure 21. As can be seen, there was little effect on the output signal.

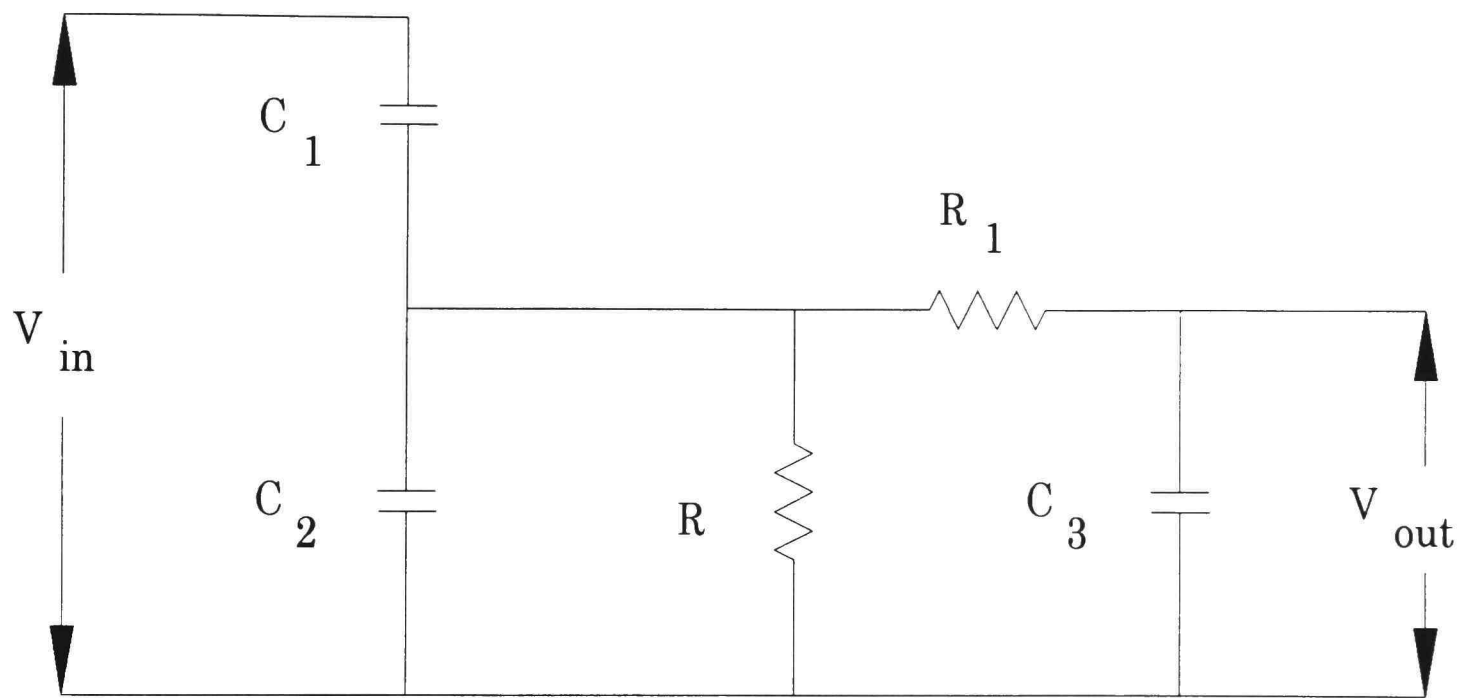


Figure 20. Circuit model used for the D-Dot probe.

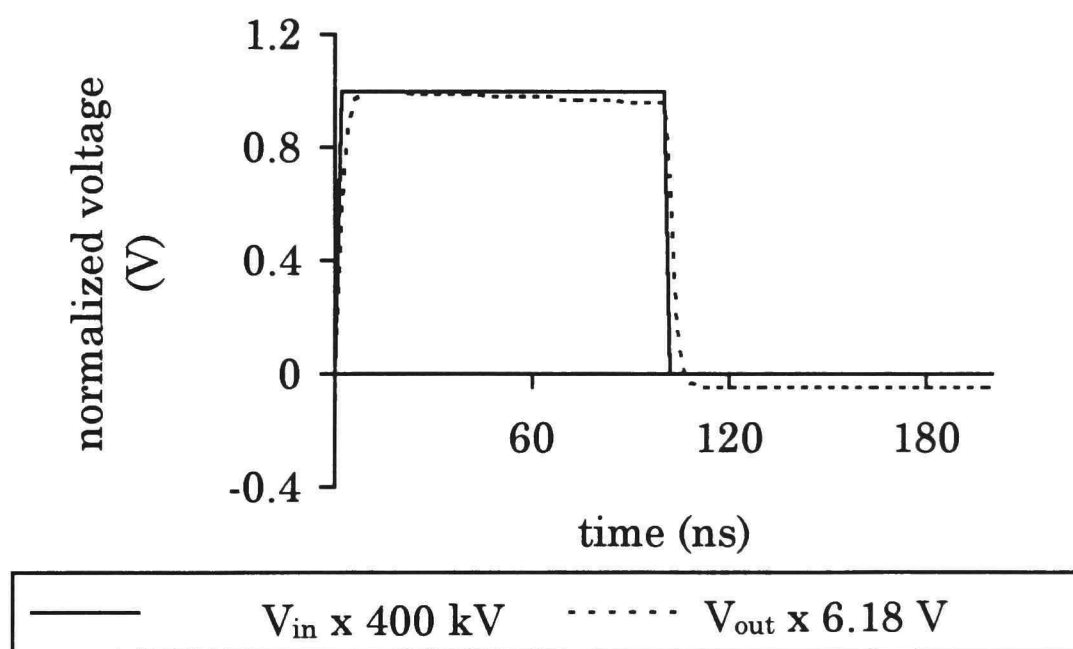


Figure 21. Normalized input and output voltages for the D-Dot probe simulation.

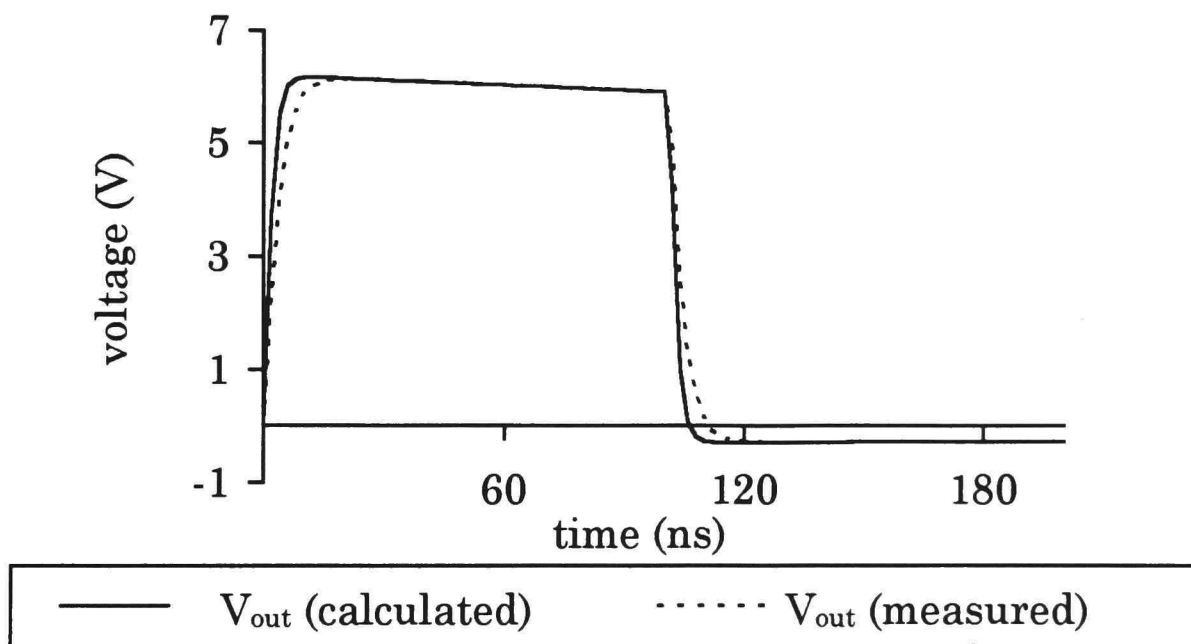


Figure 22. Comparison of D-Dot probe with calculated versus measured C_2 .

CHAPTER IV

EXPERIMENTAL DESIGN AND DATA

Experimental design

Magnetic fields

Several experiments were planned using magnets in the electrodes to look at possible effects of magnetic fields on the breakdown process. The magnets used were Cookson neodymium iron boron (NdFeB) disc magnets, 35NERR32, which were 1.27 cm in diameter and 4.7 cm in length. The field strength of the magnets was measured with a F. W. Bell Model 4048 Gauss Meter with a T-4048-001 Cal 1735 Transverse Probe. On the end of the magnet along the center line and near the surface, the magnetic field measured 0.2 T. When one of the magnets was placed in the Copper-Tungsten (CuW) electrode, the field measured at the surface of the electrode was about 15 mT.

The first experiment looked at using a single magnet in either the anode or the cathode. The polarity of the magnetic field was also investigated in this experimental series. The second experiment investigated the use of magnets in both the anode and cathode, and with the fields opposing or aligning.

The first series of trials investigated the magnet in the cathode. The procedure was to run five baseline shots, five shots with the magnetic North

Pole pointing into the gap, and five shots with the magnetic South Pole pointing into the gap. The procedure was repeated for a total of thirty shots.

Normally, when using statistics, the experiment is designed so that the data are collected in random order. However, because of the nature of pulsed power research and the difficulty in completely randomizing the shots, the shots were planned to help eliminate possible series effects. Many shots were fired on the system before the experiments were started to ensure that the system was reliable and series of shots were fired periodically between experiments to guarantee that any effects seen in the experimental trials were due to the experimental process and not a change in the pulsed power system. Analysis of Variances (ANOVA's) were calculated to find statistically significant effects. This procedure is described in Bruning and Kintz [27] and was programmed to run in MATLAB (see Appendix C). The results of the ANOVA's were then looked up in an F distribution table and a result was considered significant if its probability level (α) value was less than 0.050. At $\alpha < 0.050$, there is more than a 95% certainty that something statistically significant has occurred in the data. If the ANOVA was found to be significant, a *t*-test for a difference between two independent means was run between each of the three groups: Baseline versus North Pole, Baseline versus South Pole, and North Pole versus South Pole. The results of the *t*-test were looked up in the *t* statistic table and again, a result was considered significant if $\alpha < 0.050$.

Several parameters were analyzed for each of the data groups. The maximum voltage (V_{\max}), the effective time (τ_{eff}) which is defined as the time that the voltage is above 63% of V_{\max} , the fall-time, and the fall-rate, which is the change of voltage divided by the fall-time, were investigated. ANOVA's and, if significant, t -tests were calculated for each of these parameters.

The next series of thirty shots were run in the same fashion except with the magnet in the anode. The polarity of the charging system was reversed so that the anode was on the electrode that extended from the end of the experimental chamber. This made the data collection much easier because the experimental chamber did not have to be opened between data series to insert the magnet into the electrode. Changing the polarity seemed to have an adverse effect on the capacitors in the Marx Bank and caused several to self-destruct when the bank was fired. For this reason, a complete ANOVA was not run on the combined data with the magnet in the cathode and the magnet in the anode.

An ANOVA's was calculated for the thirty shots and t -tests were run on the three data groups for the same parameters listed above: Baseline versus North Pole, Baseline versus South Pole, and North Pole versus South Pole, and again, a result was considered significant if $\alpha < 0.050$.

The last series of magnet tests looked at the effects of using a magnet in each of the electrodes. For this series, five baseline shots were fired then a magnet was placed in each electrode. Initially, the North Pole of each

magnet was pointing towards the gap; this was labeled Opposing Fields. Five shots were fired in this configuration then the magnet in the anode was reversed so that the South Pole was pointing towards the gap; this was labeled Aligning Fields. The sequence was repeated for a total of ten shots in each data set: Baseline, Opposing Fields, and Aligning Fields. ANOVA's and, if significant, *t*-tests were run in the same fashion as described above.

Sulfur hexafluoride

SF₆ is used in many pulsed power applications because of its electro-negativity. This is used a lot in spark gap switches to increase the voltage holdoff of the switch. For this reason, the effect of adding SF₆ to the water was looked at. Ten shots were fired for a baseline, then the gas was added at the suction side of the water pump. The pressure on the gas line was increased until SF₆ bubbles were seen coming out of the drain line at the bottom of the experimental chamber. This was allowed to go on until there was about 2 cm of water displaced at the top of the experimental chamber. The gas pressure was then reduced until the water started circulating through the chamber again. Ten shots were planned but the loss of several Marx Bank capacitors made it possible to collect only four shots. The *t*-tests were calculated on the two data groups for the same parameters listed above with the results looked up in the *t* statistic table. A result was considered significant if $\alpha < 0.050$.

Two more series of experiments were run using SF₆. The second series was run the same as the first series. It consisted of ten baseline shots and ten SF₆ shots. The same *t*-tests were calculated for the second series of shots as were done on the first series. For the third experiment, the gas connection was moved to the top of the experimental chamber. The chamber was initially filled with water for the baseline shots, then the gas was added until it forced about 5 cm of water from the top of the chamber. The water was allowed to circulate through the gas layer to help draw gas bubbles into the water in the chamber. The de-ionizing bottles were bypassed so that the SF₆ would not be absorbed into the resin in the bottles. The water circulated for two hours and a series of ten shots were run. The system was left circulating for over 24 hours then the final ten shots were fired. ANOVA's were calculated for the same parameters as the first series.

Hydrochloric acid

Hydrochloric acid (HCl) was used by Ovchinnikov and Yanshin [15] to decrease the conductivity of the water in their prebreakdown research. Since they were doing prebreakdown research, they did not measure the breakdown voltages. It was decided to see if there would be any effect on V_{\max} , τ_{eff} , fall-time, and fall-rate if HCl was added to the water. Several shots were measured using different concentrations of HCl. Concentrations of 2.0×10^{-4} molar (M) and 10.0×10^{-4} M were looked at. The HCl was added to

the water and allowed to circulate only in the experimental chamber for an hour. Several shots were fired, then the water was drained from the experimental chamber. The water lines and chamber were flushed with water to ensure there was no contamination of the de-ionization bottles.

A second experiment was run using five different concentrations of HCl: 0.1×10^{-4} M, 0.5×10^{-4} M, 1.0×10^{-4} M, 5.0×10^{-4} M, and 10.0×10^{-4} M. Three shots were fired at each of the five concentration levels plus three baseline shots. ANOVA's were calculated on the five data groups and the baseline data for the same parameters listed above with the results looked up in the F statistic table. A result was considered significant if $\alpha < 0.050$. If the ANOVA was significant for a particular parameter, a series of *t*-tests were calculated to see if there were any significant differences between the baseline and the five data groups. A result was considered significant if $\alpha < 0.05$.

Polymer coatings

Two different polymer coatings were tried to see if they would have any effect on the voltage holdoff in the water gap. A thin layer of either poly(ethersulfone) (PES) or polycarbonate (PC) was air brushed onto stainless steel electrodes and then allowed to cure for at least 24 hours. A series of 15 shots with stainless steel electrodes was used for a baseline for comparison to the shots with the polymer coating. There were four sets of

electrodes with each one of the two polymers so that the following combinations could be tried: PES on both electrodes, PC on both electrodes, PES on the anode and PC on the cathode, and PC on the anode and PES on the cathode. Statistical analysis consisted of calculating a *t*-test for the τ_{eff} , V_{max} , fall-time, and fall-rate of the experimental values with the baseline. A test was considered significant if $\alpha < 0.05$.

Black wax

Stainless steel electrodes were coated with an about 1.25 mm thick coating of Apiezon-W black wax. The coating was allowed to harden for at least 24 hours before being used. Ten sets of electrodes were prepared and used for this experiment. The experimental chamber was drained after each shot. A *t*-test for the difference between two means was calculated for each of the four parameters: τ_{eff} , V_{max} , fall-time, and fall-rate. A test was considered significant if $\alpha < 0.05$.

Anodized aluminum

The last experiment consisted of two sets of aluminum electrodes made from #6061 aluminum and anodized in order to harden the surface of the electrodes. They were anodized by placing in a tank with a 20% concentration of sulfuric acid and the voltage was adjusted so that 20 amps went through the electrodes for 25 minutes. This experiment was planned to

see if the results here would be similar to Gehman et al. [9]. Eight baseline shots were used for comparison to two shots with the anodized surfaces. The same four parameters measured in the previous experiments (τ_{eff} , V_{max} , fall-time, and fall-rate) were used here and the results were analyzed with t -tests between independent means. A result was considered significant if $\alpha < 0.05$.

Data

The data for each experiment will be presented in graphic form. Each set of data will consist of a graph of the averaged signals to show the differences between the baseline and experimental groups. Each individual signal was adjusted to compensate for the starting point of the signal by adding a least-squared routine to the MATLAB data extraction program. After the individual signals were adjusted, each of the 512 data points were averaged to give the waveform for the graphs.

Four parameters were looked at for comparison between the experimental groups. These were τ_{eff} , V_{max} , fall-time, and fall-rate. The rise-time was not used because there seemed to be very little difference in the rise-time from one shot to another and was probably governed by the system rather than the closing of the water gap. The results of the four parameters are also presented in graphical form with the mean data points connected by a single line and the ± 1 standard deviation bars drawn above and below the mean points.

Magnetic fields

Figure 23 shows the average waveforms for the magnet in the anode. The three curves represent the average values for the baseline signals, the signals generated with the North Pole of the magnet facing towards the gap, and the signals generated with the South Pole of the magnet facing towards the gap. The values of τ_{eff} for each of the three groups are shown in Figure 24; V_{max} , Figure 25; fall-time, Figure 26; and fall-rate, Figure 27.

The next experimental set consisted of baseline shots and shots with the magnet placed in the cathode. Again there were three sets of signals, baseline, North Pole in, and South Pole in. The averaged waveforms are shown in Figure 28; values of τ_{eff} , Figure 29; V_{max} , Figure 30; fall-time, Figure 31; and fall-rate, Figure 32.

Two magnets were used in the last experimental series. The three sets of signals consisted of the baseline, aligning fields, and opposing fields. The averaged waveforms are shown in Figure 33; values of τ_{eff} , Figure 34; V_{max} , Figure 35; fall-time, Figure 36; and fall-rate, Figure 37.

Sulfur hexafluoride

Figure 38 shows the averaged waveforms for the first series of SF_6 experiments. The values of τ_{eff} for the two groups are shown in Figure 39; V_{max} , Figure 40; fall-time, Figure 41; and fall-rate, Figure 42. The second

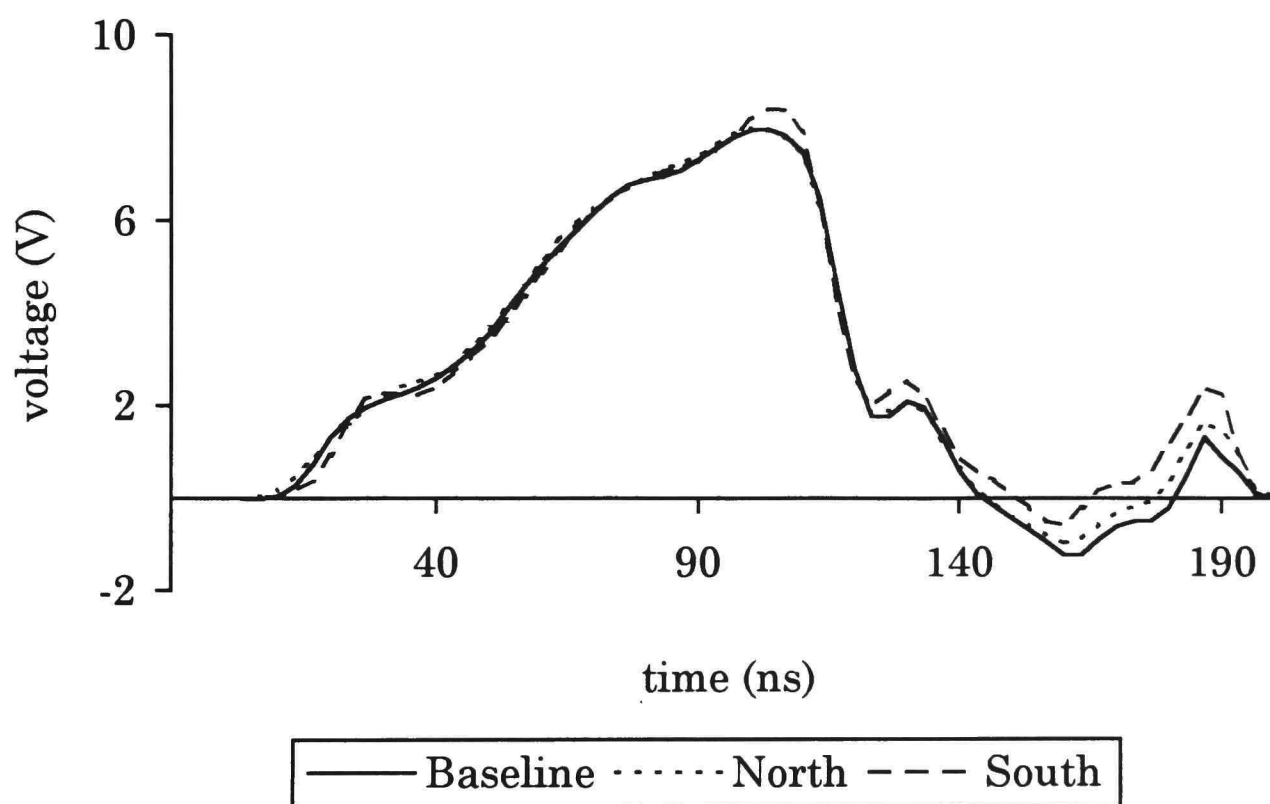


Figure 23. Average waveforms for the magnet in the anode.

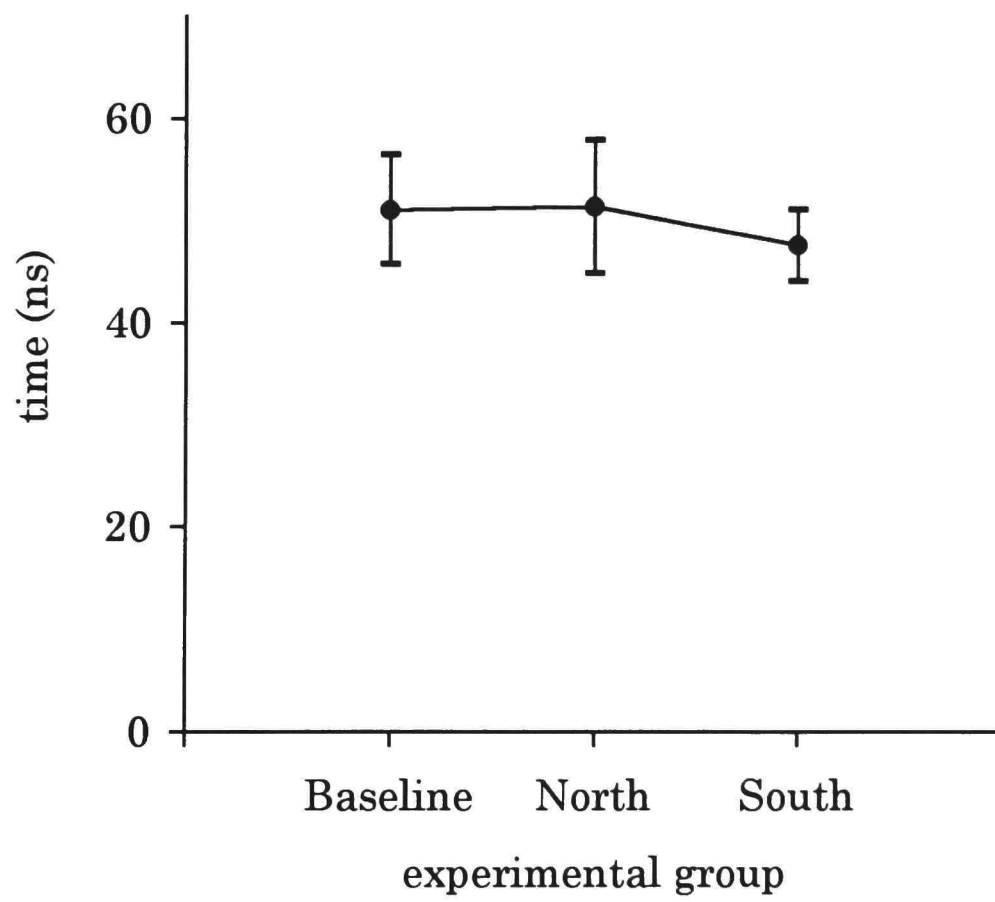


Figure 24. Effective time (τ_{eff}) with a magnet in the anode.

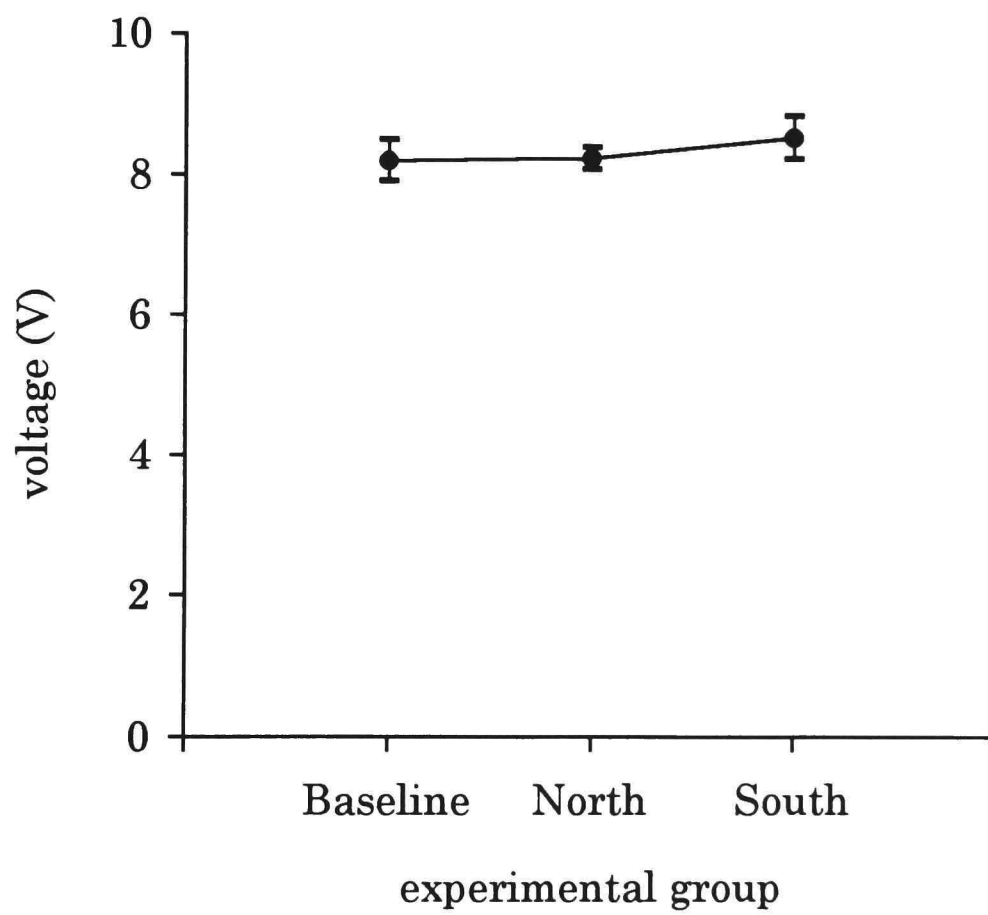


Figure 25. Maximum voltage (V_{\max}) with a magnet in the anode.

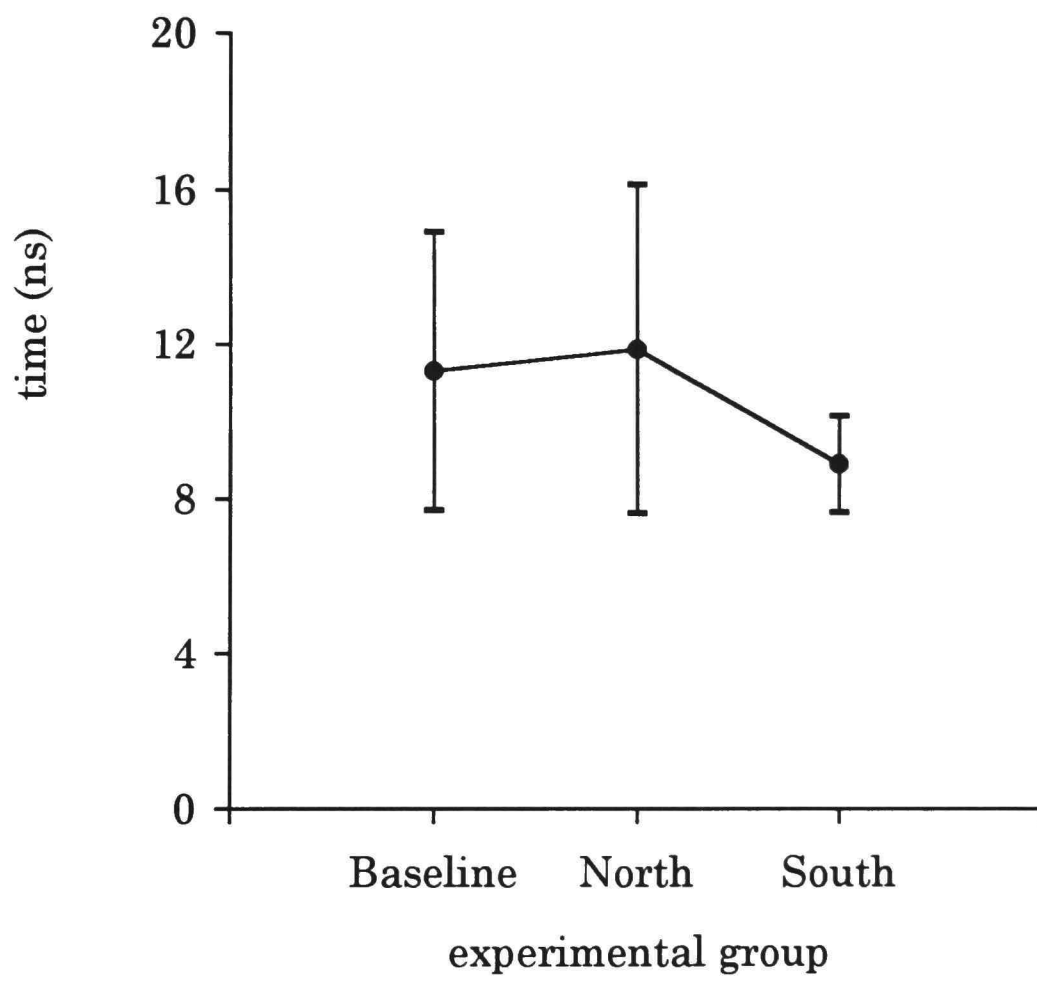


Figure 26. Fall-time with a magnet in the anode.

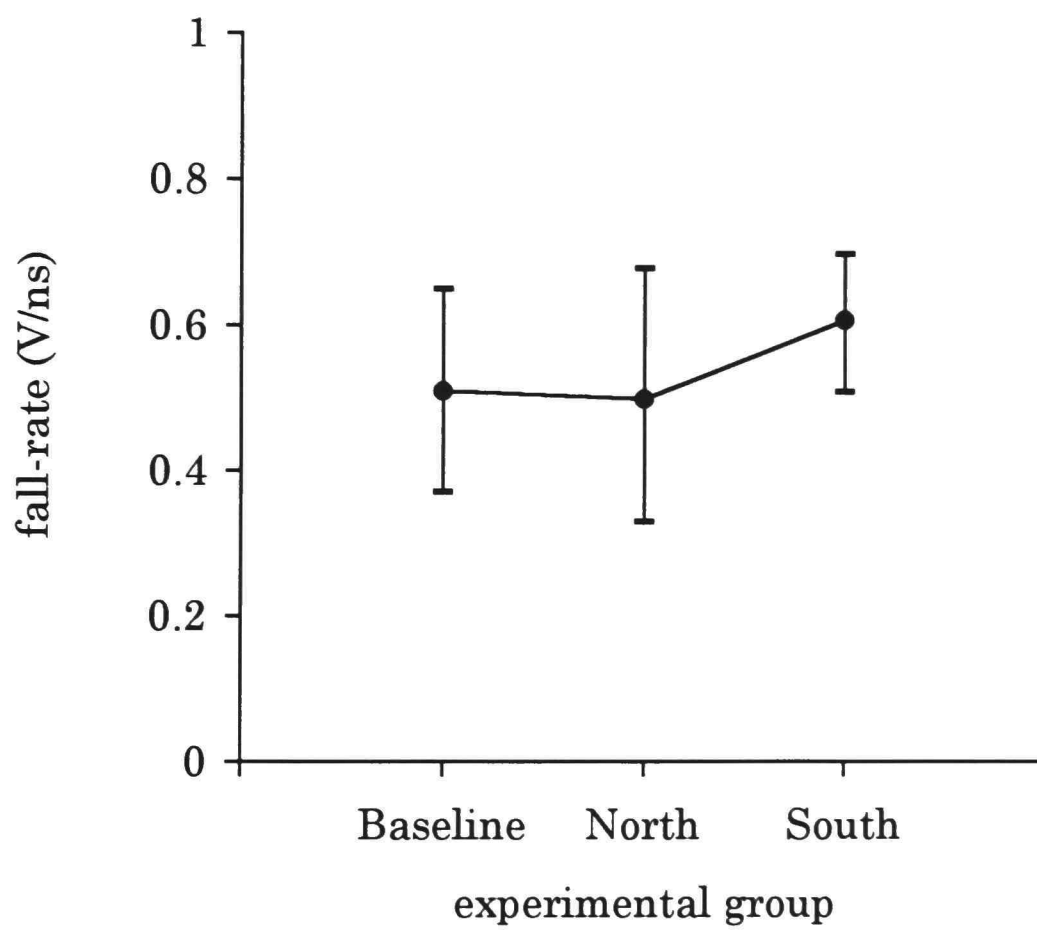


Figure 27. Fall-rate with a magnet in anode.

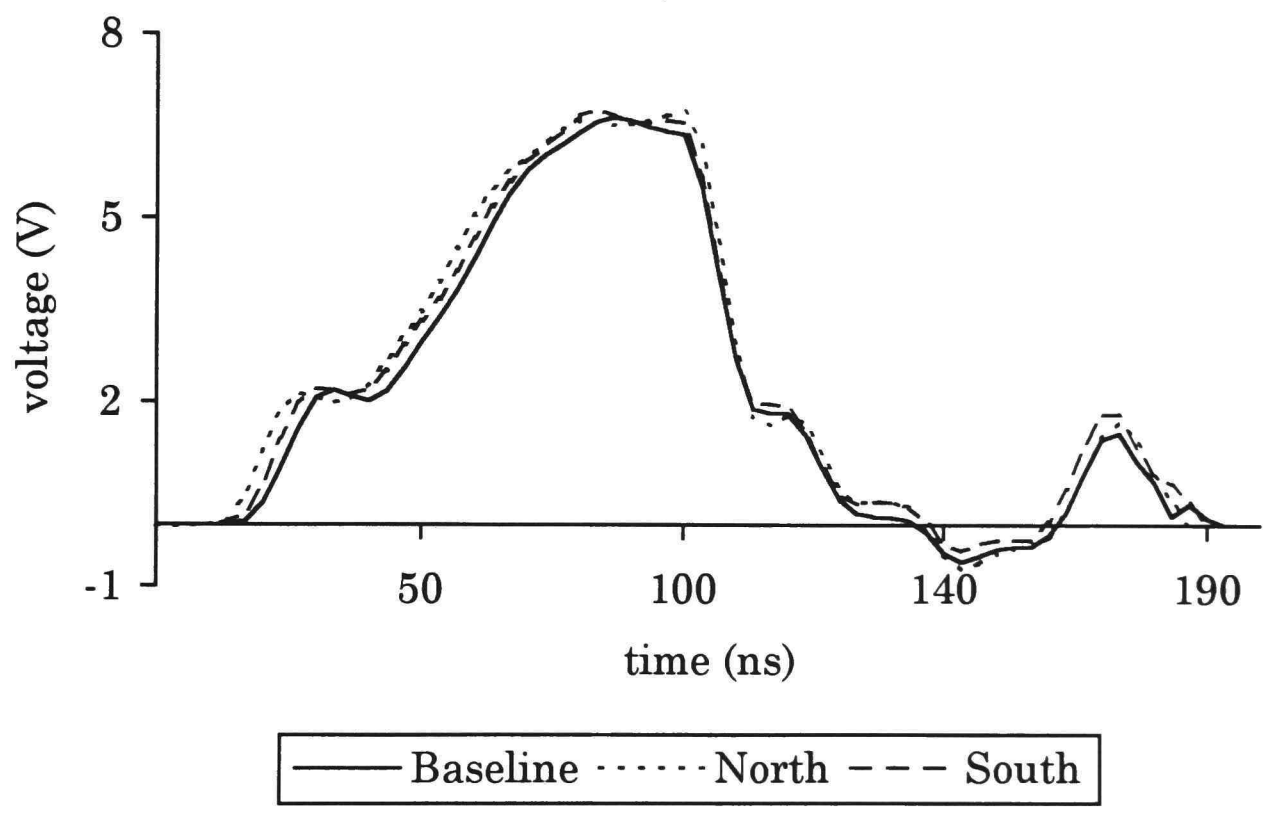


Figure 28. Average waveforms for the magnet in the cathode.

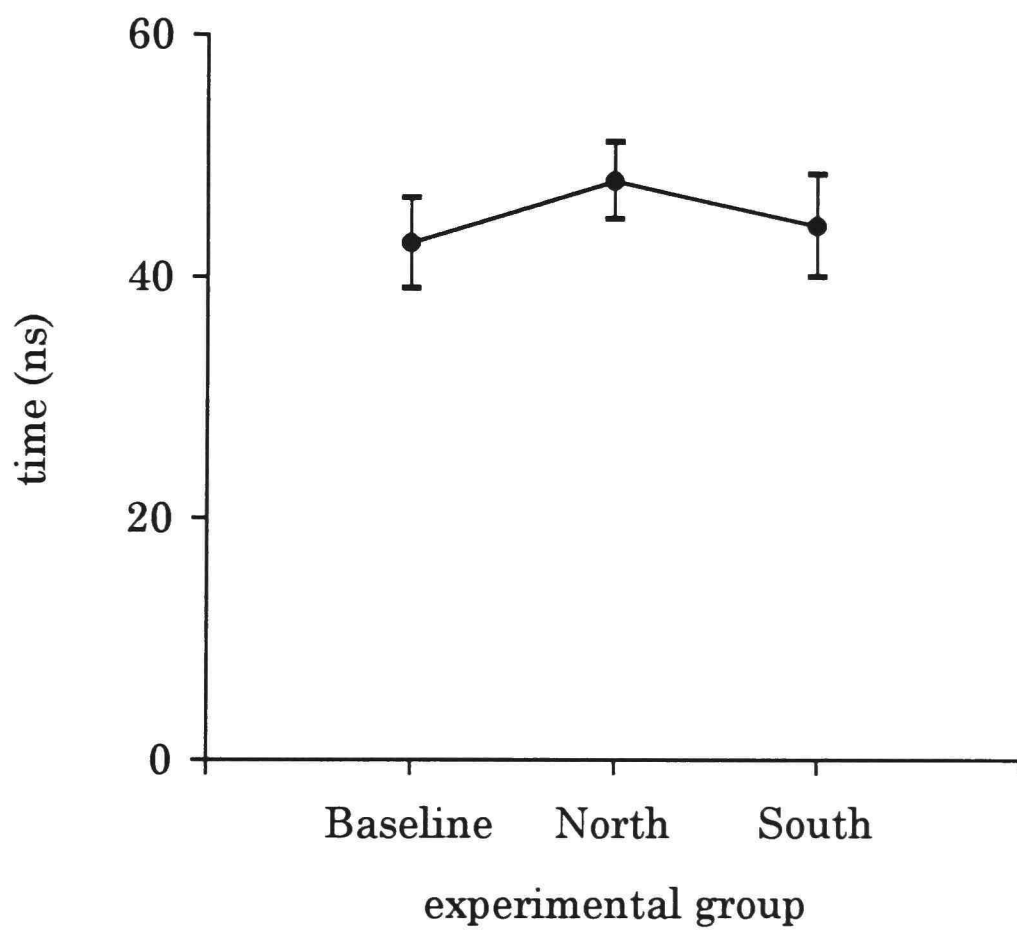


Figure 29. Effective time (τ_{eff}) with a magnet in the cathode.

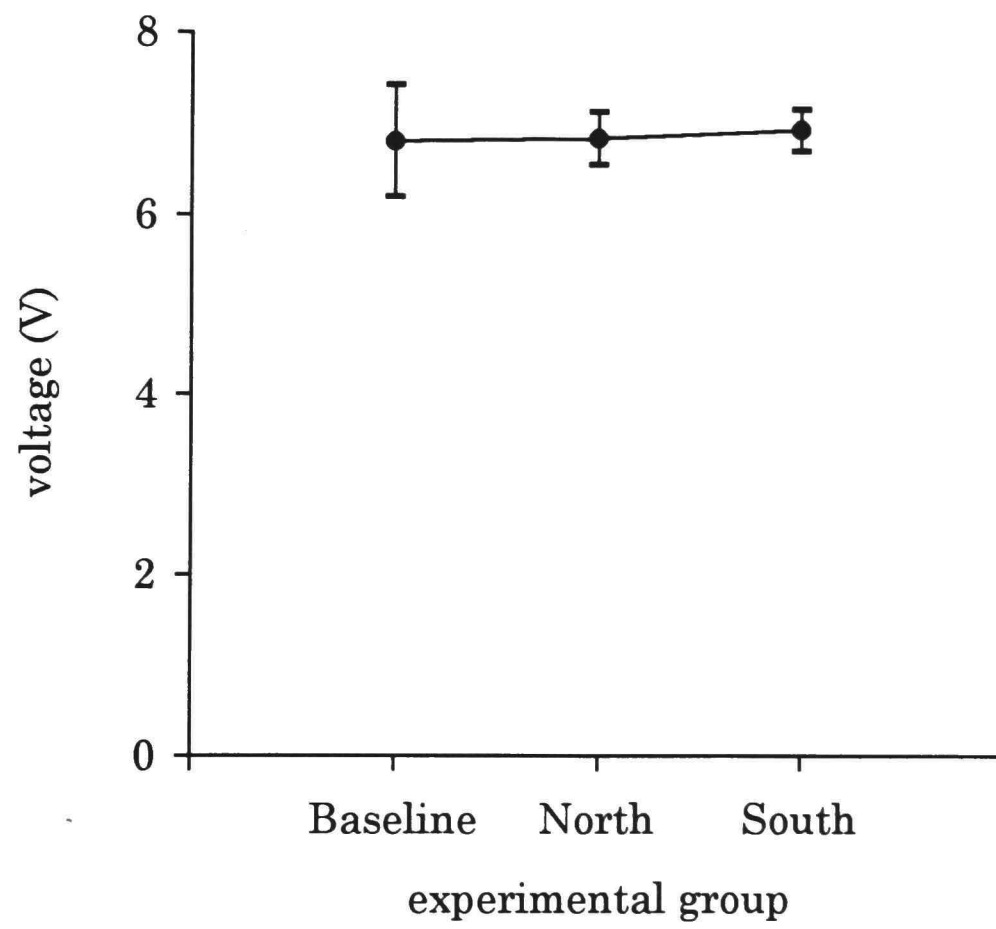


Figure 30. Maximum voltage (V_{\max}) with a magnet in the cathode.

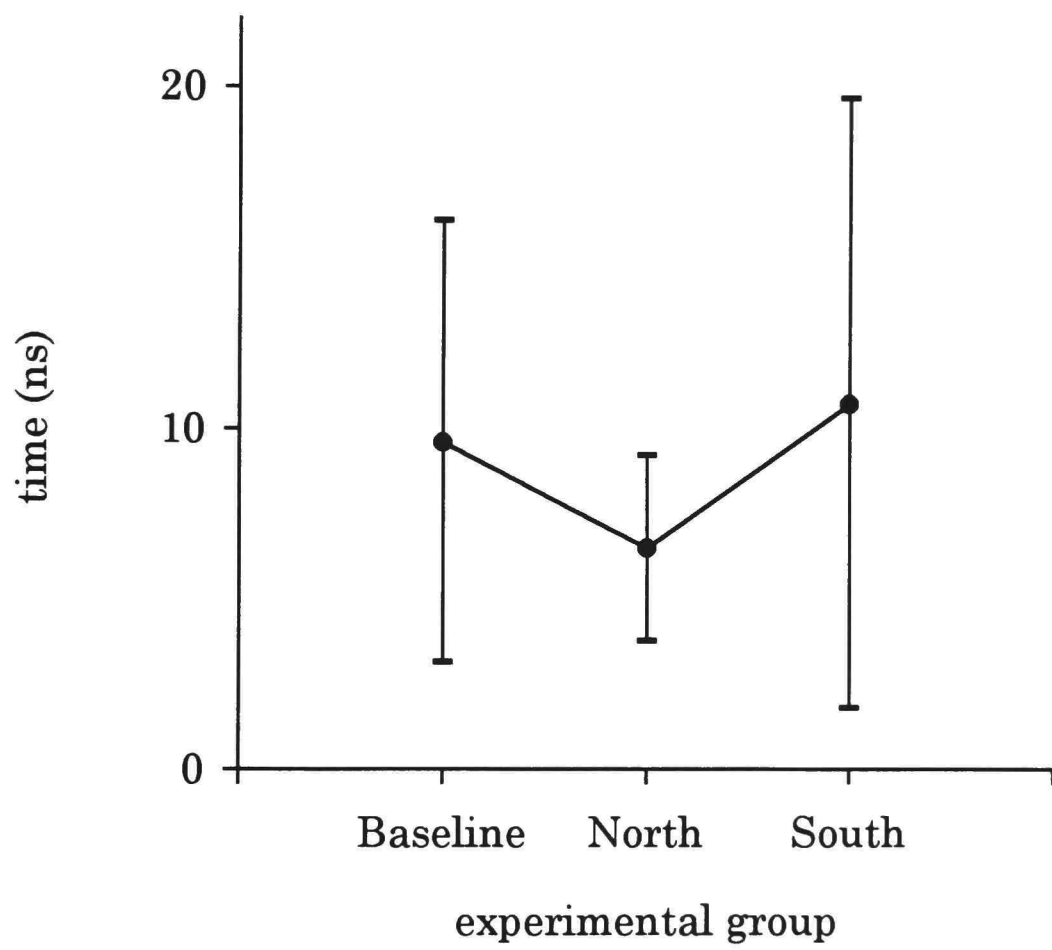


Figure 31. Fall-time with a magnet in the cathode.

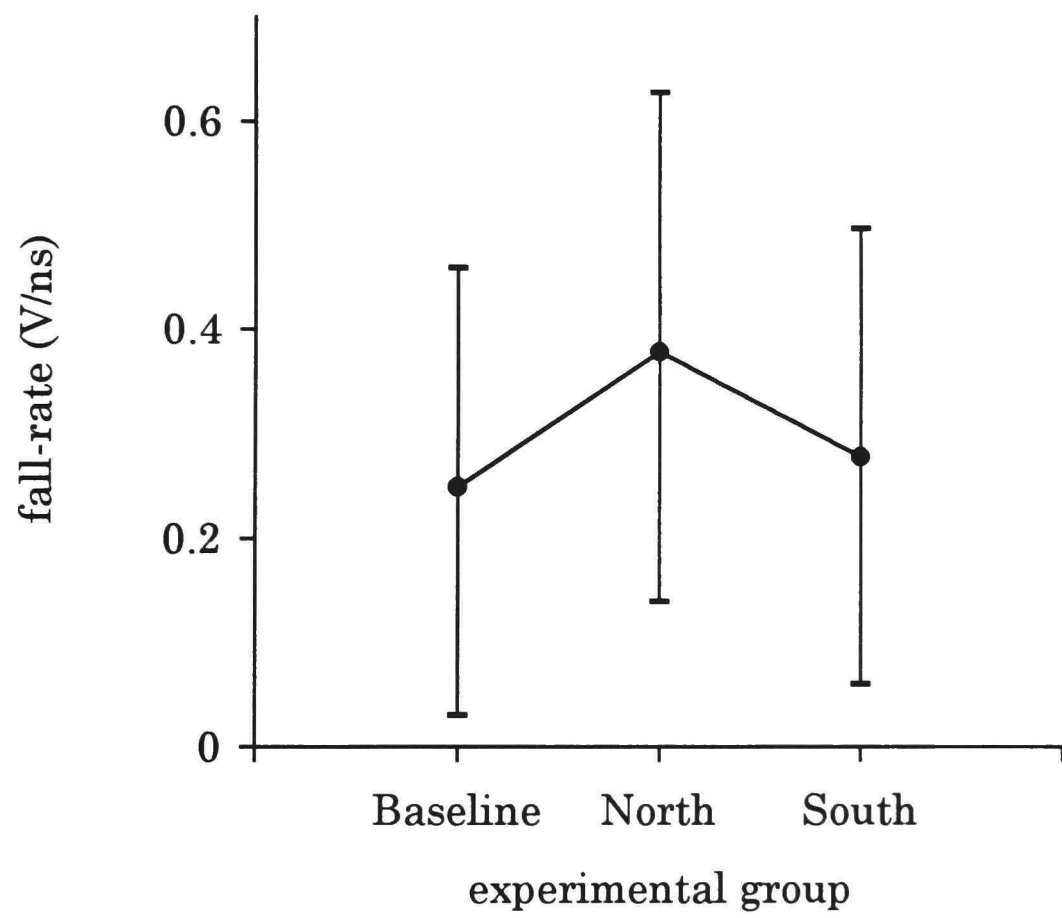


Figure 32. Fall-rate with a magnet in the cathode.

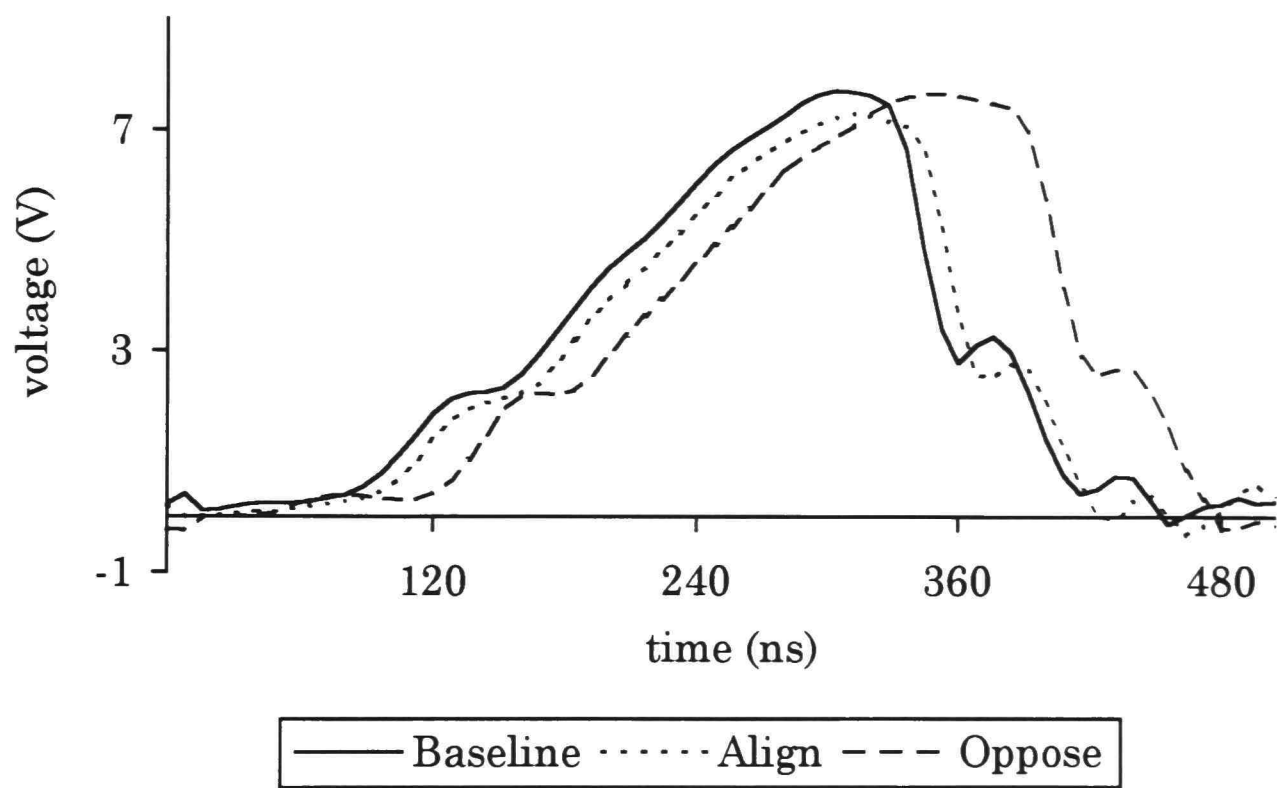


Figure 33. Average waveforms with magnets in the anode and cathode.

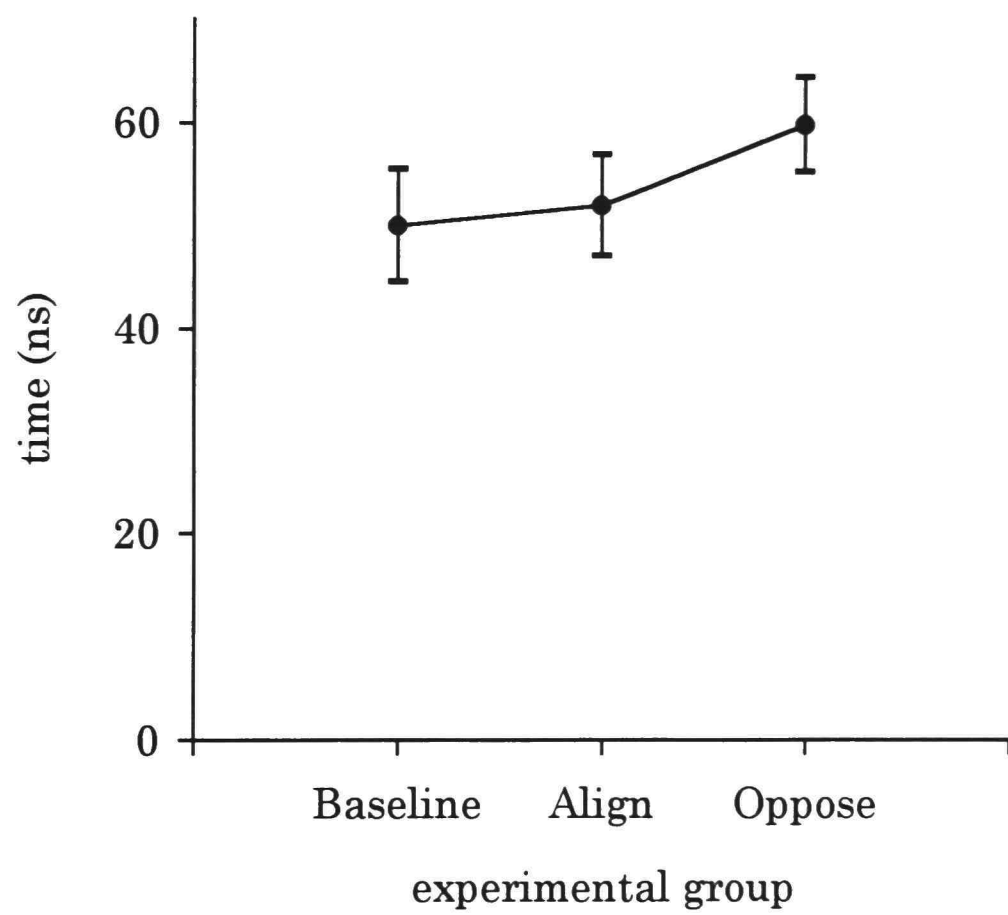


Figure 34. Effective time (τ_{eff}) with magnets in anode and cathode.

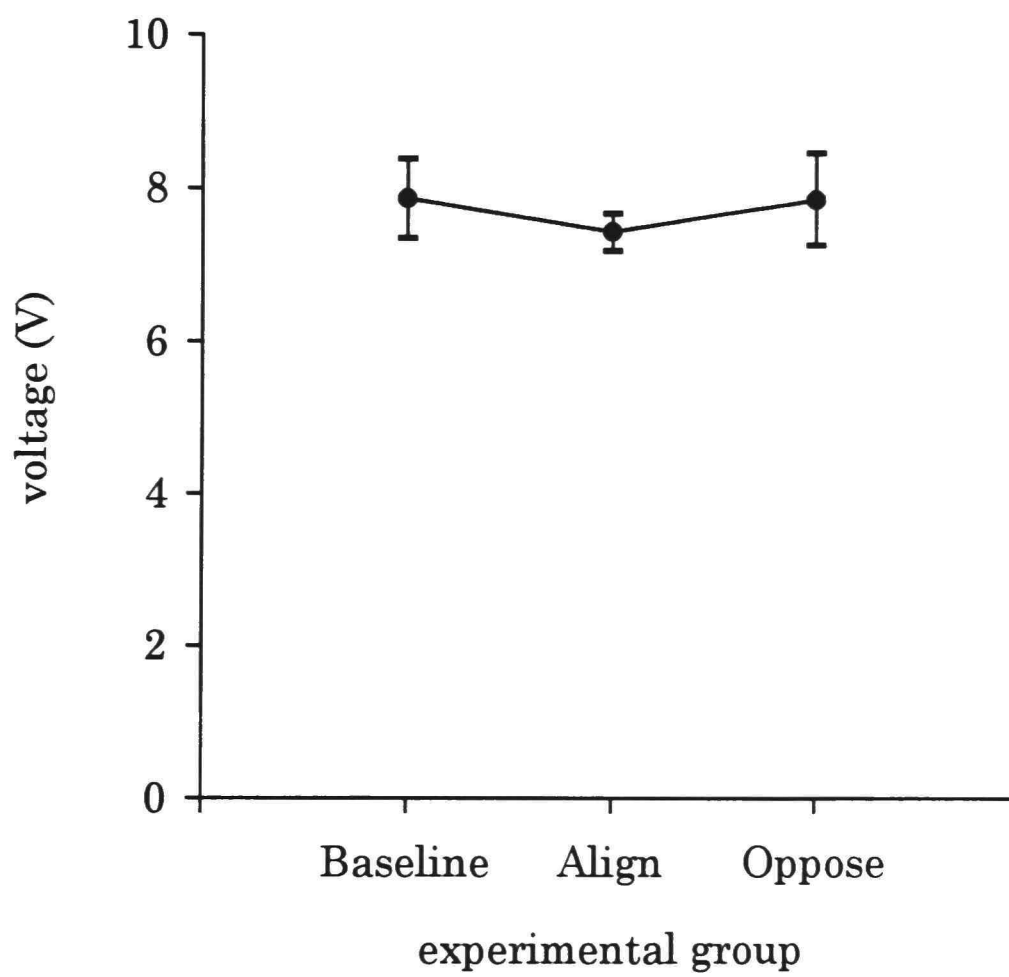


Figure 35. Maximum voltage (V_{\max}) with magnets in the anode and cathode.

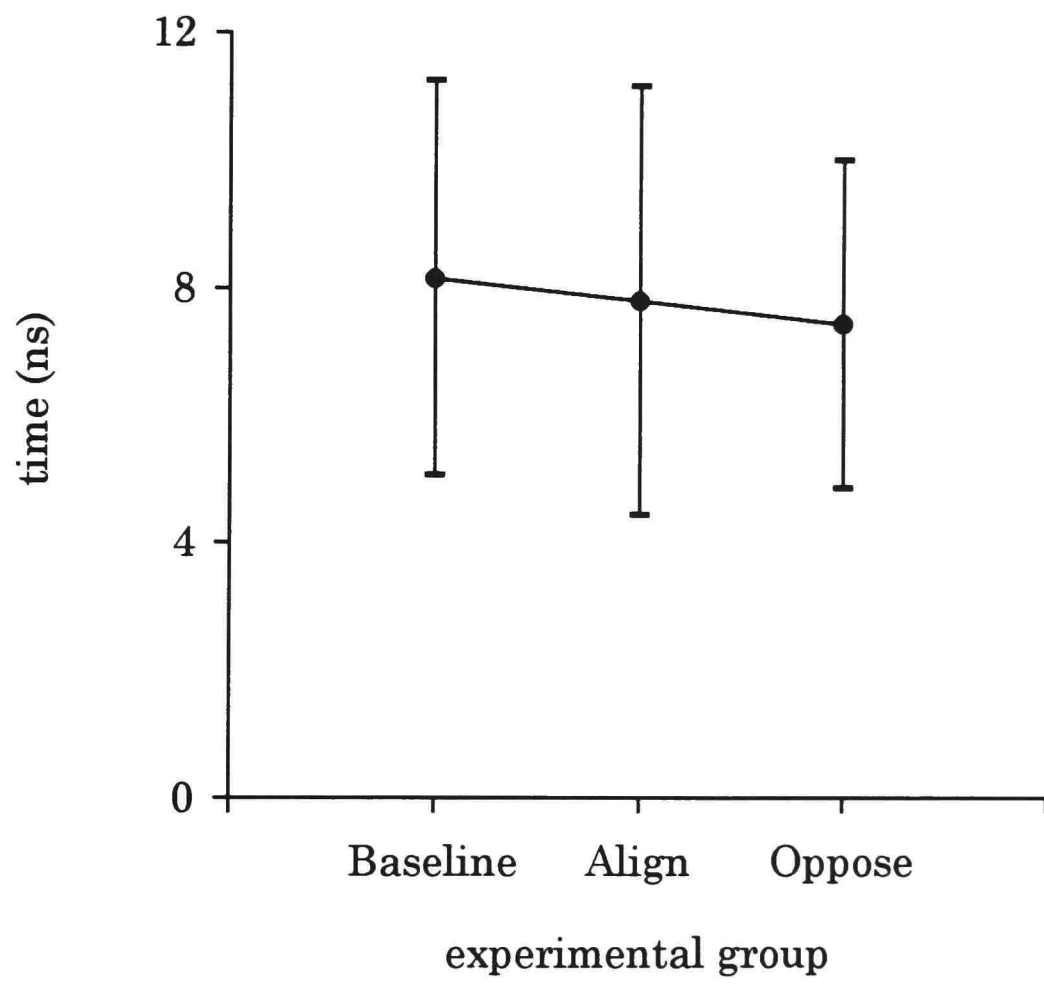


Figure 36. Fall-time with magnets in the anode and cathode.

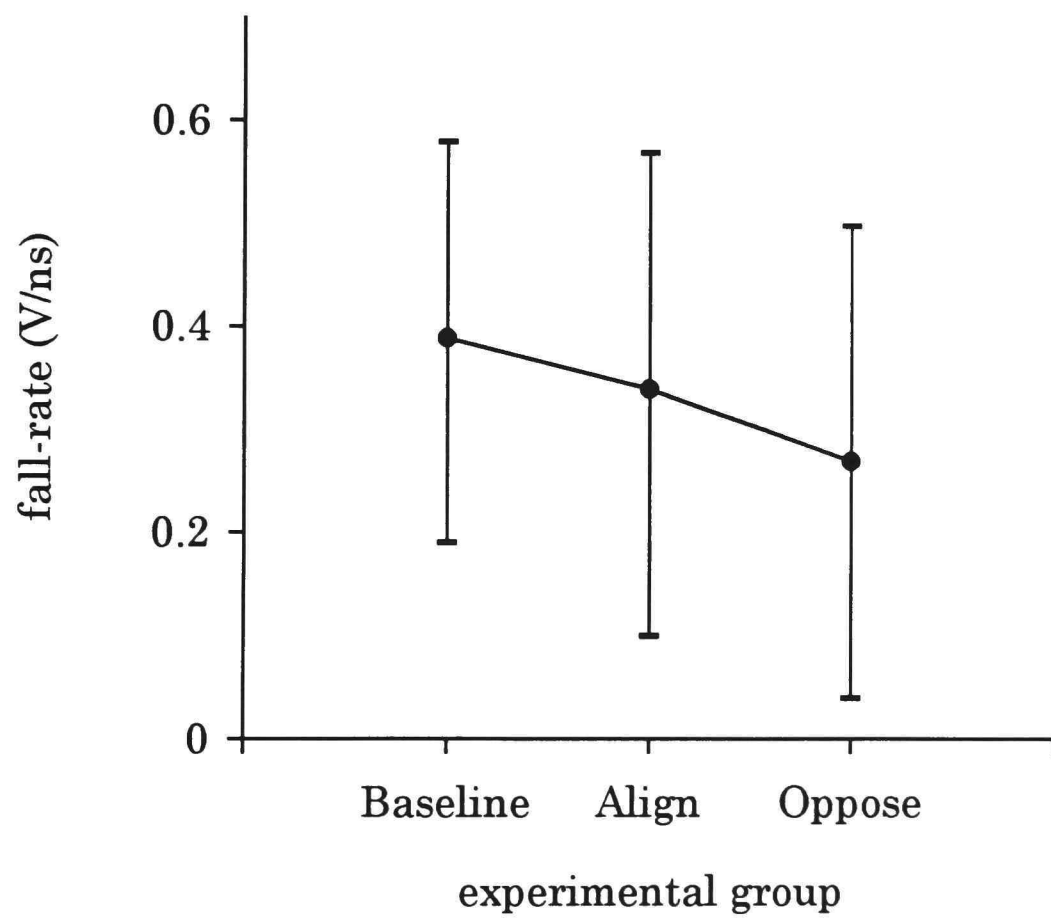


Figure 37. Fall-rate with magnets in the anode and cathode.

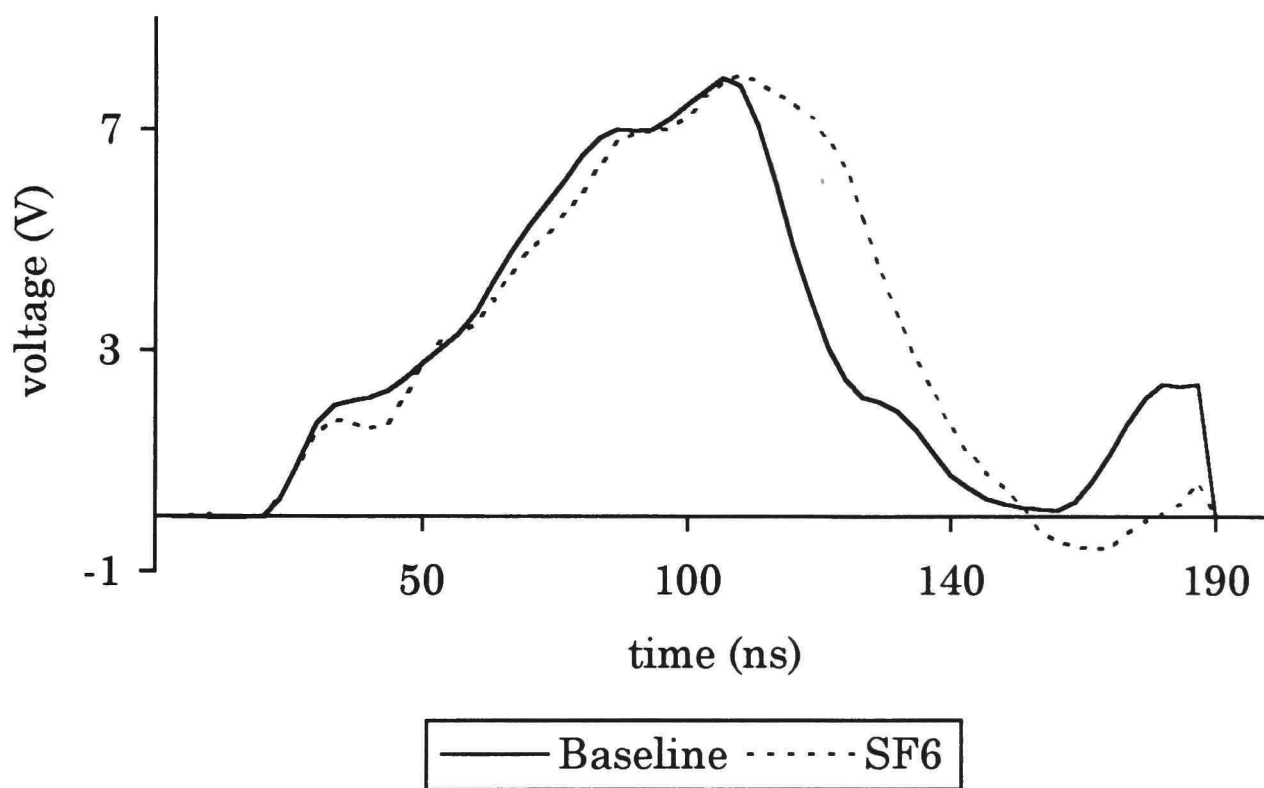


Figure 38. Average waveforms with SF₆ added to the water (first series).

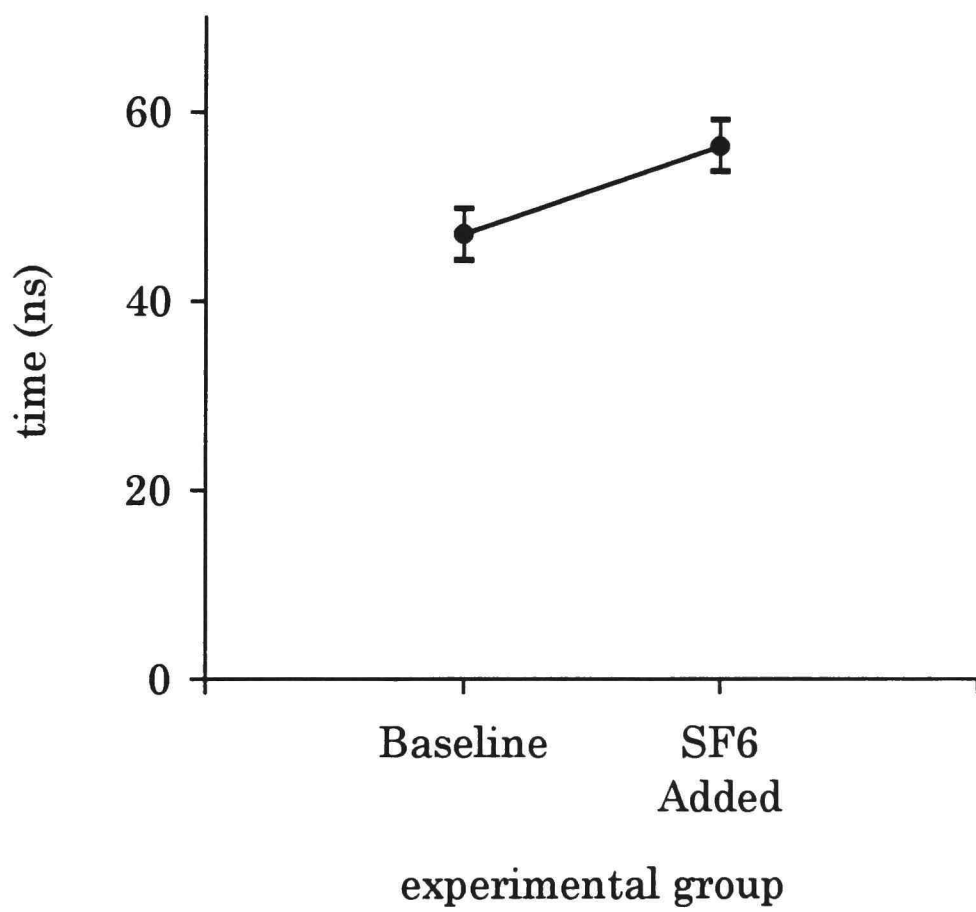


Figure 39. Effective time (τ_{eff}) with SF₆ added (first series).

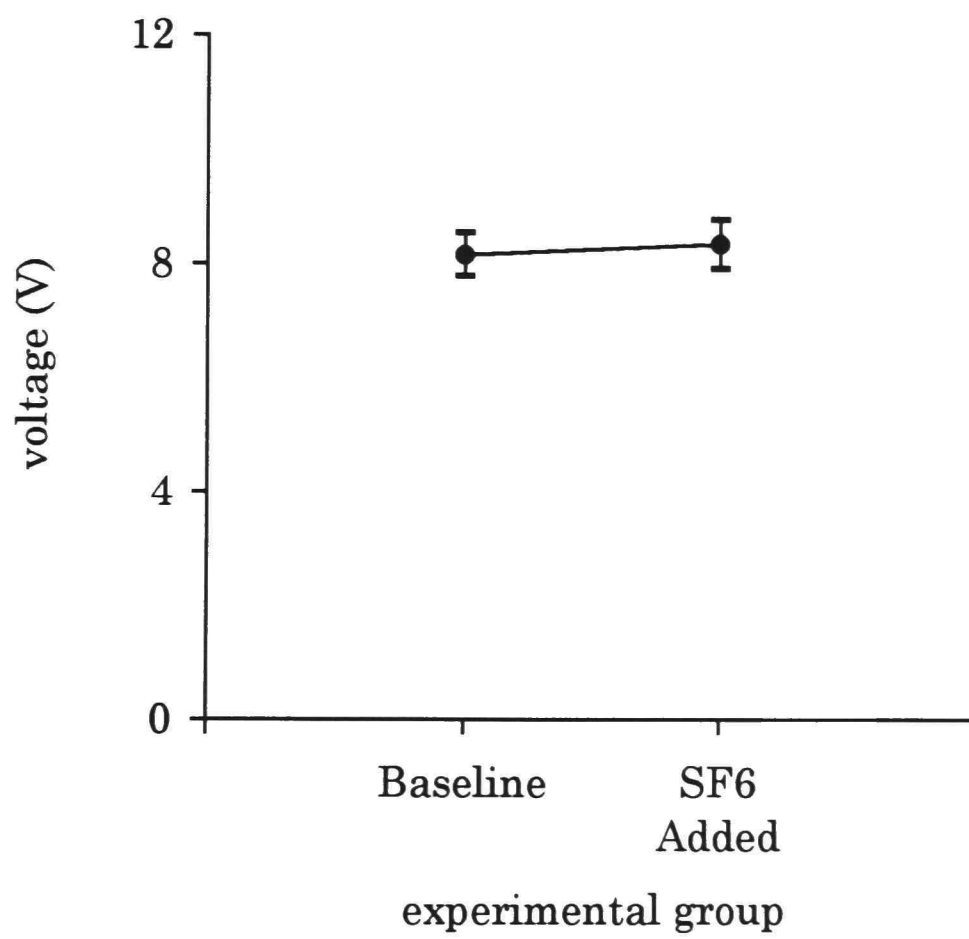


Figure 40. Maximum voltage (V_{\max}) with SF_6 added (first series).

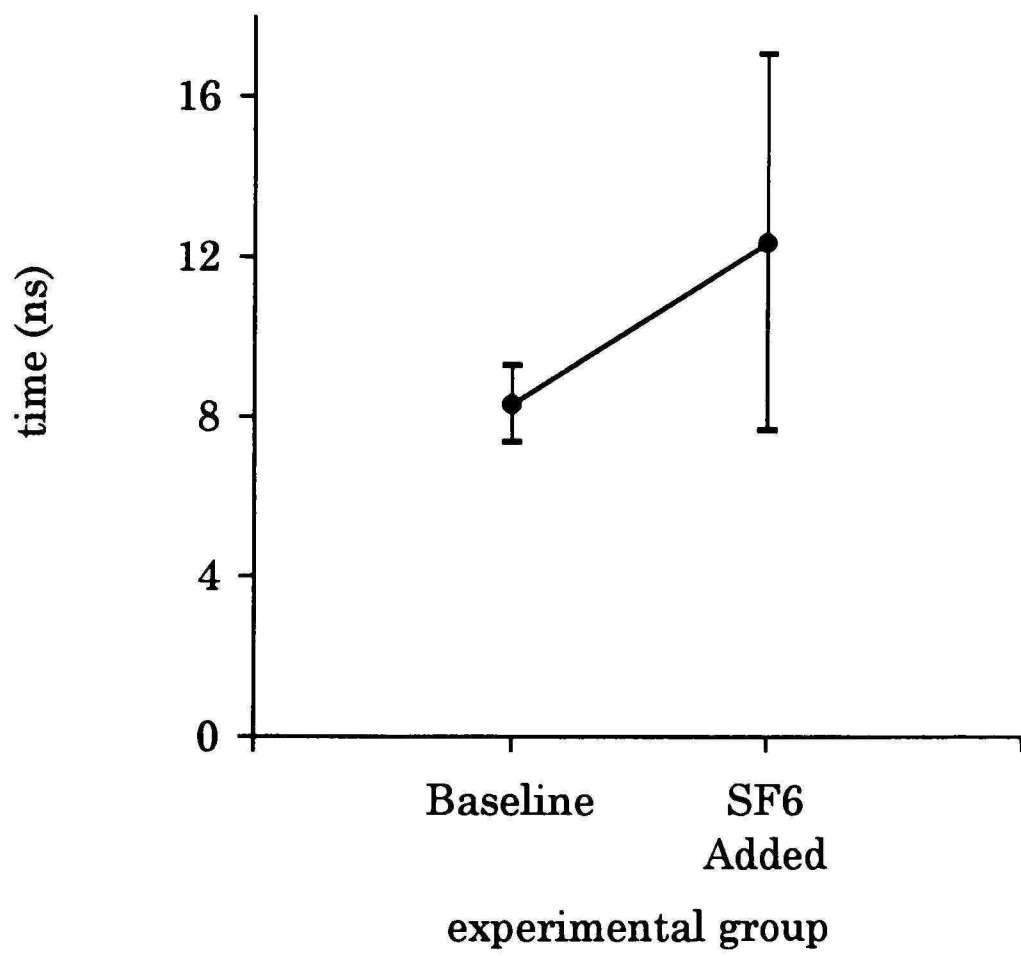


Figure 41. Fall-time with SF₆ added (first series).

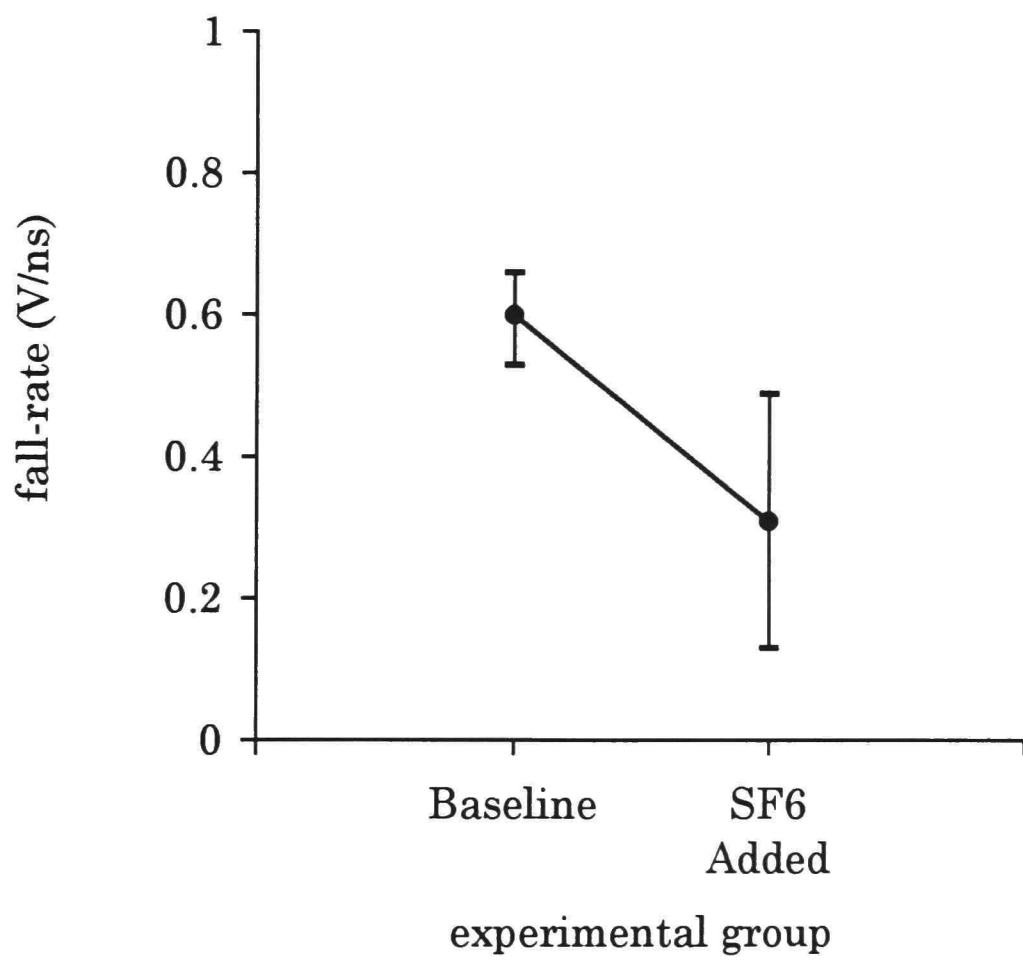


Figure 42. Fall-rate with SF₆ added (first series).

series was a repeat of the first series with the averaged waveforms in Figure 43; values of τ_{eff} , Figure 44; V_{max} , Figure 45; fall-time, Figure 46; and fall-rate, Figure 47. To show the effect the addition of the gas had on the individual waveforms, Figures 48 and 49 contain all twenty of the signals. The variation in the time-width of the signal can be seen by comparing the baseline signals in Figure 48 and the experimental signals in Figure 49.

An analog integrator was used on the last experiment using the SF_6 and accounts for the difference in the appearance of the waveforms and the absolute values of the signal parameters. Figure 50 shows the average waveforms of the three data groups: baseline, SF_6 (2 hours), and SF_6 (24 hours). The values of τ_{eff} for the two groups are shown in Figure 51; V_{max} , Figure 52; fall-time, Figure 53; and fall-rate, Figure 54.

Hydrochloric acid

Figure 55 shows the waveforms for several shots fired using two levels of HCl. The baseline signal and the 10×10^{-4} M HCl signal was captured with a 200 ns time window. The 2×10^{-4} M HCl signal was captured using a 500 ns time window. The first two signals were adjusted to fit on the 500 ns graph and accounts for the truncated appearance of the 10×10^{-4} M signal. Graphs for the four parameters used in the other experimental sets were not generated for this first set of signals. An ANOVA was not calculated for this

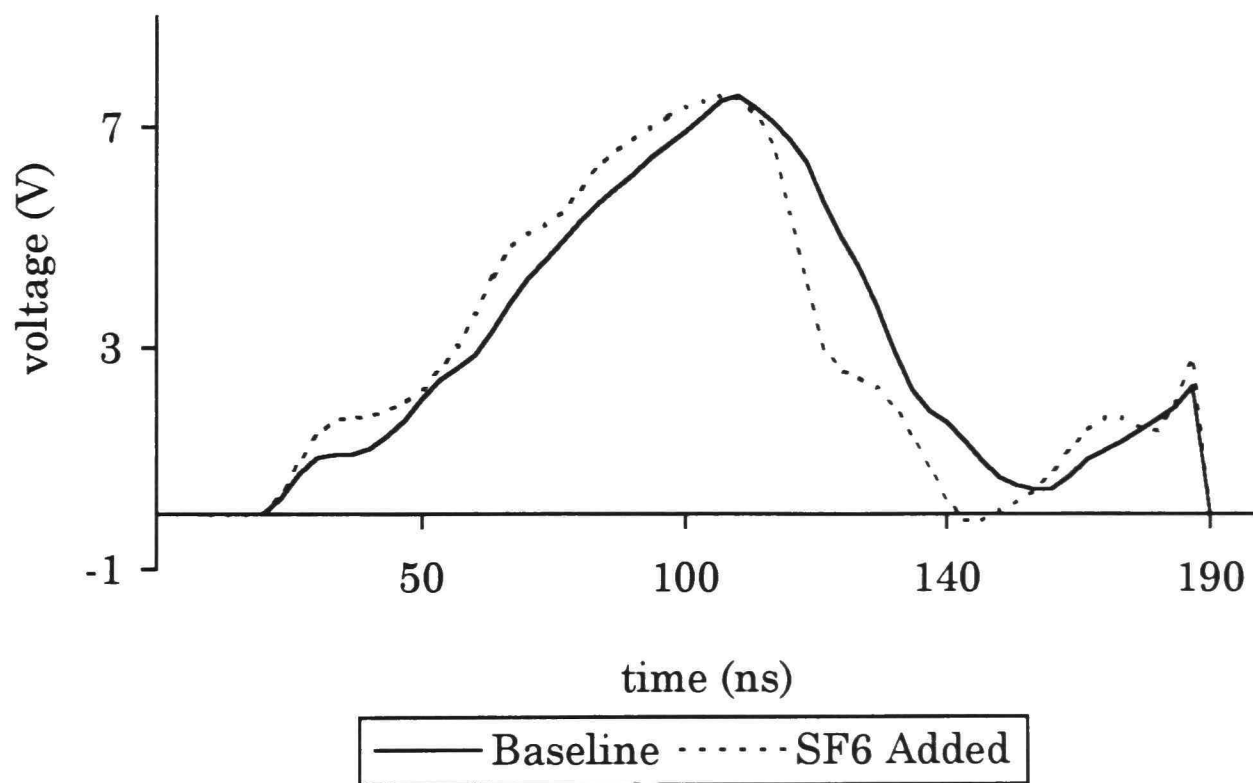


Figure 43. Average waveforms with SF₆ added to the water (second series).

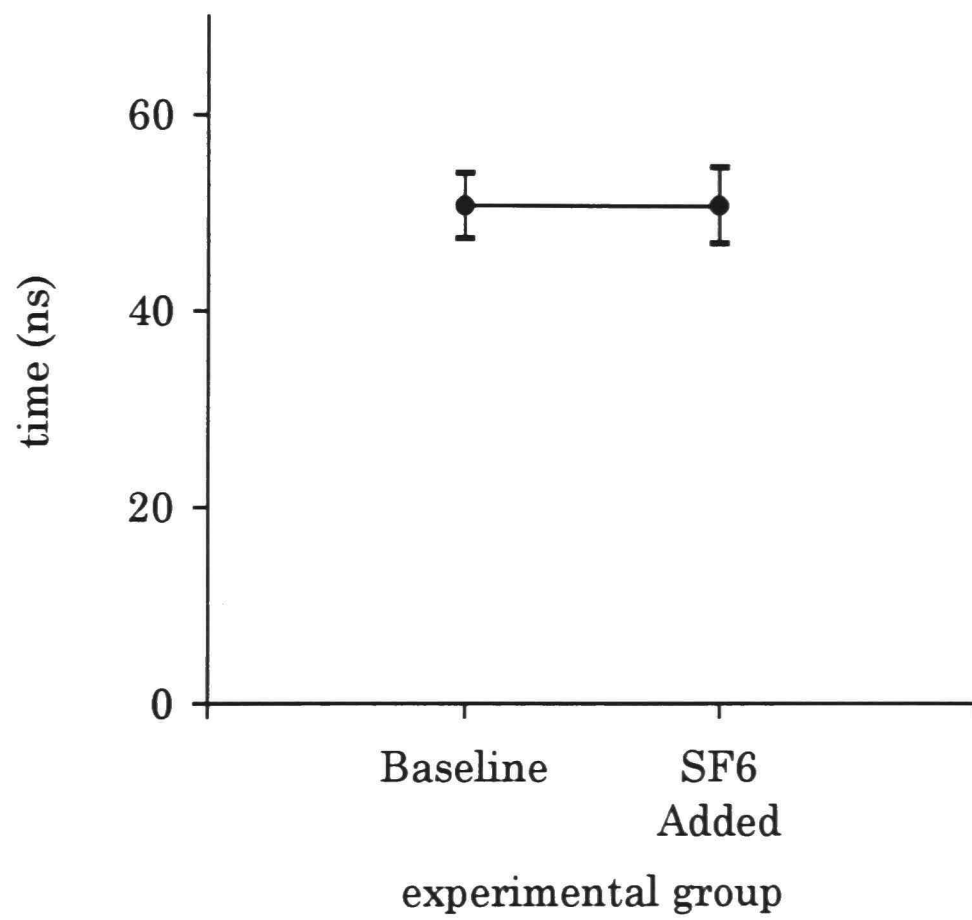


Figure 44. Effective time (τ_{eff}) with SF₆ added (second series).

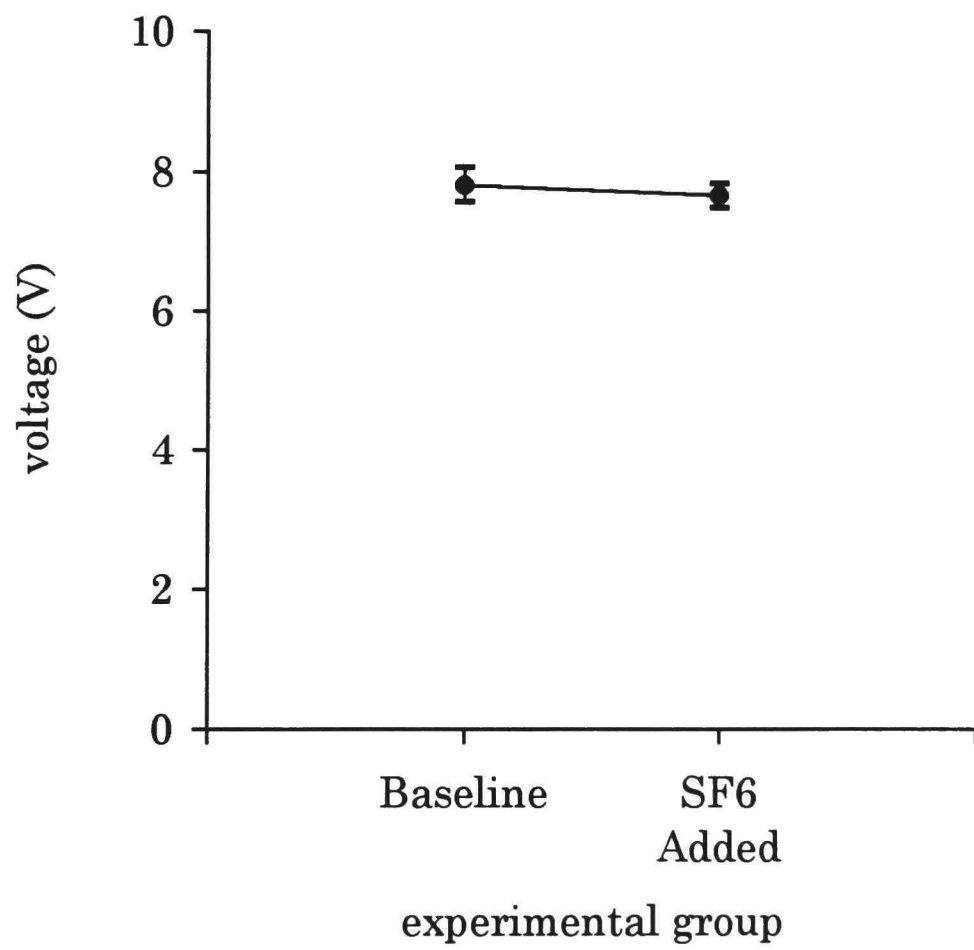


Figure 45. Maximum voltage (V_{max}) with SF₆ added (second series).

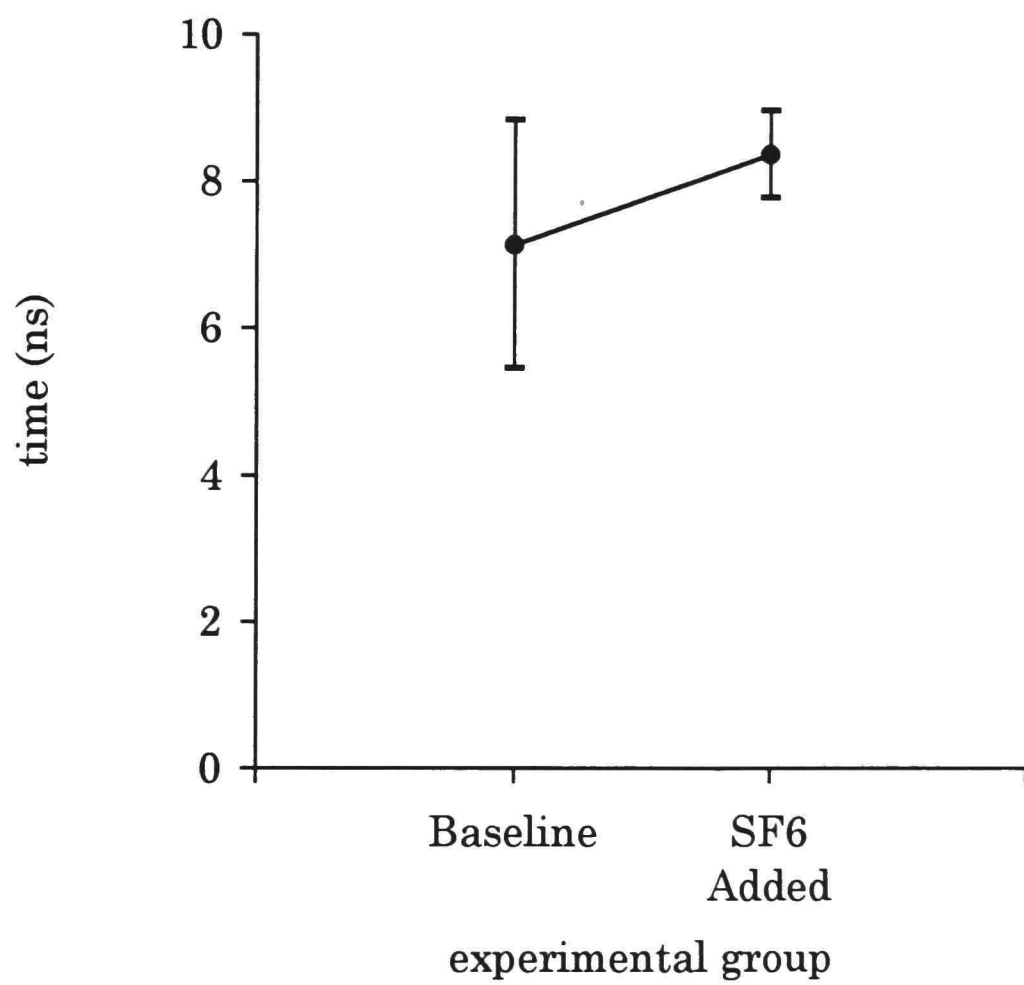


Figure 46. Fall-time with SF₆ added (second series).

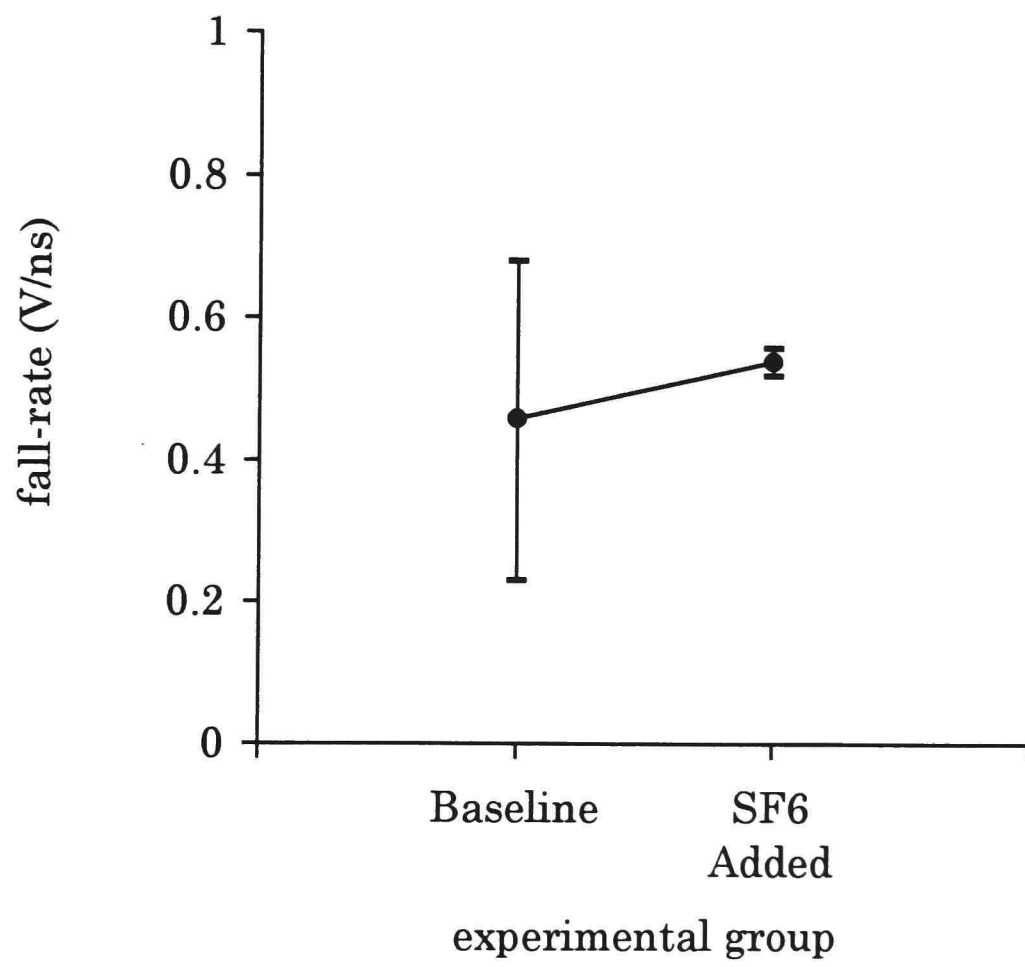


Figure 47. Fall-rate with SF₆ added (second series).

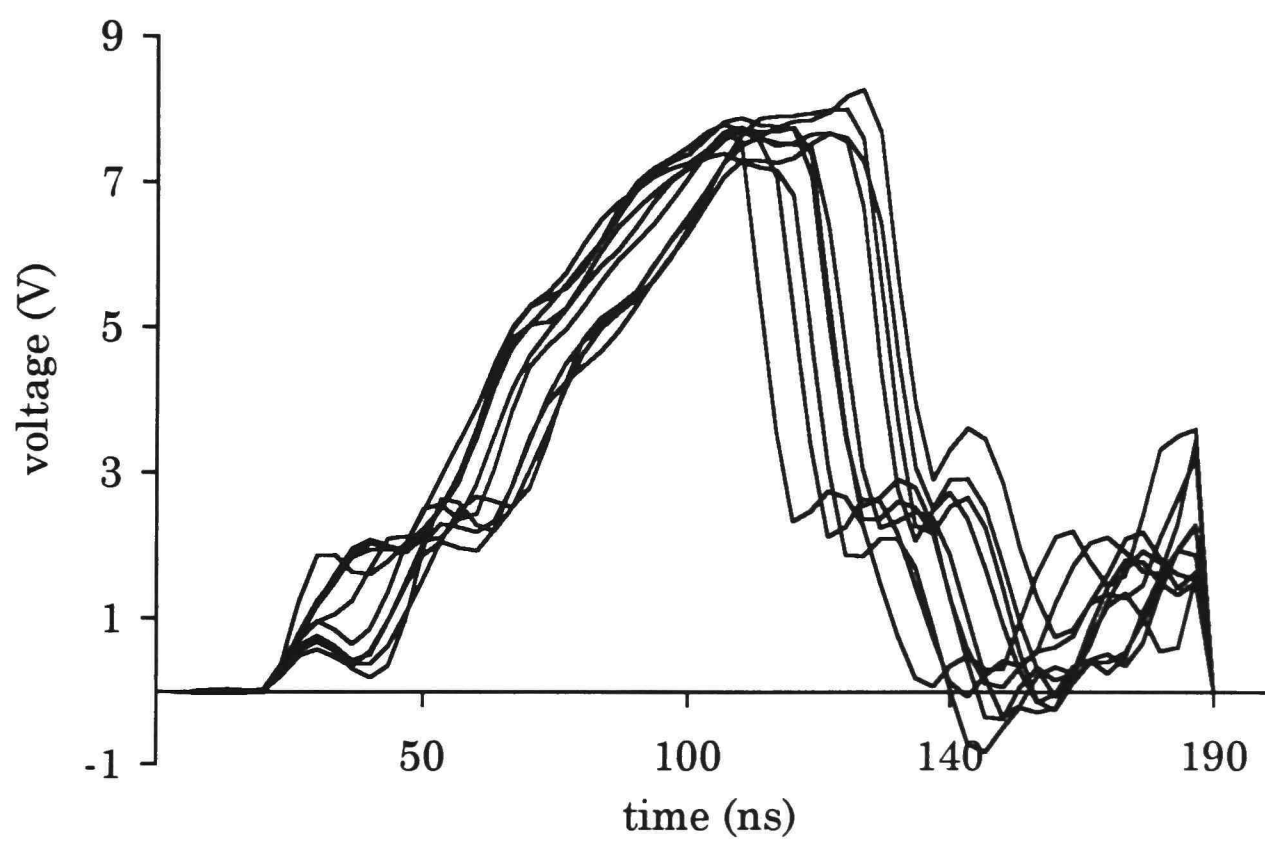


Figure 48. The ten baseline waveforms for the SF₆ second series of shots.

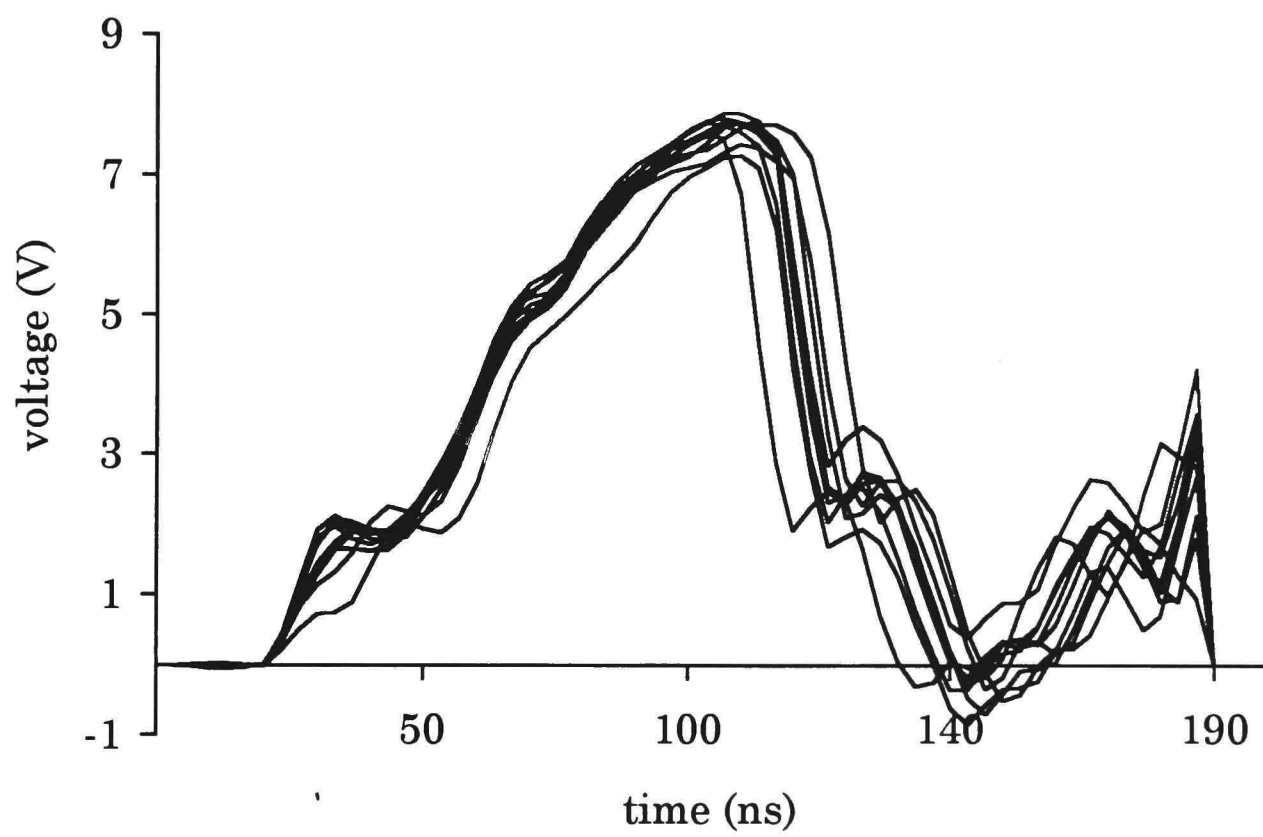


Figure 49. The ten waveforms with SF₆ added to the water (second series).

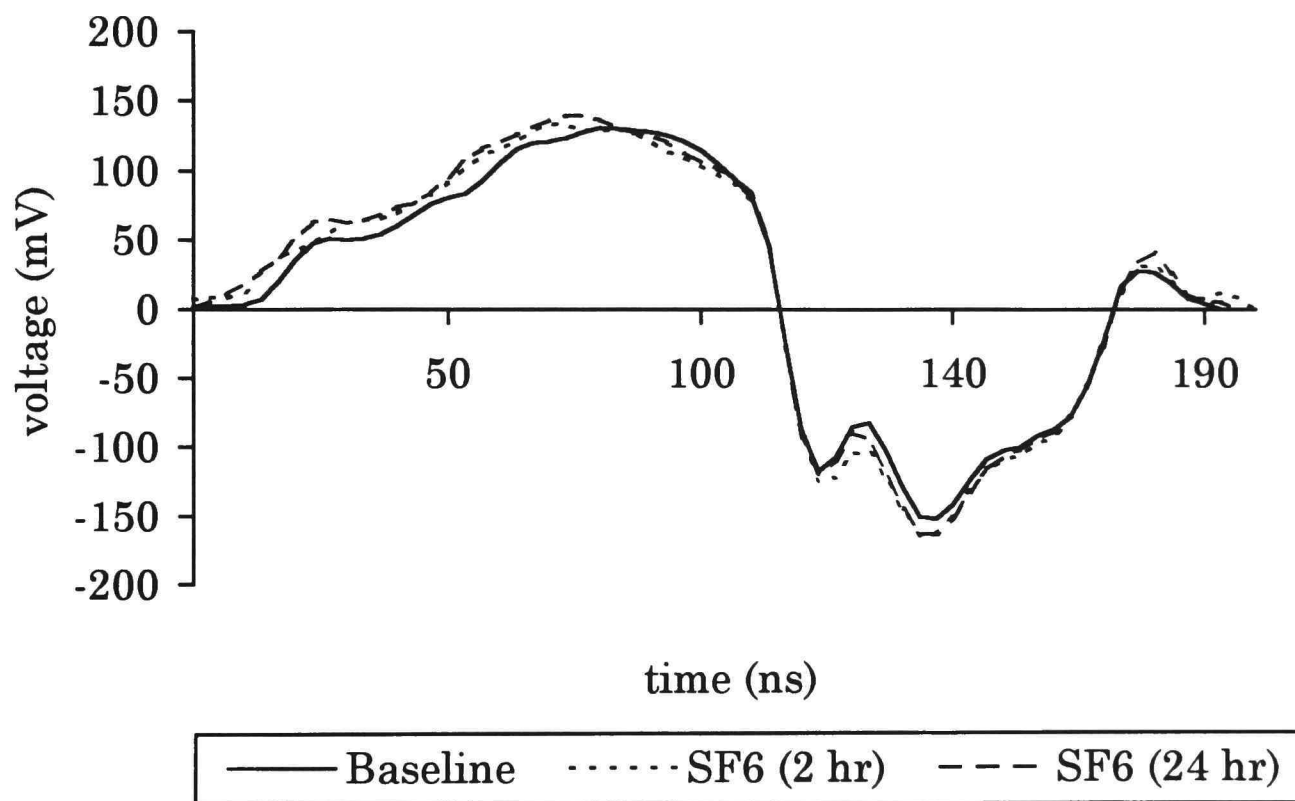


Figure 50. Average waveforms with SF₆ added to the water (third series).

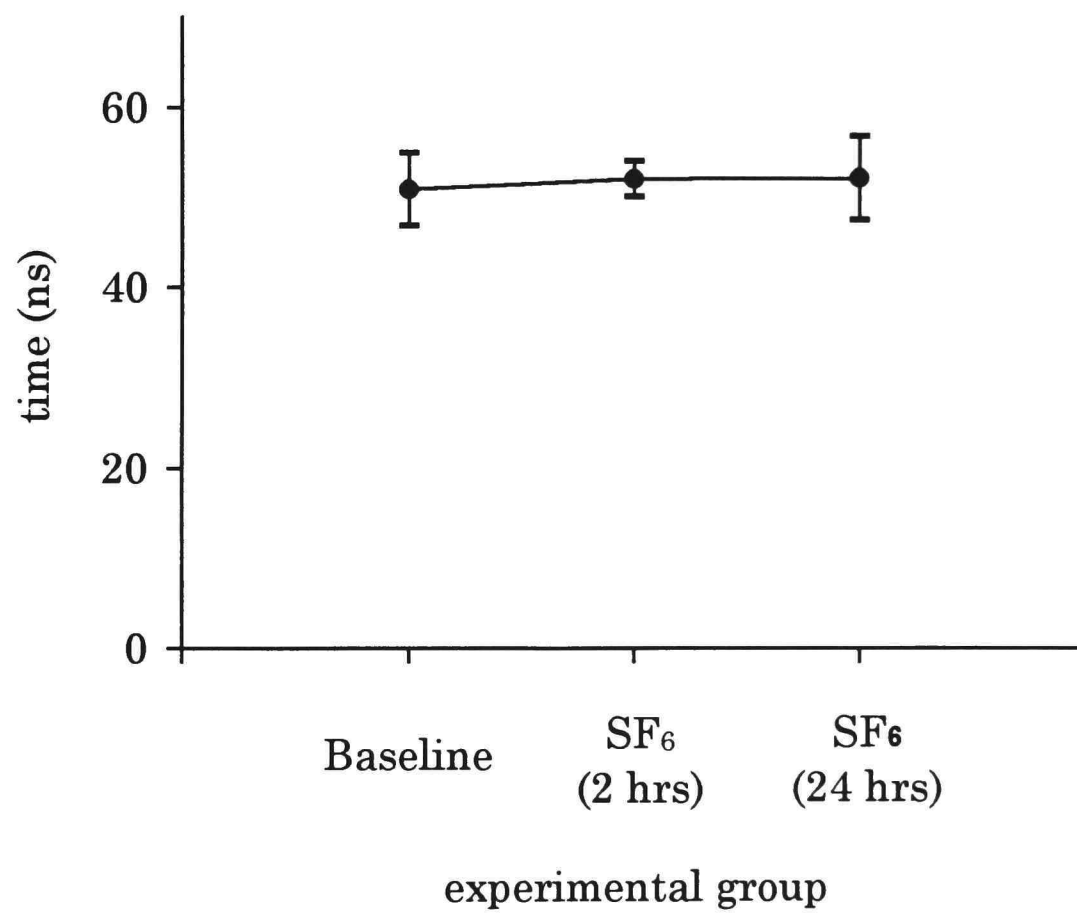


Figure 51. Effective time (τ_{eff}) with SF₆ added (third series).

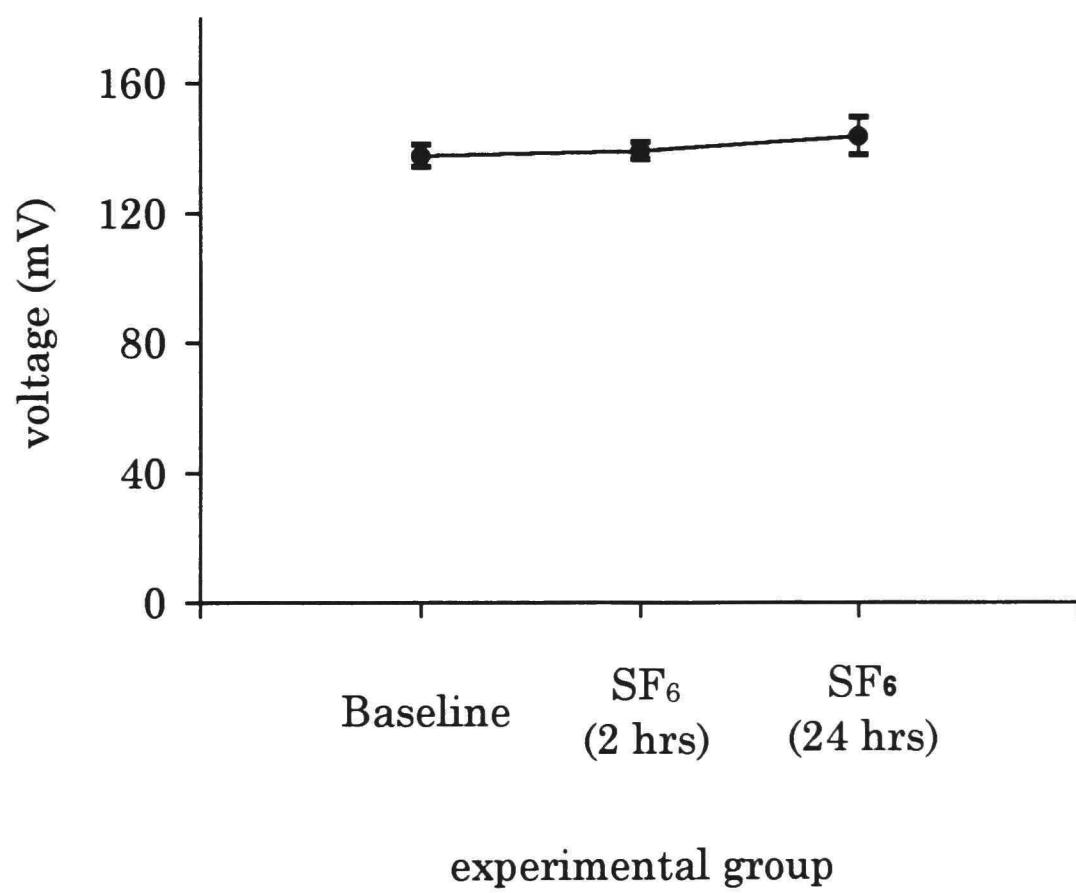


Figure 52. Maximum voltage (V_{\max}) with SF₆ added (third series).

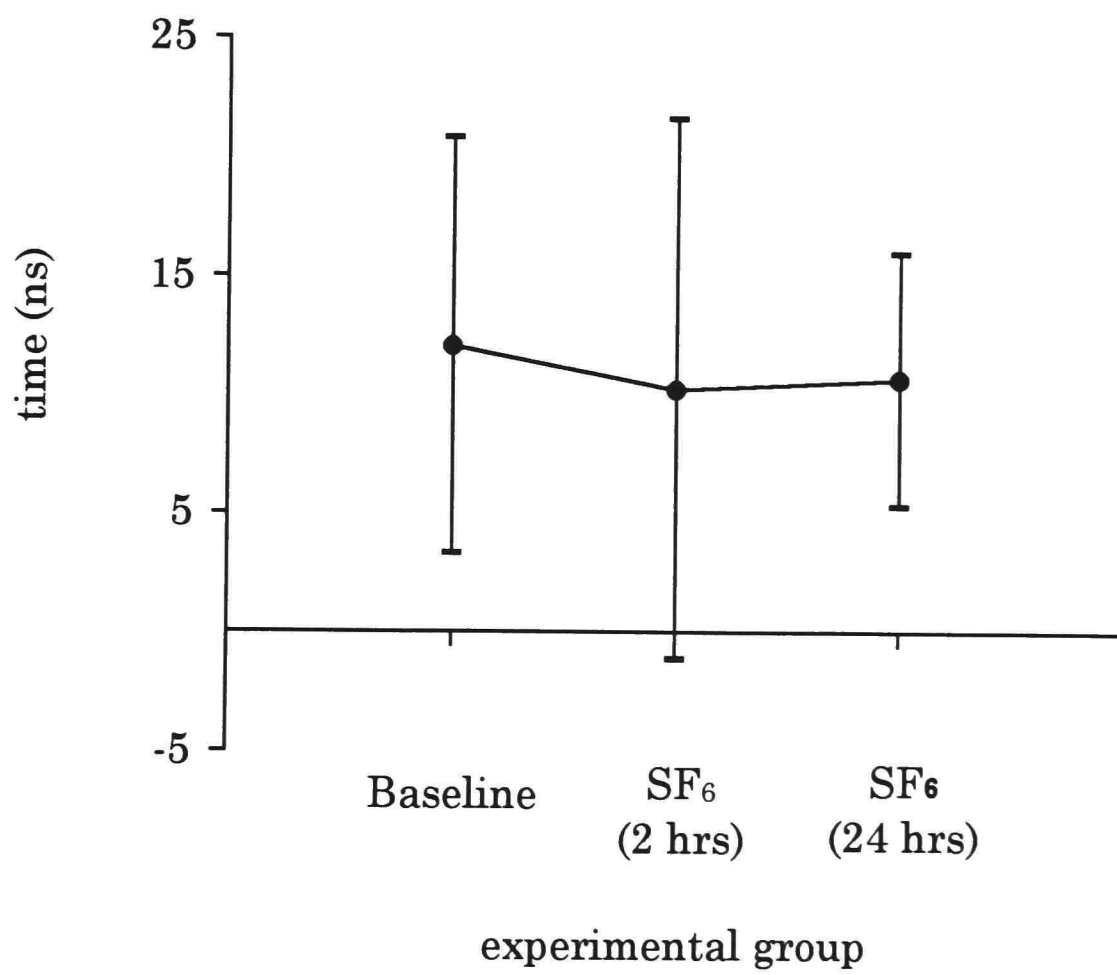


Figure 53. Fall-time with SF₆ added (third series).

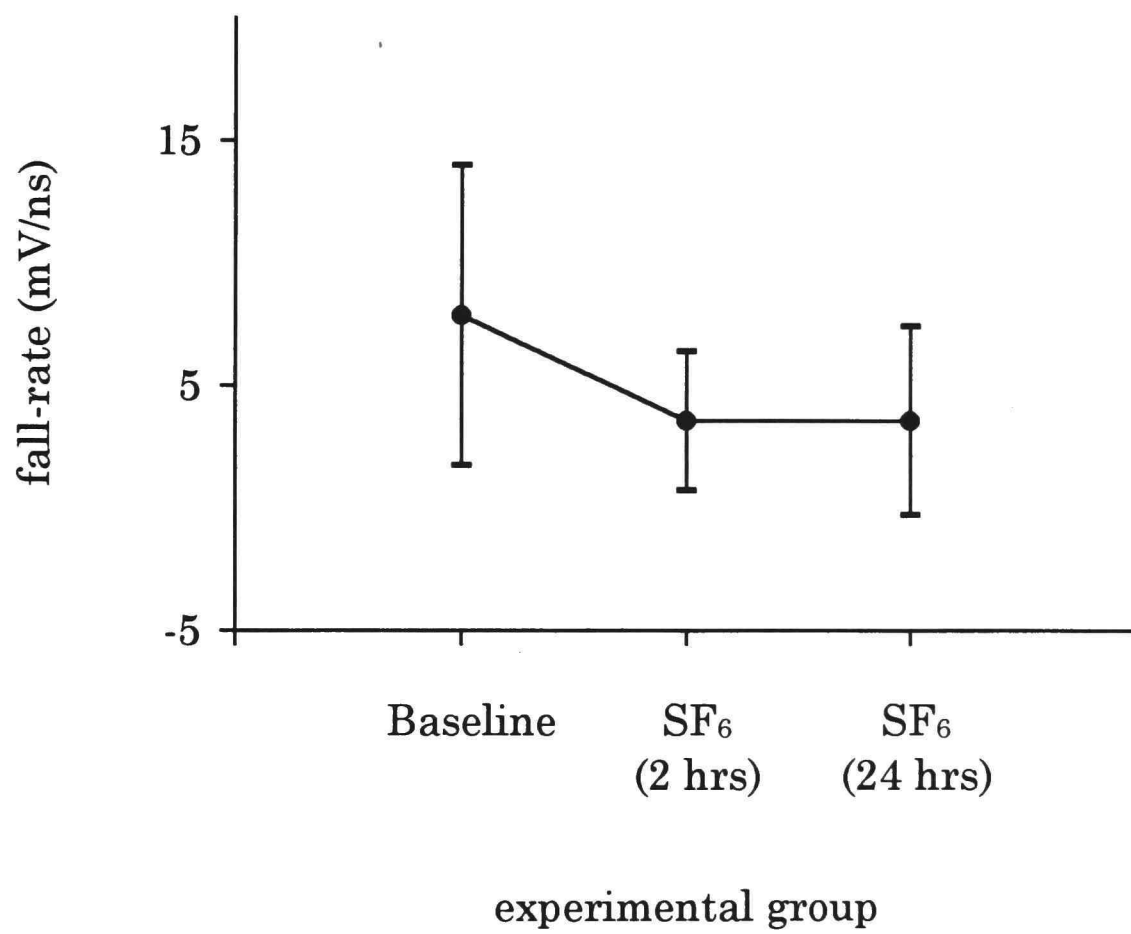


Figure 54. Fall-rate with SF₆ added (third series).

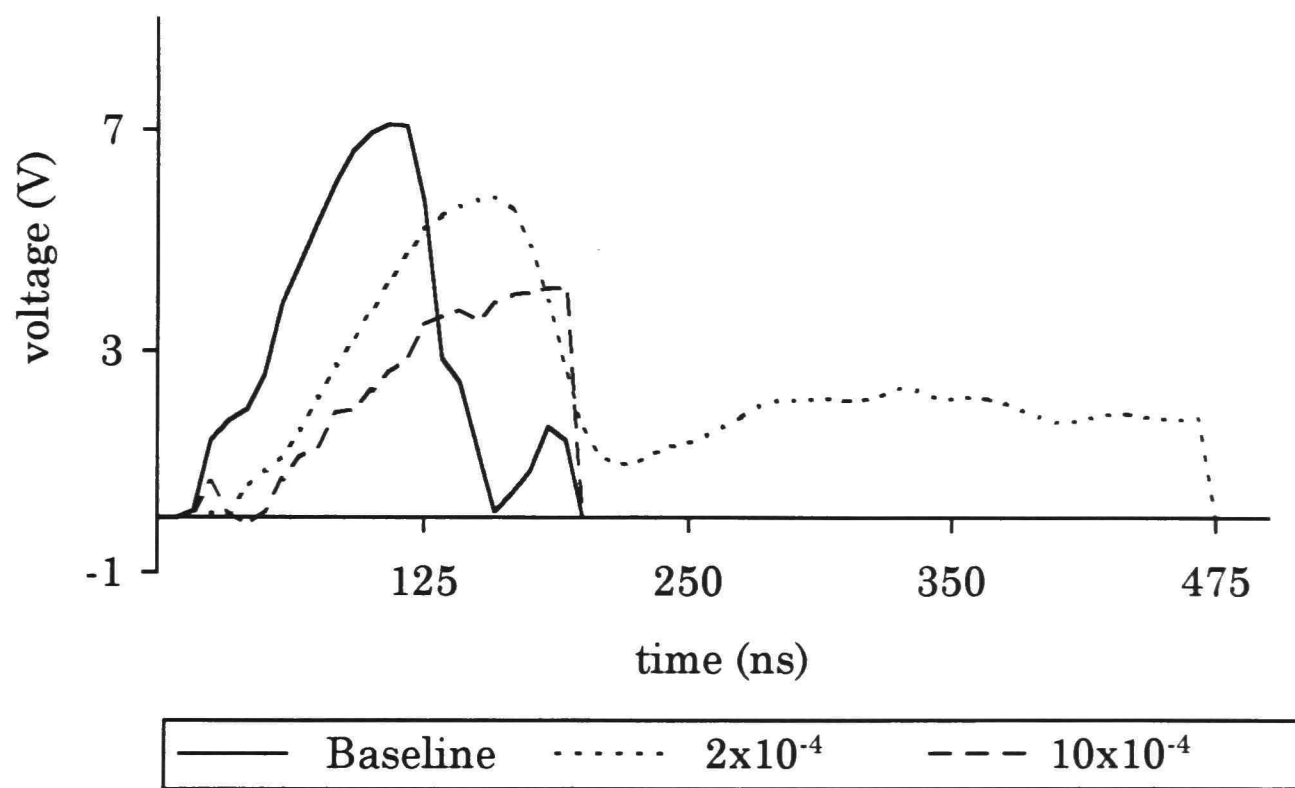


Figure 55. Waveforms for various amounts of HCl added to the water.

data because of the different time windows used and was used to plan the second experiment. The analog integrator was not used for this series.

For the second HCl experiment, five different levels of HCl were used along with the baseline. Figure 56 shows the averaged waveforms for the baseline, 0.1×10^{-4} M, 0.5×10^{-4} M, 1.0×10^{-4} M, 5.0×10^{-4} M, and 10.0×10^{-4} M. The same parameters were looked at as in the previous experiments: τ_{eff} , V_{max} , fall-time, and fall-rate. Figures 57 through 60 show the mean values and the standard deviation for each of these parameters.

Polymer coatings

Figure 61 shows the waveforms for the shots fired using the different sets of polymer coatings. Figures 62 through 65 show the mean value and the standard deviation for the baseline and the value from the one shot of each of the different sets of polymer coatings. Since there was only one shot fired with each of the four combinations of the two polymer coatings, the standard deviation could not be calculated.

Three things are significant about the series of shots with the polymer coatings. The first is the data was collected using the new Tektronix SCD5000 digitizers, the second is the use of stainless steel electrodes, and the third is the second voltage "hump" seen on the baseline shots. On some of the previous shots, there would be a small rise in the voltage after the

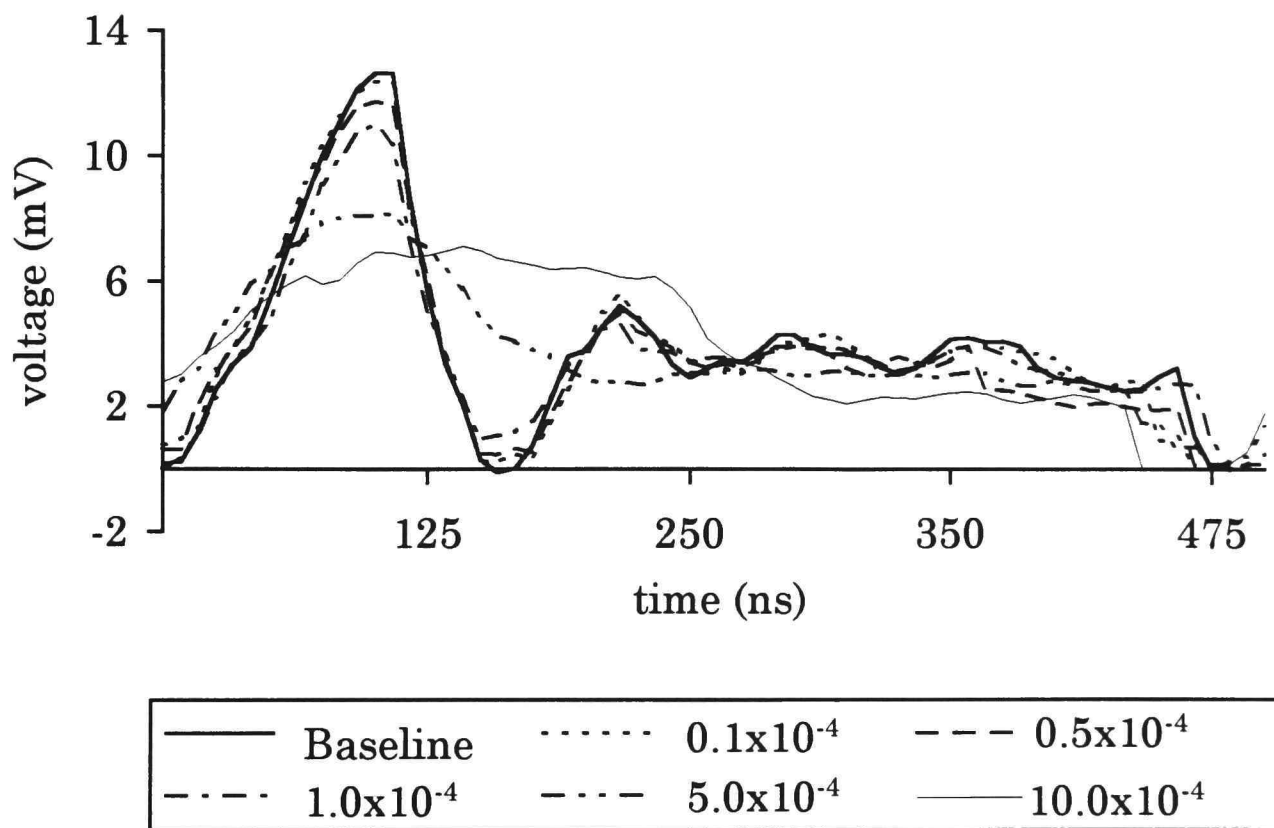


Figure 56. Average waveforms for various amounts of HCl added to the water (second series).

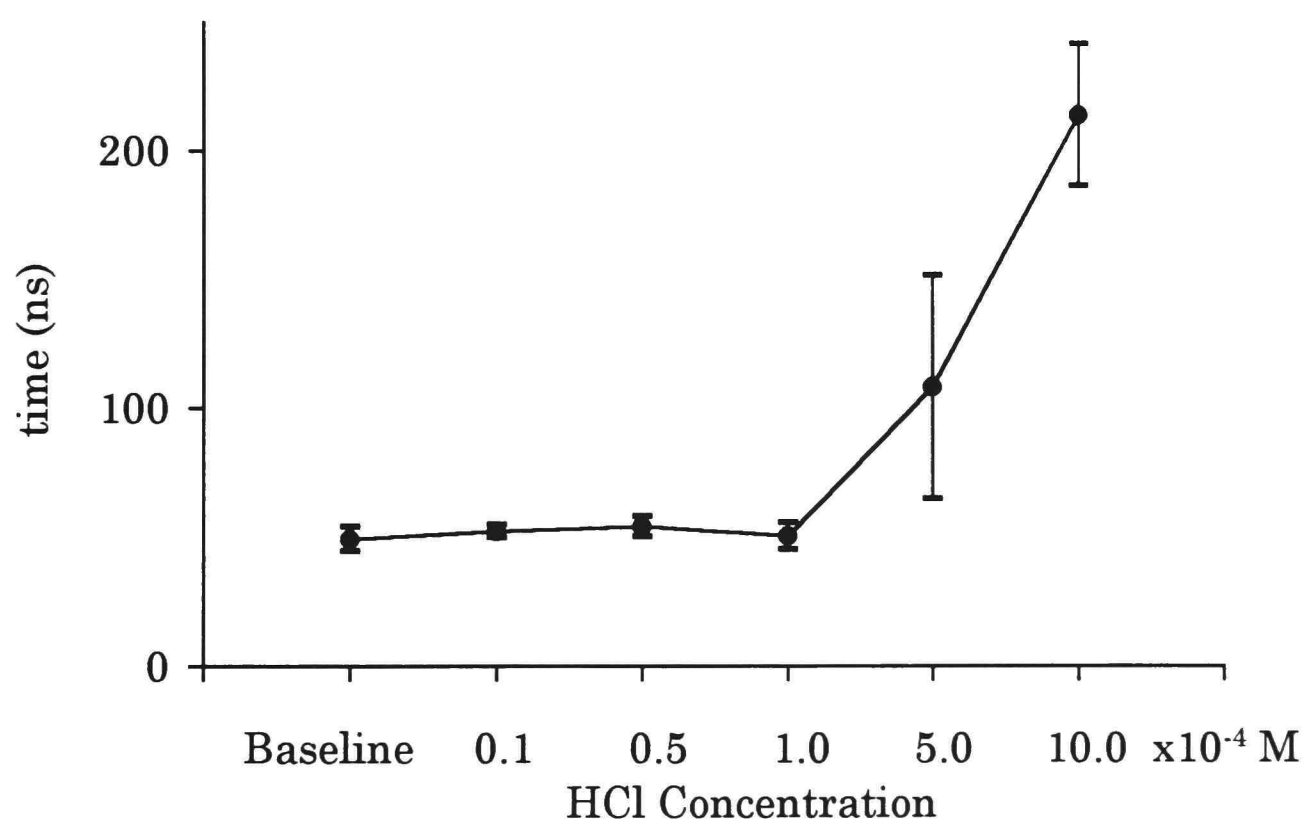


Figure 57. Effective time (τ_{eff}) with HCl added (second series).

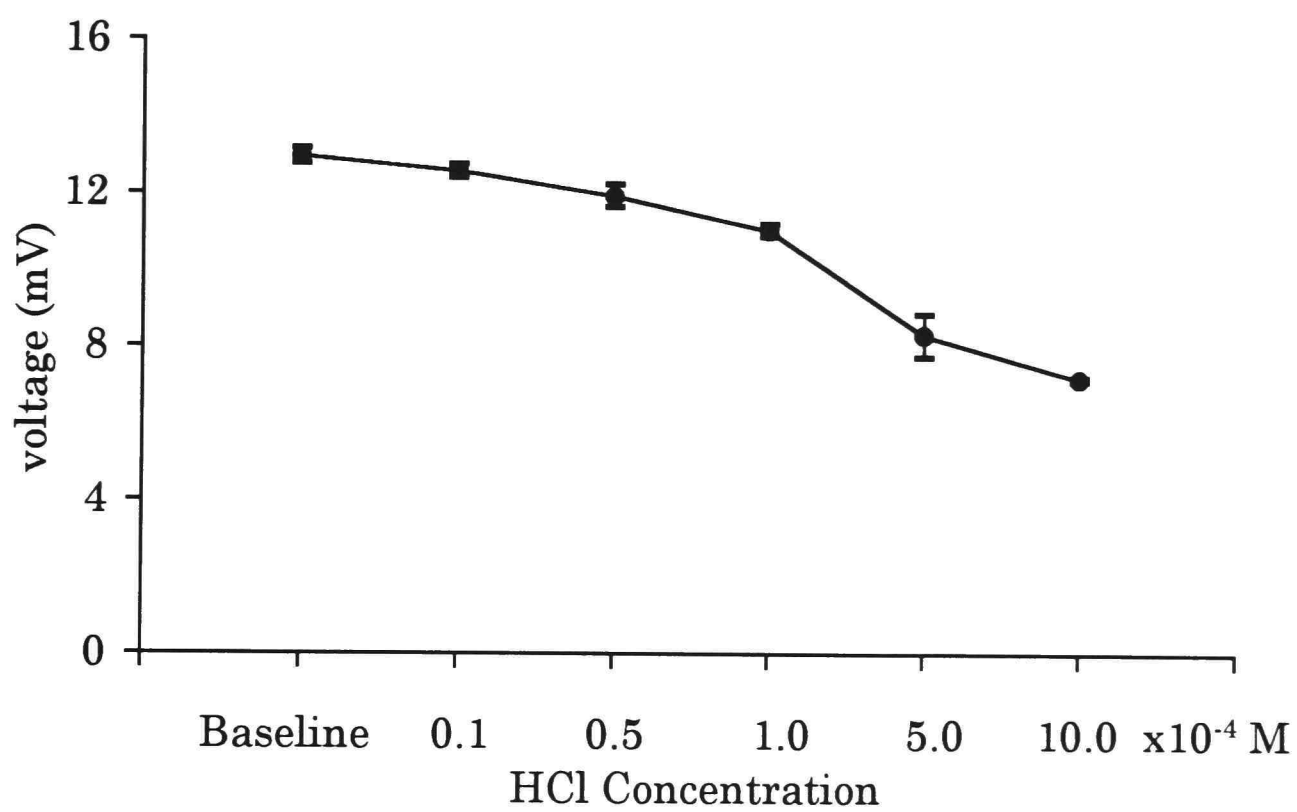


Figure 58. Maximum voltage (V_{\max}) with HCl added (second series).

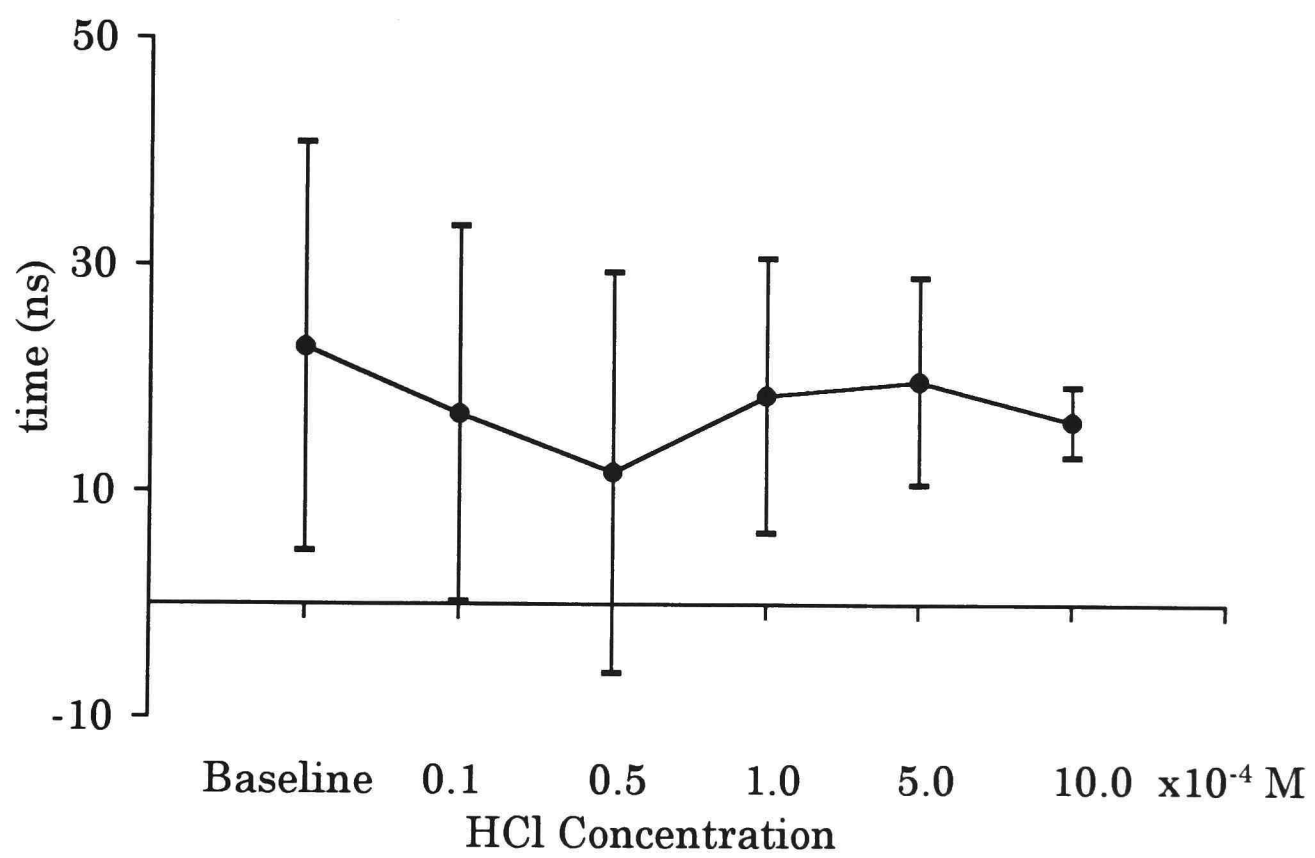


Figure 59. Fall-time with HCl added (second series).

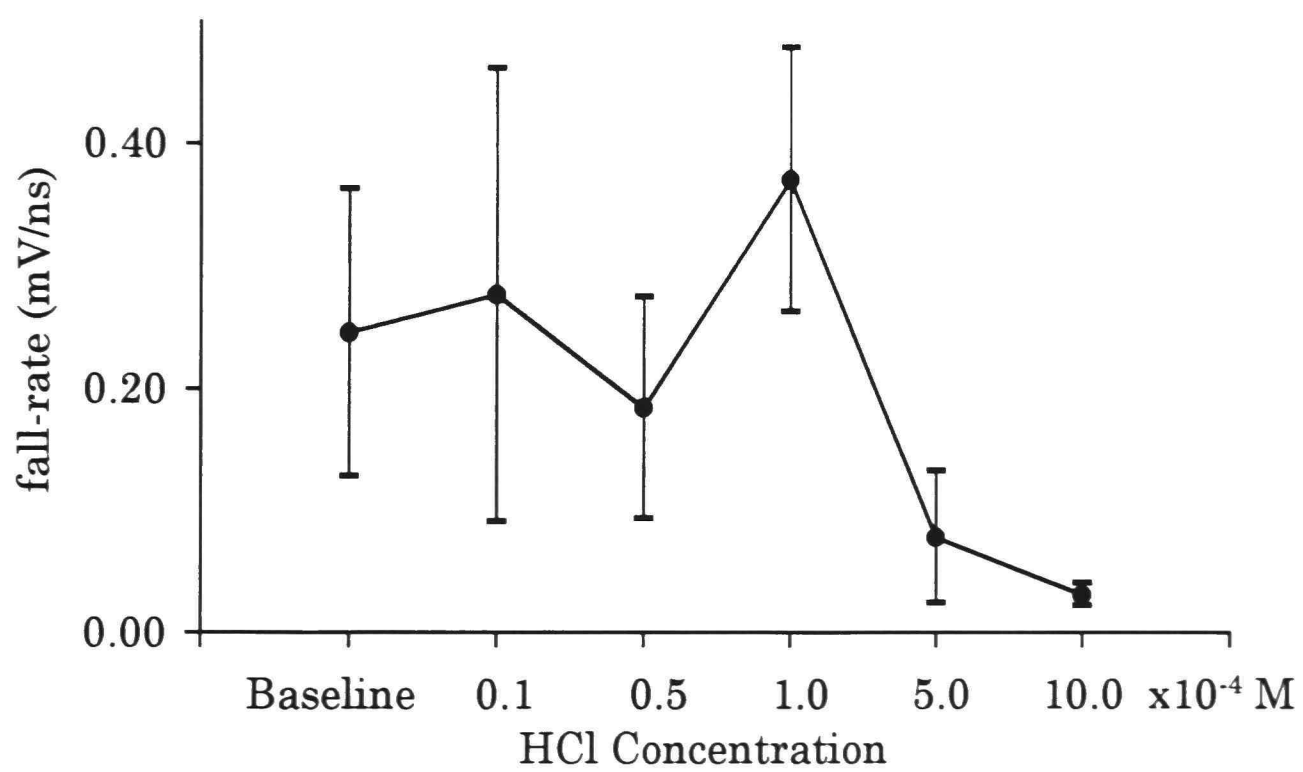


Figure 60. Fall-rate with HCl added (second series).

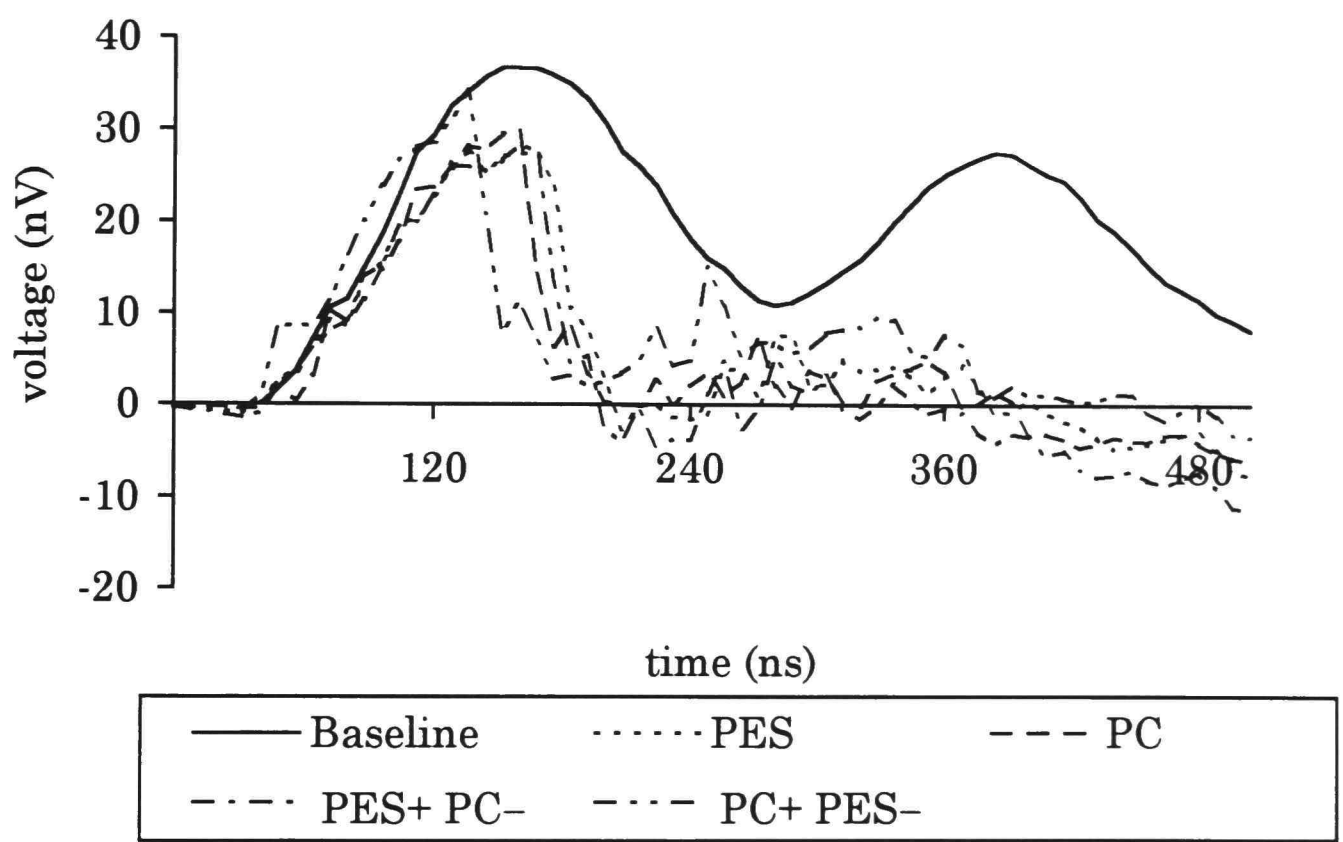


Figure 61. Average waveforms with polymer coatings on the electrodes.

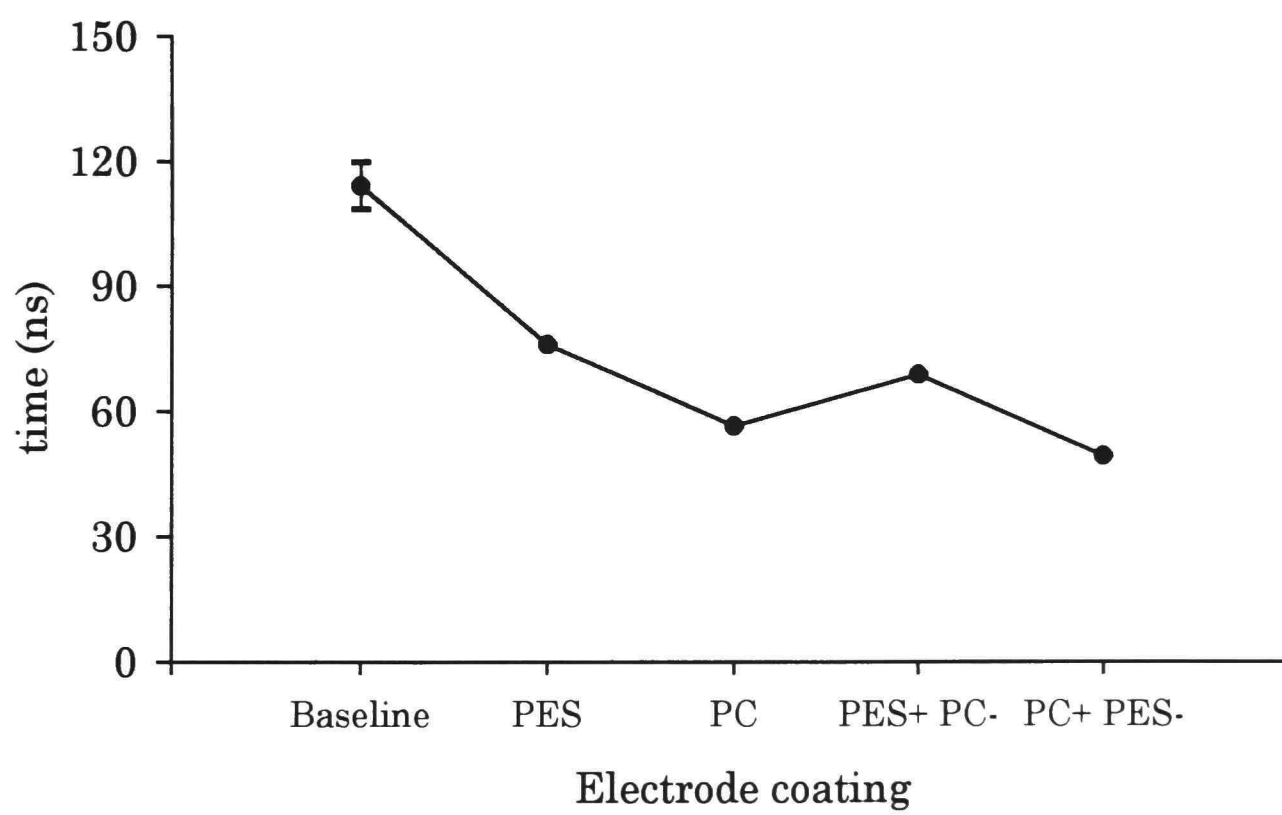


Figure 62. Effective time (τ_{eff}) with polymer coatings on the electrodes.

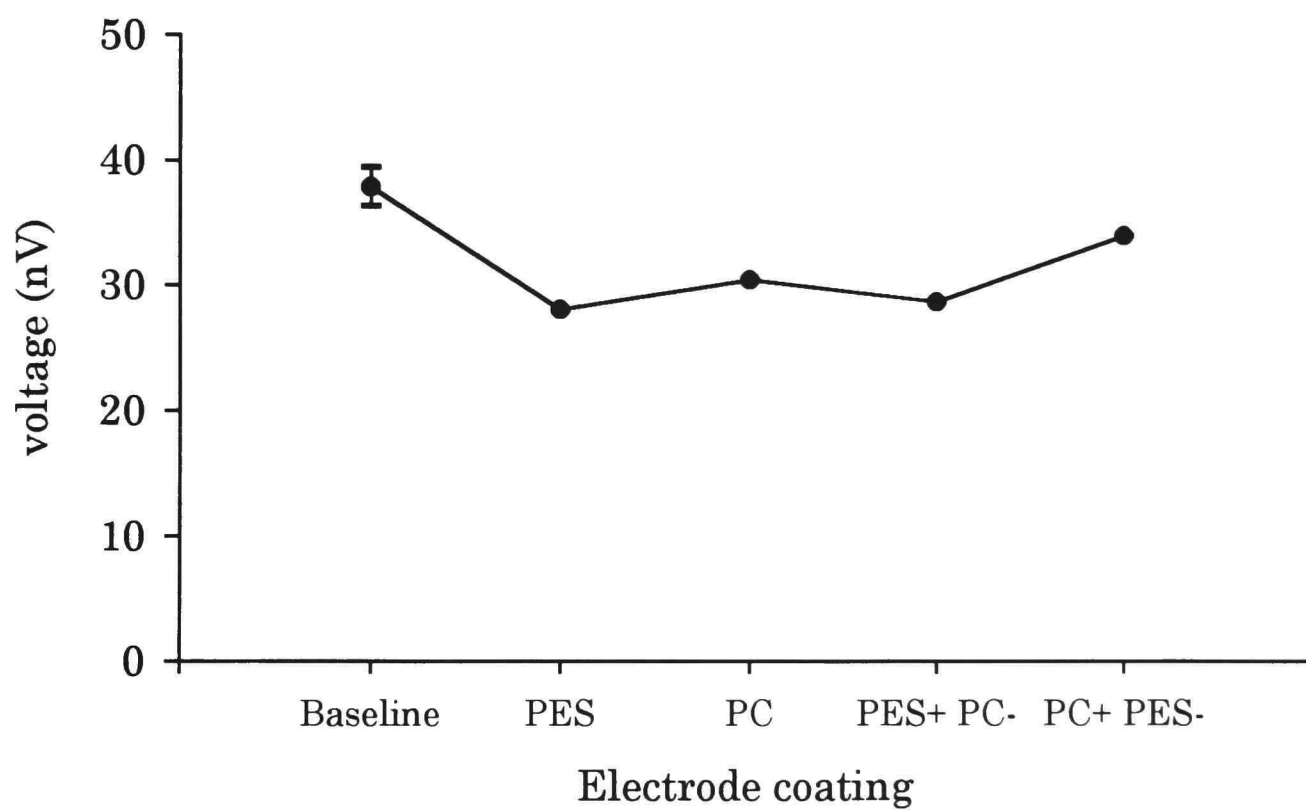


Figure 63. Maximum voltage (V_{\max}) with polymer coatings on the electrodes.

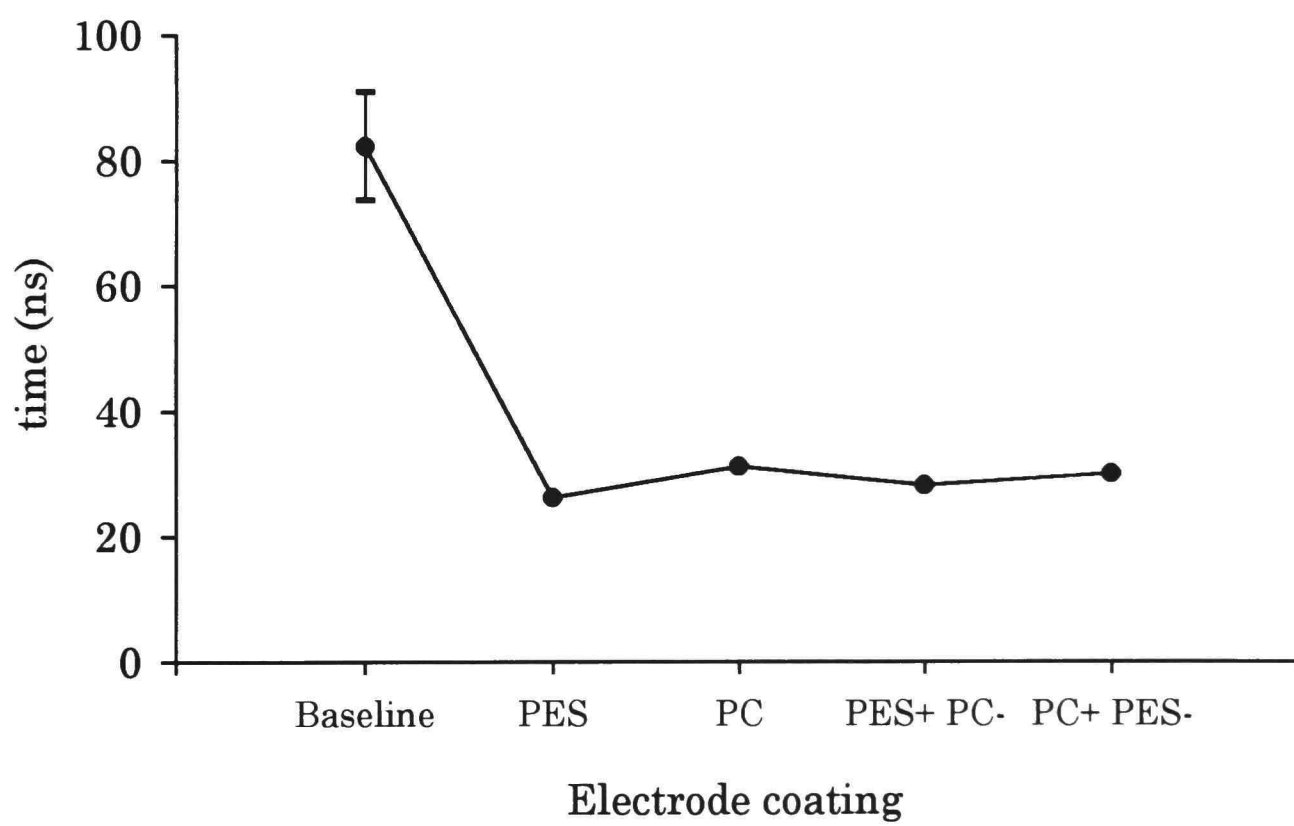


Figure 64. Fall-time with polymer coatings on the electrodes.

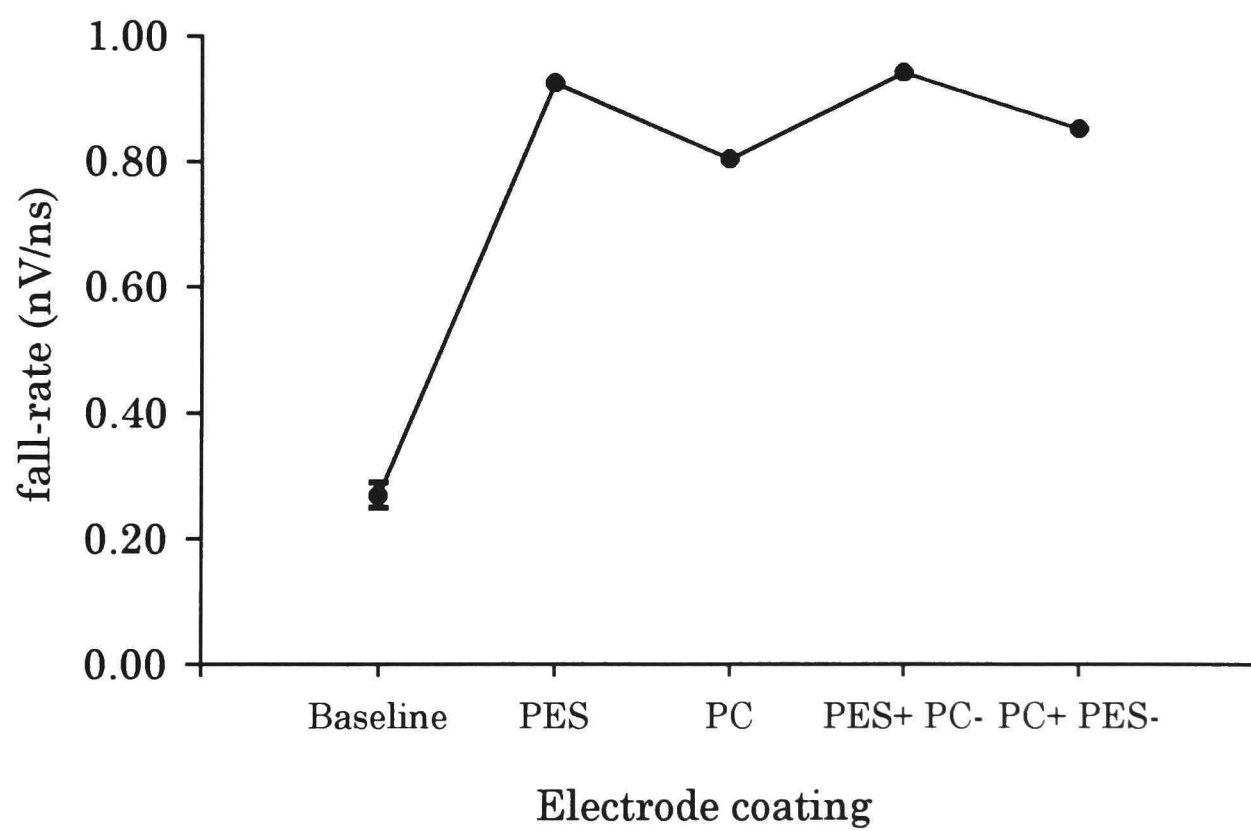


Figure 65. Fall-rate with polymer coatings on the electrodes.

voltage dropped from its maximum but it was usually insignificant when compared to the main voltage pulse. This second voltage “hump” is seen in Figure 61 (solid line) and appears to be a reflection of the initial voltage pulse. Any type of coating on the electrodes would cause the reflection to disappear. Several attempts were made to recreate this phenomena with the PSPICE model but proved to be unsuccessful. Also, when the copper tungsten electrodes were put back in the test chamber, the reflection disappeared again. The reflection seems to be caused by the use of the stainless steel electrodes but it is not clear why the type of electrode alone would cause such an effect.

Black wax

Figure 66 shows the average waveforms for the ten baseline shots and the ten shots fired with black wax on both electrodes. Figures 67 through 70 show the mean values and the standard deviations for the baseline signals and the signals with the black wax on the electrodes for each of the four parameters: τ_{eff} , V_{max} , fall-time, and fall-rate.

Anodized aluminum

Figure 71 shows the average waveforms for the eight baseline shots and the two shots with anodized aluminum electrodes. Figure 72 shows the

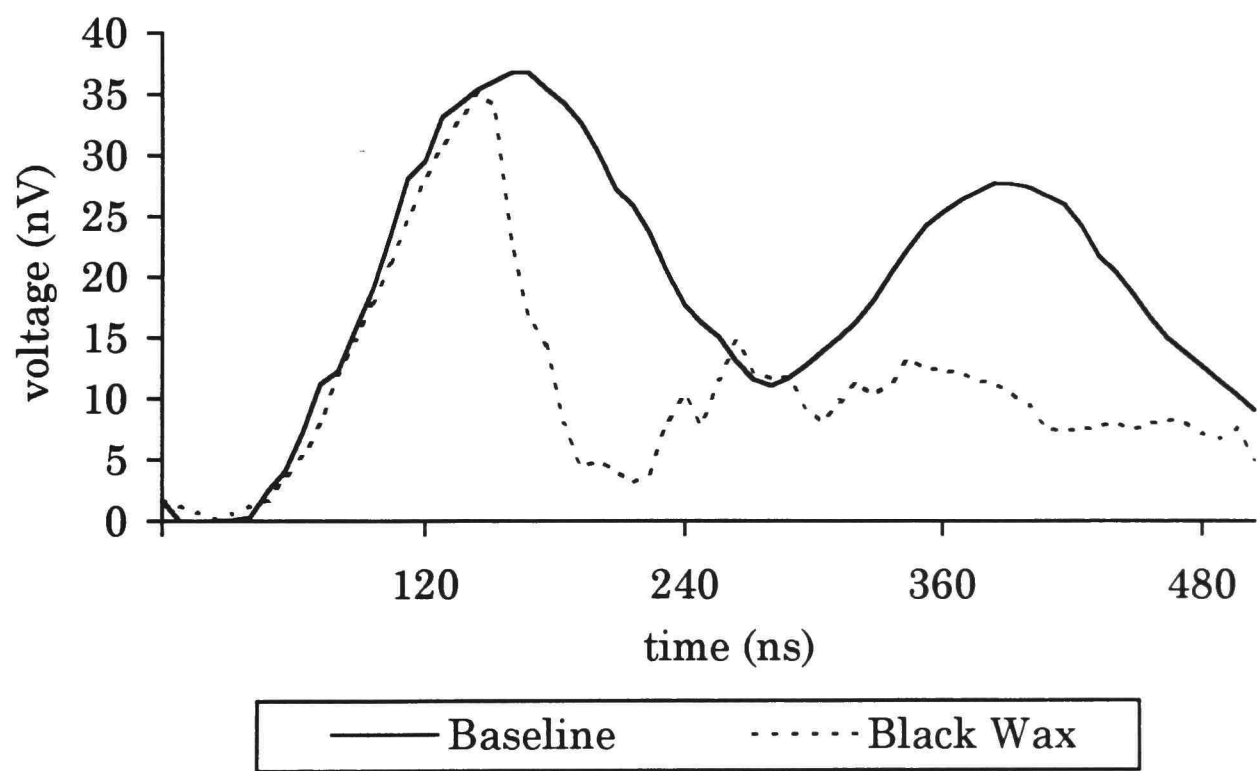


Figure 66. Average waveforms with black wax coatings on the electrodes.

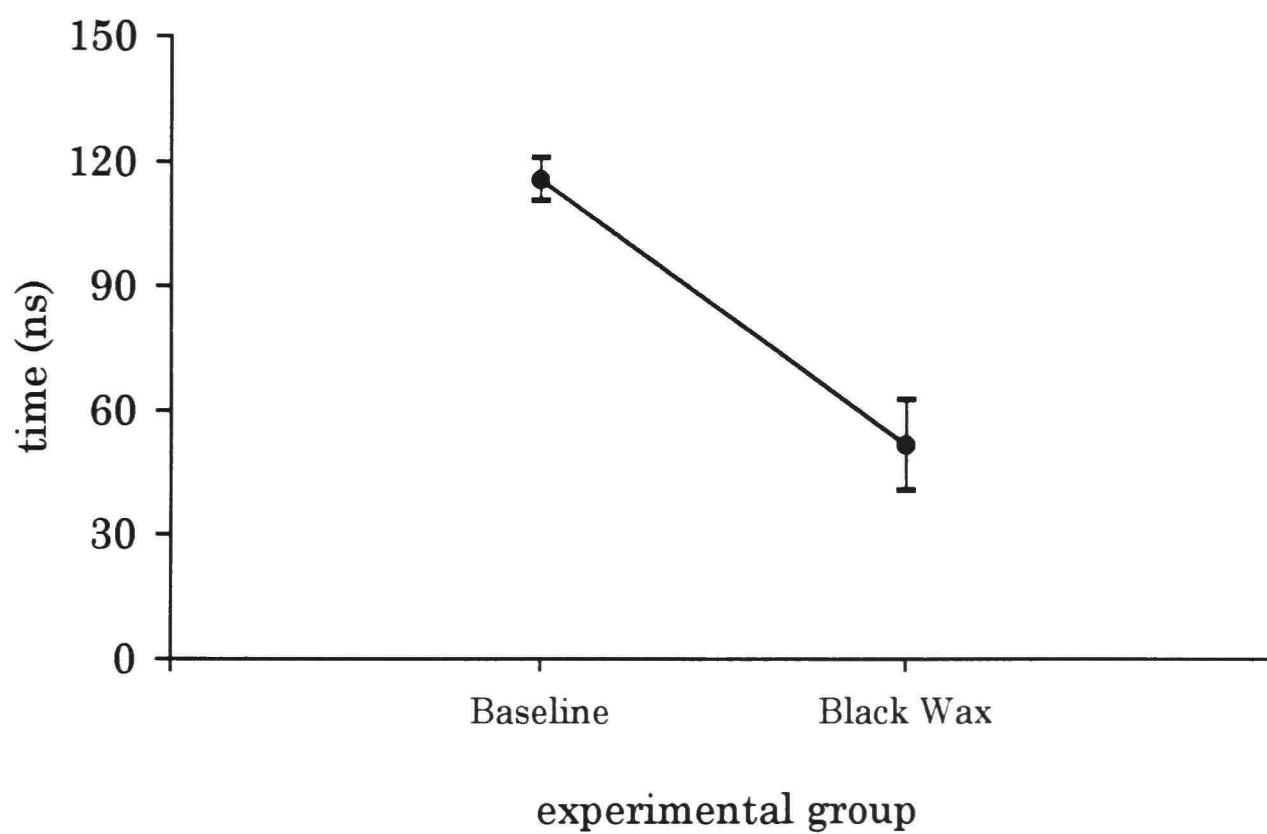


Figure 67. Effective time (τ_{eff}) with black wax coatings on the electrodes.

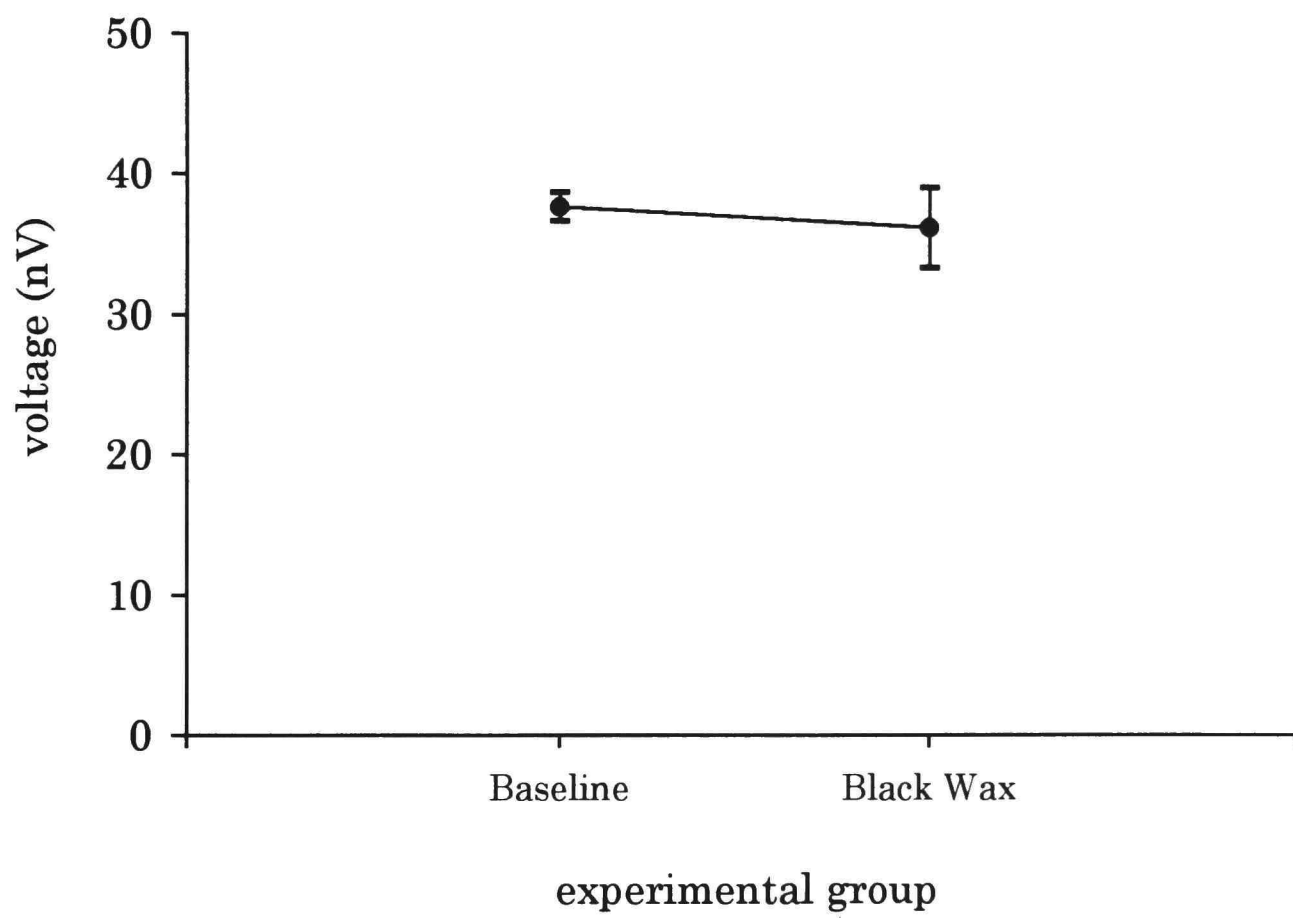


Figure 68. Maximum voltage (V_{\max}) with black wax coatings on the electrodes.

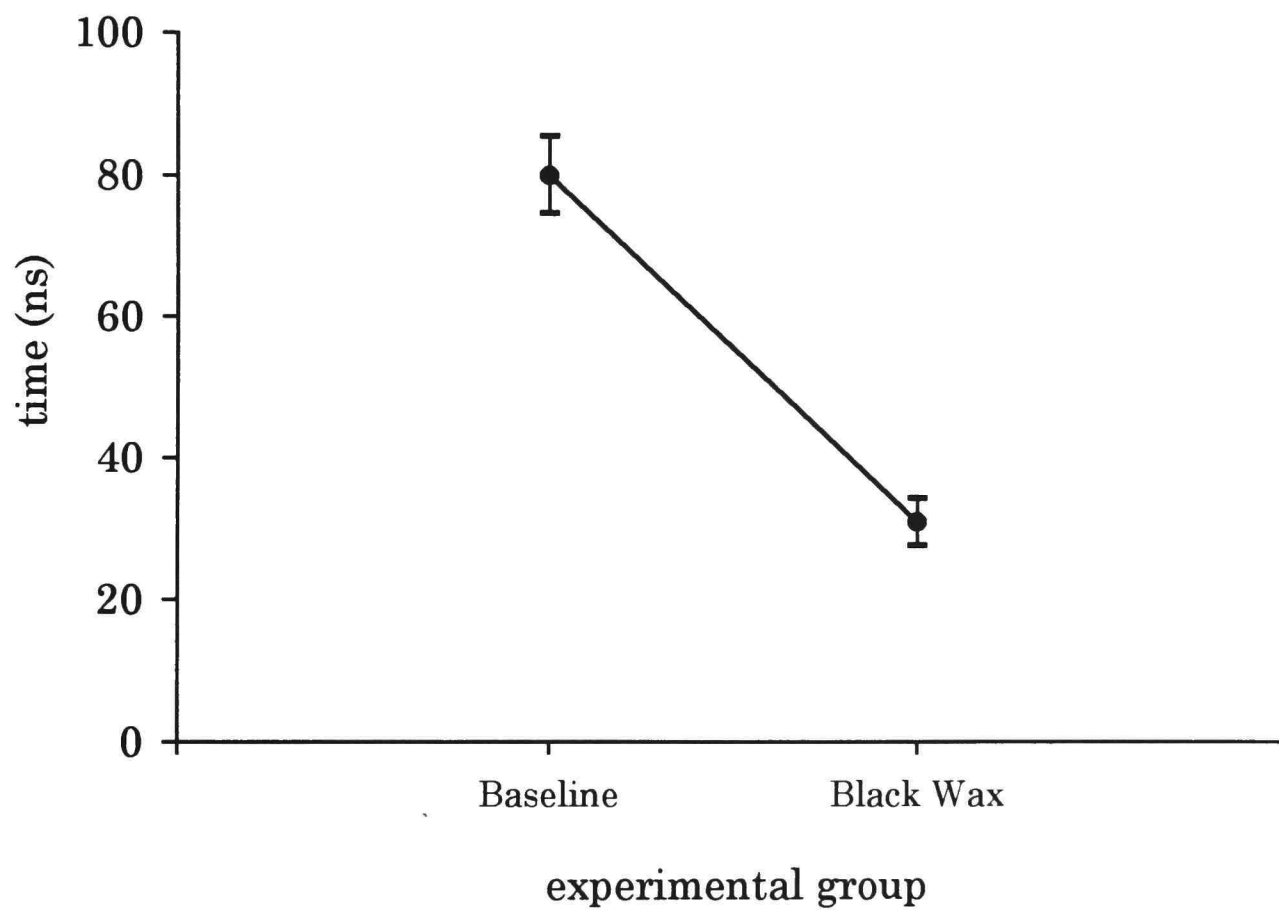


Figure 69. Fall-time with black wax coatings on the electrodes.

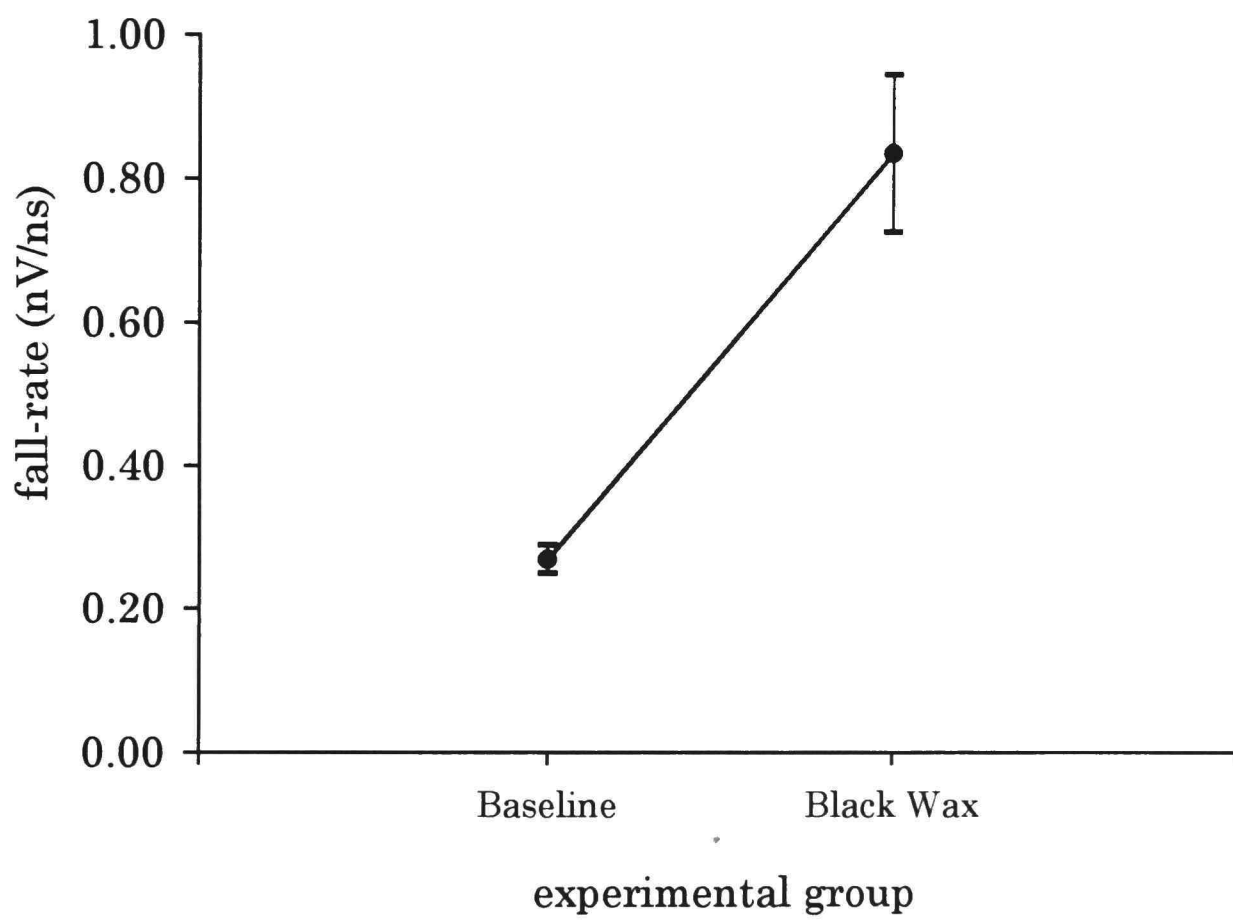


Figure 70. Fall-rate with black wax coatings on the electrodes.

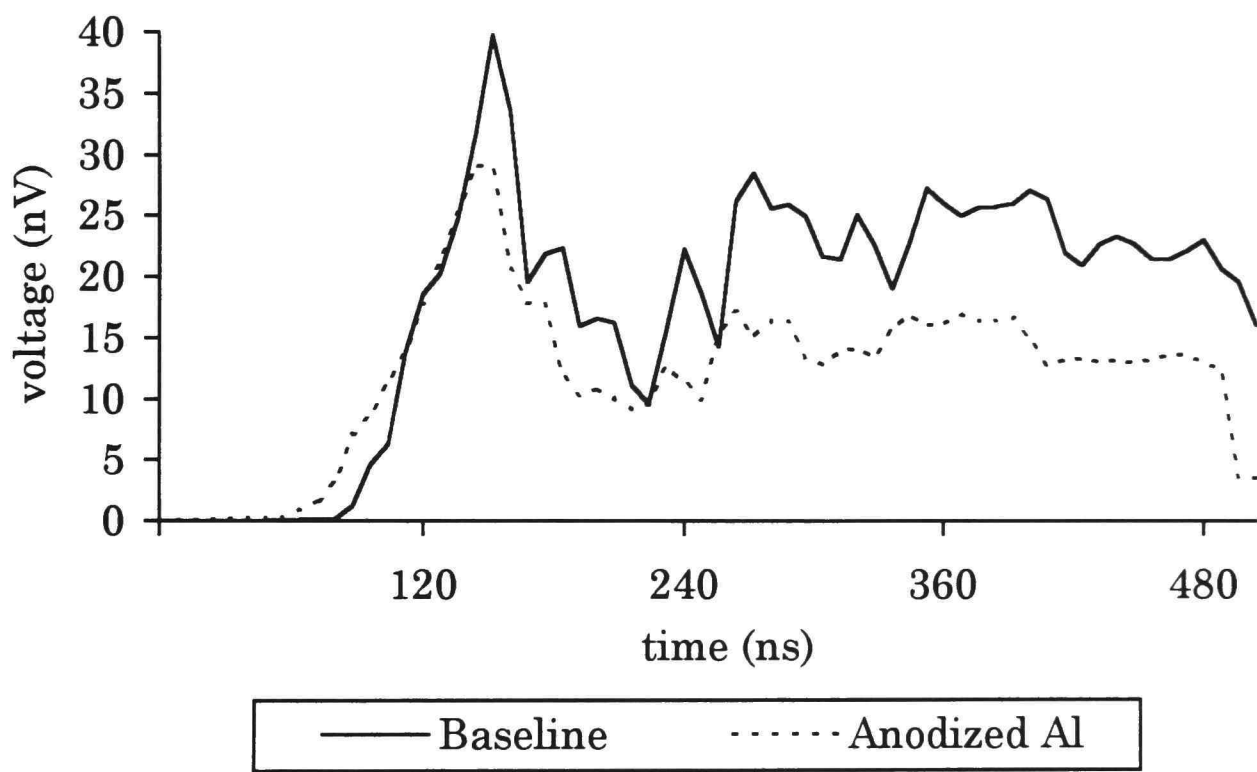


Figure 71. Average waveforms with anodized aluminum electrodes.

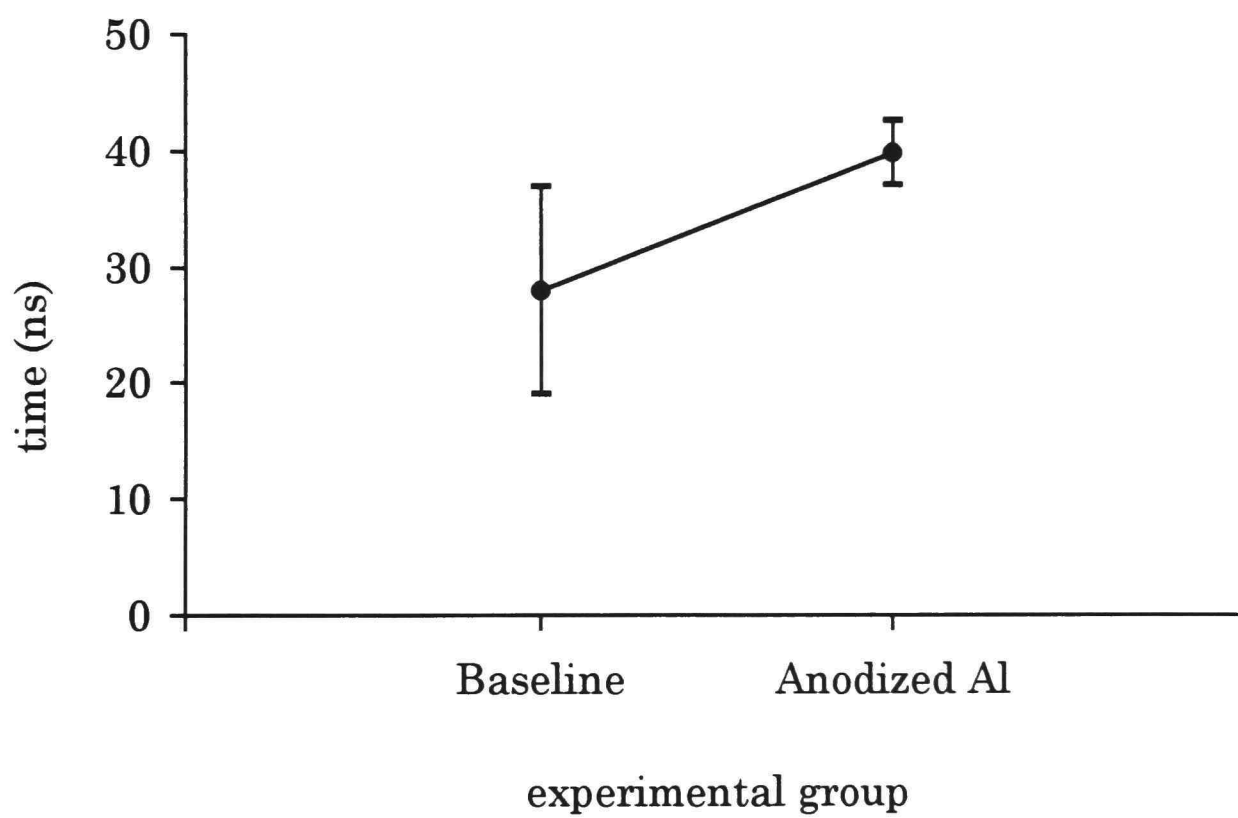


Figure 72. Effective time (τ_{eff}) with anodized aluminum electrodes.

mean values and standard deviations for the τ_{eff} of the baseline versus anodized shots. The values for V_{max} are shown in Figure 73, the fall-time values are shown in Figure 74, and the fall-rate values are in Figure 75.

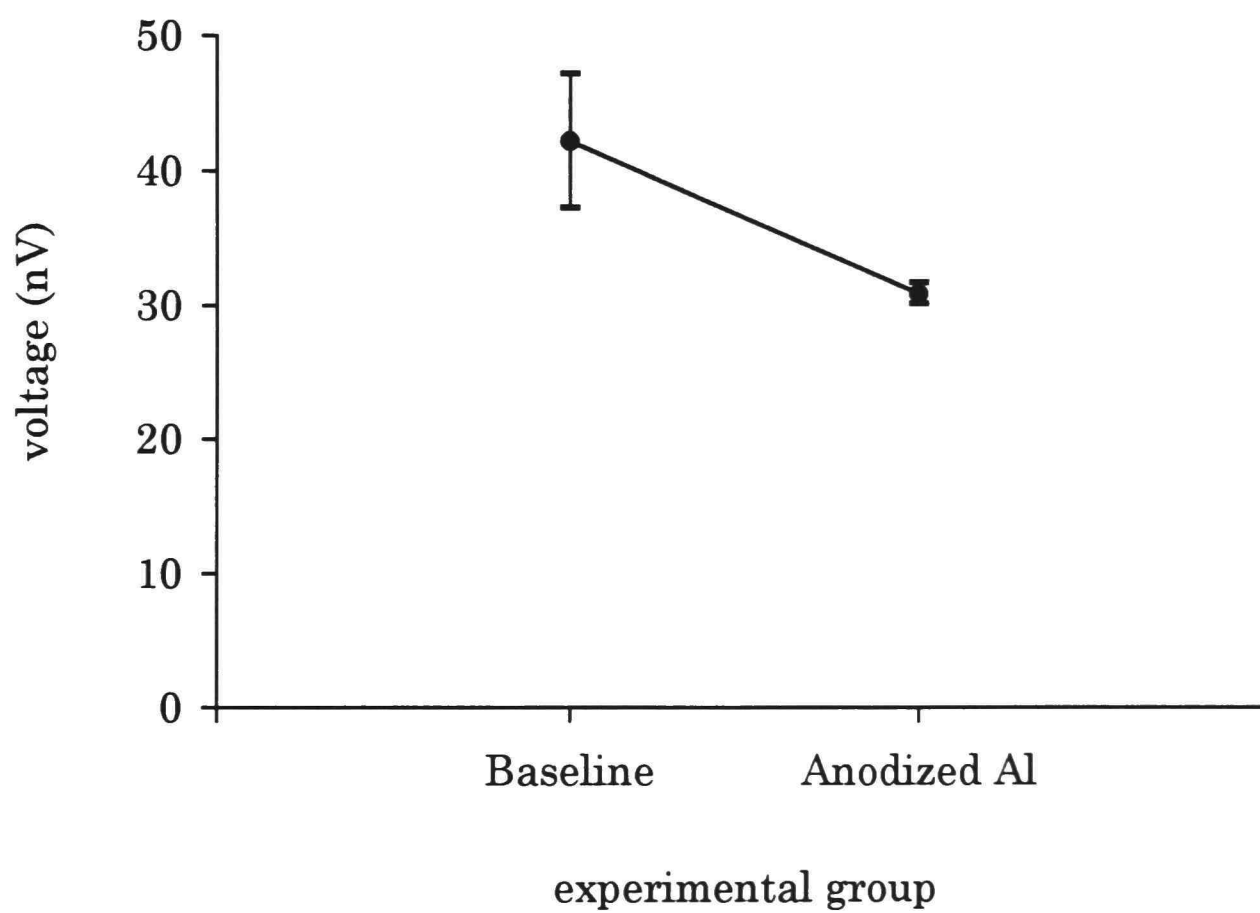


Figure 73. Maximum voltage (V_{max}) with anodized aluminum electrodes.

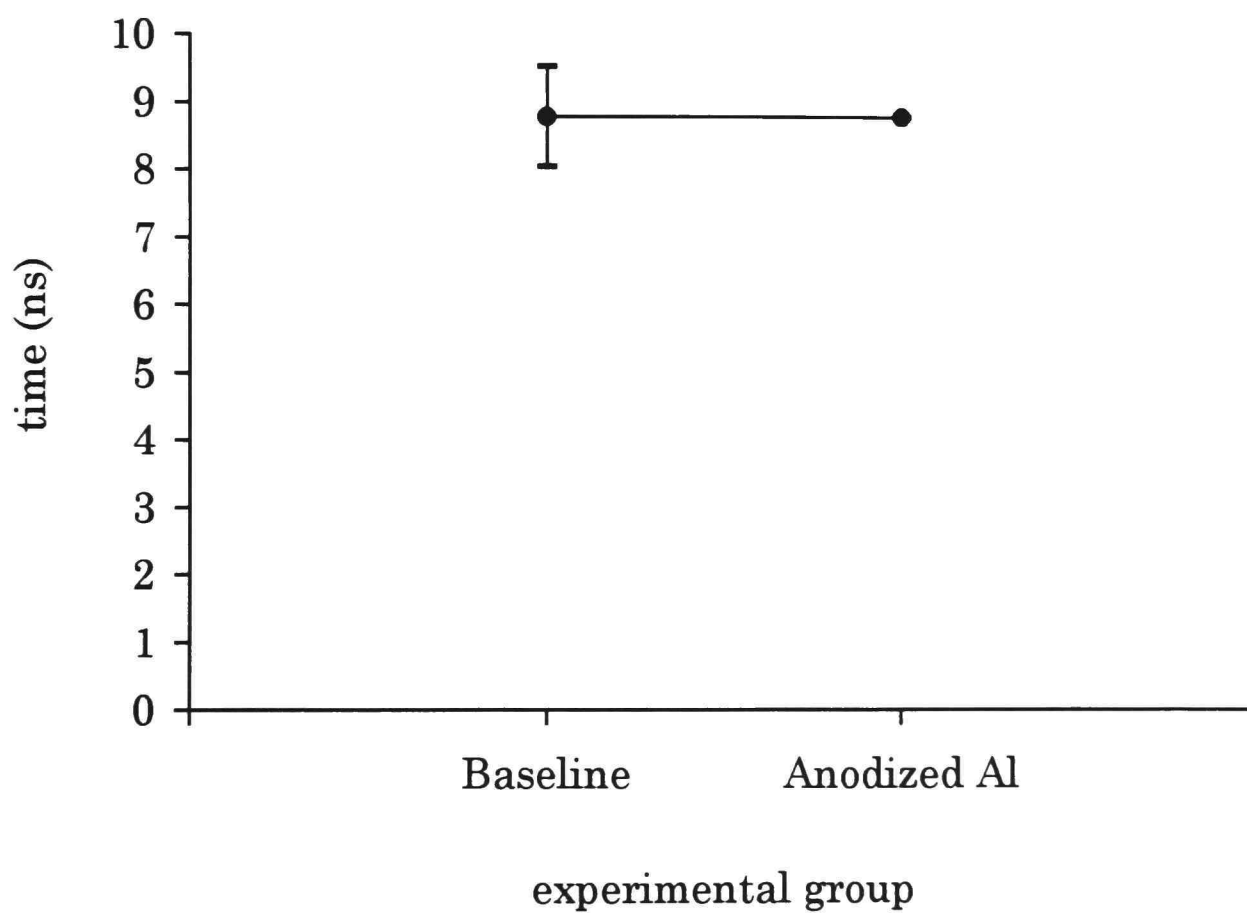


Figure 74. Fall-time with anodized aluminum electrodes.

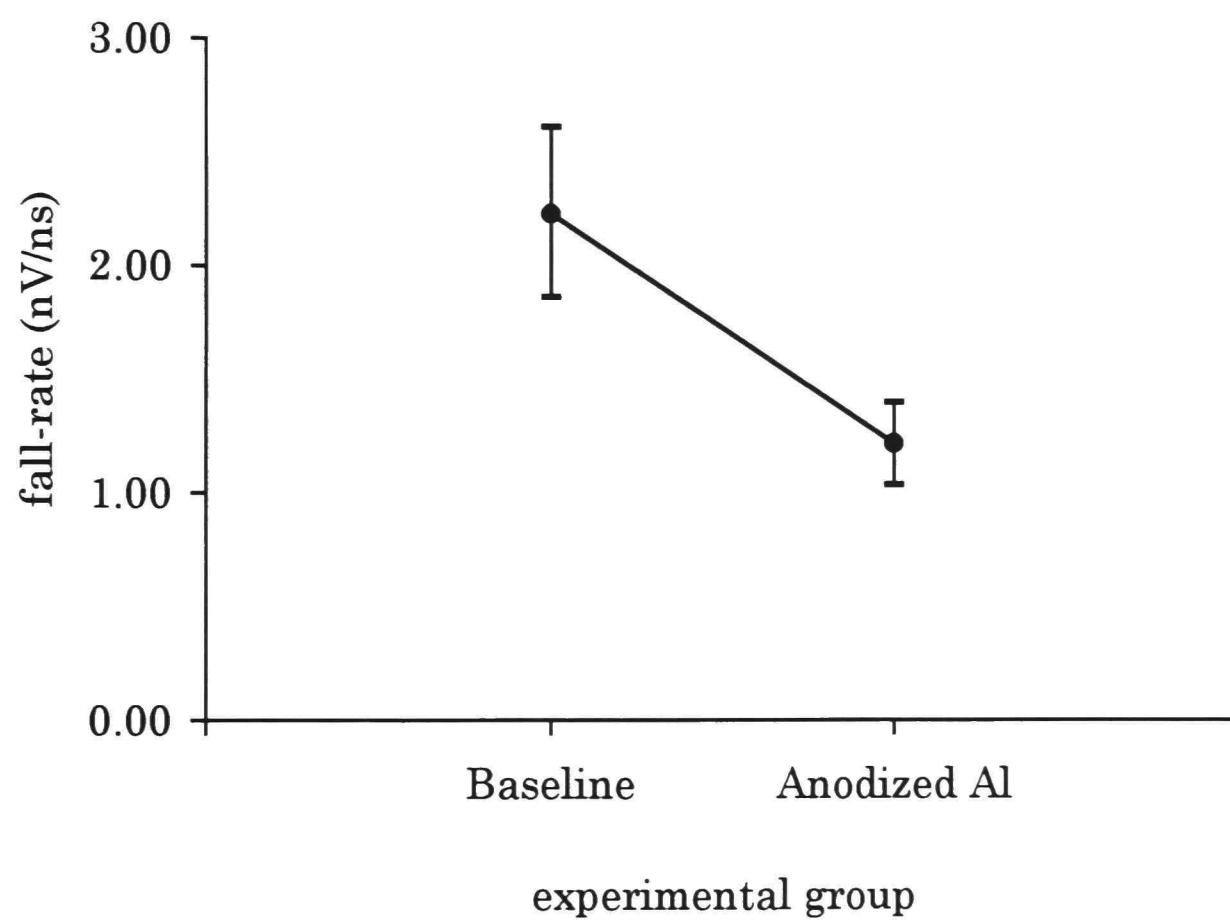


Figure 75. Fall-rate with anodized aluminum electrodes.

CHAPTER V
DATA ANALYSIS

Magnets

Anode

ANOVA's were run on each of the four parameters: τ_{eff} , V_{max} , fall-time, and fall-rate. The statistical evaluation of data from the magnet in the anode is summarized as follows:

Analysis of Variance (df = 2,27)

	F	α
τ_{eff}	1.524	not significant,
V_{max}	5.250	< 0.025,
Fall-time	2.263	not significant,
Fall-rate	1.793	not significant.

The only significant ANOVA was for V_{max} so *t*-tests were calculated for the means of the three different groups. The results are summarized as follows:

t-test (df = 18) - V_{max}

	t	α
Baseline vs. North Pole	0.449	not significant,
Baseline vs. South Pole	2.605	< 0.020,
North Pole vs. South Pole	2.754	< 0.020.

The results of the *t*-tests indicate there was a small, though, statistically significant differences between the maximum voltages of the baseline and the magnet in the anode with the South Pole pointing into the gap, and between the North Pole pointing into the gap and the South Pole

pointing into the gap. This can be seen graphically in Figure 25 with the South Pole voltage greater than the baseline and the North Pole voltages. The differences between the baseline and South Pole voltages represents a 4.0% increase in V_{\max} , while there was a 3.6% increase in voltage between the North Pole and the South Pole voltages.

Cathode

The statistical evaluation of data from the magnet in the cathode is summarized as follows:

Analysis of Variance (df = 2,27)

	F	α
τ_{eff}	5.123	< 0.025,
V_{\max}	0.299	not significant,
Fall-time	1.123	not significant,
Fall-rate	1.020	not significant.

The only significant ANOVA was for τ_{eff} so t -tests were calculated for the means of the three different groups. The results are summarized as follows:

t -test (df = 18) - τ_{eff}

	t	α
Baseline vs. North Pole	3.371	< 0.010,
Baseline vs. South Pole	0.862	not significant,
North Pole vs. South Pole	2.195	< 0.050.

The results of the t -tests indicate there were statistically significant differences between the τ_{eff} of the baseline and the magnet in the cathode with the North Pole pointing into the gap, and between the North Pole

pointing into the gap and the South Pole pointing into the gap. This can be seen graphically in Figure 29 with the North Pole voltage greater than the baseline and the South Pole voltages. The differences between the baseline and North Pole signals represents a 12.3% increase in τ_{eff} while there was a 7.7% decrease in τ_{eff} between the North Pole and the South Pole voltages.

Both

The statistical evaluation of data from the magnets in both the anode and the cathode is summarized as follows:

Analysis of Variance (df = 2,27)		
	F	α
τ_{eff}	10.910	< 0.001,
V_{max}	2.710	not significant,
Fall-time	0.134	not significant,
Fall-rate	0.659	not significant.

The only significant ANOVA was for τ_{eff} so *t*-tests were calculated for the means of the three different groups. The results are summarized as follows:

<i>t</i> -test (df = 18) - τ_{eff}		
	<i>t</i>	α
Baseline vs. Aligning field	0.874	not significant,
Baseline vs. Opposing field	4.386	< 0.001,
Aligning vs. Opposing field	3.698	< 0.010.

The results of the *t*-tests indicate there were statistically significant differences between the τ_{eff} of the baseline and the magnets in the electrodes with the fields opposing, and between the magnets in the electrodes when the

fields are aligning and opposing. This can be seen graphically in Figure 34 with the opposing fields τ_{eff} greater than both the aligning and the aligning fields τ_{eff} . The differences between the baseline and opposing field τ_{eff} represents a 19.7% increase in time, while there was a 15.1% increase in time between the aligning fields and the opposing fields τ_{eff} .

Sulfur hexafluoride

First series

The statistical evaluation of the first series SF₆ test is summarized as follows:

t-test (df = 12) - Baseline vs. SF₆ added.

	<i>t</i>	α
τ_{eff}	5.877	< 0.001,
V_{max}	0.873	not significant,
Fall-time	2.751	< 0.020,
Fall-rate	4.674	< 0.001.

The results of the *t*-tests indicate there were statistically significant differences between the baseline waveforms and the waveforms with SF₆ added to the water for τ_{eff} , fall-time, and fall-rate. This can be seen graphically in Figures 39, 41, and 42 with the effective time increasing by 20.1% with the addition of the SF₆ gas to the water while the fall-time increased by 49.0% and the fall-rate decreased by 48.3%.

Second series

The statistical evaluation of the second series SF₆ test is summarized as follows:

<i>t</i> -test (df = 18) - Baseline vs. SF ₆ added.		
	<i>t</i>	α
τ_{eff}	0.096	not significant
V _{max}	1.463	not significant
Fall-time	2.211	< 0.050
Fall-rate	1.157	not significant

The results of the *t*-tests indicate there was only a statistically significant difference between the baseline waveforms and the waveforms with SF₆ added to the water for fall-time. This can be seen graphically in Figure 46 which shows a slight increase in the fall-time. This increase represents a 17.5% change between the two groups.

Hydrochloric acid

Second series

The statistical evaluation of data generated by adding various concentrations of HCl to the water is summarized as follows:

Analysis of Variance (df = 5,12)		
	F	α
τ_{eff}	28.620	< 0.001
V _{max}	203.400	< 0.001
Fall-time	0.216	not significant
Fall-rate	4.068	< 0.025

The significant ANOVA's were for τ_{eff} , V_{max} , and fall-rate so *t*-tests were calculated for the means of the six groups. The results of the *t*-tests for τ_{eff} are summarized in Table 4.

Only five of the *t*-tests for τ_{eff} were significant. Looking at Figure 57, it appears that there was no significant effect on τ_{eff} until the concentration got to 10.0 M HCl. The 5.0 M HCl level was close to significance at the 0.05 level but was probably not because of the large variation seen at that concentration level as opposed to the first four groups. The difference between the Baseline and the 10.0 M level represents a 334% increase in the effective time. There was a 310% increase between the 0.1 M level and the 10.0 M level; 295%, 0.5 M and 10.0 M; 323%, 1.0 M and 10.0 M; and 97.6%, 5.0 M and 10.0 M. Figure 56 shows the progression of the spread of the signal as the concentration was increased.

The results of the *t*-tests for V_{max} are summarized in Table 5. In this case, all tests were significant except for the Baseline versus 0.1 M values. Figure 58 shows the decrease in V_{max} as the concentration increases. In order, the voltage dropped by 5.0% when the concentration was increased from 0.1 M to 0.5 M; 7.4%, from 0.5 M to 1.0 M; 24.8%, from 1.0 M to 5.0 M; and 13.7%, from 5.0 M to 10.0 M.

The results of the *t*-tests for the fall-rate are summarized in Table 6. Figure 60 shows wildly varying values and considerable variance in most of

Table 4. Results of the t -tests for τ_{eff} for the second HCl experiment.

t -test (df = 4)	t	α
Baseline vs. 0.1 M HCl	0.938	not significant
Baseline vs. 0.5 M HCl	1.358	not significant
Baseline vs. 1.0 M HCl	0.319	not significant
Baseline vs. 5.0 M HCl	2.339	not significant
Baseline vs. 10.0 M HCl	10.190	< 0.001
0.1 M HCl vs. 0.5 M HCl	0.728	not significant
0.1 M HCl vs. 1.0 M HCl	0.493	not significant
0.1 M HCl vs. 5.0 M HCl	2.233	not significant
0.1 M HCl vs. 10.0 M HCl	10.120	< 0.001
0.5 M HCl vs. 1.0 M HCl	0.954	not significant
0.5 M HCl vs. 5.0 M HCl	2.150	not significant
0.5 M HCl vs. 10.0 M HCl	9.938	< 0.001
1.0 M HCl vs. 5.0 M HCl	2.285	not significant
1.0 M HCl vs. 10.0 M HCl	10.090	< 0.001
5.0 M HCl vs. 10.0 M HCl	3.558	< 0.050

Table 5. Results of the t -tests for V_{\max} for the second HCl experiment

t -test (df = 4)	t	α
Baseline vs. 0.1 M HCl	2.410	not significant
Baseline vs. 0.5 M HCl	4.808	< 0.010
Baseline vs. 1.0 M HCl	12.650	< 0.001
Baseline vs. 5.0 M HCl	13.590	< 0.001
Baseline vs. 10.0 M HCl	49.090	< 0.001
0.1 M HCl vs. 0.5 M HCl	3.078	< 0.050
0.1 M HCl vs. 1.0 M HCl	10.650	< 0.001
0.1 M HCl vs. 5.0 M HCl	12.600	< 0.001
0.1 M HCl vs. 10.0 M HCl	49.920	< 0.001
0.5 M HCl vs. 1.0 M HCl	4.477	< 0.020
0.5 M HCl vs. 5.0 M HCl	9.946	< 0.001
0.5 M HCl vs. 10.0 M HCl	27.180	< 0.001
1.0 M HCl vs. 5.0 M HCl	8.197	< 0.010
1.0 M HCl vs. 10.0 M HCl	39.800	< 0.001
5.0 M HCl vs. 10.0 M HCl	3.544	< 0.050

Table 6. Results of the *t*-tests for fall-rate for the second HCl experiment

<i>t</i> -test (df = 4)	<i>t</i>	<i>a</i>
Baseline vs. 0.1 M HCl	0.242	not significant
Baseline vs. 0.5 M HCl	0.716	not significant
Baseline vs. 1.0 M HCl	1.365	not significant
Baseline vs. 5.0 M HCl	2.232	not significant
Baseline vs. 10.0 M HCl	3.147	< 0.050
0.1 M HCl vs. 0.5 M HCl	0.771	not significant
0.1 M HCl vs. 1.0 M HCl	0.768	not significant
0.1 M HCl vs. 5.0 M HCl	1.767	not significant
0.1 M HCl vs. 10.0 M HCl	2.278	not significant
0.5 M HCl vs. 1.0 M HCl	2.295	not significant
0.5 M HCl vs. 5.0 M HCl	1.729	not significant
0.5 M HCl vs. 10.0 M HCl	2.904	< 0.050
1.0 M HCl vs. 5.0 M HCl	4.175	< 0.020
1.0 M HCl vs. 10.0 M HCl	5.405	< 0.010
5.0 M HCl vs. 10.0 M HCl	1.474	not significant

the groups. For these reasons, even though some of the tests were statistically significant, they will not be used for drawing any conclusions.

Polymer coating

The results of the t -tests for τ_{eff} are summarized as follows:

t -test (df = 14) - τ_{eff}

	t	α
Baseline vs. PC	9.797	< 0.001
Baseline vs. PES	6.472	< 0.001
Baseline vs. PC+ PES-	10.960	< 0.001
Baseline vs. PES+ PC-	7.636	< 0.001

All of the t -tests for τ_{eff} were statistically significant. The change in τ_{eff} for the PC coatings on both electrodes represents a 50.4% decrease, while using the PES coatings on both electrodes decreased the τ_{eff} by 33.3%. With the PC coating on the anode and PES on the cathode, the τ_{eff} decreased by 56.4%, and, with PES on the anode and PC on the cathode, the τ_{eff} went down by 39.3%. These results can be seen in Figure 62.

The results of the t -tests for V_{max} are summarized as follows:

t -test (df = 14) - V_{max}

	t	α
Baseline vs. PC	4.629	< 0.001
Baseline vs. PES	6.106	< 0.001
Baseline vs. PC+ PES-	2.294	< 0.050
Baseline vs. PES+ PC-	5.677	< 0.001

The t -tests for V_{max} were all statistically significant. Adding the PC coating to both electrodes decreased the maximum voltage by 19.6% and decreased the voltage by 25.9% when the PES coating was used on both

electrodes. The voltage decreased by only 9.7% when the PC coating was applied to the anode and the PES coating to the cathode. A 24.1% decrease in voltage was seen with the PES coating on the anode and the PC coating on the cathode. These results can be seen in Figure 63.

The results of the *t*-tests for fall-time are summarized as follows:

t-test (df = 14) - Fall-time

	<i>t</i>	α
Baseline vs. PC	5.750	< 0.001
Baseline vs. PES	6.297	< 0.001
Baseline vs. PC+ PES-	5.859	< 0.001
Baseline vs. PES+ PC-	6.078	< 0.001

Measurements of the fall-time were statistically significant for all of the polymer coatings. A 62.2% decrease in fall-time was seen with the PC coating on both of the electrodes while a 68.1% decrease occurred with the PES coating on both electrodes. With the PC coating on the anode and the PES coating on the cathode, there was a 63.3% decrease in the fall-time of the signal. There was a 65.7% decrease in fall-time with the PES coating on the anode and the PC coating on the cathode. These results can be seen in Figure 64.

The results of the *t*-tests for fall-rate are summarized as follows:

t-test (df = 14) - Fall-rate

	<i>t</i>	α
Baseline vs. PC	24.460	< 0.001
Baseline vs. PES	30.110	< 0.001
Baseline vs. PC+ PES-	26.660	< 0.001
Baseline vs. PES+ PC-	30.980	< 0.001

The final set of t -tests were calculated for the fall-rate of the signal and were all statistically significant. Using the PC coating on both of the electrodes gave a 202.4% increase in the fall-rate while a 249.2% increase was seen with the PES coating on both electrodes. Applying a coating of PC on the anode and PES on the cathode gave a 220.6% increase in the fall-rate and a 256.3% increase with PES on the anode and PC on the cathode. These results can be seen in Figure 65.

Black wax

The statistical evaluation of data generated using a coating of black wax is summarized as follows:

t -test (df = 18)		
	t	α
τ_{eff}	16.660	< 0.001
V_{max}	1.471	not significant
Fall-time	24.270	< 0.001
Fall-rate	16.330	< 0.001

The results of the t -tests indicate there were statistically significant differences between the baseline waveforms and the waveforms with black wax on the electrodes for τ_{eff} , fall-time, and fall-rate. This can be seen graphically in Figures 66, 68, and 69 with the effective time decreasing by 55.3% with the black wax while the fall-time decreased by 61.2% and the fall-rate increased by 213.1%.

Anodized aluminum

The statistical evaluation of the data generated by using anodized aluminum electrodes is summarized as follows:

<i>t</i> -test (df = 8)		
	<i>t</i>	α
τ_{eff}	1.784	not significant
V_{max}	3.047	< 0.020
Fall-time	0.000	not significant
Fall-rate	3.570	< 0.010

The results of the *t*-tests show significant findings for V_{max} and the fall-rate. The change in the maximum voltage between the baseline shots and the shots with the anodized aluminum electrodes represents a 26.6% decrease in the voltage. This can be seen graphically in Figure 73. Figure 75 shows a 45.5% decrease in the fall-rates between the baseline shots and the experimental shots.

CHAPTER VI

CONCLUSIONS

Based on the data presented in Chapter IV and analyzed in Chapter V, it is possible to generate some ideas as to what is happening in the water during the application of a high electric field. If the reader can accept the Russian breakdown model presented in Chapter II, the results of this experiment must be able to support a breakdown process initiated by microbubbles and propagated through the water by proton transport. Looking at the previous research listed in the first part of Chapter II, the methods that had significant effects on the breakdown field strength would affect either the occurrence of microbubbles or proton transport. In particular, water pressure had some of the best results of all the methods presented. Even though it would not be practical in large systems, it is possible to double the breakdown field strength by applying very high pressures to the system. If it is microbubbles that initiate the discharge in the water gap, then applying high pressures would force out the bubbles from the electrode surface, decreasing the number of possible initiation sites, and also make the formation of bubbles from thermal heating more difficult.

Another technique used to increase the breakdown strength is to cool the water down to near freezing or, with additives, below freezing. In this

case, more thermal energy is needed for the transition from near freezing liquid to the microbubble state.

The next area that has been researched is the type of electrode material used. Of particular note is the work presented in Chapter II that looked at different materials for the anode and cathode [6]. For example, using brass and aluminum electrodes, it is possible to almost double the breakdown field strength by switching from an aluminum anode and a brass cathode to an aluminum cathode and a brass anode. This is due principally to negative charge injection. Again, looking at the Russian model, it would appear that the use of these two electrode materials together either enhance or inhibit the proton motion depending on the orientation of the electrodes.

The most promising technique for increasing the breakdown field strength is the diffusion electrodes which the Russians have claimed a quadrupling of the field strength between the electrodes [1]. By applying a diffuse conducting layer on the electrode surface, the high intensity fields forming around the microbubbles are eliminated. This allows the field to build up to a higher level until the discharge is formed by a different process such as thermal conduction in the center of the gap.

The Russians have provided us with what seems to be a good workable model of the breakdown process. The results presented in Chapter IV can now be put in context with this model. The effect of the magnetic field on the voltage output is particularly interesting because water has an electric dipole

moment but does not have a magnetic dipole moment. So the magnetic fields would have no effect on the orientation or motion of the water molecules in their natural state but would have an effect on the movement of ions through the gap between the electrodes. The radius of the path of the charged particle moving through a magnetic field is given by

$$r = \frac{mv}{qB}, \quad (24)$$

where m is the particle mass, v is the velocity, q is the charge, and B is the magnetic field strength. Ovchinnikov et al. [18] measured the electron velocity in water to be approximately 1.5×10^3 m/sec and Yanshin et al. [19] gives the proton velocity in water as 40 m/sec. With these velocities and using a magnetic field strength of 15 mT, the radii would be $0.6 \mu\text{m}$ and $27.8 \mu\text{m}$ for an electron and a proton, respectively, which are much smaller than the electrode gap. Of course, this assumes a transverse magnetic field which would not be the case here. However, with the copper-tungsten electrodes, the discharge tended to begin on the edge of the edge of the electrode rather than the center. If the initial discharge was from the edge of the electrode, then the charges would pass through almost transverse magnetic fields to get to the other electrode. The magnetic field may also affect the ability of the water molecule to interact with the proton to form the hydronium ion, thereby disrupting the current path being formed in the water.

Magnetic fields have been demonstrated to be effective for shielding high voltage systems in vacuum and there may be a similar mechanism in water. The magnetic fields employed in this experiment were very small and may account for the small changes in the output but give an inducement to continue this line of research to see if increasing the magnetic field strength will increase the breakdown field strength.

The first experiment using the SF₆ gas gave some promising results with a significant increase in the τ_{eff} . Sulfur hexafluoride was chosen because of its electro-negative quality which is why it is used in spark gap switches. The gas captures low energy electrons as they move across the gap thereby increasing the voltage holdoff of the spark gap switch. For this reason, the gas was used in the water to see if it would have a similar effect. The results seen in the first series of shots may have been due to a bad capacitor that was about to burst and is why that series was terminated. Two additional series of shots were run without the same increase in τ_{eff} seen in the first series. This may have been due to one of two things. The first was the inability to determine how much SF₆ was actually mixed into the water. It is possible that only trace amounts of the gas actually circulated in the water such that there was an insufficient quantity to cause any effect on the discharge in the gap. The other possibility is that if it is proton motion in the water that sets up the discharge, as suggested in the Russian model, then the electro-negativity of the SF₆ would have no effect on the discharge. An

interesting follow-on would be to use an electro-positive gas, such as argon or helium, to see if it would have an effect.

The Russians showed in several experiments [15] that adding HCl and similar chemicals to the water decreased the conductivity of the water during the prebreakdown period. They did not look at the field strength or voltage holdoff of the water gap. The HCl experiments were conducted to see if the decreased conductivity (increased resistivity) would relate to an increase in the field strength or voltage holdoff. The addition of HCl to the water would increase the number of H⁺ ions and was expected to interfere with the development of charge transfer by creating an excess of hydronium molecules. The other effect was the Cl⁻ ions capturing the protons as they left the electrode surface would decrease the number of protons available to start the discharge. The only effect that adding the HCl seem to have was to spread the energy over a longer time period as the concentration of HCl increased. Perhaps the phenomena seen by the Russians occurs if there is not sufficient voltage to cause a discharge in the gap.

The use of coatings has shown some potential for small surface areas but has either not been successful or not tried with larger surface areas. Polymer coatings may prove to be useful but no real conclusions can be drawn from the research conducted for this dissertation because of the limited number of trials conducted. Additional research in this area may yield some significant results. The black wax coating did not prove to be

successful. This could have been due to the method used in coating the electrode or may be due to the inability of the wax to be effective over large areas. Black wax has been shown to be effective for systems with extremely small electrode surface areas but this effect may not scale to larger sizes [7].

The results of the anodized aluminum electrode experiment indicate that anodizing the electrodes decreased the voltage holdoff level. This is inconsistent with the results that Gehman [9] demonstrated which showed that the breakdown voltage of anodized aluminum was about 15% higher than plain aluminum. Gehman used a mixture of ethylene glycol and water, cooled to -30°C , which may account for the difference in the results.

Future research should look at what is happening at the surface of the electrode on a microscopic level. The region where the metal surface and the water interface is where the electric field breakdown is initiated. By suppressing the initiation of the arc, the electric field can rise to much higher levels and will either increase the maximum voltage across the gap or increase the time that the gap can withstand the voltage before arcing. Whether it is microbubbles or high intensity field points on the surface of the electrode that cause the initiation of the arc, anything that lowers the electric fields on the surface of the electrode would be beneficial. A coating must be able to electrically “smooth” the microscopic surface of the electrode. This is essentially how the diffusion electrodes work. By having a thin layer of conductive water close to the surface of the electrode, the electric field

enhancement due to surface irregularities is lowered. This allows the field to build up until it reaches the intrinsic maximum in the gap. The diffusion electrodes would not be practical in a very large system but, as mentioned in the introduction, the Russians claimed that they have found a practical way to do what the diffusion electrodes are doing [19]. Much of the previous research has shown that there is usually a tradeoff between E_{BD} , τ_{eff} , and ϵ_r . This should be remembered when considering the Russian claims. Additional research may show that the technique developed by the Russians may yield a higher breakdown strength in the water but may, for instance, reduce the capacitance of the system.

Many techniques to increase the field strength of water have been tried with various levels of success. Some of these techniques have been very successful in a laboratory setting but would not be useful in practical system. These techniques help provide insight into the breakdown mechanism and are the key to finding a practical technique for increasing the field strength of water. A practical technique would have to be independent of the geometry of the conductor and the type of material the conductor is made of. It would have to work on systems that had either a closed or open water circulation, and must not be harmful to the filtration and de-ionization system. The technique needs to be self-healing or undisturbed if a breakdown occurs in the water. Ideally, it would not require changing the water after every shot. The use of a conductive polymer of the surface of the

electrode may prove to be a practical technique to increase the electric field strength of water.

REFERENCES

- (1) Vorov'ev, V. V., V. A. Kapitonov, E. P. Kruglyakov, and Yu. A. Tsidulko, "Breakdown of water in a system with 'diffusion' electrodes," Soviet Physics Technical Physics, Vol. 25, No. 5, pp. 598-602, May 1980.
- (2) Abramyan, E. A., V. A. Kornilov, et al., "Megavolt Energy-Concentrating Device," Soviet Physics - Doklady, Vol. 16, No. 11, pp. 983, May, 1972.
- (3) Sincerny, P. S., "Electrical Breakdown Properties of Water for Repetitively Pulsed Burst Conditions," Proceedings of the 3rd IEEE International Pulsed Power Conference, pp. 222-225, June, 1981.
- (4) Fenneman, D. B., "Pulsed High-Voltage Dielectric Properties of Ethylene Glycol/Water Mixtures," Journal of Applied Physics, Vol. 53, No. 12, pp. 8961-8968, December, 1982.
- (5) Noyel, G. A., L. J. Jorat, O. Derriche, and J. R. Huck, "Dielectric Properties of Normal Supercooled Water Obtained in Alcohol/Water Mixtures," IEEE Transactions on Electrical Insulation, Vol. 27, No. 6, pp. 1136-1143, December, 1992.
- (6) Zahn, M., Y. Ohki, K. Rhoads, M. LaGasse, and H. Matsuzawa, "Electro-Optic Charge Injection and Transport Measurements in Highly Purified Water and Water/Ethylene Glycol Mixtures," IEEE Transactions on Electrical Insulation, Vol. EI-20, No. 2, pp. 199-211, April, 1985.
- (7) Szklarczyk, M., R. C. Kainthla, and J. O' M. Bockris, "On the Dielectric Breakdown of Water: An Electrochemical Approach," Journal of Electrochemical Society, Vol. 136, No. 9, pp. 2512-2520, September, 1989.
- (8) Fenneman, D. B., and R. J. Gripshover, "Experiments on Electrical Breakdown in Water in the Microsecond Regime," IEEE Transactions on Plasma Science, Vol. PS-8, No. 3, pp. 209-213, September, 1980.

- (9) Gehman Jr., V. H., D. B. Fenneman, and R. J. Gripshover, "Electrode Surface Effects on Unipolar Charge Injection in Cooled Liquid Dielectric Mixtures," Digest of Technical Papers - 4th IEEE Pulsed Power Conference, pp. 316-322, June, 1983.
- (10) McLeod, A. R., and V. H. Gehman, Jr., "Water Breakdown Measurements of Stainless Steel and Aluminum Alloys for Long-Charging Times," Digest of Technical Papers. Sixth IEEE Pulsed Power Conference, pp. 57-59, 1987.
- (11) Kuzhekin, I. P., "Investigation of the Breakdown by Rectangular Voltage Pulses of a Liquid in an Inhomogeneous Field," Soviet Physics - Technical Physics, Vol. 11, No. 12, pp. 1585-1589, June, 1967.
- (12) Buttram, M., and M. O'Malley, "Breakdown of Water Under Long Term Stress," Digest of Technical Papers - 4th IEEE Pulsed Power Conference, pp. 327-330, 1983.
- (13) Vorov'ev, V. V., V. A. Kapitonov, and E. P. Kruglyakov, "Increase of Dielectric Strength of Water in a System with 'Diffusion' Electrodes," JETP Letters, Vol. 19, No. 2, pp. 58-59, January, 1974.
- (14) Hasted, J. B., Aqueous Dielectrics, Chapter 2: The Experimental Data for Liquid Water, Chapman and Hall, London, pp. 37-40, 1993.
- (15) Ovchinnikov, I. T., and E. V. Yanshin, "Relaxation of Proton Conduction in Water in Strong Pulsed Electric Fields," Soviet Physics - Technical Physics, Vol. 29, No. 12, pp. 1431-1432, December, 1984.
- (16) Yanshin, E. V., I. T. Ovchinnikov, and Yu. N. Vershinin, "Optical Study of Nanosecond Prebreakdown Phenomena in Water," Soviet Physics - Technical Physics, Vol. 18, No. 10, pp. 1303-1306, April, 1974.
- (17) Yanshin, E. V., K. V. Yanshin, S. M. Korobeynikov, "Space Charge and Pre-Breakdown Bubbles Formation Near Point Electrodes Under Pulse Voltage," Conference Record, Eighth International Conference on Conduction and Breakdown in Dielectric Liquids, pp. 194-198, July, 1984.

- (18) Ovchinnikov, I. T., K. V. Yanshin, and E. V. Yanshin, "Use of the Kerr Effect to Study Pulsed Electric Fields Near a Sharp Point in Water," Soviet Physics - Technical Physics, Vol. 23, No. 12, pp. 1487-1489, December, 1978.
- (19) Yanshin, E. V., S. M. Korobeynikov, I. T. Ovchinnikov, S. G. Sarin, K. V. Yanshin, V. M. Kopylov, and A. V. Klepikov, "Physical Processes Limiting the Pulse Energy Release in Liquid Dielectrics," preprint from the Digest of Technical Papers. Tenth IEEE Pulsed Power Conference, June, 1995.
- (20) Terman, F. E., Radio Engineers' Handbook, McGraw-Hill Book Company, Inc., New York, p. 53, 1943.
- (21) Coulter, T. J., A Compact Megavolt Marx Bank Generator Design, Master's thesis, Texas Tech University, Lubbock, Texas, August, 1994.
- (22) Francis, J. F., "High Voltage Pulse Techniques," Technical Report No. 5 on AFOSR Grant 74-2639 "Dense Plasma Heating and Radiation Generation," Plasma Laboratory, Department of Electrical Engineering, Texas Tech University, Lubbock, Texas, 79409, p. 102, December, 1976.
- (23) Kristiansen, M., Basic Electromagnetic Field Theory, U. S. Air Force Pulsed Power Lecture Series, Texas Tech University, No. 3, p. 18, 1978.
- (24) Kenyon, V., personal communication, Naval Surface Warfare Center, Silver Springs, Maryland, June 22, 1993.
- (25) Miller, R., personal communication, Maxwell Laboratories, San Diego, California, June 22, 1993.
- (26) Wilkinson, M., and E. Chu, "Calibration of Capacitive Voltage Probes in Water-Dielectric, High Power Pulse Generators," Maxwell Laboratories, Inc., pp. 59-68, 1982.
- (27) Bruning, J. L., and B. L. Kintz, Computational Handbook of Statistics 2nd ed., Scott, Foresman and Company, Glenview, Illinois, 1977.
- (28) Childers, K., personal communication, Physics International, San Leandro, California, January 27, 1995.

- (29) Martin, T., personal communication, Sandia National Laboratory, Albuquerque, New Mexico, January 27, 1995.

APPENDIX A

WATER BREAKDOWN FORMULAS

Describing Water Breakdown Levels

During the early 1960's, J. C. Martin did considerable experimental work on the voltage breakdown levels in water. His work was done on water at standard temperature and pressure (STP). Considerable work has been done with water under high pressure but Martin's work was not in this area. From the data collected, Martin wrote several equations to describe the data. The two most common equations are

$$F\tau_{eff}^{1/3}A^{1/10} = 0.3, \quad (25)$$

for positive polarity and

$$F\tau_{eff}^{1/3}A^{1/10} = 0.6, \quad (26)$$

for negative polarity, where F is the electric field breakdown level in MV/cm, A is the area in cm^2 , and τ_{eff} is the effective time in μs . These equations will give the electric field necessary to have a breakdown in the water for a given effective time, over a given area. For example, let $\tau_{eff} = 1 \mu\text{s}$, and $A = 1 \text{ cm}^2$, then F of the first equation is 0.3 MV/cm. If the electric field is greater than or equal to 0.3 MV/cm, then a breakdown in the water can almost be guaranteed [28]. This would be referred to operating "at the JCM level." To

operate at 60% JCM, the system is designed so that the maximum field strength, for this example, is less than or equal to 0.18 MV/cm.

What will be seen if the breakdown field of many discharges are measured is a Gaussian distribution. A typical normalized Gaussian distribution for this example would look like (Figure 76) with F from Martin's equation at the maximum of the curve. The significance of operating at 60% JCM would be the very low probability of a breakdown occurring in the water.

So, why do not all machines operate at 60% JCM?

Water is used as the insulator in pulsed power machines because it has a high relative dielectric constant (ϵ_r). This is important because the size of the machine depends on the amount of energy that can be stored in the insulator. Think of the water as the insulator in a parallel plate capacitor. The capacitance is given by

$$C = \frac{\epsilon_0 \epsilon_r A}{d}, \quad (27)$$

where ϵ_0 is the dielectric constant of vacuum, ϵ_r is the relative dielectric constant, A is the surface area of the plate, and d is the distance separating the two plates. With ϵ_r of about 80, water becomes a very popular insulator for pulsed power machines. The energy stored in a capacitor is given by

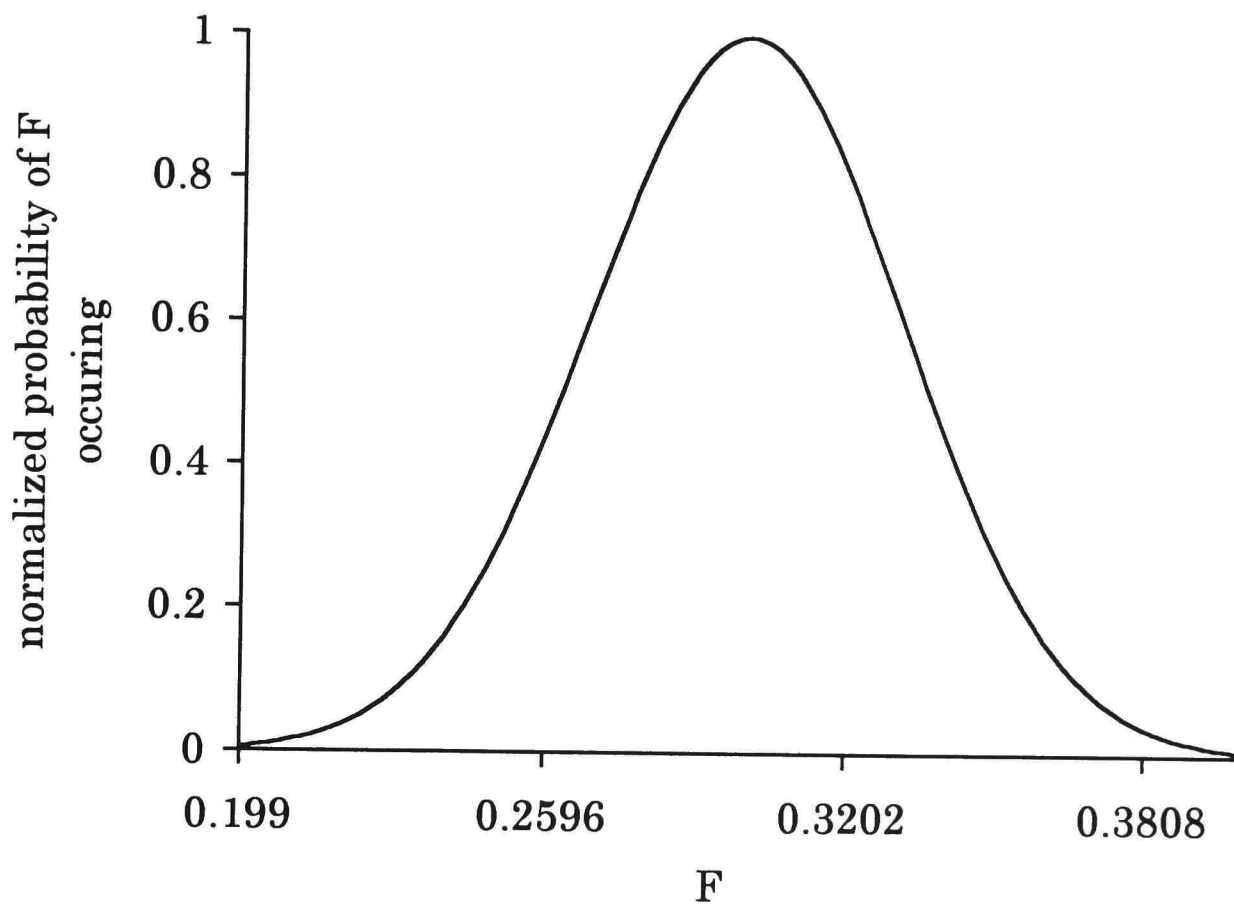


Figure 76. Typical Gaussian curve.

$$E_c = \frac{1}{2} CV^2 \quad (28)$$

The electric field strength (E) is equal to the voltage (V) divided by the distance (d). Substituting this into the energy equation gives you

$$E_c = \frac{1}{2} CE^2 d^2 \quad (29)$$

So the energy stored in the capacitor increases to the square power of the electric field. This means that if the system is operating at 60% JCM then only 36% of the energy is stored that would be stored at 100% JCM. This has a significant impact on the design of the machine. Of course, it would not be a good idea to operate at JCM level because half of the shots would not be any good because of voltage breakdown in the water capacitor. In designing a machine, the cost of the size of the machine versus the number of bad shots tolerated would have to be weighed. This would not only be the data lost on a bad shot but the damage done to the machine.

How can Sandia operate at 120% JCM?

It should be remembered that the JCM equations at the beginning of this paper were based on empirical data and not theory [29]. This means that each of the parameters has a limited range for which the equations are valid. Extrapolating the equations outside of these ranges could cause trouble. The size of the pulsed power machines that are being built today are on a much larger scale than what was available at the time Martin did his

experiments. The size and area dimensions of the Sandia machines are outside of the range of data for the JCM equations. Additional experiments were conducted by the Naval Research Laboratory in the late 1960's to expand Martin's equations. Considerable data were generated by W. H. Lupton and resulted in the Elbert-Lupton equations which are similar to the Martin equations. The major difference is the exponent for the area term. The two Elbert-Lupton equations are

$$F\tau_{eff}^{1/3}A^{0.058} = 0.23, \quad (30)$$

for positive polarity, and

$$F\tau_{eff}^{1/3}A^{0.069} = 0.557, \quad (31)$$

for negative polarity. The Sandia machines operate under the Elbert-Lupton levels. For the area dimensions involved with the Sandia machines, if the Martin equations are used, it appears that the system is operating at the 120% level. PI uses the Elbert-Lupton equations to design their machines [28]. The DOUBLE EAGLE machine was designed at 60% Elbert-Lupton and has never had a breakdown in its water line.

The curves in Figure 77 show the difference between the JCM levels and the Elbert-Lupton levels for various surface areas. The third trace is the 120% JCM level. As can be seen, for areas above 43,000 cm², the Elbert-Lupton curve crosses the 120% JCM curve.

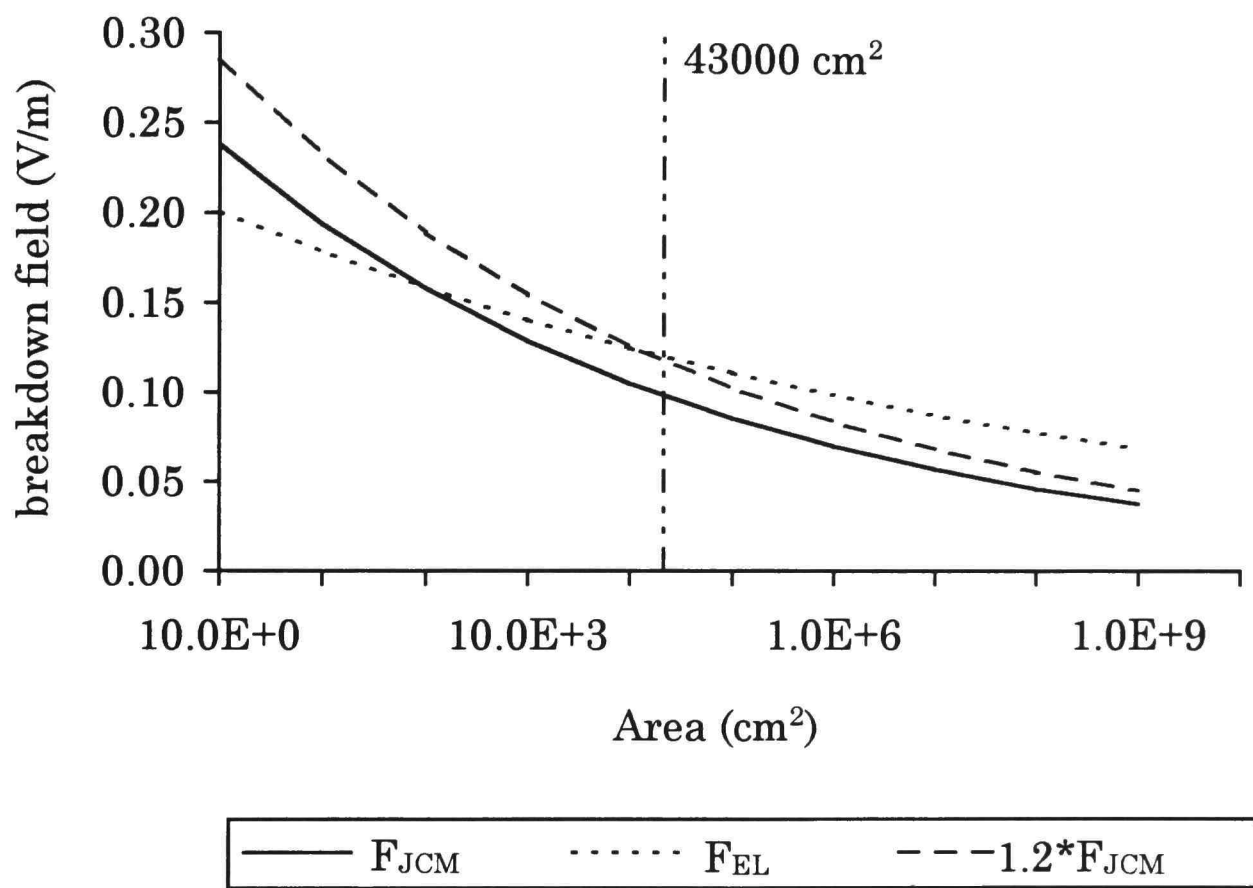


Figure 77. Comparison of the breakdown field equations (F) versus surface area (A).

The designers at Sandia [29] believe that the area term dependency disappears at very large areas, e.g., $A > 10^7 \text{ cm}^2$.

What is Texas Tech doing?

The research being conducted at Texas Tech is looking at the effects of magnetic fields, electrode coatings and water additives on E_{BD} and τ_{eff} . No one has examined the effects of magnetic fields on water before. Various additives, such as alcohol and glycol, have been used to allow the water temperature to be lowered beyond its normal freezing point in order to increase E_{BD} and τ_{eff} . Additives that affect these two parameters directly will be looked at. Several different types of coatings on the electrode surfaces have been tried. The Texas Tech Pulsed Power Laboratory will look at using polymer and wax coatings on the surface of the electrodes. The Water Breakdown System in use at Texas Tech is capable of delivering a 400 kV, 150 ns pulse to a 1.5 cm gap.

Additional Water Breakdown Level Information

Starting with the equation for energy in a capacitor,

$$E_c = \frac{1}{2} CV^2, \quad (32)$$

where E_c is in joules, C is in farads, and V is in volts. The equation for the electric field (F) for the simplest case of parallel plate geometry is

$$F = \frac{V}{d}, \quad (33)$$

where V is in volts and d is in meters. For other geometries, various field enhancement factors must be included. Combining the two equations yields

$$E_c = \frac{1}{2}CF^2d^2. \quad (34)$$

For a parallel plate capacitor, the equation for the capacitance is given by

$$C = \frac{\epsilon_o \epsilon_r A}{d}, \quad (35)$$

where $\epsilon_o = 8.85 \times 10^{-12}$ farad/meter, ϵ_r is the relative dielectric constant, A is the area of the two plates in meter², and d is the distance between the two plates in meters. Combining Eqs. (34) and (35) gives

$$E_c = \frac{1}{2} \frac{\epsilon_o \epsilon_r A}{d} F^2 d^2, \quad (36)$$

which reduces to

$$E_c = \frac{1}{2} \epsilon_o \epsilon_r A F^2 d. \quad (37)$$

By picking

$$AF^2d = \frac{2}{\epsilon_o} \text{ (volts}^2 \text{ meter)}, \quad (38)$$

then

$$E_c \sim \epsilon_r. \quad (39)$$

By graphing this along with three of the most common insulators - oil, ethylene glycol (antifreeze), water, the importance that water plays in pulsed power machines can be seen (Figure 78).

Next, the effect of the insulating medium on the amount of energy stored in the capacitor as the electric field increases can be looked at. Going back to Eq. (37)

$$E_c = \frac{1}{2} \epsilon_o \epsilon_r A F^2 d , \quad (37)$$

and setting

$$Ad = \frac{2}{\epsilon_o} (\text{m}^3) , \quad (40)$$

then

$$E_c \sim \epsilon_r F^2 . \quad (41)$$

Remember that ϵ_r for oil, ethylene glycol, and water are 2.2, 39, and 80, respectively. Figure 79 shows the effects of ϵ_r on the energy stored as the electric field (F) increases.

Next, how the energy changes with respect to the area can be shown. The four cases for water using the J. C. Martin and Elbert-Lupton equations need to be looked at. J. C. Martin showed that

$$F \tau_{eff}^{1/3} A^{1/10} = 0.3 , \quad (25)$$

for positive polarity and

$$F \tau_{eff}^{1/3} A^{1/10} = 0.6 , \quad (26)$$

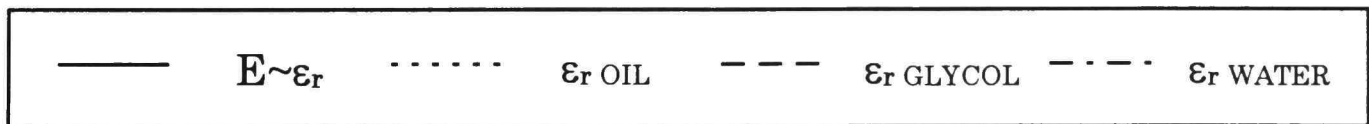
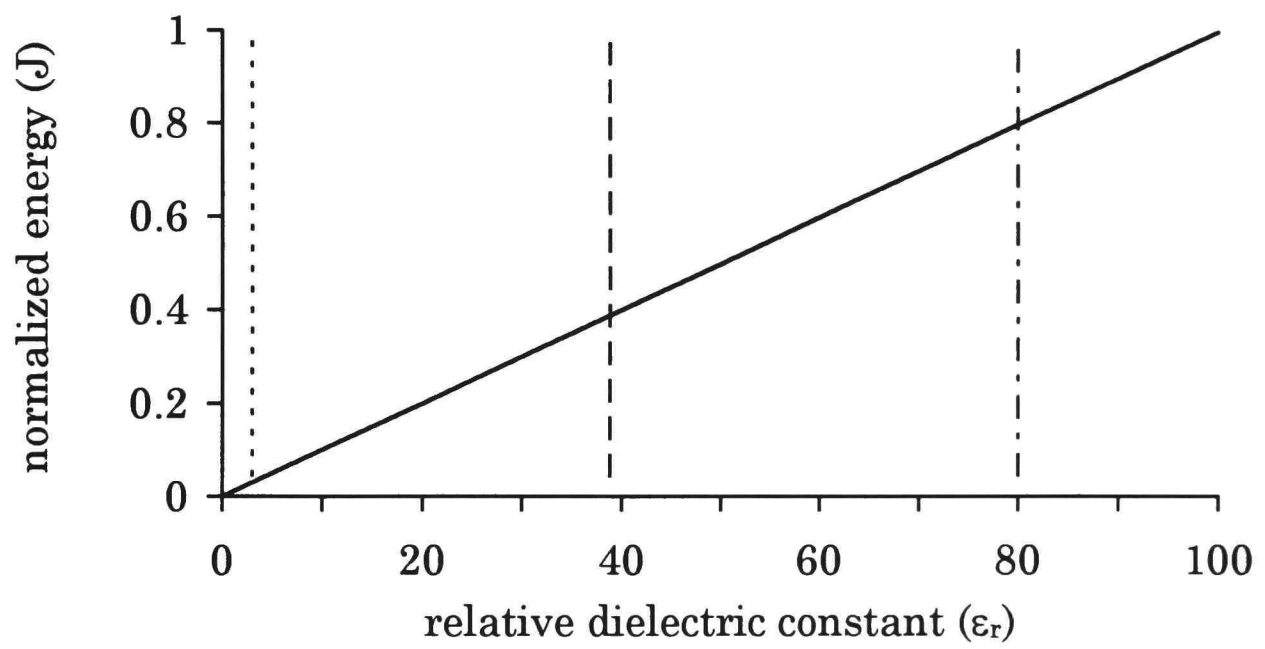


Figure 78. Normalized Energy (E_C) versus relative dielectric (ϵ_r) for $AF^2d = 2/\epsilon_0$.

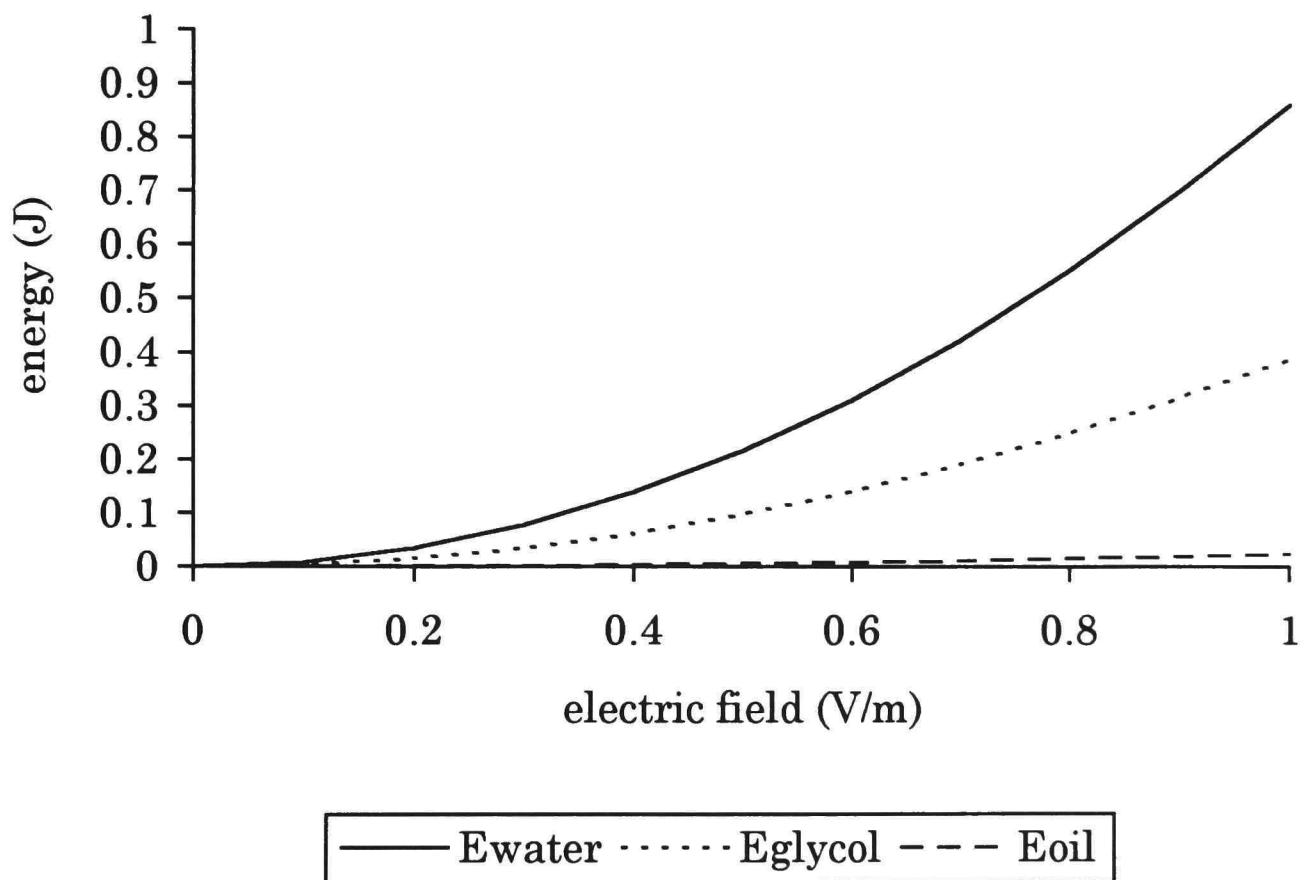


Figure 79. Normalized energy (E_c) versus normalized electric field (F) for $Ad = 2/\epsilon_0$.

for negative polarity, where F is the electric field breakdown level in MV/cm, A is the area in cm^2 , and τ_{eff} is the effective time in μs . Solving these two equations for F gives us

$$F = \frac{0.3}{\tau_{\text{eff}}^{1/3} A^{1/10}}, \quad (42)$$

and

$$F = \frac{0.6}{\tau_{\text{eff}}^{1/3} A^{1/10}}. \quad (43)$$

The significance of the polarity dependence is that in non-parallel plate geometry, e.g., coaxial, the high field electrode (the smallest one), i.e., the inner coaxial electrode, should be negative. Reversing the polarity on coaxial systems is, therefore, not a good idea. It will lower the hold-off voltage by a factor of two and thus the energy by a factor of four.

Elbert-Lupton showed that

$$F \tau_{\text{eff}}^{1/3} A^{0.058} = 0.23, \quad (30)$$

for positive polarity, and

$$F \tau_{\text{eff}}^{1/3} A^{0.069} = 0.557, \quad (31)$$

for negative polarity. Again, solving for F gives

$$F = \frac{0.23}{\tau_{\text{eff}}^{1/3} A^{0.058}}, \quad (44)$$

for positive polarity, and

$$F = \frac{0.557}{\tau_{eff}^{1/3} A^{0.069}}, \quad (45)$$

for negative polarity. A set of four energy equations which have been designated as E_{JCM+} , E_{JCM-} , E_{EL+} , and E_{EL-} for JCM positive, JCM negative, Elbert-Lupton positive, and Elbert-Lupton negative, respectively, can be derived. For E_{JCM+} , start with Eq. (37) again

$$E_c = \frac{1}{2} \varepsilon_o \varepsilon_r A F^2 d. \quad (37)$$

Substituting Eq. (42) into Eq. (37) gives

$$E_{JCM+} = \frac{1}{2} \varepsilon_o \varepsilon_r A \left(\frac{0.3}{\tau_{eff}^{1/3} A^{1/10}} \right)^2 d. \quad (46)$$

The A in Eq. (37) is in meter² while the A in Eq. (42) is in cm². The easiest way to make these terms compatible is to convert the first A to cm². This gives

$$E_{JCM+} = \frac{10^4}{2} \varepsilon_o \varepsilon_r A \left(\frac{0.3}{\tau_{eff}^{1/3} A^{1/10}} \right)^2 d. \quad (47)$$

Rearranging and combining the terms now gives

$$E_{JCM+} = \frac{10^4}{2 \tau_{eff}^{2/3}} \varepsilon_o \varepsilon_r d A \frac{(0.3)^2}{A^{2/10}}, \quad (48)$$

which gives, for a fixed d and τ_{eff} , the following proportionality relationship

$$E_{JCM+} \sim (0.3)^2 A^{(1-2/10)}. \quad (49)$$

This gives the relationship for E_{JCM+} . Doing the same for the other three equations -- Eqs. (43), (44), (45) -- gives

$$E_{JCM-} \sim (0.6)^2 A^{(1-2/10)}, \quad (50)$$

$$E_{EL+} \sim (0.23)^2 A^{(1-2 \cdot 0.058)}, \quad (51)$$

and,

$$E_{EL-} \sim (0.557)^2 A^{(1-2 \cdot 0.069)}. \quad (52)$$

Graphing these four equations gives Figure 80 which shows the relationships between the area and the energy for the four equations. As can be seen, there is a significant effect at very large areas on the amount of energy that can be stored depending on which set of equations used.

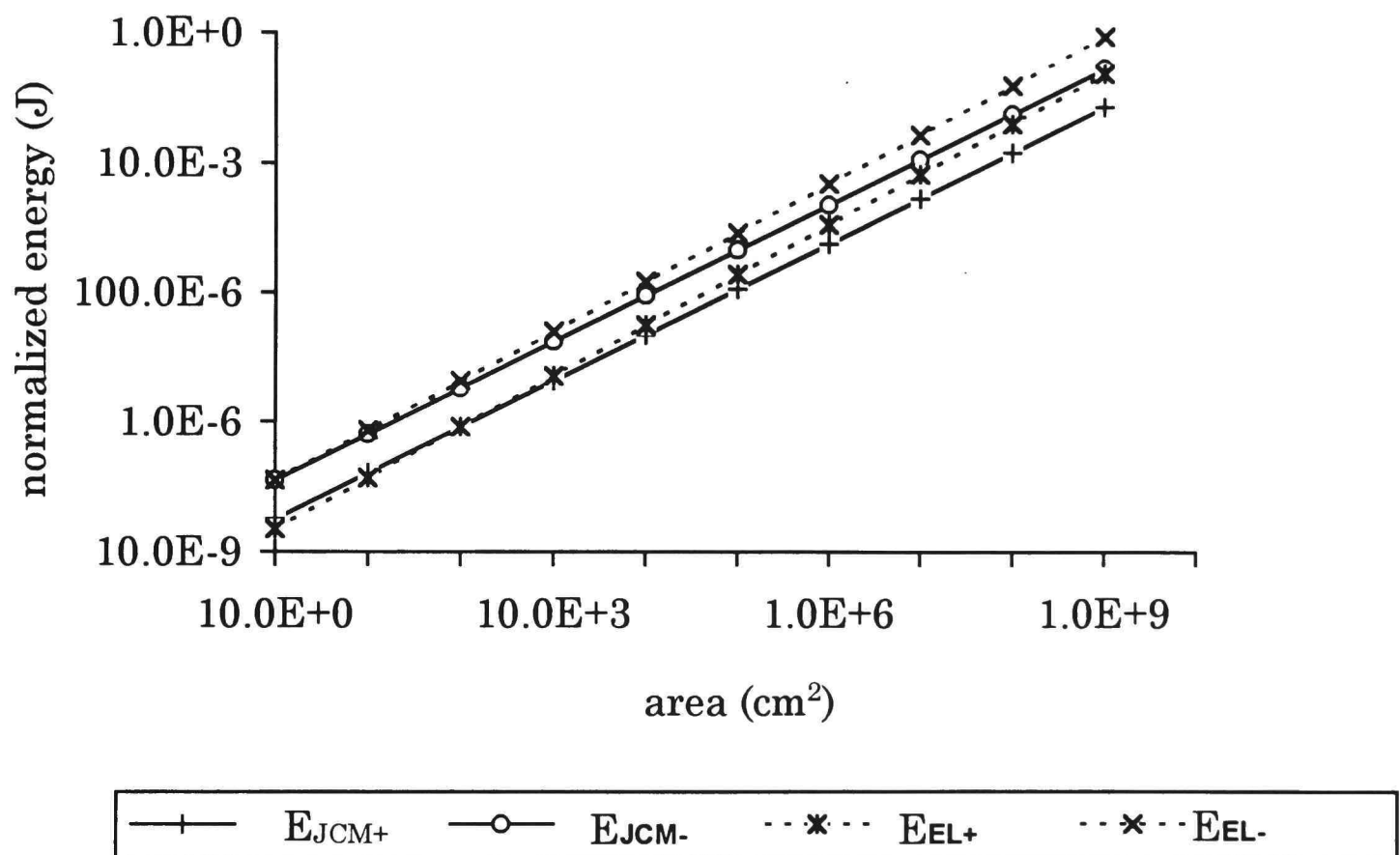


Figure 80. Normalized energy versus area for the JCM and EL equations.

APPENDIX B

D-DOT PROBE

D-Dot probe derivation

A D-Dot probe is typically used for measuring high voltage pulses in liquid (oil or water) insulated systems where direct measurement is not practical. The D-Dot probe makes use of the capacitive divider effect that the probe has on the voltage. It actually measures the derivative of the electric field. Figure 19 shows a typical D-Dot probe configuration. The probe is simply the inner conductor of a small coaxial section. It is insulated from the surrounding shell by the same insulating material as in the machine. In this case, it is transformer oil. Since the probe gives the derivative of the electric field, the signal must be fed into an integrator to give us the pulse shape of the signal trying to be measured. The probe can be designed by looking at the capacitance between the inner conductor of the machine and the probe (C_1 in Figure 19) and between the probe and the outer coaxial line of the machine (C_2). A simple RC integrator is used to give us the correct output signal. Analysis of the D-Dot probe will be based on the circuit model in Figure 20.

Since the only reactive elements in the circuit are capacitors, the following definition will be used:

$$X \equiv \frac{1}{j\omega C}. \quad (53)$$

Using the circuit model in Figure 20, write the loop equations for the circuit.

There are 3 loop equations:

$$v_{in} = i_1(X_1 + X_2) - i_2 X_2, \quad (54)$$

$$0 = -i_1 X_2 + i_2(X_2 + R) - i_3 R, \quad (55)$$

$$0 = -i_2 R + i_3(X_3 + R_1 + R), \quad (56)$$

and v_{out} is given by

$$v_{out} = i_3 X_3. \quad (57)$$

In matrix form, it looks like

$$\begin{bmatrix} X_1 + X_2 & -X_2 & 0 \\ -X_2 & X_2 + R & -R \\ 0 & -R & X_3 + R_1 + R \end{bmatrix} \begin{bmatrix} i_1 \\ i_2 \\ i_3 \end{bmatrix} = \begin{bmatrix} v_{in} \\ 0 \\ 0 \end{bmatrix}. \quad (58)$$

Using Cramer's Rule to solve for i_3

$$i_3 = \frac{\begin{vmatrix} X_1 + X_2 & -X_2 & v_{in} \\ -X_2 & X_2 + R & 0 \\ 0 & -R & 0 \end{vmatrix}}{\begin{vmatrix} X_1 + X_2 & -X_2 & 0 \\ -X_2 & X_2 + R & -R \\ 0 & -R & X_3 + R_1 + R \end{vmatrix}}. \quad (59)$$

Taking the determinants of the numerator and the denominator, gives

$$i_3 = \frac{X_2 R v_{in}}{(X_1 + X_2)(X_2 + R)(X_3 + R_1 + R) - X_2^2(X_3 + R_1 + R) - (X_1 + X_2)R^2}. \quad (60)$$

To simplify the denominator, let

$$\Delta = (X_1 + X_2)(X_2 + R)(X_3 + R_1 + R) - X_2^2(X_3 + R_1 + R) - (X_1 + X_2)R^2. \quad (61)$$

Expanding the terms

$$\Delta = X_1 X_2 X_3 + X_1 X_2 (R_1 + R) + X_1 X_3 R + X_2 X_3 R + X_1 R_1 R + X_2 R_1 R. \quad (62)$$

Factor out $X_1 X_2 X_3$

$$\Delta = (X_1 X_2 X_3) \left(1 + \frac{R_1 + R}{X_3} + \frac{R}{X_2} + \frac{R}{X_1} + \frac{R_1 R}{X_2 X_3} + \frac{R_1 R}{X_1 X_3} \right). \quad (63)$$

Finally

$$i_3 = \frac{R v_{in}}{(X_1 X_3) \left(1 + \frac{R_1 + R}{X_3} + \frac{R}{X_2} + \frac{R}{X_1} + \frac{R_1 R}{X_2 X_3} + \frac{R_1 R}{X_1 X_3} \right)}. \quad (64)$$

Using Eq. (57), then

$$\frac{v_{out}}{v_{in}} = \frac{R}{X_1 \left(1 + \frac{R_1 + R}{X_3} + \frac{R}{X_2} + \frac{R}{X_1} + \frac{R_1 R}{X_2 X_3} + \frac{R_1 R}{X_1 X_3} \right)}. \quad (65)$$

Using Eq. (53)

$$\frac{v_{out}}{v_{in}} = \frac{j\omega R C_1}{1 + j\omega [R(C_1 + C_2 + C_3) + R_1 C_3] - \omega^2 R(C_1 + C_2) R_1 C_3}, \quad (66)$$

which can be put into the form

$$\frac{V_{out}}{V_{in}} = \frac{j \frac{\omega}{\omega_1}}{\left(1 + j \frac{\omega}{\omega_2}\right) \left(1 + j \frac{\omega}{\omega_3}\right)}. \quad (67)$$

Expanding the denominator, gives

$$\left(1 + j \frac{\omega}{\omega_2}\right) \left(1 + j \frac{\omega}{\omega_3}\right) = 1 + j\omega \left(\frac{1}{\omega_2} + \frac{1}{\omega_3}\right) - \frac{\omega^2}{\omega_2 \omega_3}. \quad (68)$$

Setting this equal to the denominator of Eq. (66), gives

$$\frac{1}{\omega_2} + \frac{1}{\omega_3} = \frac{\omega_2 + \omega_3}{\omega_2 \omega_3} = R(C_1 + C_2 + C_3) + R_1 C_3, \quad (69)$$

and

$$\omega_2 \omega_3 = \frac{1}{R(C_1 + C_2)R_1 C_3}, \quad (70)$$

also from the numerator

$$\omega_1 = \frac{1}{RC_1}. \quad (71)$$

Substituting Eqs. (69), (70), and (71) into Eq. (66) gives the transfer function in the form of Eq. (67). At this point it would be useful to look at what the known quantities are and what is being solved. The value of R is known to be 50 Ω since it is the impedance of the cable connecting the D-Dot probe to the oscilloscope. The bandwidth (BW) of the system is equal to $2\pi f_3$ which is ω_3 . The BW should be at least comparable to the BW of the oscilloscope being used. Also the risetime of the signal can give us the desired BW. The integrator time constant (τ_i) should be at least 10 times the

pulsewidth of the signal that is being captured. (Note: at the time the probe was designed, it was thought that τ should be equal to the pulsewidth.) With this information, the unknowns are C_1 , C_2 , C_3 , and R_1 . At this point, some equations to solve for these values are needed.

The integrator's time constant, τ_i , is given by

$$\tau_i = R_1 C_3. \quad (72)$$

Replacing $R_1 C_3$ in Eq. (69) with τ_i and manipulating to solve for C_3 , gives

$$R(C_1 + C_2) + RC_3 = \frac{\omega_2 + \omega_3}{\omega_2 \omega_3} + \tau_i, \quad (73)$$

$$RC_3 = \frac{\omega_2 + \omega_3}{\omega_2 \omega_3} + \tau_i - R(C_1 + C_2), \quad (74)$$

and

$$C_3 = \frac{\omega_2 + \omega_3}{R\omega_2 \omega_3} + \frac{\tau_i}{R} - (C_1 + C_2). \quad (75)$$

Next, solve for ω_2 in terms of ω_3 which is the bandwidth (BW) of the system.

Using Eq. (70), solve for ω_2

$$\omega_2 = \frac{1}{R(C_1 + C_2)\tau_i \omega_3}. \quad (76)$$

The value of ω_3 is given by

$$\omega_3 = 2\pi \text{BW}. \quad (77)$$

From the Tektronix's catalog, the relationship

$$\text{BW} = \frac{0.35}{t_r}, \quad (78)$$

is given where t_r is the risetime of the pulse being measured. Combining Eqs. (77) and (78) gives

$$\omega_3 = \frac{0.7\pi}{t_r}. \quad (79)$$

Next, a Bode plot will be used to develop a relationship between the input and output voltages and the frequencies. Figure 81 shows what a typical transfer function with one zero and two poles looks like [Eq. (67)]. The asymptote for the zero, in this case ω_1 , rises at 20 dB/decade. It crosses the 0 dB line at ω_1 . The 0 dB line is equal to the input voltage (v_{in}). The curve will rise at 20 dB/decade from the left side of the plot until it gets to the value of the first pole (ω_2). At that point, the curve flattens out until it gets to ω_3 then it will drop at 20 dB/decade. The value of the voltage along this curve is the output voltage. Of particular interest is the flat part of the curve, since this will be the maximum voltage out (v_{out}) of the D-Dot probe. To get a relationship between v_{in}/v_{out} , the number of decades between ω_1 and ω_2 must be determined, which is

$$\text{Decades} = \log\left(\frac{\omega_1}{\omega_2}\right). \quad (80)$$

Since the rate of change is 20 dB/decade, the difference between v_{in} and v_{out} is $20 \log(\omega_1/\omega_2)$. Since v_{in} and v_{out} are in dB, the equation can be written as

$$v_i(\text{dB}) - v_o(\text{dB}) = 20 \log\left(\frac{\omega_1}{\omega_2}\right). \quad (81)$$

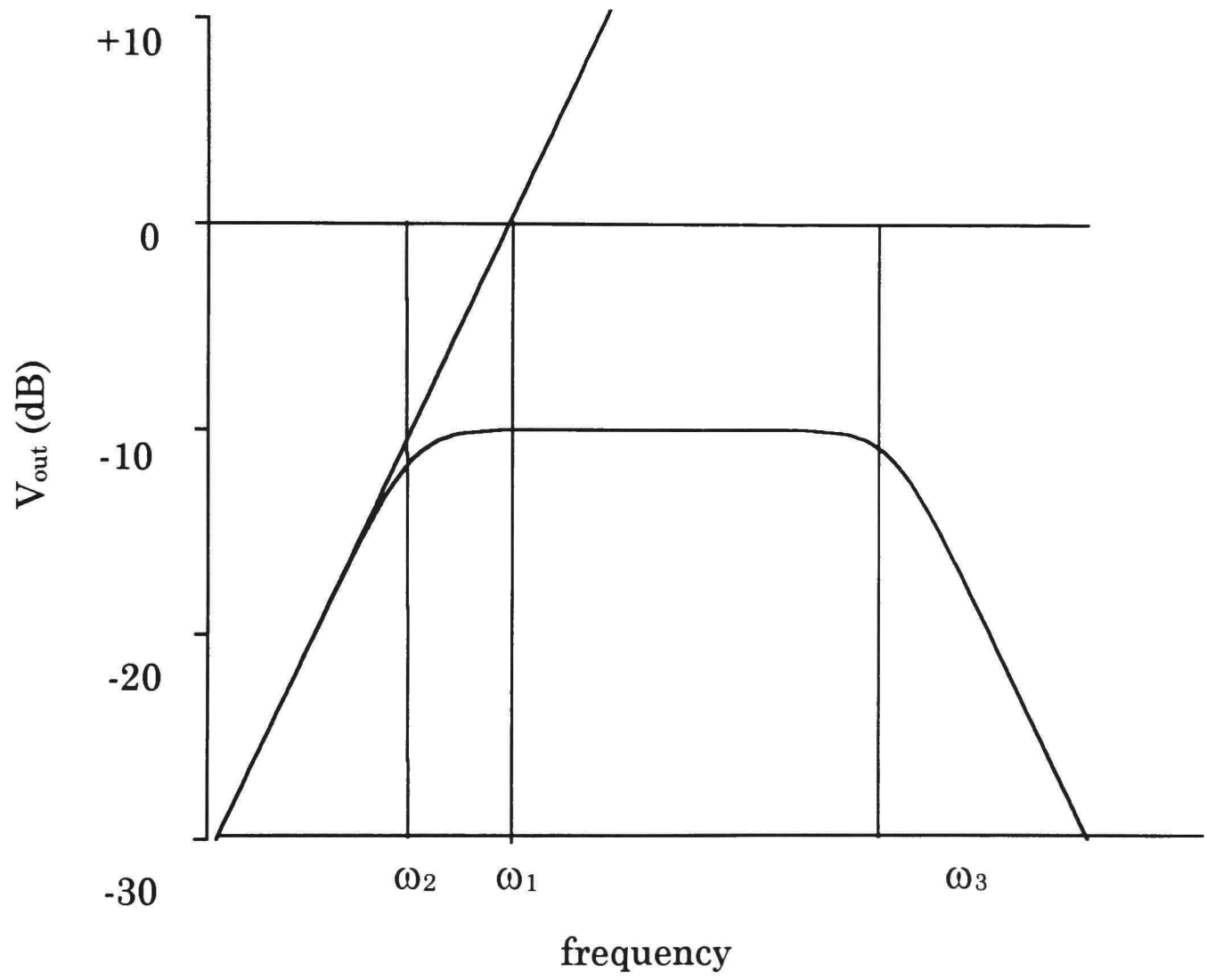


Figure 81. Typical Bode plot with one zero and two poles.

Using the definition of dB, Eq. (81) is

$$20\log(v_i) - 20\log(v_o) = 20\log\left(\frac{\omega_1}{\omega_2}\right), \quad (82)$$

which is

$$20\log\left(\frac{v_i}{v_o}\right) = 20\log\left(\frac{\omega_1}{\omega_2}\right), \quad (83)$$

dividing both sides by 20 and taking the inverse log gives

$$\frac{v_i}{v_o} = \frac{\omega_1}{\omega_2}, \quad (84)$$

and, finally

$$v_o = \frac{\omega_2}{\omega_1} v_i. \quad (85)$$

With Eq. (85), the values needed to design the D-Dot probe can be derived. The final solution will be an iterative process. First of all, C_2 needs to be much greater than C_1 . The reason for this is discussed in Wilkinson's [26] paper and it also has an effect on the physical design of the probe.

$$C_2 = 50C_1, \quad (86)$$

was chosen to coincide with the capacitor values used in Wilkinson's paper. Eqs. (71), (72), (75), (76), (85), and (86) are needed to design the probe. The risetime of the signal was known, so Eq. (78) was used to get an idea of the bandwidth that was needed. Eq. (78) gives the minimum bandwidth so this value was multiplied by ten. From this value, ω_3 is derived from Eq. (77).

Using Mathcad, the following constants were used:

$$\begin{aligned}
R &= 50 \Omega, \\
\tau_i &= 2 \mu\text{s}, \\
C_1 &= 0.5 \text{ pF}, \\
C_2 &= 50C_1, \\
\omega_3 &= 2\pi 100 \text{ MHz}, \\
&\text{and,} \\
v_{\text{in}} &= 1 \text{ MV}.
\end{aligned} \tag{87}$$

The value of τ_i was selected at 2 μs to coincide with the system's pulsewidth. This is the minimum integration time that should be used. C_1 was chosen from the value used in Wilkinson's article. From Eq. (78), with a risetime of 30 ns, the bandwidth would be 11.16 MHz. Ten times this value gives about 100 MHz, so ω_3 is set to $2\pi 100$ MHz. The following equations were then entered into Mathcad:

$$\omega_2 = \frac{1}{R(C_1 + C_2)\tau_i\omega_3}, \tag{76}$$

$$\omega_1 = \frac{1}{RC_1}, \tag{71}$$

$$v_o = \frac{\omega_2}{\omega_1} v_i, \tag{85}$$

$$C_3 = \frac{\omega_2 + \omega_3}{R\omega_2\omega_3} + \frac{\tau_i}{R} - (C_1 + C_2), \tag{75}$$

and,

$$R_1 = \frac{\tau_i}{C_3}. \tag{72}$$

By adjusting the values in Eq. (87), the values of v_{out} , C_2 , C_3 , and R_1 can be calculated. The value of v_{out} needs to be maximized which is inversely

proportional to the bandwidth and the integration time. Also C_1 should be as small as possible since it determines the overall size of the probe. Certain values of C_1 and the bandwidth will cause R_1 and C_3 to go negative. By adjusting the values of Eq. (87), reasonable values for the probe can be derived.

After finding the values needed for the components, then the dimensions of the probe must be derived. C_1 can be estimated as a parallel plate capacitor. The equation for C_1 is given by

$$C_1 = \frac{\epsilon_r \epsilon_0 \pi r^2}{d} \quad (88)$$

Solve for the radius (r)

$$r = \sqrt{\frac{C_1 d}{\epsilon_r \epsilon_0 \pi}} \quad (89)$$

C_2 can be thought of as a coaxial capacitor and the capacitance is given by

$$C_2 = \frac{2\pi\epsilon_r \epsilon_0 l}{\ln\left(\frac{b}{r}\right)} \quad (90)$$

Solve for the length (l)

$$l = \frac{C_2 \ln\left(\frac{b}{r}\right)}{2\pi\epsilon_r \epsilon_0}, \quad (91)$$

where b is the radius of the outer conductor, which is the radius of the probe plus the gap thickness (t_g) between the inner and outer conductors of the

probe (Figure 82). The value of t_g is somewhat arbitrary. The gap should be large enough to prevent voltage breakdown across the gap, yet small enough to make l manageable. Starting with t_g equal to 1 cm, it was adjusted to get a reasonable length. If l is too small, then it may be physically difficult to mount the probe on the system.

For the D-Dot probe for the Water Breakdown Experiment, the dimensions were

$$\begin{aligned}
 R_1 &= 1.21 \text{ k}\Omega, \\
 C_1 &= 0.65 \text{ pF}, \\
 C_2 &= 32.50 \text{ pF}, \\
 C_3 &= 1.66 \text{ nF}, \\
 r &= 2.96 \text{ cm}, \\
 t_g &= 0.69 \text{ cm}, \\
 b &= 3.65 \text{ cm}, \\
 d &= 8.26 \text{ cm} \\
 &\text{and,} \\
 l &= 5.56 \text{ cm}.
 \end{aligned} \tag{92}$$

The only change in the initial conditions is $C_1 = 0.65 \text{ pF}$ instead of 0.5 pF .

This was necessary to get reasonable values of C_3 and R_1 . For the parameters listed above, V_{out} would equal 15.6 V for V_{in} of 1 MV .

D-Dot probe construction

From the values listed in Eq. (44) above, a set of drawings was generated. The body of the probe was made of aluminum with the insulator

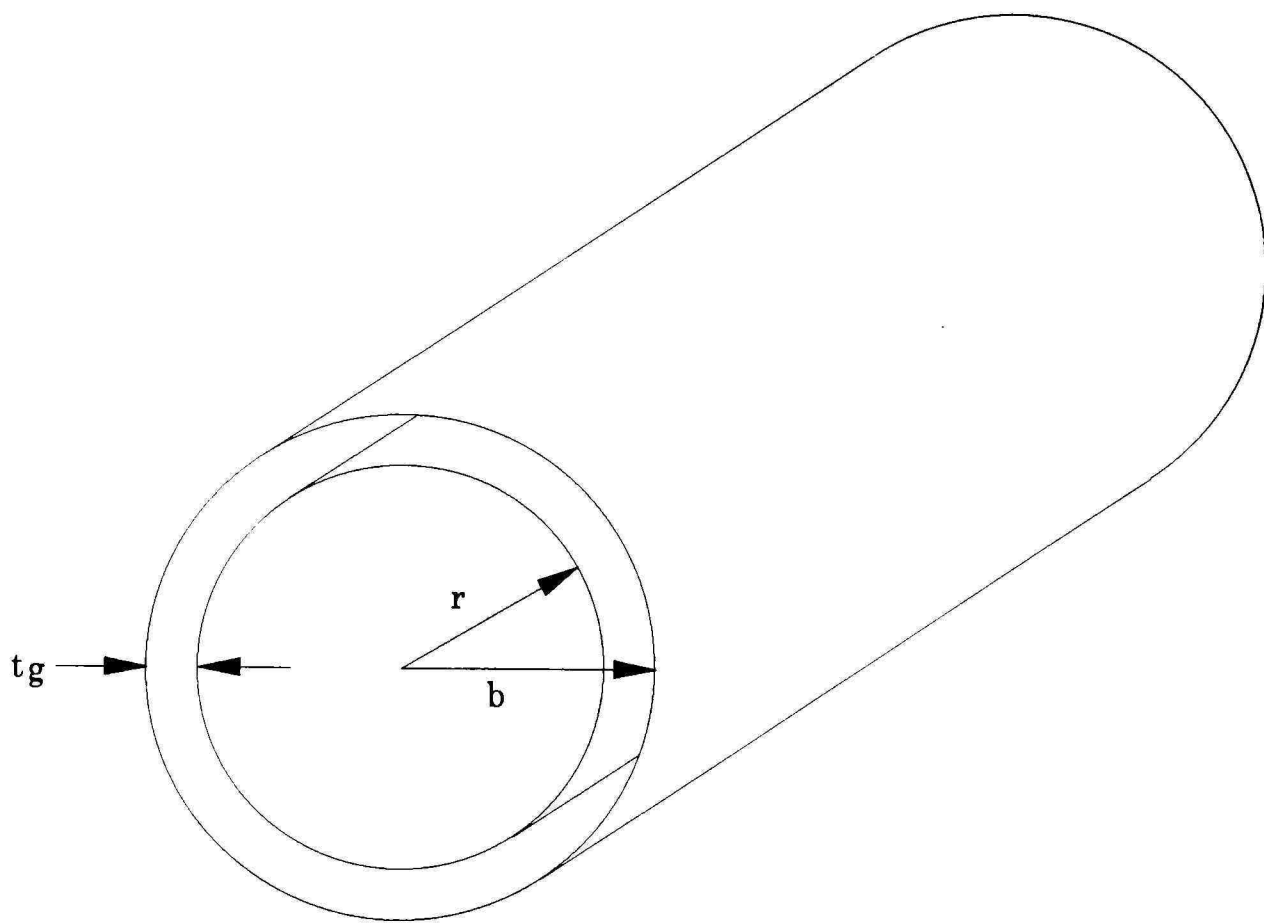


Figure 82. Coaxial geometry for Eqs. (90) and (91).

made from nylon. A mounting plate was welded to the coaxial line so that the probe could be bolted to the coaxial line without the need for any bolt heads to protrude into the line. A test setup was built from copper sheeting and consisted of two cone shaped end pieces which were bolted to the ends of the coaxial line section. A line pulser was used to test the probe. A 1 kV, 400 ns pulse was injected into the test setup which was terminated into a 50 Ω load. Measurements were made of the input voltage and the output voltage from the probe with the results shown in Figure 83. The top trace was the input signal measured with a Tektronix P-6015, 75 MHz bandwidth, probe. The bottom trace was the output of the D-Dot probe. It is interesting to note that the output of the D-Dot probe gives a better representation of the input signal than the Tektronix probe did. The frequency response of the Tektronix probe was only 75 MHz while the D-Dot was designed for 100 MHz. From the sharpness of the curve on the bottom of Figure 83, it appears that the bandwidth of the D-Dot probe is much higher than 100 MHz.

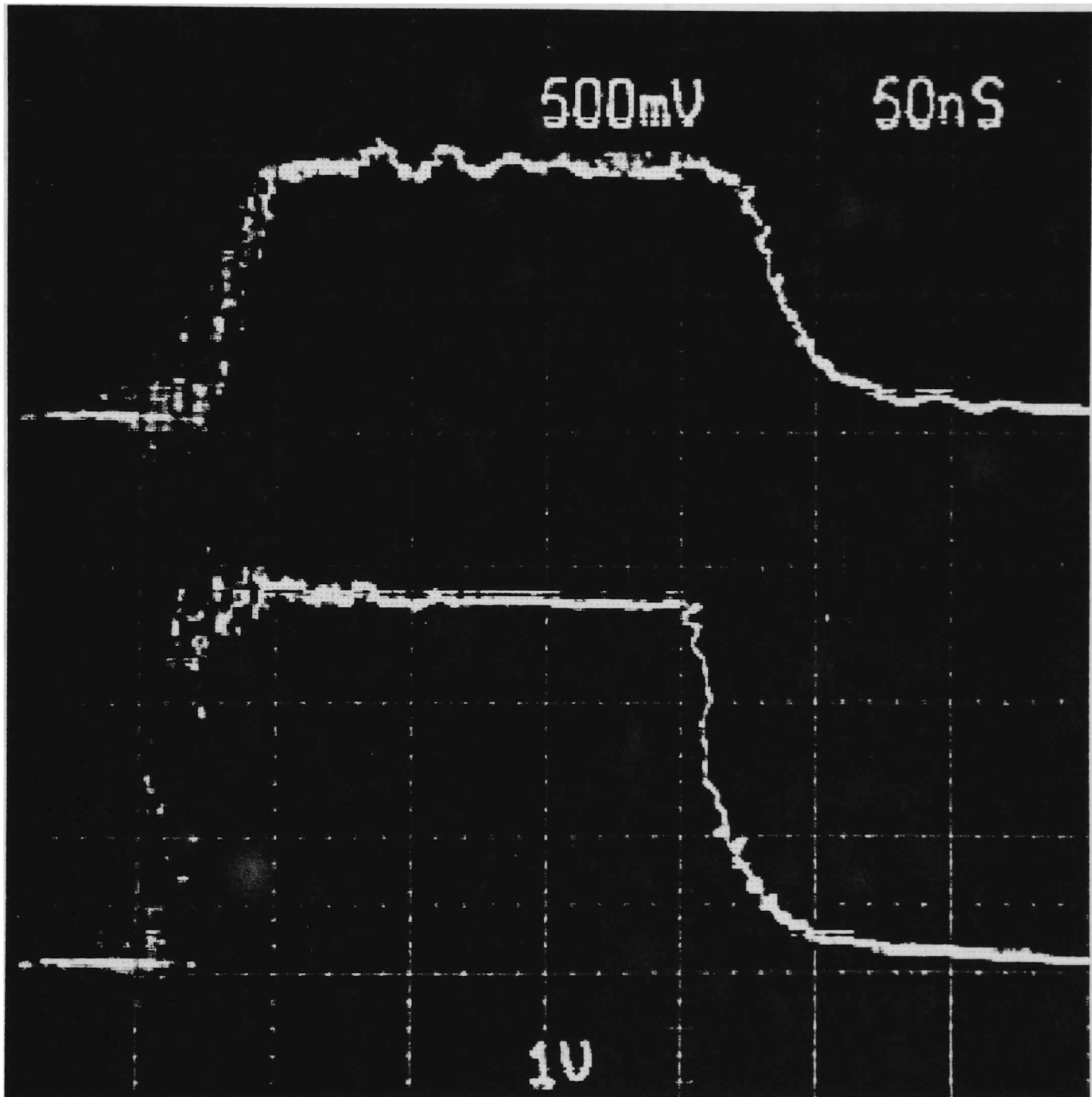


Figure 83. Output of the D-Dot probe. The top trace was the input signal measured with a 75 MHz bandwidth probe. The bottom trace was the output of the D-Dot probe.

APPENDIX C

MATLAB PROGRAMS

Notes: (1) All MATLAB comments are preceded by a percent sign and (2) MATLAB commands that exceeded the margin spacing were continued with a hanging indent. In the actual program file, the margins would have to be set so the whole command would be on one line. (3) Two sets of programs are given here as a representation of the type of programming that was done to analyze the data. The first set of programs -- WAX1.M, WAX1A.M, and WAX1B.M -- is an example of a set of data analyzed using only *t*-tests and the second set -- HCL1.M, HCL1A.M, and HCL1B.M -- is an example of a set of data analyzed using first an ANOVA and then *t*-tests. The function calls used by these programs follow the main programs.

WAX1.M

```
clear
```

```
% This program loads the ASCII files and renames the data. Baseline data  
% variables start with a "b" while the wax data shots start with a "w".  
% Baseline shots - same as for the polymer coating shots.
```

```
load base02.asc
```

```
ba= base02(:,2);
```

```
clear base02  
  
load base03.asc  
  
bb= base03(:,2);  
  
clear base03  
  
load base04.asc  
  
bc= base04(:,2);  
  
clear base04  
  
load base05.asc  
  
bd= base05(:,2);  
  
clear base05  
  
load base06.asc  
  
be= base06(:,2);  
  
clear base06  
  
load base07.asc  
  
bf= base07(:,2);  
  
clear base07  
  
load base08.asc  
  
bg= base08(:,2);  
  
clear base08  
  
load base09.asc  
  
bh= base09(:,2);
```

```
clear base09

load base10.asc

bi= base10(:,2);

clear base10

load base11.asc

bj= base11(:,2);

clear base11

% WAX shots

load wax01.asc

wa= wax01(:,2);

clear wax01

load wax02.asc

wb= wax02(:,2);

clear wax02

load wax03.asc

wc= wax03(:,2);

clear wax03

load wax04.asc

wd= wax04(:,2);

clear wax04

load wax05.asc
```

```
we= wax05(:,2);  
  
clear wax05  
  
load wax06.asc  
  
wf= wax06(:,2);  
  
clear wax06  
  
load wax07.asc  
  
wg= wax07(:,2);  
  
clear wax07  
  
load wax08.asc  
  
wh= wax08(:,2);  
  
clear wax08  
  
load wax09.asc  
  
wi= wax09(:,2);  
  
clear wax09  
  
load wax10.asc  
  
wj= wax10(:,2);  
  
clear wax10  
  
% Adjust the shots so they all overlap  
  
[bb]=adjust(ba,bb);  
  
[bc]=adjust(ba,bc);  
  
[bd]=adjust(ba,bd);
```

```

[be]=adjust(ba,be);
[bf]=adjust(ba,bf);
[bg]=adjust(ba,bg);
[bh]=adjust(ba,bh);
[bi]=adjust(ba,bi);
[bj]=adjust(ba,bj);
[wb]=adjust(wa,wb);
[wc]=adjust(wa,wc);
[wd]=adjust(wa,wd);
[we]=adjust(wa,we);
[wf]=adjust(wa,wf);
[wg]=adjust(wa,wg);
[wh]=adjust(wa,wh);
[wi]=adjust(wa,wi);
[wj]=adjust(wa,wj);

% Get "mean" waveforms. Take the mean of each set of data points.

for xx=1:512

temp1=[ba(xx) bb(xx) bc(xx) bd(xx) be(xx) bf(xx) bg(xx) bh(xx) bi(xx) bj(xx)];

    baseline(xx)=mean(temp1);

temp2=[wa(xx) wb(xx) wc(xx) wd(xx) we(xx) wf(xx) wg(xx) wh(xx) wi(xx)

    wj(xx)];

```

```
wax(xx)=mean(temp2);  
end %(xx)  
  
tm=(0:511)/512*500; % timeline values (x-axis) for plots.  
  
% Plot average waveforms.  
  
plot(tm,baseline/1e-9,tm,wax/1e-9)  
  
title('Baseline vs Black Wax Coating - Average Values (Adjusted)')  
  
xlabel('ns')  
  
ylabel('nV')  
  
save wax1
```

WAX1A.M

```
% This program extracts the data needed for the statistical analysis and for  
% the graphs.
```

```
clear
```

```
load wax1
```

```
% Correct the waveform in order to calculate the fall-time and fall-rate
```

```
ba=fixcurve(ba,300);
```

```
bb=fixcurve(bb,300);
```

```
bc=fixcurve(bc,300);
```

```
bd=fixcurve(bd,300);
```

```
be=fixcurve(be,300);
```

```
bf=fixcurve(bf,300);
```

```
bg=fixcurve(bg,300);
```

```
bh=fixcurve(bh,300);
```

```
bi=fixcurve(bi,300);
```

```
bj=fixcurve(bj,300);
```

```
wa=fixcurve(wa,200);
```

```
wb=fixcurve(wb,200);
```

```
wc=fixcurve(wc,200);
```

```
wd=fixcurve(wd,200);
```

```
we=fixcurve(we,200);
```

```

wf=fixcurve(wf,200);

wg=fixcurve(wg,200);

wh=fixcurve(wh,200);

wi=fixcurve(wi,200);

wj=fixcurve(wj,200);

tlength=500e-9; % length of scope display

tx=tlength/512; % time between points

% Set up vectors for teff, Vmax, fall-time, and fall-rate for both the baseline

% and the wax data.

teffbaseline=zeros(1,10);

maxbaseline=zeros(1,10); % Vmax

falltimebase=zeros(1,10);

fallratebase=zeros(1,10);

teffwax=zeros(1,10);

maxwax=zeros(1,10);

falltimewax=zeros(1,10);

fallratewax=zeros(1,10);

% BASELINE = ba,bb,...,bj

% Calculate teff, Vmax, fall-time, and fall-rate for each signal

tempa=max(ba);

tempb=find(ba(1:300)>=.63*tempa);

```

```

teffbaseline(1)=(tempb(length(tempb))-tempb(1))*tx;
maxbaseline(1)=tempa;
falltimebase(1)=falltime(ba,tlength);
fallratebase(1)=fallrate(ba,tlength);
tempa=max(bb);
tempb=find(bb(1:300)>=.63*tempa);
teffbaseline(2)=(tempb(length(tempb))-tempb(1))*tx;
maxbaseline(2)=tempa;
falltimebase(2)=falltime(bb,tlength);
fallratebase(2)=fallrate(bb,tlength);
tempa=max(bc);
tempb=find(bc(1:300)>=.63*tempa);
teffbaseline(3)=(tempb(length(tempb))-tempb(1))*tx;
maxbaseline(3)=tempa;
falltimebase(3)=falltime(bc,tlength);
fallratebase(3)=fallrate(bc,tlength);
tempa=max(bd);
tempb=find(bd(1:300)>=.63*tempa);
teffbaseline(4)=(tempb(length(tempb))-tempb(1))*tx;
maxbaseline(4)=tempa;
falltimebase(4)=falltime(bd,tlength);

```

```

fallratebase(4)=fallrate(bd,tlength);

tempa=max(be);

tempb=find(be(1:300)>=.63*tempa);

teffbaseline(5)=(tempb(length(tempb))-tempb(1))*tx;

maxbaseline(5)=tempa;

falltimebase(5)=falltime(be,tlength);

fallratebase(5)=fallrate(be,tlength);

tempa=max(bf);

tempb=find(bf(1:300)>=.63*tempa);

teffbaseline(6)=(tempb(length(tempb))-tempb(1))*tx;

maxbaseline(6)=tempa;

falltimebase(6)=falltime(bf,tlength);

fallratebase(6)=fallrate(bf,tlength);

tempa=max(bg);

tempb=find(bg(1:300)>=.63*tempa);

teffbaseline(7)=(tempb(length(tempb))-tempb(1))*tx;

maxbaseline(7)=tempa;

falltimebase(7)=falltime(bg,tlength);

fallratebase(7)=fallrate(bg,tlength);

tempa=max(bh);

tempb=find(bh(1:300)>=.63*tempa);

```

```

teffbaseline(8)=(tempb(length(tempb))-tempb(1))*tx;
maxbaseline(8)=tempa;
falltimebase(8)=falltime(bh,tlength);
fallratebase(8)=fallrate(bh,tlength);
tempa=max(bi);
tempb=find(bi(1:300)>=.63*tempa);
teffbaseline(9)=(tempb(length(tempb))-tempb(1))*tx;
maxbaseline(9)=tempa;
falltimebase(9)=falltime(bi,tlength);
fallratebase(9)=fallrate(bi,tlength);
tempa=max(bj);
tempb=find(bj(1:300)>=.63*tempa);
teffbaseline(10)=(tempb(length(tempb))-tempb(1))*tx;
maxbaseline(10)=tempa;
falltimebase(10)=falltime(bj,tlength);
fallratebase(10)=fallrate(bj,tlength);
maxbasemean=mean(maxbaseline);
maxbasestd=std(maxbaseline);
teffbasemean=mean(teffbaseline);
teffbasestd=std(teffbaseline);
falltimebasemean=mean(falltimebase);

```

```

falltimebasestd=std(falltimebase);
fallratebasemean=mean(fallratebase);
fallratebasestd=std(fallratebase);

% WAX

tempa=max(wa);
tempb=find(wa>=.63*tempa);
teffwax(1)=(tempb(length(tempb))-tempb(1))*tx;
maxwax(1)=tempa;
falltimewax(1)=falltime(wa,tlength);
fallratewax(1)=fallrate(wa,tlength);
tempa=max(wb);
tempb=find(wb>=.63*tempa);
teffwax(2)=(tempb(length(tempb))-tempb(1))*tx;
maxwax(2)=tempa;
falltimewax(2)=falltime(wb,tlength);
fallratewax(2)=fallrate(wb,tlength);
tempa=max(wc);
tempb=find(wc>=.63*tempa);
teffwax(3)=(tempb(length(tempb))-tempb(1))*tx;
maxwax(3)=tempa;
falltimewax(3)=falltime(wc,tlength);

```

```

fallratewax(3)=fallrate(wc,tlength);

tempa=max(wd);

tempb=find(wd>=.63*tempa);

teffwax(4)=(tempb(length(tempb))-tempb(1))*tx;

maxwax(4)=tempa;

falltimewax(4)=falltime(wd,tlength);

fallratewax(4)=fallrate(wd,tlength);

tempa=max(we);

tempb=find(we>=.63*tempa);

teffwax(5)=(tempb(length(tempb))-tempb(1))*tx;

maxwax(5)=tempa;

falltimewax(5)=falltime(we,tlength);

fallratewax(5)=fallrate(we,tlength);

tempa=max(wf);

tempb=find(wf>=.63*tempa);

teffwax(6)=(tempb(length(tempb))-tempb(1))*tx;

maxwax(6)=tempa;

falltimewax(6)=falltime(wf,tlength);

fallratewax(6)=fallrate(wf,tlength);

tempa=max(wg);

tempb=find(wg>=.63*tempa);

```

```

teffwax(7)=(tempb(length(tempb))-tempb(1))*tx;
maxwax(7)=tempa;
falltimewax(7)=falltime(wg,tlength);
fallratewax(7)=fallrate(wg,tlength);
tempa=max(wh);
tempb=find(wh>=.63*tempa);
teffwax(8)=(tempb(length(tempb))-tempb(1))*tx;
maxwax(8)=tempa;
falltimewax(8)=falltime(wh,tlength);
fallratewax(8)=fallrate(wh,tlength);
tempa=max(wi);
tempb=find(wi>=.63*tempa);
teffwax(9)=(tempb(length(tempb))-tempb(1))*tx;
maxwax(9)=tempa;
falltimewax(9)=falltime(wi,tlength);
fallratewax(9)=fallrate(wi,tlength);
tempa=max(wj);
tempb=find(wj>=.63*tempa);
teffwax(10)=(tempb(length(tempb))-tempb(1))*tx;
maxwax(10)=tempa;
falltimewax(10)=falltime(wj,tlength);

```

```

fallratewax(10)=fallrate(wj,tlength);

maxwaxmean=mean(maxwax);

maxwaxstd=std(maxwax);

teffwaxmean=mean(teffwax);

teffwaxstd=std(teffwax);

falltimewaxmean=mean(falltimewax);

falltimewaxstd=std(falltimewax);

fallratewaxmean=mean(fallratewax);

fallratewaxstd=std(fallratewax);

% Group the means and standard deviations for each of the four parameters.

maxmeans=[maxbasemean maxwaxmean];

maxstds=[maxbasestd maxwaxstd];

teffmeans=[teffbasemean teffwaxmean];

teffstds=[teffbasestd teffwaxstd];

falltimemeans=[falltimebasemean falltimewaxmean];

falltimestds=[falltimebasestd falltimewaxstd];

fallratemeans=[fallratebasemean fallratewaxmean];

fallratestds=[fallratebasestd fallratewaxstd];

% Plot the data.

xy=[0 6 0 ceil(max(teffmeans/1e-9)+max(teffstds/1e-9))*1.25];

axis(xy)

```

```

plot(teffmeans/1e-9)
errorbars(teffmeans/1e-9,teffstds/1e-9)
ylabel('ns')
title('Baseline vs Black Wax - teff')
pause
print
xy=[0 6 0 ceil(max(maxmeans/1e-9)+max(maxstds/1e-9))*1.25];
axis(xy)
plot(maxmeans/1e-9)
errorbars(maxmeans/1e-9,maxstds/1e-9)
ylabel('nV')
title('Baseline vs Black Wax - Maximum Voltage')
pause
print
xy=[0 6 0 ceil(max(falltimemeans/1e-9)+max(falltimestds/1e-9))*1.25];
axis(xy)
plot(falltimemeans/1e-9)
errorbars(falltimemeans/1e-9,falltimestds/1e-9)
ylabel('ns')
title('Baseline vs Black Wax - Falltime')
pause

```

```
print
xy=[0 6 0 2.5];
axis(xy)
plot(fallratemeans)
errorbars(fallratemeans,fallratestds)
ylabel('nV/ns')
title('Baseline vs Black Wax - Fallrate')
print
save wax1a
```

WAX1B.M

```
% This program does the statistical analysis of the data.

clear

load wax1a

% t-tests

% Vmax

df=18;

disp(['Baseline vs. Black Wax'])

disp([' '])

disp(['t-test (df = ',num2str(df),') - Vmax'])

M=[maxbaseline' maxwax'];

ttest % ttest does a series of t-tests on the data in the matrix M

% Calculate the percent change between the two means.

change(maxbaseline,maxwax);

% Teff

M=[teffbaseline' teffwax'];

disp([' '])

disp(['t-test (df = ',num2str(df),') - teff'])

ttest;

change(teffbaseline,teffwax);

disp([' '])
```

```
% Fall-time  
  
M=[falltimebase' falltimewax'];  
  
disp(['t-test (df = ',num2str(df),') - Fall-time'])  
  
disp([' '])  
  
ttest;  
  
change(falltimebase,falltimewax);  
  
% Fall-rate  
  
M=[fallratebase' fallratewax'];  
  
disp(['t-test (df = ',num2str(df),') - fall-rate'])  
  
disp([' '])  
  
ttest;  
  
change(fallratebase,fallratewax);
```

HCL2.M

% This program loads and renames ASCII data

load hc2ba.asc

ba=hc2ba;

clear hc2ba

load hc2bb.asc

bb=hc2bb;

clear hc2bb

load hc2bc.asc

bc=hc2bc;

clear hc2bc

load hc21a.asc

a1=hc21a;

clear hc21a

load hc21b.asc

b1=hc21b;

clear hc21b

load hc21c.asc

c1=hc21c;

clear hc21c

load hc22a.asc

```
a2=hc22a;
clear hc22a
load hc22b.asc
b2=hc22b;
clear hc22b
load hc22c.asc
c2=hc22c;
clear hc22c
load hc23a.asc
a3=hc23a;
clear hc23a
load hc23b.asc
b3=hc23b;
clear hc23b
load hc23c.asc
c3=hc23c;
clear hc23c
load hc24a.asc
a4=hc24a;
clear hc24a
load hc24b.asc
```

```
b4=hc24b;

clear hc24b

load hc24c.asc

c4=hc24c;

clear hc24c

load hc25a.asc

a5=hc25a;

clear hc25a

load hc25b.asc

b5=hc25b;

clear hc25b

load hc25c.asc

c5=hc25c;

clear hc25c

% baseline = ba,bb,bc

% series 1 = a1,b1,c1  0.1 M HCl

% series 2 = a2,b2,c2  0.5 M HCl

% series 3 = a3,b3,c3  1.0 M HCl

% series 4 = a4,b4,c4  5.0 M HCl

% series 5 = a5,b5,c5  10.0 M HCl

% Adjust waveforms for "best fit"
```

```

[bb]=adjust(ba,bb);
[bc]=adjust(ba,bc);
[b1]=adjust(a1,b1);
[c1]=adjust(a1,c1);
[b2]=adjust(a2,b2);
[c2]=adjust(a2,c2);
[b3]=adjust(a3,b3);
[c3]=adjust(a3,c3);
[b4]=adjust(a4,b4);
[c4]=adjust(a4,c4);
[b5]=adjust(a5,b5);
[c5]=adjust(a5,c5);

% Get average waveforms

for xx=1:512

    temp1=[ba(xx) bb(xx) bc(xx)];
    baseline(xx)=mean(temp1);
    temp1=[a1(xx) b1(xx) c1(xx)];
    set1(xx)=mean(temp1);
    temp1=[a2(xx) b2(xx) c2(xx)];
    set2(xx)=mean(temp1);
    temp1=[a3(xx) b3(xx) c3(xx)];

```

```

set3(xx)=mean(temp1);

temp1=[a4(xx) b4(xx) c4(xx)];

set4(xx)=mean(temp1);

temp1=[a5(xx) b5(xx) c5(xx)];

set5(xx)=mean(temp1);

end %(xx)

[set1]=adjust(baseline,set1);

[set2]=adjust(baseline,set2);

[set3]=adjust(baseline,set3);

[set4]=adjust(baseline,set4);

[set5]=adjust(baseline,set5);

tm=(0:511)/512*500; % timeline values (x-axis)

% Plot average signals

plot(tm,baseline*1e3,tm,set1*1e3,tm,set2*1e3,tm,set3*1e3,tm,set4*1e3,tm,
      set5*1e3)

title('Baseline vs HCl - Average Values')

xlabel('ns')

ylabel('mV')

save hcl2

```

HCL2A.M

```
% This program calculates the teff, Vmax, fall-time, and fall-rate for each of  
% the five data sets and the baseline.
```

```
clear
```

```
load hcl2
```

```
% Scale the data by 1000
```

```
ba=ba*1000;
```

```
bb=bb*1000;
```

```
bc=bc*1000;
```

```
a1=a1*1000;
```

```
b1=b1*1000;
```

```
c1=c1*1000;
```

```
a2=a2*1000;
```

```
b2=b2*1000;
```

```
c2=c2*1000;
```

```
a3=a3*1000;
```

```
b3=b3*1000;
```

```
c3=c3*1000;
```

```
a4=a4*1000;
```

```
b4=b4*1000;
```

```
c4=c4*1000;
```

```
a5=a5*1000;

b5=b5*1000;

c5=c5*1000;

tlength=500e-9; % length of scope display

tx=tlength/512; % time between each data point

% Set up vectors and matrices (M) for each of the parameters

teffbaseline=zeros(1,3);

teffhcl1=zeros(1,3);

teffhcl2=zeros(1,3);

teffhcl3=zeros(1,3);

teffhcl4=zeros(1,3);

teffhcl5=zeros(1,3);

Mteff=zeros(3,6);

maxbaseline=zeros(1,3);

maxhcl1=zeros(1,3);

maxhcl2=zeros(1,3);

maxhcl3=zeros(1,3);

maxhcl4=zeros(1,3);

maxhcl5=zeros(1,3);

Mmax=zeros(3,6);

falltimebaseline=zeros(1,3);
```

```

falltimehcl1=zeros(1,3);
falltimehcl2=zeros(1,3);
falltimehcl3=zeros(1,3);
falltimehcl4=zeros(1,3);
falltimehcl5=zeros(1,3);
Mfalltime=zeros(3,6);
fallratebaseline=zeros(1,3);
fallratehcl1=zeros(1,3);
fallratehcl2=zeros(1,3);
fallratehcl3=zeros(1,3);
fallratehcl4=zeros(1,3);
fallratehcl5=zeros(1,3);
Mfallrate=zeros(3,6);

% Calculate teff, Vmax, fall-time, and fall-rate for each of the data sets
% baseline = ba,bb,bc
tempa=max(ba);
tempb=find(ba>=.63*tempa);
teffbaseline(1)=(tempb(length(tempb))-tempb(1))*tx;
maxbaseline(1)=tempa;
falltimebase(1)=falltime(ba,tlength);
fallratebase(1)=fallrate(ba,tlength);

```

```

tempa=max(bb);

tempb=find(bb>=.63*tempa);

teffbaseline(2)=(tempb(length(tempb))-tempb(1))*tx;

maxbaseline(2)=tempa;

falltimebase(2)=falltime(bb,tlength);

fallratebase(2)=fallrate(bb,tlength);

tempa=max(bc);

tempb=find(bc>=.63*tempa);

teffbaseline(3)=(tempb(length(tempb))-tempb(1))*tx;

maxbaseline(3)=tempa;

falltimebase(3)=falltime(bc,tlength);

fallratebase(3)=fallrate(bc,tlength);

teffbasemean=mean(teffbaseline);

teffbasestd=std(teffbaseline);

maxbasemean=mean(maxbaseline);

maxbasestd=std(maxbaseline);

falltimebasemean=mean(falltimebase);

falltimebasestd=std(falltimebase);

fallratebasemean=mean(fallratebase);

fallratebasestd=std(fallratebase);

% series 1 = a1,b1,c1 (0.1 M HCl)

```

```

tempa=max(a1);

tempb=find(a1>=.63*tempa);

teffhcl1(1)=(tempb(length(tempb))-tempb(1))*tx;

maxhcl1(1)=tempa;

falltimehcl1(1)=falltime(a1,tlength);

fallratehcl1(1)=fallrate(a1,tlength);

tempa=max(b1);

tempb=find(b1>=.63*tempa);

teffhcl1(2)=(tempb(length(tempb))-tempb(1))*tx;

maxhcl1(2)=tempa;

falltimehcl1(2)=falltime(b1,tlength);

fallratehcl1(2)=fallrate(b1,tlength);

tempa=max(c1);

tempb=find(c1>=.63*tempa);

teffhcl1(3)=(tempb(length(tempb))-tempb(1))*tx;

maxhcl1(3)=tempa;

falltimehcl1(3)=falltime(c1,tlength);

fallratehcl1(3)=fallrate(c1,tlength);

teffhcl1mean=mean(teffhcl1);

teffhcl1std=std(teffhcl1);

maxhcl1mean=mean(maxhcl1);

```

```

maxhcl1std=std(maxhcl1);

falltimehcl1mean=mean(falltimehcl1);

falltimehcl1std=std(falltimehcl1);

fallratehcl1mean=mean(fallratehcl1);

fallratehcl1std=std(fallratehcl1);

% series 2 = a2,b2,c2 (0.5 M HCl)

tempa=max(a2);

tempb=find(a2>=.63*tempa);

teffhcl2(1)=(tempb(length(tempb))-tempb(1))*tx;

maxhcl2(1)=tempa;

falltimehcl2(1)=falltime(a2,tlength);

fallratehcl2(1)=fallrate(a2,tlength);

tempa=max(b2);

tempb=find(b2>=.63*tempa);

teffhcl2(2)=(tempb(length(tempb))-tempb(1))*tx;

maxhcl2(2)=tempa;

falltimehcl2(2)=falltime(b2,tlength);

fallratehcl2(2)=fallrate(b2,tlength);

tempa=max(c2);

tempb=find(c2>=.63*tempa);

teffhcl2(3)=(tempb(length(tempb))-tempb(1))*tx;

```

```

maxhcl2(3)=tempa;

falltimehcl2(3)=falltime(c2,tlength);

fallratehcl2(3)=fallrate(c2,tlength);

teffhcl2mean=mean(teffhcl2);

teffhcl2std=std(teffhcl2);

maxhcl2mean=mean(maxhcl2);

maxhcl2std=std(maxhcl2);

falltimehcl2mean=mean(falltimehcl2);

falltimehcl2std=std(falltimehcl2);

fallratehcl2mean=mean(fallratehcl2);

fallratehcl2std=std(fallratehcl2);

% series 3 = a3,b3,c3 (1.0 M HCl)

tempa=max(a3);

tempb=find(a3>=.63*tempa);

teffhcl3(1)=(tempb(length(tempb))-tempb(1))*tx;

maxhcl3(1)=tempa;

falltimehcl3(1)=falltime(a3,tlength);

fallratehcl3(1)=fallrate(a3,tlength);

tempa=max(b3);

tempb=find(b3>=.63*tempa);

teffhcl3(2)=(tempb(length(tempb))-tempb(1))*tx;

```

```

maxhcl3(2)=tempa;

falltimehcl3(2)=falltime(b3,tlength);

fallratehcl3(2)=fallrate(b3,tlength);

tempa=max(c3);

tempb=find(c3>=.63*tempa);

teffhcl3(3)=(tempb(length(tempb))-tempb(1))*tx;

maxhcl3(3)=tempa;

falltimehcl3(3)=falltime(c3,tlength);

fallratehcl3(3)=fallrate(c3,tlength);

teffhcl3mean=mean(teffhcl3);

teffhcl3std=std(teffhcl3);

maxhcl3mean=mean(maxhcl3);

maxhcl3std=std(maxhcl3);

falltimehcl3mean=mean(falltimehcl3);

falltimehcl3std=std(falltimehcl3);

fallratehcl3mean=mean(fallratehcl3);

fallratehcl3std=std(fallratehcl3);

% series 4 = a4,b4,c4 (5.0 M HCl)

tempa=max(a4);

tempb=find(a4>=.63*tempa);

teffhcl4(1)=(tempb(length(tempb))-tempb(1))*tx;

```

```

maxhcl4(1)=tempa;

falltimehcl4(1)=falltime(a4,tlength);

fallratehcl4(1)=fallrate(a4,tlength);

tempa=max(b4);

tempb=find(b4>=.63*tempa);

teffhcl4(2)=(tempb(length(tempb))-tempb(1))*tx;

maxhcl4(2)=tempa;

falltimehcl4(2)=falltime(b4,tlength);

fallratehcl4(2)=fallrate(b4,tlength);

tempa=max(c4);

tempb=find(c4>=.63*tempa);

teffhcl4(3)=(tempb(length(tempb))-tempb(1))*tx;

maxhcl4(3)=tempa;

falltimehcl4(3)=falltime(c4,tlength);

fallratehcl4(3)=fallrate(c4,tlength);

teffhcl4mean=mean(teffhcl4);

teffhcl4std=std(teffhcl4);

maxhcl4mean=mean(maxhcl4);

maxhcl4std=std(maxhcl4);

falltimehcl4mean=mean(falltimehcl4);

falltimehcl4std=std(falltimehcl4);

```

```

fallratehcl4mean=mean(fallratehcl4);

fallratehcl4std=std(fallratehcl4);

% series 5 = a5,b5,c5 (10.0 M HCl)

tempa=max(a5);

tempb=find(a5>=.63*tempa);

teffhcl5(1)=(tempb(length(tempb))-tempb(1))*tx;

maxhcl5(1)=tempa;

falltimehcl5(1)=falltime(a5,tlength);

fallratehcl5(1)=fallrate(a5,tlength);

tempa=max(b5);

tempb=find(b5>=.63*tempa);

teffhcl5(2)=(tempb(length(tempb))-tempb(1))*tx;

maxhcl5(2)=tempa;

falltimehcl5(2)=falltime(b5,tlength);

fallratehcl5(2)=fallrate(b5,tlength);

tempa=max(c5);

tempb=find(c5>=.63*tempa);

teffhcl5(3)=(tempb(length(tempb))-tempb(1))*tx;

maxhcl5(3)=tempa;

falltimehcl5(3)=falltime(c5,tlength);

fallratehcl5(3)=fallrate(c5,tlength);

```

```

teffhcl5mean=mean(teffhcl5);

teffhcl5std=std(teffhcl5);

maxhcl5mean=mean(maxhcl5);

maxhcl5std=std(maxhcl5);

falltimehcl5mean=mean(falltimehcl5);

falltimehcl5std=std(falltimehcl5);

fallratehcl5mean=mean(fallratehcl5);

fallratehcl5std=std(fallratehcl5);

% Put means and standard deviations into vectors

teffmeans=[teffbasemean teffhcl1mean teffhcl2mean teffhcl3mean
           teffhcl4mean teffhcl5mean ]*1e9;

teffstds=[teffbasestd teffhcl1std teffhcl2std teffhcl3std teffhcl4std teffhcl5std
          ]*1e9;

maxmeans=[maxbasemean maxhcl1mean maxhcl2mean maxhcl3mean
          maxhcl4mean maxhcl5mean];

maxstds=[maxbasestd maxhcl1std maxhcl2std maxhcl3std maxhcl4std
         maxhcl5std];

falltimemeans=[falltimebasemean falltimehcl1mean falltimehcl2mean
              falltimehcl3mean falltimehcl4mean falltimehcl5mean]*1e9;

falltimestds=[falltimebasestd falltimehcl1std falltimehcl2std falltimehcl3std
              falltimehcl4std falltimehcl5std]*1e9;

```

```

fallratemeans=[fallratebasemean fallratehcl1mean fallratehcl2mean
    fallratehcl3mean fallratehcl4mean fallratehcl5mean]/1e9;
fallratestds=[fallratebasestd fallratehcl1std fallratehcl2std fallratehcl3std
    fallratehcl4std fallratehcl5std]/1e9;
% Set up matrices for t-tests
Mteff=[teffbaseline' teffhcl1' teffhcl2' teffhcl3' teffhcl4' teffhcl5'];
Mmax=[maxbaseline' maxhcl1' maxhcl2' maxhcl3' maxhcl4' maxhcl5'];
Mfalltime=[falltimebase' falltimehcl1' falltimehcl2' falltimehcl3' falltimehcl4'
    falltimehcl5'];
Mfallrate=[fallratebase' fallratehcl1' fallratehcl2' fallratehcl3' fallratehcl4'
    fallratehcl5'];
% Plot the data
xy=[0 7 0 ceil(max(means+stds)*1.25)];
axis(xy)
plot(means)
errorbars(means,stds)
ylabel('ns')
title('Baseline vs HCl Added to the Water (2nd Series) - Mean teff')
text(.6,25,'Baseline')
text(1.6,25,'0.1e-4')
text(2.6,25,'0.5e-4')

```

```

text(3.6,25,'1.0e-4')
text(4.6,30,'5.0e-4')
text(5.6,150,'10.0e-4')

pause

print

xy=[0 7 0 ceil(max(maxmeans+maxstds)*1.25)];

axis(xy)

plot(maxmeans)

errorbars(maxmeans,maxstds)

ylabel('mV')

title('Baseline vs HCl Added to the Water (2nd Series) - Mean Maximum
      Voltage')

text(.6,14,'Baseline')

text(1.6,13,'0.1e-4')

text(2.6,12.5,'0.5e-4')

text(3.6,12,'1.0e-4')

text(4.6,10,'5.0e-4')

text(5.6,8,'10.0e-4')

pause

print

xy=[0 7 -15 ceil(max(falltimemeans+falltimestds)*1.25)];

```

```

axis(xy)

plot(falltimemeans)

errorbars(falltimemeans,falltimestds)

ylabel('ns')

title('Baseline vs HCl Added to the Water (2nd Series)- Mean Falltime')

text(.6,45,'Baseline')

text(1.6,35,'0.1e-4')

text(2.6,35,'0.5e-4')

text(3.6,35,'1.0e-4')

text(4.6,35,'5.0e-4')

text(5.6,25,'10.0e-4')

pause

print

xy=[0 7 -1 1];

axis(xy)

plot(fallratemeans)

errorbars(fallratemeans,fallratestds)

ylabel('mV/ns')

title('Baseline vs HCl Added to the Water (2nd Series)- Mean Fallrate')

text(.6,-.25,'Baseline')

text(1.6,-.25, '0.1e-4')

```

```
text(2.6,-.25, '0.5e-4')
```

```
text(3.6,-.25, '1.0e-4')
```

```
text(4.6,-.25, '5.0e-4')
```

```
text(5.6,-.25, '10.0e-4')
```

```
print
```

```
save hcl2a
```

HCL2B.M

```
% This program does the statistical analysis of the HCl data.

clear

load hcl2a

% Calculate the ANOVA's

[F,sst,ssb,ssw,msb,msw,dfsst,dfssb,dfssw]=anova(Mteff);

disp([' '])

disp(['Analysis of Variance (df = ',num2str(dfssb),',',num2str(dfssw),')'])

disp(['      F      a'])

disp(['teff      ',num2str(F)])

[F,sst,ssb,ssw,msb,msw,dfsst,dfssb,dfssw]=anova(Mmax);

disp(['Vmax      ',num2str(F)])

[F,sst,ssb,ssw,msb,msw,dfsst,dfssb,dfssw]=anova(Mfalltime);

disp(['Falltime  ',num2str(F)])

[F,sst,ssb,ssw,msb,msw,dfsst,dfssb,dfssw]=anova(Mfallrate);

disp(['Fallrate   ',num2str(F)])

% Calculate the t-tests for each set of data

disp([' '])

disp([' '])

disp(['teff'])

multi_t(Mteff);
```

`disp([' '])`

`disp(['Vmax'])`

`multi_t(Mmax);`

`disp([' '])`

`disp(['Falltime'])`

`multi_t(Mfalltime);`

`disp([' '])`

`disp(['Fallrate'])`

`multi_t(Mfallrate);`

ADJUST.M

```
function [z]=adjust(x,y)

% ADJUST rotates one curve so that the sum of squared difference is at
% a minimum
% Function call is
% [z]=adjust(x,y)
% where z is the curve y rotated to best fit curve x.
% x is not changed.

checkx=size(x);

checky=size(y);

if checkx(1)==1,x=x';end %if

if checky(1)==1,y=y';end %if

tempadj1=y;

ssdiv=zeros(length(y),1);

for i=1:length(y)

ssdiv(i)=sum((x-tempadj1).^2);

tempadj1=rotate(y,i);

end

tempadj3=find(ssdiv==min(ssdiv));

z=rotate(y,tempadj3);
```

ANOVA.M

```
function [F,dfssb,dfssw]=anova(M)

% ANOVA - calculates the Analysis of Variance of an LxM size Matrix.

%     The columns of the matrix represents the trial groups. The program

% returns the F value and the degrees of freedom needed to look up the

% results in a F table.

%     Function call is:

%     [F,sst,ssb,ssw,msb,msw,dfsst,dfssb,dfssw]=anova(M)

%     where dfssb is the degrees of freedom between the groups and dfssw

% is the degrees of freedom within the groups.

[l m]=size(M);

a=sum(M(:));

b=M.^2;

c=sum(b(:));

n=l*m;

correct=a^2/n;

sst=c-correct;

d=sum(M);

d=d.^2;

e=sum(d);

f=e/l;
```

$ssb = f \cdot \text{correct};$

$ssw = sst - ssb;$

$dfsst = n - 1;$

$dfssb = m - 1;$

$dfssw = dfsst - dfssb;$

$mst = sst / dfsst;$

$msb = ssb / dfssb;$

$msw = ssw / dfssw;$

$F = msb / msw;$

CHANGE.M

```
function [x]=CHANGE(a,b)

% CHANGE - calculates the percent change between the means of two
%          vectors
%          Function call is
%          [x]=CHANGE(a,b)
%          where a and b are two vectors

x=((mean(b)-mean(a))/mean(a))*100;

disp(['Change = ',num2str(x),' %'])
```

FALLRATE.M

```
function fallrt=fallrate(u,tlength)

% FALLRATE calculates (V90-V10)/(t90-t10) - the time rate of change of
% the voltage during the fall time of the function u. tlength is the scope
% display time.

% Function call is in the form

% [y]=fallrate(x,t)

% where x is a 1xN vector and t is the length of the total time of the
% function.

txmax=find(u==max(u));

txmin=length(u);

for i=txmax:txmin

if u(i)<u(i+1),minval=i;,break,end

end

vmax=u(txmax);

vmin=u(minval);

v90=.9*(vmax-vmin)+vmin;

v10=.1*(vmax-vmin)+vmin;

y=find(u(1:minval)>v90);

i90=y(length(y));

y=find(u(1:minval)>v10);
```

```
i10=y(length(y));
```

```
deltav=v90-v10;
```

```
deltat=(i10-i90)*tlength/512;
```

```
fallrt=deltav/deltat;
```

FALLTIME.M

```
function falltm=falltime(u,tlength)

% FALLTIME calculates the 10%-90% falltime of the function u.

%   Function call is in the form

%           [y]=falltime(x,t)

%   where x is a 1xN vector and t is the length of the total time.

txmax=find(u==max(u));

txmin=length(u);

for i=txmax:txmin

if u(i)<u(i+1),minval=i;,break,end

end

vmax=u(txmax);

vmin=u(minval);

v90=.9*(vmax-vmin)+vmin;

v10=.1*(vmax-vmin)+vmin;

y=find(u(1:minval)>v90);

i90=y(length(y));

y=find(u(1:minval)>v10);

i10=y(length(y));

falltm=(i10-i90)*tlength/512;
```

FIXCURVE.M

```
function [y]=fixcurve(u,maxnum)

% FIXCURVE - corrects the small bumps on the falling part of the voltage
%           signal.
%           Function call is
%           [y]=FIXCURVE(u,n)
%           where u is the signal vector and n is the point value of the
%           bottom of the curve.

n=find(u==max(u));

m=find(u(n:maxnum)==min(u(n:maxnum)));

o=m+n-1;

for i=n+1:o
if u(i)>u(i-1), u(i)=u(i-1);, end

end

y=u;
```

MULTI T.M

```
function(M)

% This program takes an m x n matrix (M) and returns the t-test for each
% pair of data series (columns). No variables are returned but the values of
% the t-tests are printed on the screen.

[row,col]=size(M);

for count1=1:col-1

    for count2=count1+1:col

M1=M(:,count1);

M2=M(:,count2);

sd1=sum(M1.^2)-sum(M1)^2/row;

sd2=sum(M2.^2)-sum(M2)^2/row;

tempta=(sd1+sd2)/((row-1)*row);

t=abs(mean(M1)-mean(M2))/sqrt(tempta);

df=2*(row-1);

disp([' '])

disp(['t',num2str(count1),',',num2str(count2),'= ',num2str(t),

    ' df=',num2str(df)])

end %(count2)

end %(count1)
```

TTEST.M

```
% This program is a subroutine that calculates the various t-tests between  
% the columns of the matrix M. It prints out the results directly to the  
% screen. This program can only be used on data sets that are equal  
% lengths.
```

```
[row,col]=size(M);
```

```
for count1=1:col-1
```

```
    for count2=count1+1:col
```

```
        M1=M(:,count1);
```

```
        M2=M(:,count2);
```

```
        sd1=sum(M1.^2)-sum(M1)^2/row;
```

```
        sd2=sum(M2.^2)-sum(M2)^2/row;
```

```
        tempta=(sd1+sd2)/((row-1)*row);
```

```
        t=abs(mean(M1)-mean(M2))/sqrt(tempta);
```

```
        df=2*(row-1);
```

```
        disp([' '])
```

```
        disp(['t',num2str(count1),',',num2str(count2),'= ',num2str(t)])
```

```
    end %(count2)
```

```
end %(count1)
```

APPENDIX D
ASSEMBLY LANGUAGE PROGRAMS

Notes: (1) All Assembly Language comments are preceded by a semicolon and (2) Assembly Language commands that exceeded the margin spacing were continued with a hanging indent. In the actual program file, the margins would have to be set so that the whole command would be on one line.

WAVEFORM Program

```
;      This program was written to change the filenames of the RAW video
; files created by DCS01GPH. It was written in Assembly Language and
; compiled with A86, which is similar to Microsoft's Assembly Language
; compiler. The way the program works is to first run the DOS command
;
;          DIR *.RAW /B /O-D /-P
; and save the output to the file WAVEFORM.TMP. The switch /B just
; displays the filenames without any other information, /O-D, lists the latest
; file first based on the file creation date and time, /-P turns off the page
; display mode (screen stops after it fills a page then waits for a key to be
; pressed before displaying another screen).
;
;      The program then opens the file WAVEFORM.TMP and reads the first
```

; 8 bytes (filename) and saves it in the location LAST_FILE, This is the last
; RAW file that was created by DCS. It checks to see if the filename is 5 to 8
; bytes long and shifts the filename extension if there are less than 8 bytes in
; the filename.

; Next, the program loads the file WAVEFORM.FIL which contains the
; previous filename that was used (ex: 95052403). It increments this
; filename and displays it on the screen to confirm that it is correct. If it
: isn't correct, enter the correct filename.

; The program then runs the DOS command COPY to create a new RAW
; image file with the new filename. I had the program copy the file rather
; than rename it. In case something goes wrong you will always have the
; original file. Next, the program runs the DOS program RAW2VID to
; display the image on the monitor. If this is the correct image, then the
; program is finished. I have tried to include as much error catching as
; reasonably possible. If you have problem that involve the DOS programs,
; check to make sure that those programs are in the same subdirectory as this
; program (except for DIR and COPY). If you have any other problems, you
; will have to find someone that can debug an assembly language program or
; see if you can track me down.

JMP START

COMMAND_LINE DB "\COMMAND.COM",0

DEFAULT_COMMAND DB 2EH, "/C DIR ???????.RAW /B /O-D /-P > "

TEMP_FILE DB "WAVEFORM.TMP", 0

DEFAULT_COMMAND2 DB 21H, "/C COPY "

COPY1 DB 8H DUP(0), ".RAW "

COPY2 DB "LASTFILE.RAW"

DEFAULT_COMMAND3 DB 17H, "/C RAW2VID "

RAW2VID1 DB 8H DUP(0), ".RAW"

DEFAULT_COMMAND4 DB 27H, "/C RAW2BIN "

RAW2BIN1 DB 8H DUP(0), ".RAW \PSTYLER2\X.RAW"

OLD_FILE DB "WAVEFORM.FIL", 0

PRINT1 DB "IS THE FILE NAME GOING TO BE "

LAST_FILE DB 8H DUP(20H), 0, "\$"

NEW_FILE DB 8H DUP(0H), 0

PARAMETER_BLOCK DB 0AH DUP(0)

FILE_HANDLE DW 0

LINEFEED DB 0AH, 0DH, "\$"

QUESTION_MARK DB "? (Y/N ENTER=Y) \$"

PRINT2 DB "ENTER CORRECT FILE NAME > \$"

CORRECT_FILE DB 09H, 0, 09H DUP(20H)

PRINT3 DB "COPYING "

COPY3 DB "12345678.RAW TO "

COPY4 DB "LASTFILE.RAW \$"

ERRMSG1 DB "UNABLE TO OPEN CHNGNAME.TMP, CHECK TO SEE IF
IT EXISTS.",0DH,0AH,"IF NOT, ERROR OCCURED CREATING THE
DIRECTORY FILE.",0DH,0AH,"\$"

ERRMSG2 DB "UNABLE TO READ CHNGNAME.TMP, CHECK TO SEE IF
IT EXISTS.",0DH,0AH,"CHECK THE FILE BEFORE ROCEEDING.",
0DH, 0AH, "\$"

ERRMSG3 DB "UNABLE TO CLOSE CHNGNAME.TMP, CHECK TO SEE
IF IT EXISTS.",0DH,0AH,"CHECK THE FILE BEFORE
PROCEEDING.",0DH, 0AH, "\$"

ERRMSG4 DB "UNABLE TO OPEN CHNGNAME.FIL, CHECK TO SEE IF
IT EXISTS.",0DH,0AH,"IF NOT, CREATE CHNGNAME.FIL.", 0DH,
0AH, "\$"

ERRMSG5 DB "UNABLE TO READ CHNGNAME.FIL, CHECK TO SEE IF
IT EXISTS.",0DH,0AH,"CHECK THE FILE BEFORE
PROCEEDING.", 0DH, 0AH, "\$"

ERRMSG6 DB "UNABLE TO CLOSE CHNGNAME.FIL, CHECK TO SEE IF
IT EXISTS.",0DH,0AH,"CHECK THE FILE BEFORE
PROCEEDING.", 0DH, 0AH, "\$"

ERRMSG8 DB "UNABLE TO WRITE TO CHNGNAME.FIL, CHECK TO
SEE IF IT EXISTS.",0DH,0AH,"CHECK THE FILE BEFORE

```

PROCEEDING.", 0DH, 0AH,"$"

ERRMSG10 DB "UNABLE TO DELETE CHNGNAME.TMP, CHECK TO
SEE IF IT EXISTS.",0DH,0AH,"DELETE THE FILE BEFORE
RUNNING PROGRAM AGAIN.",0DH,0AH,"$"

PRINT4 DB "IS THIS THE CORRECT VIDEO FILE? (Y/N ENTER=Y) $"
PRINT5 DB "WRONG FILE WAS CONVERTED, CHECK RAW FILE
CREATED BY DCS",0DH,0AH,"AND PROGRAM WILL
TERMINATE.$"

PRINT6 DB "RAW FILE HAS BEEN COPIED TO \PSTYLER2\X.RAW",
0DH, 0AH,"$"

START:

MOV BX,1000H ; allocate memory space to run DOS commands

MOV AH,4AH

INT 21H

MOV AX,CS

MOV DS,AX

MOV ES,AX

MOV WORD PTR [PARAMETER_BLOCK+2],OFFSET
DEFAULT_COMMAND

MOV WORD PTR [PARAMETER_BLOCK+4],DS

MOV WORD PTR [PARAMETER_BLOCK+6],SS

```

```
MOV WORD PTR [PARAMETER_BLOCK+8],SP
MOV DX,OFFSET COMMAND_LINE
MOV BX, OFFSET PARAMETER_BLOCK
MOV AL,0
MOV AH,4BH ; run DOS command
INT 21H
MOV AH,3DH ; Open temp file
MOV DX,OFFSET TEMP_FILE
MOV AL,0
INT 21H
JNC ERROR1 ; Check for error
MOV DX,OFFSET ERRMSG1
CALL PRINT_LINE ; Print error message
JMP EXIT_PROGRAM ; Exit program
ERROR1:
MOV FILE_HANDLE,AX
MOV BX,AX ; FILE HANDLE
MOV AH,3FH
MOV DX,OFFSET NEW_FILE
MOV CX, 8H ; Number of bytes
INT 21H
```

```
JNC ERROR2 ; Check for error

MOV DX,OFFSET ERRMSG2

CALL PRINT_LINE ; Print error message

JMP EXIT_PROGRAM ; Exit program

ERROR2:

MOV AH,3EH ; Close temp file

MOV BX,FILE_HANDLE

INT 21H

JNC ERROR3 ; Check for error

MOV DX,OFFSET ERRMSG3

CALL PRINT_LINE ; Print error message

JMP EXIT_PROGRAM ; Exit program

ERROR3:

MOV AH,3DH ; Open CHNGNAME.FIL

MOV DX,OFFSET OLD_FILE

MOV AL,0

INT 21H

JNC ERROR4 ; Check for error

MOV DX,OFFSET ERRMSG4

CALL PRINT_LINE ; Print error message

JMP EXIT_PROGRAM ; Exit program
```

ERROR4:

MOV FILE_HANDLE,AX

MOV BX,AX ; File handle

MOV AH,3FH ;Load file

MOV DX,OFFSET LAST_FILE

MOV CX, 8H ; Number of bytes

INT 21H

JNC ERROR5 ; Check for error

MOV DX,OFFSET ERRMSG5

CALL PRINT_LINE ; Print error message

JMP EXIT_PROGRAM ; Exit program

ERROR5:

MOV AH,3EH ; Close chngname.fil

MOV BX,FILE_HANDLE

INT 21H

JNC ERROR6 ; Check for error

MOV DX,OFFSET ERRMSG6

CALL PRINT_LINE ; Print error message

JMP EXIT_PROGRAM ; Exit program

ERROR6:

INC LAST_FILE+7

```

CMP LAST_FILE+7,3AH ; look to see if the last digit of the filename is
JNZ INC_END ; greater than 9, if so change to 0, and increment
MOV LAST_FILE+7,30H ; the 10's digit
INC LAST_FILE+6
INC_END:
; CHECK NEW FILENAME
CHECK_NAME:
MOV DX, OFFSET PRINT1 ; asks for input to see if the filename is correct
CALL PRINT_LINE
MOV DX, OFFSET QUESTION_MARK
CALL PRINT_LINE
; Get keyboard input
KEYBOARD1:
MOV AH,08H
INT 21H
CMP AL,"Y"
JZ KEYBOARD2
CMP AL,"y"
JZ KEYBOARD2
CMP AL,0DH
JZ KEYBOARD4

```

```
CMP AL,"N"

JZ KEYBOARD3

CMP AL,"n"

JNZ KEYBOARD1

KEYBOARD3:

; Get correct file name if filename is wrong, prompt for correct name

CALL PRINT_YN

MOV DX, OFFSET PRINT2

CALL PRINT_LINE

MOV AH,0AH ; Buffered keyboard input to get new filename

MOV DX, OFFSET CORRECT_FILE

INT 21H

MOV CX,8 ; Move the correct filename to LAST_FILE

MOV SI,OFFSET CORRECT_FILE+2

MOV DI,OFFSET LAST_FILE

REPZ

MOVSB

MOV AH,09H

MOV DX, OFFSET LINEFEED

INT 21H

JMP CHECK_NAME
```

KEYBOARD2:

CALL PRINT_YN

JMP KEYBOARD_END

KEYBOARD4:

MOV AL,"Y"

JMP KEYBOARD2

KEYBOARD_END:

; Copy the original raw file to the new raw file

; Move the file names to the copy command line

MOV CX,8

MOV SI,OFFSET NEW_FILE

MOV DI,OFFSET COPY1

REPZ

MOVSB

MOV CX,8

MOV SI,OFFSET LAST_FILE

MOV DI,OFFSET COPY2

REPZ

MOVSB

; Check for periods in the new filename for filenames that only have less than

; 8 characters.

; 7 Characters

CMP BYTE PTR [COPY1+7],2EH

JNZ CHECK1

MOV CX,3

MOV SI,OFFSET COPY1+9

MOV DI,OFFSET COPY1+8

REPZ

MOVSB

MOV BYTE PTR [COPY1+0BH],20H

CHECK1:

;6 Characters

CMP BYTE PTR [COPY1+6],2EH

JNZ CHECK2

MOV CX,2

MOV SI,OFFSET COPY1+0AH

MOV DI,OFFSET COPY1+8

REPZ

MOVSB

MOV BYTE PTR [COPY1+0AH],20H

MOV BYTE PTR [COPY1+0BH],20H

CHECK2:

;5 Characters

CMP BYTE PTR [COPY1+5],2EH

JNZ CHECK3

MOV BYTE PTR [COPY1+8],"W"

MOV BYTE PTR [COPY1+09H],20H

MOV BYTE PTR [COPY1+0AH],20H

MOV BYTE PTR [COPY1+0BH],20H

CHECK3:

;4 Characters

CMP BYTE PTR [COPY1+4],2EH

JNZ CHECK4

MOV BYTE PTR [COPY1+08H],20H

MOV BYTE PTR [COPY1+09H],20H

MOV BYTE PTR [COPY1+0AH],20H

MOV BYTE PTR [COPY1+0BH],20H

CHECK4:

; Print COPY statement to the screen

MOV CX,0CH

MOV SI,OFFSET COPY1

MOV DI,OFFSET COPY3

REPZ

```
MOVSB
MOV CX,0CH
MOV SI,OFFSET COPY2
MOV DI,OFFSET COPY4
REPZ
MOVSB
MOV DX,OFFSET PRINT3
CALL PRINT_LINE
MOV DX, OFFSET LINEFEED
CALL PRINT_LINE
;Copy files
MOV AX,CS
MOV DS,AX
MOV ES,AX
MOV WORD PTR [PARAMETER_BLOCK+2],OFFSET
DEFAULT_COMMAND2
MOV WORD PTR [PARAMETER_BLOCK+4],DS
MOV WORD PTR [PARAMETER_BLOCK+6],SS
MOV WORD PTR [PARAMETER_BLOCK+8],SP
MOV DX,OFFSET COMMAND_LINE
MOV BX, OFFSET PARAMETER_BLOCK
```

```

MOV AL,0

MOV AH,4BH ; call DOS command (COPY)

INT 21H

;Save last file name in the file CHNGNAME.FIL

MOV AH,3DH ; Open CHNGNAME.FIL

MOV DX,OFFSET OLD_FILE

MOV AL,1 ; Open file for writing

INT 21H

JNC ERROR7 ; Check for error

MOV DX,OFFSET ERRMSG4

CALL PRINT_LINE ; Print error message

JMP EXIT_PROGRAM ; Exit program

ERROR7:

MOV FILE_HANDLE,AX

MOV BX,AX ; File handle

MOV AH,40H ; Write to a file

MOV DX,OFFSET LAST_FILE

MOV CX, 8H ; Number of bytes

INT 21H

JNC ERROR8 ; Check for error

MOV DX,OFFSET ERRMSG8

```

```
CALL PRINT_LINE ; Print error message
JMP EXIT_PROGRAM ; Exit program
ERROR8:
MOV AH,3EH ; Close CHNGNAME.FIL
MOV BX,FILE_HANDLE
INT 21H
JNC ERROR9 ; Check for error
MOV DX,OFFSET ERRMSG6
CALL PRINT_LINE ; Print error message
JMP EXIT_PROGRAM ; Exit program
ERROR9:
; Delete temp file
MOV AH,41H ; Delete file
MOV DX,OFFSET TEMP_FILE
INT 21H
JNC ERROR10 ; Check for error
MOV DX,OFFSET ERRMSG10
CALL PRINT_LINE ; Print error message
JMP EXIT_PROGRAM ; Exit program
ERROR10:
; DOS command to run RAW2VID
```

;Move filename to command lines

MOV CX,8

MOV SI,OFFSET LAST_FILE

MOV DI,OFFSET RAW2VID1

REPZ

MOVSB

MOV CX,8

MOV SI,OFFSET LAST_FILE

MOV DI,OFFSET RAW2BIN1

REPZ

MOVSB

MOV AX,CS

MOV DS,AX

MOV ES,AX

MOV WORD PTR [PARAMETER_BLOCK+2],OFFSET

DEFAULT_COMMAND3

MOV WORD PTR [PARAMETER_BLOCK+4],DS

MOV WORD PTR [PARAMETER_BLOCK+6],SS

MOV WORD PTR [PARAMETER_BLOCK+8],SP

MOV DX,OFFSET COMMAND_LINE

MOV BX, OFFSET PARAMETER_BLOCK

```
MOV AL,0
MOV AH,4BH ; run DOS command (RAW2VID)
INT 21H
;CHECK TO SEE IF IT IS THE CORRECT FILE
MOV DX,OFFSET PRINT4
CALL PRINT_LINE
; Get keyboard input
KEYBOARD5:
MOV AH,08H ;Get keyboard input
INT 21H
CMP AL,"Y"
JZ KEYBOARD6
CMP AL,"y"
JZ KEYBOARD6
CMP AL,0DH
JZ KEYBOARD8
CMP AL,"N"
JZ KEYBOARD7
CMP AL,"n"
JNZ KEYBOARD5
KEYBOARD7:
```

```

; If the file is wrong, print error message and exit

CALL PRINT_YN

MOV DX,OFFSET PRINT5

CALL PRINT_LINE

JMP EXIT_PROGRAM

KEYBOARD6:

CALL PRINT_YN

JMP KEYBOARD_END2

KEYBOARD8:

MOV AL,"Y"

JMP KEYBOARD6

KEYBOARD_END2:

; DOS command to run RAW2BIN LASTFILE.RAW \PSTYLER2\X.RAW

; which saves the binary data from LASTFILE.RAW as the file

;\PSTYLER2\X.RAW

MOV AX,CS

MOV DS,AX

MOV ES,AX

MOV WORD PTR [PARAMETER_BLOCK+2],OFFSET

DEFAULT_COMMAND4

MOV WORD PTR [PARAMETER_BLOCK+4],DS

```

```

MOV WORD PTR [PARAMETER_BLOCK+6],SS
MOV WORD PTR [PARAMETER_BLOCK+8],SP
MOV DX,OFFSET COMMAND_LINE
MOV BX, OFFSET PARAMETER_BLOCK
MOV AL,0
MOV AH,4BH ; run DOS command (RAW2BIN)
INT 21H
MOV DX,OFFSET PRINT6 ; print message to screen that the file has been
CALL PRINT_LINE ; converted and saved as \PSTYLER2\X.RAW
JMP EXIT_PROGRAM
;The end if all goes right
;SUBROUTINES
PRINT_YN:
MOV DL,AL
MOV AH,02H
INT 21H
MOV AH,09H
MOV DX, OFFSET LINEFEED
INT 21H
RET
PRINT_LINE:

```

MOV AH,09H

INT 21H

RET

EXIT_PROGRAM:

MOV AH,49H ; Free allocated memory

INT 21H

MOV AH,4CH

INT 21H ; Exit program

STRIPASC Program

; This program is used to strip the header information from the ASC
; files. While you are in DCS, save the waveform in the ASCII format. This
; will give you 20 lines of header information followed by 512 data points
; separated by line feeds. After stripping the header, you can import the data
; into MATLAB.

JMP START

FILENAME DB 10H DUP(0)

LINE1 DB "ERROR: UNABLE TO OPEN FILE. INCLUDE EXTENSION.",
0DH, 0AH, "\$"

LINE2 DB "ERROR: UNABLE TO READ FILE.", 0DH,0AH,"\$"

LINE3 DB "FILE HAS PROBABLY ALREADY BEEN STRIPPED.",
0DH,0AH,"\$"

LINE4 DB "ERROR: SOMETHING IS WRONG WITH THE FILE.", 0DH,
0AH, "NEEDS TO BE CHECKED", 0DH, 0AH, "\$"

LINE5 DB "ERROR: UNABLE TO CLOSE FILE.", 0DH,0AH,"\$"

LINE6 DB "ERROR: UNABLE TO CLEAR FILE.", 0DH,0AH,"\$"

LINE7 DB "ERROR: UNABLE TO SAVE FILE.", 0DH,0AH,"\$"

FILE_HANDLE DW ?

FILE_SIZE DW ?

START:

```
MOV CL,[80H] ; These 8 lines move the information from the DOS line
MOV CH,0 ; to the filename block
DEC CX
CLD
MOV SI,82H
MOV DI, OFFSET FILENAME
REPZ
MOVSB
MOV AH,3DH ; Open the file
MOV DX,OFFSET FILENAME
MOV AL,2
INT 21H
JNC ST1
MOV DX,OFFSET LINE1 ; Print error message
JMP PRINT_LINE
ST1:
MOV [FILE_HANDLE],AX
MOV BX,AX
MOV AH,3FH ; Read the file
MOV DX,OFFSET END_MARKER
MOV CX,0FF00H ; Maximum number of bytes
```

```

INT 21H

JNC ST2

MOV DX,OFFSET LINE2 ; Print error message

JMP PRINT_LINE

ST2:

MOV [FILE_SIZE],AX

;Close file

MOV AH,3EH

MOV BX,[FILE_HANDLE]

INT 21H

JNC ST2A

MOV DX,OFFSET LINE5

JMP PRINT_LINE

ST2A:

MOV BX,OFFSET END_MARKER

CMP BYTE PTR [BX],"W" ; Check to see if the file has already been
                        ; stripped or not.

JZ ST3

CMP BYTE PTR [BX],"-" ; See if it is negative

JNZ ST5

INC BX ; If it is '-', then check the next character

```

ST5:

CMP BYTE PTR [BX],30H ; If the file starts with a number then it has
; probably been stripped

JL ST4

CMP BYTE PTR [BX],39H

JG ST4

;If the program gets here, then the file has probably already been stripped

MOV DX,OFFSET LINE3 ; Print message that the file is probably

JMP PRINT_LINE ; already stripped

ST4: ; The first character was not a 'W' or a

MOV DX,OFFSET LINE4 ; number - something is wrong with the file

JMP PRINT_LINE

ST3: ; Strip the header

; Find the beginning of the data string look for 'Y' then 'D'

MOV DI,OFFSET END_MARKER

MOV AL,"Y" ; Look for 'Y'

MOV CX,300H ; Look at the first 300H bytes

PUSH BX ; Save bx

MOV BX,100H

CMP BH,BL ; Set zero flag

REPZ SCASB

```

MOV AL,"D"      ; Look for 'D'

CMP BH,BL      ; Set zero flag

REPZ SCASB

POP BX

ADD DI,5       ; Gets DI to the last of the header

MOV CX,[FILE_SIZE]

SUB CX,DI

ADD CX,OFFSET END_MARKER

MOV [FILE_SIZE],CX

MOV SI,DI

INC SI

MOV DI,OFFSET END_MARKER

REPZ MOVSB

; This next section checks to see if there is any unwanted information after
; the 512 data points

PUSH BX

MOV DI,OFFSET END_MARKER

MOV AL,0DH    ; Line feed

MOV CX,512

ST8:

PUSH CX

```

```
MOV CX,100H
MOV BX,100H ; To set zero flag
CMP BH,BL
REPNZ SCASB
POP CX
LOOP ST8
POP BX
MOV AX,DI
MOV BX,OFFSET END_MARKER
SUB AX,BX
MOV FILE_SIZE,AX
MOV AH,3CH ; Clear old file
MOV DX, OFFSET FILENAME
MOV CX,0
INT 21H
JNC ST6B
MOV DX,OFFSET LINE6
JMP PRINT_LINE
ST6B:
MOV AH,3DH ; Open the file
MOV DX,OFFSET FILENAME
```

```
MOV AL,2
INT 21H
JNC ST6A
MOV DX,OFFSET LINE1
JMP PRINT_LINE
ST6A:
; Save file
MOV AH,40H
MOV DX,OFFSET END_MARKER
MOV CX,[FILE_SIZE]
MOV BX,[FILE_HANDLE]
INT 21H
JNC ST6
MOV DX,OFFSET LINE7
JMP PRINT_LINE
ST6:
;Close file
MOV AH,3EH
MOV BX,[FILE_HANDLE]
INT 21H
JNC ST7
```

MOV DX,OFFSET LINE5

ST7:

EXIT_PROGRAM:

MOV AH,4CH

INT 21H

PRINT_LINE:

MOV AH,9

INT 21H

JMP EXIT_PROGRAM

END_MARKER DB 0

APPENDIX E
READING LIST

- Abramyan, E. A., V. A. Kornilov, et al., "Megavolt Energy-Concentrating Device," Soviet Physics - Doklady, Vol. 16, No. 11, pp. 983, May, 1972.
- Adamian, Y. A., V. V. Titkov, and G. A. Shneerson, "Water Line with the Electrostatic Concentrator," Digest of Technical Papers, Ninth IEEE International Pulsed Power Conference, pp. 103-106, June, 1993.
- Alkhimov, A. P., V. V. Vorob'ev, V. F. Klimkin, A. G. Ponomarenko, and R. I. Soloukhin, "The Development of Electrical Discharge in Water," Soviet Physics - Doklady, Vol. 15, No. 10, pp. 959-961, April, 1971.
- Angell, C. A., Water a Comprehensive Treatise, Volume 7, Water and Aqueous Solutions at Subzero Temperatures, Chapter 1, "Supercooled Water," Edited by Felix Franks, Plenum Press, New York, NY, pp. 1-81.
- Antonov, E. A., L. N. Gnatyuk, B. M. Stepanov, Yu. I. Filenko, and V. Ya. Tsarfin, "Holographic Investigation of Electrical Explosions of Conductors," High Temperature, Vol. 10, No. 6, pp. 1087-1091, 1971.
- Arensburg, A., and S. Wald, "X-Ray Diagnostics of a Plasma-Jet-Liquid Interaction in Electrothermal Guns," Journal of Applied Physics, Vol. 73, No. 5, pp. 2145-2154, March, 1993.
- Atten, P., and A. Saker, "Streamer Propagation Over a Liquid/Solid Interface," IEEE Transactions on Electrical Insulation, Vol. 28, No. 2, pp. 230-242, April, 1993.
- Babula, E., A. Sierota, S. Zoledziowski, and J. H. Calderwood, "The Effect of Moisture on Partial Discharges in Dielectric Liquids," Conference Record, Eight International Conference on Conduction and Breakdown in Dielectric Liquids, pp. 209-213, July, 1984.
- Baksht, R. B., I. M. Datsko, A. F. Korostelev, V. V. Loskutov, A. V. Luchinskii, and A. A. Chertov, "Nanosecond electrical explosion of thin wires," Soviet Journal of Applied Physics, Vol. 9, No. 6, pp. 706-710, 1983.

- Balygin, I.E., "Electrical Breakdown of Liquid Dielectrics (A Review)," Translation of Elektrichestvo (Electricity), No. 1, pp. 89, 1954. Foreign Technology Report FTD-HT-23-772-72, 20 October 1972.
- Bartnikas, R., "Dielectric Loss in Insulating Liquids," IEEE Transactions on Electrical Insulation, Vol. EI-2, No. 1, April, 1967.
- Bell, W. R., "Influence of Specimen Size on the Dielectric Strength of Transformer Oil," IEEE Transactions on Electrical Insulation, Vol. EI-12, No. 4, August, 1977.
- Berger, N., and P. Jay, "A New Impregnant for HV Power Capacitors," IEEE Transactions on Electrical Insulation, Vol. EI-21, No. 1, pp. 59-63, February, 1986.
- Berger, T. L., "Effects of Surrounding Medium on Electrically Exploded Aluminum Foil Fuses," IEEE Transactions on Plasma Science, Vol. PS-8, No. 3, pp. 213-216, September, 1980.
- Bernardes, J., and M. F. Rose, "Electrical Breakdown Characteristics of Sodium Chloride - Water Mixtures," Digest of Technical Papers - 4th IEEE Pulsed Power Conference, pp. 308-311, June, 1983.
- Beroual, A., "Behavior of Charged and Uncharged Bubbles in Dielectric Liquids Subjected to Electric Stress," Journal of Applied Physics, Vol. 71, No. 3, pp. 1142-1145, February, 1992.
- Beroual, A., "Electronic and Gaseous Processes in the Prebreakdown Phenomena of Dielectric Liquids," Journal of Applied Physics, Vol. 73, No. 9, pp. 4528-4533, May, 1993.
- Beroual, A., and R. Tobazeon, "Prebreakdown Phenomena in Liquid Dielectrics," IEEE Transactions on Electrical Insulation, Vol. EI-21, No. 4, pp. 613-627, August, 1986.
- Beruchev, N. G., E. P. Bol'shakov, et al., "Nanosecond High-Current Electron Accelerator," Instruments and Experimental Techniques, Vol. 26, Pt 1, No. 6, pp. 1259-1265, November-December, 1983.

- Binns, D. F., and A. Jaberansari, "Effect of Temperature on the Electrical Breakdown of Conductor Samples in R-Temp and Envirotemp," Conference Record, Eighth International Conference on Conduction and Breakdown in Dielectric Liquids, pp. 250-254, July, 1984.
- Birlaskedaran, S., and M. Darveniza, "Microdischarges from Particles in Transformer Oil," IEEE Transactions on Electrical Insulation, Vol. EI-11, No. 4, pp. 162-163, December, 1976.
- Borsi, H., and U. Schroder, "Initiation and Formation of Partial Discharges in Mineral-Based Insulating Oil," IEEE Transactions on Dielectrics and Electrical Insulation, Vol. 1, No. 3, pp. 419-425, June, 1994.
- Bozzo, R., G. Coletti, P. Molfino, and G. Molinari, "Electrode Systems for Dielectric Strength Controlling the Electro-Dielectrophoretic Effects," Conference Record, Eighth International Conference on Conduction and Breakdown in Dielectric Liquids, pp. 265-269, July, 1984.
- Brzostek, E., and J. Kedzia, "Static Electrification in Aged Transformer Oil," IEEE Transactions on Electrical Insulation, Vol. EI-21, No. 4, pp. 609-612, August, 1986.
- Burton, J. K., D. Conte, et al., "Multiple Channel Switching in Water Dielectric Pulse Generators," Proceedings of the 5th Symposium on Engineering Problems of Fusion Research, pp. 679-683, 1973.
- Buttram, M., and M. O'Malley, "Breakdown of Water Under Long Term Stress," Digest of Technical Papers - 4th IEEE Pulsed Power Conference, pp. 327-330, 1983.
- Camarcat, N., J. Delvaux, B. Etlicher, D. Mosher, G. Raboisson, and A. Perronnet, "Electrical pulsed power generators of the 1 TW class," Laser and Particle Beams, Vol. 3, part 4, pp. 415-455, 1985.
- Cesari, S., and S. Yakov, "Considerations About the Impulse Breakdown and Power Frequency Partial Discharge Inception Voltages of Insulating Liquids," Conference Record, Eighth International Conference on Conduction and Breakdown in Dielectric Liquids, pp. 230-234, July, 1984.
- Chadband, W. G., "On Variations in the Propagation of Positive Discharges Between Transformer Oil and Silicone Fluids," Journal Physics D: Applied Physics, Vol. 13, pp. 1299-1307, 1980.

- Chadband, W. G., "The Ubiquitous Positive Streamer," IEEE Transactions on Electrical Insulation, Vol. 23, No. 4, pp. 697-706, August, 1988.
- Chadband, W. G., and T. M. Sufian, "Experimental Support for a Model of Positive Streamer Propagation in Liquid Insulation," IEEE Transactions on Electrical Insulation, Vol. EI-20, No. 2, pp. 239-246, April, 1985.
- Chiu, C., C. W. Smith, and J. H. Calderwood, "Investigation of a Critical Region Between Corona and Discharge Channels in Highly Stressed Dielectric Liquids," Conference Record, Eighth International Conference on Conduction and Breakdown in Dielectric Liquids, pp. 164-170, July, 1984.
- Colson, S. D., and T. H. Dunning, Jr., "The Structure of Nature's Solvent: Water," Science, Vol. 265, pp. 43-44, July, 1994.
- Curry, R., P.D'A. Champney, C. Eichenberger, J. Fockler, D. Morton, R. Sears, I. Smith, R. Conrad, "The Development and Testing of Subnanosecond-Rise, Kilohertz Oil Switches for the Generation of High-Frequency Impulses," IEEE Transactions on Plasma Science, Vol. 20, No. 3, pp. 383-392, June, 1992.
- Danikas, M., "Technical Report: Particles in Transformer Oil," IEEE Electrical Insulation Magazine, Vol. 7, No. 2, pp. 39-40, March/April, 1991.
- Demidov, B. A., M. V. Ivkin, V. A. Petrov, and S. D. Fanchenko, "A High-Voltage Water Spark Gap with Laser Firing," Instruments and Experimental Techniques, Vol. 17, No. 1, pp. 131-133, 1974.
- Denholm, A. S., J. J. Moriarty, W. R. Bell, J. R. Uglum, G. K. Simcox, J. Hipple, and S. V. Nablo, "Review of Dielectrics and Switching," Technical Report No. AFWL-TR-72-88, AFWL/DYX, Kirtland AFB, New Mexico 87117, 1988, (Limited Distribution).
- Devins, J. C., S. J. Rzas, and R. J. Schwabe, "Breakdown and Prebreakdown Phenomena in Liquids," Journal of Applied Physics, Vol. 52, No. 7, pp. 4531-4545, July, 1981.
- Dimeler, G. R., I. W. Mills, and J. J. Melchiorre, "The Scope of Hydrogenation as a Refining Tool for the Manufacture of Transformer Oils," IEEE Transactions on Electrical Insulation, Vol. EI-4, No. 1, pp. 7-12, 1969.

- Dingjiu, L., and C. Shoushen, "The Breakdown Voltage of Deionized Water and Transformer Oil in the Microsecond and Nanosecond Regions," Proceedings, Second International Conference on Properties and Applications of Dielectric Materials, Vol. 1, pp. 63-66, 1988.
- Dotoku, K., H. Yamada, and S. Sakamoto, "Field Emission into Nonpolar Organic Liquids," Journal of Chemical Physics, Vol. 69, No. 3, pp. 1121-1125, August, 1978.
- Duval, M., and C. Lamarre., "The Characterization of Electrical Insulating Oils by High-Performance Liquid Chromatography," IEEE Transactions on Electrical Insulation, Vol. EI-12, No. 5, pp. 340-348, October, 1977.
- Duval, M., and D. Cauchon, "Paraffinic Transformer Oils for Use at Low Temperatures," IEEE Transactions on Electrical Insulation, Vol. EI-18, No. 6, pp. 586-590, December, 1983.
- Eish, T. D., Y. A. Abed, and G. M. El-Salam, "Breakdown Phenomena in Transformer Oil Subjected to Direct Voltages with Ripple," Conference Record, Eighth International Conference on Conduction and Breakdown in Dielectric Liquids, pp. 245-249, July, 1984.
- El-Sulaiman, A. A., and A. S. Ahmed, "Effects of Field Strength and Filtration on Burst Phenomena in Aged Transformer Oil Under High Non-Uniform DC Field," IEEE Transactions on Electrical Insulation, Vol. EI-18, No. 2, pp. 163-166, April, 1983.
- Energy Sciences, Inc., "The Influence of Hydrostatic Pressure Upon the Dielectric Properties of Deionized Water," Performed under Contract No. F29601-71-C-0034, Air Force Weapons Laboratory, Kirtland AFB, NM, May, 1972.
- Etlicher, B., N. Camarcot, C. Bruno, G. Roboisson, and A. Perronnet, "Scaling of the J. C. Martin breakdown equations to generators of the 1-TW class," Digest of Technical Papers - 4th IEEE Pulsed Power Conference, pp. 331-334, 1983.
- Federov, V. M., "High Power Nanosecond Discharge Channel in Water," 5th Megagauss Conference, pp. 319-326, 1990.
- Felici, N. J., "Blazing a Fiery Trail with the Hounds," IEEE Transactions on Electrical Insulation, Vol. 23, No. 4, pp. 497-503, August, 1988.

- Fenneman, D. B., "Pulsed High-Voltage Dielectric Properties of Ethylene Glycol/Water Mixtures," Journal of Applied Physics, Vol. 53, No. 12, pp. 8961-8968, December, 1982.
- Fenneman, D. B., and R. J. Gripshover, "Experiments on Electrical Breakdown in Water in the Microsecond Regime," IEEE Transactions on Plasma Science, Vol. PS-8, No. 3, pp. 209-213, September, 1980.
- Fenneman, D. B., and R. J. Gripshover, "High Power Dielectric Properties of Water Mixtures," Digest of Technical Papers - 4th IEEE Pulsed Power Conference, pp. 302-307, June, 1983.
- Fleszynski, J., and B. Lutynski, "Macroparticle-Initiated Breakdown of Insulating Oil," Conference Record, Eighth International Conference on Conduction and Breakdown in Dielectric Liquids, pp. 275-279, July, 1984.
- Forster E. O., "Critical Assessment of the Electrical Breakdown Process In Dielectric Fluids," IEEE Transactions on Electrical Insulation, Vol. EI-20, No. 5, pp. 891-896, October, 1985.
- Forster, E. O., "Electric Conductance in Liquid Hydrocarbons," IEEE Transactions on Electrical Insulation, Vol. EI-2, No. 1, pp. 10-18, April, 1967.
- Forster, E. O., "Partial Discharges and Streamers in Liquid Dielectrics, the Significance of the Inception Voltage," IEEE Transactions on Electrical Insulation, Vol. 28, No. 6, pp. 941-946, December, 1993.
- Forster, E. O., "Progress in the Field of Electric Properties of Dielectric Liquids," IEEE Transactions on Electrical Insulation, Vol. 25, No. 1, pp. 45-53, February, 1990.
- Forster, E. O., "Research in the Dynamics of Electrical Breakdown in Liquid Dielectrics," IEEE Transactions on Electrical Insulation, Vol. EI-15, No. 3, pp. 182-185, June, 1980.
- Forster, E. O., and P. Wong, "High Speed Laser Schlieren Studies of Electrical Breakdown in Liquid Hydrocarbons," IEEE Transactions on Electrical Insulation, Vol. EI-12, No. 4, pp. 435-442, December, 1977.

- Frei, C. J., "Weibull Statistical Analysis of Dielectric Breakdown in N-Hexane," Conference Record, Eighth International Conference on Conduction and Breakdown in Dielectric Liquids, pp. 217-224, July, 1984.
- Friedman, M., and M. Ury, "Chemically Enhanced Opening Switch for Generating High-Voltage Pulses," Review of Scientific Instruments, Vol. 48, No. 3, pp. 279-281, March, 1977.
- Fuhr, J., and W. F. Schmidt, "Time-Resolved Current-Voltage Measurement of the Spark Breakdown in Liquid N-Hexane," Conference Record, Eighth International Conference on Conduction and Breakdown in Dielectric Liquids, pp. 235-240, July, 1984.
- Fuhr, J., W. F. Schmidt, and S. Sato, "Spark Breakdown of Liquid Hydrocarbons. I. Fast Current and Voltage Measurements of the Spark Breakdown in Liquid n-hexane," Journal of Applied Physics, Vol. 59, No. 11, pp. 3694-3701, June, 1986.
- Fuhr, J., and W. F. Schmidt, "Spark Breakdown of Liquid Hydrocarbons. II. Temporal Development of the Electric Spark Resistance in n-pentane, n-hexane, 2,2 dimethylbutane, and n-decane," Journal of Applied Physics, Vol. 59, No. 11, pp. 3702-3708, June, 1986.
- Garton, G. C., E. C. Rogers, and E. H. Reynolds, "Discussion on Dielectric Loss and Voltage Breakdown in Liquid Nitrogen and Hydrogen," IEEE Transactions on Electrical Insulation, pp. 47-48, March, 1971.
- Gavrilov, G. N., V. V. Petukhov, A. G. Ryabinin, G. A. Ryabinin, and T. V. Brublevskaia "Total Hydrodynamic Efficiency of an Underwater Electric Discharge," Soviet Physics - Technical Physics, Vol. 22, No. 7, pp. 868-870, July, 1977.
- Gavrilov, I. M., V. R. Kukhta, V. V. Lopatin, and P. G. Petrov, "Dynamics of Prebreakdown Phenomena in a Uniform Field in Water," IEEE Transactions on Dielectrics and Electrical Insulation, Vol. 1, No. 3, pp. 496-502, June, 1994.
- Gehman Jr., V. H., D. B. Fenneman, and R. J. Gripshover, "Electrode Surface Effects on Unipolar Charge Injection in Cooled Liquid Dielectric Mixtures," Digest of Technical Papers - 4th IEEE Pulsed Power Conference, pp. 316-322, June, 1983.

- Girdinio, P., G. Liberti, P. Molfino, G. Molinari, and A. Viviani, "A New Class of Uniform Field Electrodes for Dielectric Strength Tests in Dielectric Liquids," Conference Record, Eighth International Conference on Conduction and Breakdown in Dielectric Liquids, pp. 225-229, July, 1984.
- Gomer, R., "Field Emission and Field Ionization in Condensed Phases," Accounts of Chemical Research, Vol. 5, No. 2, pp. 41-48, February, 1972.
- Graneau, P., and P. N. Graneau, "Electrodynamic Explosions in Liquids," Applied Physics Letters, Vol. 46, No. 5, pp. 468-470, March, 1985.
- Guenther, A. H., G. L. Zigler, J. R. Bettis, and R. P. Copeland, "Laser triggered switching of a pulsed, charged, oil filled spark gap," Review of Scientific Instruments, Vol. 46, No. 7, pp. 914-920, 1975.
- Hakim, R. M., "The Effect of Oxidation on the Dielectric Properties of an Insulating Oil," IEEE Transactions on Electrical Insulation, Vol. EI-7, No. 4, pp. 185-195, December, 1972.
- Hakim, R. M., "The Properties of an Insulating Oil and Its Fractions at Low Temperatures," IEEE Transactions on Electrical Insulation, Vol. EI-10, No. 4, pp. 124-134, December, 1975.
- Hakim, R. M., R. G. Oliver, and H. St-Onge, "The dielectric properties of silicone fluids," Erratum: IEEE Transactions on Electrical Insulation, Vol. EI-13, No. 1, p. 65, 1978.
- Halpern, B., and R. Gomer, "Field Emission in Liquids," The Journal of Chemical Physics, Vol. 51, No. 3, pp. 1031-1047, August, 1969.
- Halpern, B., and R. Gomer, "Field Ionization in Liquids," The Journal of Chemical Physics, Vol. 51, No. 3, pp. 1048-1056, August, 1969.
- Hasted, J. B., Aqueous Dielectrics, Chapman and Hall, London, 1993.
- Hasted, J. B., Water a Comprehensive Treatise, Volume 1, The Physics and Physical Chemistry of Water, Chapter 7, "Liquid Water: Dielectric Properties," Edited by Felix Franks, Plenum Press, New York, NY, pp. 255-309, 1972.

- Hasted, J. B., Water a Comprehensive Treatise, Volume 2, Water in Crystalline Hydrates Aqueous Solutions of Simple Nonelectrolytes, Chapter 7, "Dielectric Properties," Edited by Felix Franks, Plenum Press, New York, NY, pp. 405-458, 1973.
- Hausler, E., and L. Stein, "Fokussierbare Unterwasserimpulsschallquellen," Acustica, Vol. 49, No. 4, pp. 273-279, 1981, (German).
- Hayashi, M., O. Yamamoto, H. Isa, C. Uenosono, Y. Mino, and T. Tani, "Studies on Corona in Transformer Oil by Measurement of Space Charge," Conference Record, Eighth International Conference on Conduction and Breakdown in Dielectric Liquids, pp. 204-208, July, 1984.
- Hebner, R. E., E. F. Kelley, E. O. Forster, and G. J. Fitzpatrick, "Observation of Prebreakdown and Breakdown Phenomena in Liquid Hydrocarbons Under Nonuniform Field Conditions," Conference Record, Eighth International Conference on Conduction and Breakdown in Dielectric Liquids, pp. 185-189, July, 1984.
- Henson, B. L., "Corona Discharge from Fine Points in Liquid Helium," Physics Letters, Vol. 33A, No. 2, pp. 91-92, October, 1970.
- Hosticka, C., "Dependence of Uniform/Nonuniform Field Transformer Oil Breakdown on Oil Composition," IEEE Transactions on Electrical Insulation, Vol. EI-14, No. 1, pp. 43-50, February, 1979.
- Huck, J. R., G. A. Noyel, and L. J. Jorat, "Dielectric Properties of Supercooled Glycerol-Water Solutions," IEEE Transactions on Electrical Insulation, Vol. 23, No. 4, pp. 627-638, August, 1988.
- Inuishi, Y., "Effect of Space Charge and Structure on Breakdown of Liquid and Solid," IEEE Transactions on Electrical Insulation, Vol. EI-17, No. 6, pp. 488-492, December, 1982.
- Itahashi, S., M. Sone, and H. Mitsui, "Effect of dissolved water in several kinds of liquid dielectrics on conduction," Proceedings of the 1991 CEIDP, pp. 482-487.
- Jaksts, A. and A. D. Cross, "High Speed Streak Photography of the Breakdown of Transformer Oil and the Dependence of its Nature on Local Stored Energy," IEEE Transactions on Electrical Insulation, Vol. EI-18, No. 6, pp. 599-604, December, 1983.

- Jefferies, M., and K. Mathes, "Dielectric Loss and Voltage Breakdown in Liquid Nitrogen and Hydrogen," IEEE Transactions on Electrical Insulation, Vol. EI-5, No. 3, pp. 83-91, September, 1970.
- Johnson, D. L., and J. P. VanDevender, "Low Prepulse, High Power Density Water Dielectric Switching," Digest of Technical Papers - 2nd IEEE International Pulsed Power Conference, pp. 191-194, June, 1979.
- Johnson, D. L., and J. P. VanDevender, and T. H. Martin, "High Power Density Water Dielectric Switching," IEEE Transactions on Plasma Science, Vol. PS-8, No. 3, pp. 204-209, September, 1980.
- Jones, H. M., and E. E. Kunhardt, "Development of Pulsed Dielectric Breakdown in Liquids," Journal of Physics D: Applied Physics, Vol. 28, No. 1, p. 178, 1995.
- Jones, H. M., and E. E. Kunhardt, "Electron Impact Ionization and Dielectric Breakdown in Liquid Xe and Ar," Conference Record of the 1994 IEEE International Symposium on Electrical Insulation, pp. 442-445, June 1994.
- Jones, H. M., and E. E. Kunhardt, "Monte Carlo Investigation of Electron-Impact Ionization in Liquid Xenon," Physical Review B, Vol. 48, No. 13, pp. 9382-9387, October 1993.
- Jones, H. M., and E. E. Kunhardt, "Pulsed Dielectric Breakdown of Pressurized Water and Salt Solutions," Journal of Applied Physics, Vol. 77, No. 2, p. 795, 1995.
- Jones, H. M., and E. E. Kunhardt, "Submicrosecond Breakdown and Prebreakdown Phenomena in Water: Influence of Pressure, Conductivity, and Gap Separation," Conference Record of the 1994 IEEE International Symposium on Electrical Insulation, pp. 442-445, June 1994.
- Jones, H. M., and E. E. Kunhardt, "The Influence of Pressure and Conductivity on the Pulsed Breakdown of Water," IEEE Transactions on Dielectrics and Electrical Insulation, Vol. 1, No. 6, pp. 1016-1025, December, 1994.
- Kadish, A., and W. B. Maier, II, "Electromagnetic Radiation from Abrupt Current Changes in Electrical Discharges." Journal of Applied Physics, Vol. 70, No. 11, pp. 6700-6711, December, 1991.

- Kaneko, T., M. Hara, and M. Akazaki, "Effects of Voltage on Dielectric Breakdown Characteristics in Gaps Partially Immersed in Liquid Nitrogen," Conference Record, Eighth International Conference on Conduction and Breakdown in Dielectric Liquids, pp. 270-274, July, 1984.
- Kang, B. P., "Stability of Electrical-Insulating Oils," IEEE Transactions on Electrical Insulation, Vol. EI-5, No. 2, pp. 41-46, June, 1970.
- Kang, B. P., "Thermal Dependency of Viscosity, Power Factor, and Ion Content of Electrical Insulating Oils-III Predictions of Power Factor of Oil Blends Through the Concept of Ion Content," IEEE Transactions on Electrical Insulation, Vol. EI-2, No. 2, pp. 121-128, August, 1967.
- Kang, B. P., "Thermal Dependency of Viscosity, Power Factor, and Ion Content of Electrical Insulating Oils-II Characteristics of Blended Insulating Oils," IEEE Transactions on Electrical Insulation, Vol. EI-2, No. 1, pp. 55-69, April, 1967.
- Kao, K., and J. McMath, "Time-Dependent Pressure Effect in Liquid Dielectrics," IEEE Transactions on Electrical Insulation, Vol. EI-5, No. 3, pp. 64-68, September, 1969.
- Kao, K., and M. Rashwan, "On the Thermal Activation Energy for high-Field Electric Conduction in Dielectric Liquids," IEEE Transactions on Electrical Insulation, Vol. EI-13, No. 2, pp. 86-93, April, 1978.
- Kao, K. C., "Theory of high-field electric conduction and breakdown in dielectric liquids," IEEE Transactions on Electrical Insulation, Vol. EI-11, No. 4, pp. 121-128, 1976.
- Kedzia, J., and E. Brozostek, "Static Electrification in Transformer Oil as a Measure of its Aging," IEEE Transactions on Electrical Insulation, Vol. EI-19, No. 2, pp. 101-106, April, 1984.
- Kelly, E. F., and R. E. Hebner Jr., "Electro-Optic Field Measurement at a Needle Tip and Streamer Initiation in Nitrobenzene," 1986 Annual Report Conference on Electrical Insulation and Dielectric Phenomena, IEEE, pp. 272-277, 1986.
- Kelly, E. F., and R. E. Hebner Jr., "The Electric Field Distribution Associated with Prebreakdown Phenomena in Nitrobenzene," Journal of Applied Physics, Vol. 52, No. 1, pp. 191-195, January, 1981.

- Khalifa, M., and A. Nousseir, "Temporal Variation of Conduction Currents in Liquid Insulants Under High Direct Voltages," IEEE Transactions on Electrical Insulation, Vol. EI-11, No. 2, pp. 51-54, June, 1976.
- Kitani, I., and K. Arii, "Impulse Tree and Discharge Light in PMMA Subjected to Nanosecond Pulses," IEEE Transactions on Electrical Insulation, Vol. EI-19, No. 4, pp. 281-287, August, 1984.
- Klimkin, V., "Mechanisms of Electrical Breakdown of Water from Pointed Anode in the Nanosecond Range," Soviet Technical Physics Letters, Vol. 16, No. 2, pp. 146-147, February, 1990.
- Koldamasov, A. I., "Plasma Formation in Cavitating Dielectric Liquid," Soviet Physics - Technical Physics, Vol. 36, No. 2, pp. 234-235, 1991.
- Korobeynikov, S. M., and E. V. Yanshin, "Bubble Model: Time Dependent Pressure Effect in Liquids," Conference Record of the 10th International Conference on Conduction and Breakdown in Dielectric Liquids, pp. 360-364, 1990.
- Korobeynikov, S. M., and E. V. Yanshin, "Dynamics of the Electrostriction Pressure in a Fluid Near a Spherical Electrode," Soviet Physics - Technical Physics, Vol. 28, No. 10, pp. 1288-1290, October, 1983.
- Kovsharov, N. F., A. V. Luchinskii, et al., "SNOP-3 Pulse Generator," Instruments and Experimental Techniques, Vol. 30, No. 6, Part 1, pp. 1367-1373, May, 1988.
- Krasucki, Z., High Voltage Technology, Chapter 7, "Breakdown of Commercial Liquid and Liquid-Solid Dielectrics," Edited by L. L. Alston, Oxford University Press, London, pp. 129-143, 1968,
- Krivitskii, E. V., "On the Destruction of Phase Uniformity in Liquid Dielectrics Subjected to a Pulsed Voltage," Soviet Physics - Technical Physics, Vol. 36, No. 1, pp. 4-7, January, 1991.
- Krivitskii, E. V., V. D. Kustovskii, and A. P. Slivinskii, "Effect of the Initial Conditions on the Dynamics of an Underwater Spark. I. Effect of the Parameters of the Generator and the Medium," Soviet Physics - Technical Physics, Vol. 25, No. 8, pp. 993-998, August, 1980.
- Kuffel, E., and W. S. Zaengl, High Voltage Engineering, Section 5.14.2, Breakdown in Liquids, Pergamon Press, New York, pp. 411-421, 1984.

- Kuleshov, V. M., S. L. Nedoseev, V. P. Smirnov, and A. M. Spektor, "Switching characteristics of a discharge in water," Soviet Physics - Technical Physics, Vol. 19, No. 1, pp. 150-151, 1974.
- Kuskova, N. I., "Mechanisms of Electrical Breakdown in Water," Soviet Technical Physics Letters, Vol. 15, No. 12, December, 1989.
- Kuzhekin, I. P., "Investigation of the Breakdown by Rectangular Voltage Pulses of a Liquid in an Inhomogeneous Field," Soviet Physics - Technical Physics, Vol. 11, No. 12, pp. 1585-1589, June, 1967.
- Lagunov, V. M., and V. M. Fedorov, "Use of Water Insulation in the Pulsed Current Sources and Electron Accelerators of the Novosibirsk Institute of Nuclear Physics," Soviet Journal of Applied Physics, Vol. 4, No. 3, pp. 396-403, May-June, 1978.
- Lee, W. M., and R. D. Ford, "Pressure Measurements Correlated with Electrical Explosion of Metals in Water," Journal of Applied Physics, Vol. 64, No. 8, pp. 3851-3854, October, 1988.
- Lesaint, O., and R. Tobazeon, "Study of the Generation by Acute Electrodes of a Gaseous Phase in Dielectric Liquids Subjected to High A. C. or Step Voltages," Conference Record, Eighth International Conference on Conduction and Breakdown in Dielectric Liquids, pp. 176-179, July, 1984.
- Lewis, T. J., High Voltage Technology, Chapter 6, The Electrical Conduction and Strength of Pure Liquids, Edited by L. L. Alston, Oxford University Press, London, pp. 111-127, 1968.
- Lhiaubet, C., and R. M. Meyer, "Method of Indirect Determination of the Anodic and Cathodic Voltage Drops in Short High-Current Electric Discharges in a Dielectric Liquid," Journal of Applied Physics, Vol. 52, No. 6, pp. 3929-3934, June, 1981.
- Lischer, D. W., and A. Ramrus, "Laser Initiated Conduction of an Overvolted Water Spark Gap," Digest of Technical Papers - 3rd IEEE International Pulsed Power Conference, IEEE, New York, NY, pp. 478-481, 1981.

- Mahajan, S. M., and T. S. Sudarshan, "Measurement of the Space Charge Field in Transformer Oil Using its Kerr Effect," IEEE Transactions on Dielectrics and Electrical Insulation, Vol. 1, No. 1, pp. 63-70, February, 1994.
- Maksiejewski, J. L., "The Breakdown Process of a Liquid Trigatron," IEEE Transactions on Electrical Insulation, Vol. 23, No. 2, pp. 227-230, April, 1988.
- Maksiejewski, J. L., "The Effect of Additives on the Time Characteristics of a Liquid Trigatron," IEEE Transactions on Electrical Insulation, Vol. EI-22, No. 3, pp. 237-239, June, 1987.
- Maksiejewski, J. L., "Time-Lags of Triggered Spark Gaps in Liquid Hydrocarbons," Conference Record, Eighth International Conference on Conduction and Breakdown in Dielectric Liquids, pp. 260-264, July, 1984.
- Maruska, H. P., E. O. Forster, and J. H. Enard, "Electrical Transport Processes in Heavy hydrocarbon Fluids," IEEE Transactions on Electrical Insulation, Vol. EI-20, No. 6, pp. 947-955, December, 1985.
- Mathes, K. N., "Influence of Electrical Discharges in Oil and Combinations of Oil and Paper." IEEE Transactions on Electrical Insulation, Vol. EI-11, No. 4, pp. 164-180, December, 1976.
- McClintock, P. V. E., "Field Emission in Liquid Helium," Physics Letters, Vol. 29A, No. 8, pp. 453-454, June, 1969.
- McGrath, P. B., and H. I. Marsden, "DC-Induced prebreakdown Events in N-Hexane," IEEE Transactions on Electrical Insulation, Vol. EI-21, No. 4, pp. 669-672, August, 1986.
- McKenny, P. J., and P. B. McGrath, "Anomalous Positive Point Prebreakdown Behavior in Dielectric Liquids," IEEE Transactions on Electrical Insulation, Vol. EI-19, No. 2, pp. 93-100, April, 1984.
- McLeod, A. R., and V. H. Gehman, Jr., "Water Breakdown Measurements of Stainless Steel and Aluminum Alloys for Long-Charging Times," Digest of Technical Papers. Sixth IEEE Pulsed Power Conference, pp. 57-59, 1987.

- Megahed, I. Y., and A. A. Zaky, "Influence of Temperature and Pressure on Conduction Currents in Transformer Oil," IEEE Transactions on Electrical Insulation, Vol. EI-4, No. 4, pp. 99-103, December, 1969.
- Mel'nikov, N. P., G. A. Ostroumov, and M. Yu. Stoyak, "The Development of an Electric Discharge in Aqueous Electrolytes," Soviet Physics - Doklady, Vol. 8, No. 2, pp. 176, August, 1963.
- Melchiorre, J. J., and I. W. Mills, "Factors Affecting Stability of Electrical Insulating Oils," IEEE Transactions on Electrical Insulation, Vol. EI-2, No. 2, pp. 150-155, 1967.
- Messerschmitt, J., "Investigations of the Pressure Dependence of Electrical Breakdown of Purified Water and Saline Solutions," Digest of Technical Papers, Ninth IEEE International Pulsed Power Conference, pp. 56-58, June, 1993.
- Miller, A. R., "Sub-Ohm Coaxial Pulse Generators, Blackjack 3, 4, and 5," 3rd IEEE International Pulsed Power Conference, pp. 200-205, 1981.
- Moore, W. B., R. W. Stinnett, and D. H. McDaniel, "Supermite Vacuum Interface Design," Digest of Technical Papers. 5th IEEE Pulsed Power Conference, pp. 315-318, 1985.
- Morcos, I., and F. Rizk, "A Surface Chemistry Approach to the Study of Solid Electrodes in Insulating Liquids," IEEE Transactions on Electrical Insulation, Vol. EI-12, No. 4, pp. 309-312, August, 1977.
- Nakao, Y., H. Itoh, Y. Sakai, and H. Tagashira, "Studies of the Creepage Discharge on the Surface of Liquids," IEEE Transactions on Electrical Insulation, Vol. 23, No. 4, pp. 677-687, August, 1988.
- Nelson, J. K., "Dielectric Fluids in Motion," IEEE Electrical Insulation Magazine, Vol. 10, No. 3, pp. 16-28, May/June, 1994.
- Nosseir, A., "Effect of Dissolved Gases, Stress, and Gap Spacing on High-Field Conductivity in Liquid Insulants," IEEE Transactions on Electrical Insulation, Vol. EI-10, No. 2, pp. 58-62, June, 1975.
- Noyel, G. A., L. J. Jorat, O. Derriche, and J. R. Huck, "Dielectric Properties of Normal Supercooled Water Obtained in Alcohol/Water Mixtures," IEEE Transactions on Electrical Insulation, Vol. 27, No. 6, pp. 1136-1143, December, 1992.

- Ohashi, A., and M. Ueda, "Thermal Breakdown of Silicone Liquids Under Pulsed High-Frequency Field," IEEE Transactions on Electrical Insulation, Vol. EI-8, No. 4, pp. 128-133, December, 1973.
- Oliveri, S., and R. Kattan, "Numerical Study of Single-Vapor-Bubble Dynamics in Insulating liquids Initiated by electrical Current Pulses," Journal of Applied Physics, Vol. 71, No. 1, pp. 108-112, January, 1982.
- Ovchinnikov, I. T., and E. V. Yanshin, "A High-Voltage Pulse Electrooptical Bridge," Instruments and Experimental Techniques, Vol. 26, No. 1, pp. 100-103, 1983.
- Ovchinnikov, I. T., and E. V. Yanshin, "Dipolar-Ion-Mediated Relaxation of Conduction in Water Associated with High-Voltage Impurities," Soviet Physics - Technical Physics, Vol. 29, No. 12, pp. 1430-1431, December, 1984.
- Ovchinnikov, I. T., and E. V. Yanshin, "Relaxation of Proton Conduction in Water in Strong Pulsed Electric Fields," Soviet Physics - Technical Physics, Vol. 29, No. 12, pp. 1431-1432, December, 1984.
- Ovchinnikov, I. T., K. V. Yanshin, and E. V. Yanshin, "Investigating Prebreakdown Fields in Water by Means of the Kerr Effect," Soviet Physics - Technical Physics, Vol. 19, No. 2, pp. 294-295, August, 1974.
- Ovchinnikov, I. T., K. V. Yanshin, and E. V. Yanshin, "Use of the Kerr Effect to Study Pulsed Electric Fields Near a Sharp Point in Water," Soviet Physics - Technical Physics, Vol. 23, No. 12, pp. 1487-1489, December, 1978.
- Pellinen, D. G., and I. Smith, "A reliable multimegavolt voltage divider," Review of Scientific Instruments, Vol. 43, No. 2, pp. 299-301, 1972.
- Perkins, J. R., "Selection of Materials for Use as Electrical Insulation-A Philosophical and Systematic Approach," IEEE Transactions on Electrical Insulation, Vol. EI-6, No. 3, pp. 106-110, September, 1971.
- Perret, J., "Study of the Dielectric Breakdown of Insulating Mineral Oils Under Impulse Voltages," IEEE Transactions on Electrical Insulation, Vol. EI-16, No. 4, pp. 339-345, August, 1981.

- Petrovic, K., and D. Vitorvic, "Examination of Insulating Oils for Transformers by Instrumental Methods," IEEE Transactions on Electrical Insulation, Vol. EI-18, No. 6, pp. 591-598, December, 1983.
- Pompili, M., C. Mazzetti, and E. O. Forster, "Partial Discharge Distributions in Liquid Dielectrics," IEEE Transactions on Electrical Insulation, Vol. 27, No. 1, pp. 99-105, February, 1992.
- Prikhod'ko, N. "Electrical Breakdown of Dielectrics With a Dipole Structure," Translation of Tomsk Universitet Sibirskiy Fiziko-Tekhnicheskiv Institut Trudy, (High Voltage Laboratory), Vol. 6, No. 2, pp. 114-119, 1945. Foreign Technology Report NO. FTD-HC-23-1176-72, 20 July 1972.
- Qui, Y., A. Sun, and E. Kuffel, "Improved Dielectric Strength of SF6 Gas with a Trichlorotrifluoroethane Vapor Additive," IEEE Transactions on Electrical Insulation, Vol. EI-22, No. 6, pp. 763-768, December, 1987.
- Rabe, J. G., and W. F. Schmidt, "Discussion: Decomposition Products of Silicone Liquids due to Electric Discharges," IEEE Transactions on Electrical Insulation, Vol. EI-18, No. 6, pp. 662-663, December, 1983.
- Ramu, T. S., and Y. N. Rao, "On the Evaluation of Conductivity of Mixtures of Liquid Dielectrics," IEEE Transactions on Electrical Insulation, Vol. EI-7, No. 2, pp. 55-60, June, 1972.
- Rao, Y. N., and T. S. Ramu, "Determination of the Permittivity and Loss Factor of Mixtures of Liquid Dielectrics," IEEE Transactions on Electrical Insulation, Vol. EI-7, No. 4, December, 1972.
- Ridah, S., "Shock Waves in Water," Journal of Applied Physics, Vol. 64, No. 1, pp. 152-158, July, 1988.
- Rudenko, N. S., and V. I. Tsvetkov, "An Investigation of the Electric Strength of Some Liquid Dielectrics Subject to Nanosecond Voltage Pulses," Soviet Physics - Technical Physics, Vol. 10, No. 10, pp. 1417-1419, April, 1966.
- Rudenko, N. S., and V. I. Tsvetkov, "Study of the Pulse Electrical Strength of Some Liquids," Soviet Physics - Technical Physics, Vol. 9, No. 6, pp. 837-839, December, 1964.

- Rzad, S. J., and J. C. Devins, "The Influence of a DC Bias on Streamers Produced by Step Voltages in Transformer Oil and Over Solid-Liquid Interfaces," IEEE Transactions on Electrical Insulation, Vol. EI-18, No. 1, pp. 1-10, February, 1983.
- Sacchi, C. A., "Laser-Induced Electric Breakdown in Water," Journal of the Optical Society Am B, Vol. 8, No. 2, pp. 337-344, February, 1991.
- Saikan, S. and F. Shimizu, "Water Spark Gap for a Nitrogen Laser," Review of Scientific Instruments, Vol.46, No. 12, pp. 1700-1701, December, 1975.
- Sakamoto, S., and H. Yamada, "Optical Study of Conduction and Breakdown in Dielectric Liquids," IEEE Transactions on Electrical Insulation, Vol. EI-15, No. 3, pp. 171-181, June, 1980.
- Sarin, S. G., E. V. Yanshin, and S. M. Korobeynikov, "EHD Instabilities Registration in Liquids," Proceedings of the 3rd International Conference on Properties and Applications of Dielectric Materials, pp. 898-900, July, 1991.
- Sawada, T., and T. Kitamori, "Detection of Ultrafine Particles in Ultrapure Water by Laser-Induced Breakdown Acoustic Effect," IEE 1988 Ultrasonics Symposium, pp. 711-716, 1988.
- Sazama, F. J., and V. L. Kenyon, "A Streamer Model for High-Voltage Water Switches," IEEE Transactions on Plasma Science, Vol. PS-8, No. 3, pp. 198-203, September, 1980.
- Schmidt, W. F., "Elementary Processes in the Development of the Electrical Breakdown of Liquids (A Review)," IEEE Transactions on Electrical Insulation, Vol. EI-17, No. 6, pp. 478-483, December, 1982.
- Schmidt, W. F., and W. Schnabel, "Electron Injection into Dielectric Liquids by Field Emission," Zeitschrift fur Naturforschung A (Astrophysik, Physik, und Physikalische Chemie), Vol. 26A, No. 1, pp. 169-170, 1971.
- Schnabel, W., and W. Schmidt, "Polymerization by High Electric Fields: Field Emission and Field Ionization," Journal of Polymer Science, Symposium No. 42, 273-280, 1973.

- Schwinkendorf, W. E., "Development of Water as a High Energy Density Dielectric," Air Force Weapons Laboratory, Kirtland Air Force Base, New Mexico, December, 1976, Report No. AFWL-TR-76-113 (Limited Distribution).
- Schwinkendorf, W. E., "Review of Electrical Breakdown Processes in Water," Air Force Weapons Laboratory, Kirtland Air Force Base, New Mexico, December, 1976, Report No. AFWL-TR-76-110 (Limited Distribution).
- Schwinkendorf, W. E., "Study of Conduction and Electrical Breakdown of Dielectric Liquids," Air Force Weapons Laboratory, Kirtland Air Force Base, New Mexico, December, 1976, Report No. AFWL-TR-76-112 (Limited Distribution).
- Sharbaugh, A. H., and P. K. Watson, "The Electric Strength of Hexane Vapor and Liquid in the Critical Region," Journal of Applied Physics, Vol. 48, No. 3, pp. 943-950, March, 1977.
- Sharbaugh, A. H., J. C. Devins and S. J. Rzas, "Progress in the Field of Electric Breakdown in Dielectric Liquids," IEEE Transactions on Electrical Insulation, Vol. EI-13 No. 4, pp. 249-276, August, 1978.
- Sharbaugh, A. H., J. C. Devins, and S. J. Rzas, "Review of past work on liquid breakdown," IEEE Transactions on Electrical Insulation, Vol. EI-15, No. 3, pp. 167-170, June, 1980.
- Shaw, D. G., and S. W. Cichanowski, "A Changing Capacitor Technology-Failure Mechanisms and Design Innovations," IEEE Transactions on Electrical Insulation, Vol. EI-16, No. 5, pp. 399-413, October, 1981.
- Shipman Jr., J. D., "Design and Performance of the new multichannel Oil Output Switch on the Gamble IIA Water Dielectric Pulse Power Generator at NRL," Digest of Technical Papers - 3rd IEEE International Pulsed Power Conference, IEEE, New York, NY, pp. 475-477, 1981.
- Shirai, M., and T. Ishii, "Evolution of Hydrogen from Insulating Oil in Transformers," IEEE Transactions on Electrical Insulation, Vol. EI-12, No. 4, pp. 266-272, August, 1977.
- Shirai, M., S. Shimoji, and T. Ishii, "Thermodynamic study on the thermal decomposition of insulating oil," IEEE Transactions on Electrical Insulation, Vol. EI-12, No. 4, pp. 272-280, 1977.

- Sincerny, P. S., "Electrical Breakdown Properties of Water for Repetitively Pulsed Burst Conditions," Proceedings of the 3rd IEEE International Pulsed Power Conference, pp. 222-225, June, 1981.
- Skvarenina, T. L., "An Introduction to Electrical Breakdown in Dielectrics," USAF Air Command and Staff College, Maxwell AFB, AL, Report No. 85-2470, April, 1985.
- Spence, P. W., Y. G. Chen, G. Frazier, and H. Calvin, "Inductance and Resistance Characteristics of Single-Site Untriggered Water Switches in Water Transfer Capacitor Circuits," Digest of Technical Papers - 2nd IEEE International Pulsed Power Conference, pp. 359-362, June, 1979.
- Srebrov, B. A., L. P. Dishkova, and F. I. Kuzmanova, "Electrical Breakdown of a Small Gap Filled with Distilled Water," Soviet Technical Physics Letters, Vol. 16, No. 1, pp. 70-71, January, 1990.
- Stekol'nikov, I. S., and V. Ya. Ushakov, "Discharge Phenomena in Liquids," Soviet Physics - Technical Physics, Vol. 10, No. 9, pp. 1307-1313, March, 1966.
- Stricklett, K., and R. Brunt, "Partial Discharge and Dielectric Liquid Research," Research for Electric Energy Systems - An Annual Report, pp. 32-45, December, 1991.
- Sueda, H., and K. C. Kao, "Prebreakdown Phenomena in High-Viscosity Dielectric Liquids," IEEE Transactions on Electrical Insulation, Vol. EI-17, No. 3, pp. 221-227, June, 1982.
- Sufian, T. M., and W. G. Chadband, "Positive Streamer Propagation in Liquid Insulation," Conference Record, Eighth International Conference on Conduction and Breakdown in Dielectric Liquids, pp. 153-158, July, 1984.
- Suzuki, T., and S. Murakami, "Decomposition Products of Silicone Liquid due to Electric Discharge," IEEE Transactions on Electrical Insulation, Vol. EI-18, No. 2, pp. 152-157, April, 1983.
- Suzuki, T., H. Hiramoto, and M. Umeda, "Dependence of Breakdown Voltage of Silicone Liquid on Temperature," IEEE Transactions on Electrical Insulation, Vol. EI-18, No. 4, pp. 462-590, August, 1983.

- Szklarczyk, M., R. C. Kainthla, and J. O'M. Bockris, "On the Dielectric Breakdown of Water: An Electrochemical Approach," Journal of Electrochemical Society, Vol. 136, No. 9, pp. 2512-2520, September, 1989.
- Tobazeon, R., "Prebreakdown Phenomena in Dielectric Liquids," IEEE Transactions on Dielectrics and Electrical Insulation, Vol. 1, No. 6, pp. 1132-1147, December, 1994.
- Tobazeon, R., and D. Philippe, "Prebreakdown Currents and Optical Events in Insulating Liquids Subjected to a Voltage Step in Point-Plane Geometry," Conference Record, Eighth International Conference on Conduction and Breakdown in Dielectric Liquids, pp. 190-193, July, 1984.
- Tobazeon, R., J. C. Filippini, and C. Marteau, "On the Measurement of the Conductivity of Highly Insulating Liquids," IEEE Transactions on Dielectrics and Electrical Insulation, Vol. 1, No. 6, pp. 1000-1004, December, 1994.
- Toriyama, Y., and U. Shinohara, "Electric Breakdown Field Intensity of Water and Aqueous Solutions," Physics Review, Vol. 51, No. 8, pp. 680, April, 1937.
- Tsukioka, H., K. Sugawara, E. Mori, S. Hukumori, and S. Sakai, "New Apparatus for Detecting H₂, CO, and CH₄ Dissolved in Transformer Oil," IEEE Transactions on Electrical Insulation, Vol. EI-18, No. 4, pp. 409-419, August, 1983.
- Ushakov, V. Ya., "Development of a Discharge in a Liquid Dielectric with Ramp Function Voltage Pulses," Soviet Physics - Technical Physics, Vol. 10, No. 10, pp. 1420-1423, April, 1966.
- VanDevender, J. P., "The Resistive Phase of a High Voltage Water Spark," Journal of Applied Physics, Vol. 49, No. 5, pp. 2616-2620, May, 1978.
- VanDevender, J. P., and T. H. Martin, "Untriggered water switching," IEEE Transactions on Nuclear Science, Vol. NS-22, No. 3, pp. 979-982, 1975.
- Van Heesch, E. J. M., R. H. P. Lemmens, B. Franken, K. J. Ptasinski, and F. L. S. Geurts, "Pulsed Corona for Breaking up Air Bubbles in Water," IEEE Transactions on Dielectrics and Electrical Insulation, Vol. 1, No. 3, pp. 426-431, June, 1994.

- Von Hippel, A., "The Dielectric Relaxation Spectra of Water, Ice, and Aqueous Solutions, and their Interpretation. 1. Critical Survey of the Status-quo for Water," IEEE Transactions on Electrical Insulation, Vol. 23, No. 5, pp. 801-816, October, 1988.
- Von Hippel, A., "The Dielectric Relaxation Spectra of Water, Ice, and Aqueous Solutions, and their Interpretation. 2. Tentative Interpretation of the Relaxation Spectrum of Water in the Time and Frequency Domain," IEEE Transactions on Electrical Insulation, Vol. 23, No. 5, pp. 817-823, October, 1988.
- Von Hippel, A., "The Dielectric Relaxation Spectra of Water, Ice, and Aqueous Solutions, and their Interpretation. 3. Proton Organization and Proton Transfer in Ice," IEEE Transactions on Electrical Insulation, Vol. 23, No. 5, pp. 825-840, October, 1988.
- Vorob'ev, V. V., V. A. Kapitonov, and E. P. Kruglyakov, "Increase of Dielectric Strength of Water in a System with 'Diffusion' Electrodes," JETP Letters, Vol. 19, No. 2, pp. 58-59, January, 1974.
- Vyvolokin, A. E., "Generation of SHF-Fields by Nontraditional Sources," Digest of Technical Papers, Ninth IEEE International Pulsed Power Conference, pp. 616-617, June, 1993.
- Watson, P. K., and A. H. Sharbaugh, "The Electric Strength of Nitrogen at Elevated Pressures and Small Gap Spacings," Journal of Applied Physics, Vol. 40, No. 1, pp. 328-334, January, 1969.
- Watson, P. K., W. G. Chadband, and W. Y. Mak, "Bubble Growth in Viscous and Non-Viscous Liquids Following a Localized Electrical Discharge," Conference Record, Eighth International Conference on Conduction and Breakdown in Dielectric Liquids, pp. 180-184, July, 1984.
- Weber, B. V., R. J. Commisso, G. Cooperstein, J. M. Grossmann, D. D. Hinshelwood, D. Mosher, J. M. Neri, P. F. Ottinger, and S. J. Stephanakis, "Plasma Erosion Opening Switch Research at NRL," IEEE Transactions on Plasma Science, Vol. PS-15, No. 6, pp. 635-648, December, 1987.
- Wilkinson, G. M., "Time-Dependent Capacitance Effects in Water Dielectric Switching," Digest of Technical Papers - 4th IEEE Pulsed Power Conference, pp. 323-326, June, 1983.

- Wilkinson, G. M., and A. R. Miller, "Untriggered, Multisite Switching in Water at Microsecond Charging Times," presented at the 1986 High Voltage Workshop, (limited distribution).
- Wong, P. P., and E. O. Forster, "The Dynamics of Electrical Breakdown in Liquid Hydrocarbons," IEEE Transactions on Electrical Insulation, Vol. EI-17, No. 3, pp. 203-220, June, 1982.
- Xie, H. K., and K. C. Kao, "A Study of the Low-Density Regions Developed in Liquefied Polyethylene Under High Electric Fields," Conference Record, Eighth International Conference on Conduction and Breakdown in Dielectric Liquids, pp. 199-203, July, 1984.
- Yamada, H., and T. Sato, "Electro-Optical Measurement of Pre-Breakdown Current in Dielectric Liquids," Conference Record, Eighth International Conference on Conduction and Breakdown in Dielectric Liquids, pp. 171-175, July, 1984.
- Yamashita, H., E. O. Forster, and M. Pompili, "Streamer Formation in Perfluoropolyether Under Impulse Conditions," IEEE Transactions on Electrical Insulation, Vol. 28, No. 3, pp. 324-329, June, 1993.
- Yamashita, H., T. Okada, and H. Amano, "Pre-Breakdown Current and Light Emission in Transformer Oil," Conference Record, Eighth International Conference on Conduction and Breakdown in Dielectric Liquids, pp. 159-163, July, 1984.
- Yamazawa, K., M. Uemura, H. Yamashita, and E. O. Foster, "Pulse Measurements Using LED in Dielectric Liquids Under Impulse Voltages," IEEE Transactions on Dielectrics and Electrical Insulation, Vol. 1, No. 3, pp. 391-396, June, 1994.
- Yanshin, E. V., and I. T. Ovchinnikov, "High Field Conduction Measurements in Water by Pulse Electrooptical Bridge," Conference Record of the 8th International Conference on Conduction and Breakdown in Dielectric Liquids, pp. 83-87, July, 1984.
- Yanshin, E. V., K. V. Yanshin, S. M. Korobeynikov, "Space Charge and Pre-Breakdown Bubbles Formation Near Point Electrodes Under Pulse Voltage," Conference Record, Eighth International Conference on Conduction and Breakdown in Dielectric Liquids, pp. 194-198, July, 1984.

- Yanshin, E. V., I. T. Ovchinnikov, and Yu. N. Vershinin, "Optical Study of Nanosecond Prebreakdown Phenomena in Water," Soviet Physics - Technical Physics, Vol. 18, No. 10, pp. 1303-1306, April, 1974.
- Yasufuku, S., "Calorimetric Measurements of Water Dissolved in Dielectric Fluids," IEEE Transactions on Electrical Insulation, Vol. EI-17, No. 5, pp. 464-468, October, 1982.
- Yasufuku, S., "General Properties of Mixtures of Naphthenic Insulating Oil with Alkylbenzenes," IEEE Transactions on Electrical Insulation, Vol. EI-14, No. 6, pp. 343-346, December, 1979.
- Yasufuku, S., and Y. Ishioka, "General Properties of Mixtures of Paraffinic Insulating Oil with Alkylbenzenes," IEEE Transactions on Electrical Insulation, Vol. EI-15, No. 5, pp. 429-433, October, 1980.
- Yasufuku, S., J. Ise, and S. Kobayashi, "Radiation-Induced Degradation Phenomena in Electrical Insulating Oils," IEEE Transactions on Electrical Insulation, Vol. EI-13, No. 1, pp. 45-50, February, 1978.
- Yasufuku, S., T. Umemura, and T. Tanii, "Electric Conduction Phenomena and Carrier Mobility Behavior in Dielectric Fluids," IEEE Transactions on Electrical Insulation, Vol. EI-14, No. 1, pp. 28-35, February, 1979.
- Yehia, S., and A. A. Zaky, "Some Factors Affecting the Direct Breakdown Voltage of Silicone Oil Under Nonuniform Fields," IEEE Transactions on Electrical Insulation, Vol. EI-18, No. 1, pp. 86-88, February, 1983.
- Yoshino, K., "Dependence of Dielectric Breakdown of Liquids on Molecular Structure," IEEE Transactions on Electrical Insulation, Vol. EI-15, No. 3, pp. 186-200, June, 1980.
- Yoshino, K., "Electrical Conduction and Dielectric Breakdown in Liquid Dielectrics," IEEE Transactions on Electrical Insulation, Vol. EI-21, No. 6, pp. 847-853, December, 1986.
- Yoshino, K., S. H. Kim, K. Kaneto, and Y. Inuishi, "Dielectric Breakdown of Liquid Helium and Influence of Electrode Coating," Conference Record, Eighth International Conference on Conduction and Breakdown in Dielectric Liquids, pp. 241-244, July, 1984.

- Young, D. R., "Electric Breakdown in CO₂ from Low Pressures to the Liquid State," Journal of Applied Physics, Vol. 21, pp. 222-231, March, 1950.
- Zahn, M., "Transform Relationship Between Kerr-Effect Optical Phase Shift and Nonuniform Electric Field Distributions," IEEE Transactions on Dielectrics and Electrical Insulation, Vol. 1, No. 2, pp. 235-246, April, 1994.
- Zahn, M., S. Voldman, T. Takada, and D. B. Fenneman, "Charge Injection and Transport in High Voltage Water/Glycol Capacitors," Journal of Applied Physics, Vol. 54, No. 1, pp. 315-325, January, 1983.
- Zahn, M., Y. Ohki, K. Rhoads, M. LaGasse, and H. Matsuzawa, "Electro-Optic Charge Injection and Transport Measurements in Highly Purified Water and Water/Ethylene Glycol Mixtures," IEEE Transactions on Electrical Insulation, Vol. EI-20, No. 2, pp. 199-211, April, 1985.
- Zaky, A. A., and I. Megahed, "Effect of Organic Additives, Gas Phase, Stress, and Temperature on the Gassing Characteristics of Insulating Liquids," IEEE Transactions on Electrical Insulation, Vol. EI-7, No. 3, pp. 145-152, September, 1972.
- Zaky, A. A., I. Y. Megahed, and S. A. Yehia, "The Direct Breakdown Voltage of Silicone Oil Under Uniform Fields," Conference Record, Eighth International Conference on Conduction and Breakdown in Dielectric Liquids, pp. 255-259, July, 1984.
- Zaky, A. A., I. Y. Megahed, M. S. Khalil, "Effect of Dissolved Gases, Organic Additives and Field Configuration on Co-Field Motion in Insulating Oils," IEEE Transactions on Electrical Insulation, Vol. EI-14, No. 1, pp. 21-27, February, 1979.
- Zaky, A. A., M. E. Zein Eldine, and R. Hawley, "Influence of electrode coatings on the breakdown strength of transformer oil," Nature, Vol. 202, pp. 687-688, 1964.
- Zavtrak, S. T., and E. V. Korobko, "Behavior of Gas Bubbles in Liquid Dielectrics in the Presence of an External Electric Field," Soviet Physics - Technical Physics, Vol. 36, No. 3, March, 1991.

Zutavern, F., and M. Buttram, "Area and Time Dependence of the Breakdown of Water Under Long Term Stress," Annual Report. IEEE 1983 Conference on Electrical Insulation and Dielectric Phenomena, pp. 251-256, 1983.

